ENGINEERED ANTIGEN-SPECIFIC REGULATORY T CELLS

by

Nicholas Aaron James Dawson

B.Sc., The University of British Columbia, 2013

A THESIS SUBMITTED IN PARTIAL FULFILLMENT OF

THE REQUIREMENTS FOR THE DEGREE OF

DOCTOR OF PHILOSOPHY

in

THE FACULTY OF GRADUATE AND POSTDOCTORAL STUDIES

(Experimental Medicine)

THE UNIVERSITY OF BRITISH COLUMBIA

(Vancouver)

October 2019

The following individuals certify that they have read, and recommend to the Faculty of Graduate and Postdoctoral Studies for acceptance, the dissertation entitled:

ENGINEERED ANTIGEN-SPECIFIC REGULATORY T CELLS

submitted by Nicholas Aaron James Dawson in partial fulfillment of the requirements for

the degree of Doctor of Philosophy

in Experimental Medicine

Examining Committee:

Megan K Levings
Supervisor

Soren Gantt
Supervisory Committee Member

Laura Sly
University Examiner

Andrew Weng
University Examiner

Additional Supervisory Committee Members:

Kenneth Harder
Supervisory Committee Member

Scott Tebbutt
Supervisory Committee Member

Raewyn Broady
Supervisory Committee Member

Abstract

Achieving transplant tolerance with regulatory T cell (Treg) adoptive immunotherapy is currently under investigation as a therapy to reduce graft rejection, improve long-term outcomes, and patient quality of life. Initial approaches involve expansion of naturally-occurring Tregs, either polyclonal or antigen-specific, however both of these approaches have several technical limitations that restrict implementation at a large-scale. To circumvent these limitations, this work describes an alternate approach to generate antigen-specific Tregs by expressing a chimeric antigen receptor specific for HLA-A*02:01 (A2-CAR), which activates Tregs in the presence of HLA-A*02:01, a tissue antigen allele that is commonly mismatched between transplant donor and recipient. In the first CAR Treg studies, the antigen-binding region (scFv) of the A2-CAR was derived from the mouse BB7.2 hybridoma, which could cause immunogenic responses and limit its efficacy in humans. Additionally, most CAR Treg studies to date employ CD28 and CD3 signaling domains to activate the cell, but alternative co-receptor signaling moieties have not been adequately tested. Two major improvements to CAR Treg technology are explored: (1) the scFv is humanized to reduce the immunogenicity of the CAR construct itself, rendering it less likely to cause immune responses in humans and (2) a collection of a variety of co-receptor intracellular domains are tested in place of CD28 to determine whether alternative signals can bestow Tregs with more beneficial functional properties. In the final chapter, a method for staining FOXP3, the Treg master transcription factor, using mass cytometry is described to enable thorough tracking of $FOXP3^+$ Tregs and the rest of the immune compartment in patient samples from various tissues. Collectively, this body of work furthers our understanding of Treg immunotherapies and provides further support for their use in transplant settings.

Lay Summary

Patients fortunate enough to receive an organ transplant must tolerate immunosuppressive prescriptions their entire lives to prevent organ rejection. This work builds on a novel treatment that uses a special immune cell called a regulatory T cell, which suppresses immune responses, engineered to express a new protein that redirects the cell protect the newly transplanted organ. This will reduce the need for lifelong immunosuppression by retraining the immune system to see the new organ as safe, instead of as a foreign entity. My research improves on this technology in two ways: (1) alter the engineered protein to make it more invisible to the immune system allowing the treatment to last longer in patients and (2) optimize the signals the cell receives when it encounters the organ, creating a stronger immune suppressive forcefield around the organ. I also describe a new method that can be used to track these cells after injection.

Preface

The work performed in this thesis contributes to three main bodies of work, which are either published or in preparation for publication. Some of the results in this thesis are the subject of patent applications, either pending or in preparation. These are detailed below, including a breakdown of my and other's contributions to these projects.

Chapter 3: Systematic testing and specificity mapping of alloantigen-specific chimeric antigen receptors in T regulatory cells

The entirely of this work is published and has USA patents pending:

- Dawson, N.A.J., Lamarche, C., Hoeppli, R.E., Bergqvist, P., Fung, V.C.W., McIver, E., Huang, Q., Gillies, J., Speck, M., Orban, P.C., Bush, J.W., Mojibian, M., Levings, M.K. Systematic testing and specificity mapping of alloantigen-specific chimeric antigen receptors in regulatory T cells. *JCI Insight* **4,** (2019).
- Patent application numbers: PCT/CA2018/051167 and PCT/CA2018/051174

I designed the cloning strategy, experimental plan, all in vitro assays; performed cell preparation for all experiments, in vitro expression, activation, activation cross-reactivity, suppression, in vivo luciferase assays; helped with preparation of mice for skin transplant. I also performed data analysis for all in vitro studies and designed the analysis for the cross-reactivity studies, generated all of the figures, wrote the manuscript and supervised EM and QH. CL optimized the FlowPRA assay, performed the FlowPRA and activation cross-reactivity experiments, in vivo luciferase experiments and also wrote the manuscript. PB designed the humanized single chain antibody sequences. RH designed and also performed the luciferase experiment, xenogeneic GVHD experiment. VF also performed the luciferase and xenogeneic GVHD experiment. EM

assisted with cell preparation and quantification of skin transplant experiment. QH assisted with cell preparation and in vitro experiment setup. JG made lentivirus. MS, MM performed human skin transplant experiments and analyzed the human skin transplant data. PO helped design the cloning strategy. JB performed the histology scoring of human skin transplant experiments. MKL supervised the work and also wrote the manuscript.

Chapter 4: Functional effects of chimeric antigen receptor co-receptor signaling domains in human Tregs

This work is in manuscript preparation and has patents in preparation under the working title:

- Dawson, N.A.J., Sanchez, I.R., Novakovsky, G., Fung, V.C.W., Huang, Q., McIver, E., Sun, G., Gillies, J., Speck, M., Orban, P.C., Mojibian, M., Levings, M.K. Functional effects of chimeric antigen receptor co-receptor signaling domains in human Tregs.

I designed and cloned all of the constructs, designed and optimized all of the experiments, performed cell preparation, all in vitro and in vivo studies except the long-term culture experiments, which I designed and oversaw execution and data analysis. I analyzed all the data, except the RNA sequencing differential expression analysis, which I oversaw. IRS performed long-term culture experiments, analyzed the data and assisted with in vivo xenogeneic GVHD experiments. GN performed RNA differential gene expression analysis. QH and EM helped with cell preparation and in vitro assay setup. GS performed transient expression experiments under my supervision. VF and JG made lentivirus. MS and MM helped with cell injection for in vivo studies. PO helped design the cloning strategy. MKL supervised the work and provided guidance.

Chapter 5: An optimized method to measure human FOXP3$^+$ regulatory T cells from multiple tissue types using mass cytometry

The entirety of this work is published:

- Dawson, N.A.J., Lam, A.J., Cook, L., Hoeppli, R.E., Broady, R., Pesenacker, A.M., Levings, M.K. An optimized method to measure human FOXP3$^+$ regulatory T cells from multiple tissue types using mass cytometry. *Eur. J. Immunol.* **48,** 1415–1419 (2018).

I designed the fixation and permeabilization strategy for mass cytometry, all the experiments, and performed/analyzed all the experiments comparing buffer systems, antigen-specific Treg whole blood staining, tissue Treg comparison and some of the flow versus mass cytometry experiments. I made the figures and wrote the manuscript. AL also performed the flow versus mass cytometry experiments and analyzed those data. LC helped perform the antigen-specific assays and analyze those data. RH, RB, AP provided tissue samples and criticism of the manuscript. MKL supervised the work and also wrote the manuscript.

The following reviews have also been published and were also used in introduction sections of this thesis:

- Dawson, N.A.J. & Levings, M.K. Antigen-specific regulatory T cells: are police CARs the answer? *Translational Research* 1–6 (2017). doi:10.1016/j.trsl.2017.06.009
- Dawson, N.A.J., Vent-Schmidt, J. & Levings, M.K. Engineered Tolerance: Tailoring Development, Function, and Antigen-Specificity of Regulatory T Cells. *Front Immunol* **8,** 1460 (2017).

Table of Contents

List of Tables

List of Figures

List of Abbreviations

A2	HLA-A2 (HLA-A*02:01)
ACCENSE	automatic classification of cellular expression by non-linear stochastic embedding
ADP	adenosine diphosphate
Ag	antigen
AIRE	autoimmune regulator
Allo	allogeneic
AML	acute myeloid leukemia
AMP	adenosine monophosphate
ANOVA	analysis of variance
APC	antigen-presenting cell
ATP	adenosine triphosphate
CAR	chimeric antigen receptor
CCR	chemokine (C-C motif) receptor
CD	cluster of differentiation
CCL	CC chemokine ligand
CEA	carcinoembryonic antigen
CM	central memory
CMV	cytomegalovirus
CNS	conserved non-coding sequence
CPD	cell proliferation dye
Ct	cycle threshold
CTLA-4	cytotoxic T lymphocyte-associated protein 4
DNA	deoxyribonucleic acid
EAE	experimental autoimmune encephalomyelitis
EGFR	epidermal growth factor receptor
EM	effector memory
EMRA	CD45RA+ effector memory
FACS	fluorescence-activated cell sorting
FcγR	Fc gamma receptor
FMO	fluorescence-minus-one
FOXP3	forkhead box protein 3
FSC	forward scatter
FVD	fixable viability dye
FVIII	factor VIII
GARP	glycoprotein A repetitions predominant
GITR	glucocorticoid-induced TNFR family-related gene
Gly	glycine
GVHD	graft-versus-host disease
HER2	human epidermal growth factor receptor 2
HLA	human leukocute antigen
hs	homo sapiens
HSCT	hematopoietic stem cell transplant
IBD	inflammatory bowel disease

ICOS	inducible T cell co-stimulator
IDO	indolamine 2,3-dioxygenase
IFN	interferon
Ig	immunoglobulin
IgG	immunoglobulin type G
IL	interleukin
ITAM	immunoreceptor tyrosine-based activation motif
ITIM	immunoreceptor tyrosine-based inhibitory motif
IPEX	immunodysregulation polyendocrinopathy enteropathy X-linked
i.v.	intravenous
JIA	juvenile idiopathic arthritis
LAG-3	lymphocyte activating protein 3
LAP	latency-associated peptide
mAb	monoclonal antibody
MFI	mean fluorescence intensity
MHC	major histocompatibility complex
mm	mus musculus
MMO	metal-minus-one
MOG	myelin oligodendrocyte glycoprotein
mTOR	mammalian target of rapamycin
(Δ)NGFR	(truncated) nerve growth factor receptor
NK	natural killer
NOD	non-obese diabetic
NSG	NOD/SCID IL-2Rγ^{null}
PBMC	peripheral blood mononuclear cells
PD-1	programmed cell death protein 1
PFA	paraformaldehyde
PI3K	phophoinositide 3-kinase
pTreg	peripherally-induced Treg
PRA	panel reactive
RNA	ribonucleic acid
RT-PCR	reverse transcription polymerase chain reaction
scFv	single chain variable fragment; single chain antibody
SEB	staphylococcus enterotoxin B
SEM	standard error of the mean
Ser	serine
SMAC	supramolecular activation cluster
SOT	solid organ transplant
SSC	side scatter
STAT	signal transducer and activator of transcription proteins
T1D	type 1 diabetes
Tconv	conventional T cell
TCR	T cell receptor
TGFβ	transforming growth factor β
Th	T helper

TM	transmembrane
TNBS	trinitrobenzenesulfonic acid
TNF	tumor necrosis factor
TNFR	tumor necrosis factor receptor
TNP	trinitrophenyl
tTreg	thymic-derived Treg
Treg	regulatory T cell
TSDR	Treg-specific demethylated region
Vh	variable heavy chain
Vl	variable light chain
xeno	xenogeneic

Acknowledgements

Most importantly, thank you to my supervisor and mentor of seven years, Megan Levings. It was an absolute honour to learn and be a part of such an exciting time in your career.

Thanks to Agnieszka Kielczewska, who, perhaps unknowingly, encouraged me to do a Ph.D.

I would also like to thank Paul Orban for your wisdom, training and impromptu discussions.

Thank you to all of the individuals that put their time into these projects, both directly and indirectly: Avery, Jess, Isaac, Caroline, Majid, Maddy, Emma, Grace, Michelle, Romy, Rosa, Jana, Vivian. It truly took a small army to pull off this ambitious work.

Thank you to all of my other lab mates, both past and present.

Thank you to Don and Angela for always supporting me and Janelle in the best way you can.

Lastly, thank you to my committee members, collaborators and funding sources for supporting my training and these research projects.

To my loving wife,

who was left at the airport when both she and a shipment of cells arrived at the same time.

Your love, sacrifice and support are unwavering.

Chapter 1: Introduction

1.1 $CD4^+$ T helper cells in the adaptive immune response

$CD4^+$ T helper cells are an arm of the adaptive immune system that coordinates immune responses and develop in the thymus from bone marrow-derived lymphocyte progenitors[1-3]. During development in the thymus, T cell precursors, or thymocytes, undergo T cell receptor (TCR) rearrangement to determine their antigen specificity and ultimately their lineage within the T cell subset[1,3]. The majority of thymocytes rearrange the α and β chains of their TCR before their γδ chains, becoming either $CD4^+$ or $CD8^+$ αβ T cells[4]. The functions of γδ T cells will not be further discussed here. After TCR rearrangement, αβ thymocytes, upregulate both CD4 and CD8 co-receptors and undergo *positive selection* in the thymus cortex[3]. During positive selection, $CD4^+CD8^+$ double-positive T cells interact with self-antigens presented by major histocompatibility complex (MHC; human leukocyte antigen (HLA) in humans) class I or class II molecules on cortical thymic epithelial cells[5]. The majority of thymocytes bind neither and die from neglect[5]. Thymocytes that do bind MHC class II receive a signal to downregulate the CD8 co-receptor to become single positive CD4+ T cell (and vice-versa if the cell binds MHC class I) before moving to the thymic medulla to undergo *negative selection*, sometimes referred to as *clonal deletion*[5]. Here, single positive CD4 thymocytes that bind MHC-self peptides presented by medullary thymic epithelial cells and bone marrow derived antigen-presenting cells (APCs) with too high affinity are instructed to die via apoptosis[5]. Indeed, medullary thymic epithelial cells have been licensed to promiscuously express extrathymic, tissue-restricted antigens in the thymus by expressing the autoimmune regulator (AIRE) protein, which recruits chromatin remodeling and RNA polymerase machinery[6,7]. Bone marrow-derived APCs, such as dendritic

cells and B cells, can bring additional antigens from the periphery that add further to the self-antigen repertoire presented in the thymus medulla[5]. $CD4^+$ thymocytes that do not bind MHC-self peptides with too high affinity in the thymus medulla are not "selected out" and exit the thymus as naïve $CD4^+$ T cells[5].

In the periphery and secondary lymphoid organs, naïve $CD4^+$ T cells require multiple activating signals from professional APCs, such as dendritic cells, B cells or macrophages[8,9]. The first activating signal comes from TCR pairing with its cognate MHC-peptide complex and stabilized by interaction of the CD4 co-receptor with MHC, which forms the centre of the interface between the two cells called the *immunological synapse*, or *supramolecular activation complex (SMAC)*[8,9]. A second activating signal comes from interactions between additional T cell co-receptors and ligands expressed on APCs, such as CD28/B7 or 4-1BB/4-1BBL interaction, further stabilizing the SMAC[8,9]. While the first signal provides positively activating signals to the cell, ligation of the second set of co-receptors prolongs the interaction with the APC and synergizes with TCR signals, further activating the cell[8,9]. Both signals are necessary, and any one signal is not sufficient to fully activate the T cell: T cells that receive only the first signal without a second signal become refractory to additional stimulation, enter a state of anergy and eventually die from neglect[8,9]. A third signal that determines the $CD4^+$ T helper lineage (ie. Th1, Th2, Th17, Tfh, etc) is provided by the cytokine milieu surrounding the T cell when it receives the first two activation signals[9]. Each $CD4^+$ T helper lineage is specialized to provide activation and maturation signals to other immune cells tailored specifically for the type of immune response required (reviewed in[2]). After activation, the cell proliferates creating clonal populations of effector memory and central memory cells marked by downregulation of CD45RA and upregulation of CD45RO isoforms[10]. Central memory cells are responsible for

maintenance of long-term immunological memory and express CCR7, the chemokine receptor for CCL19/20, trafficking signals that emanate from the lymph node. The effector memory pool, which have higher effector potential and cytokine producing capabilities and lack CCR7, retracts during resolution of an immune response[9,10].

1.2 T regulatory cells

Ever since Medawar and colleagues performed their seminal studies on tolerance in the 1950's[11], immunologists have been working to understand the mechanisms that control immune recognition of self. First proposed as a thymic-derived T suppressor subset in 1970[12], subsequent studies have characterized a subset of $CD4^+$ T helper cells called T regulatory cells (Tregs) that are absolutely required to maintain immunological tolerance in the periphery. The non-redundant and critical nature of Tregs is evidenced most clearly in patients with deleterious mutations in forkhead box P3 (FOXP3), the Treg master transcription factor, resulting in immunodysregulation polyendocrinopathy enteropathy X-linked (IPEX) syndrome[13]. IPEX patients have severe autoimmunity in the form of severe enteropathy, type 1 diabetes, lymphadenopathy, psoriasis, eczema and hypothyroidism due to unchecked T cell activation and a lack of $FOXP3^+$ Tregs in the periphery[13]. Indeed, Tregs have been shown to suppress the proliferation, expression of "activation" markers and pro-inflammatory cytokine production of many cell types, including but not limited to, $CD8^+$ and $CD4^+$ T cells, mature dendritic cells and B cells[14]. In humans, Tregs express high levels of the high-affinity IL-2 receptor α chain (CD25) and low levels of the IL-7 receptor α chain (CD127)[15].

The suppressive phenotype of Tregs is mostly driven by expression of FOXP3, which directly represses IL-2, IL-4 and IFNɣ[16], classic pro-inflammatory cytokines, and drives

expression of cytotoxic lymphocyte-associated antigen 4 (CTLA-4), latency-associated peptide (LAP) and glycoprotein A repetitions predominant (GARP), proteins involved in the suppressive mechanisms of Tregs[14]. Expression of high levels of FOXP3 is driven by epigenetic modifications within a non-coding enhancer element within the *Foxp3* gene locus called the Treg-specific demethylated region (TSDR)[17,18]. Cells with a highly demethylated TSDR region, are thought to be committed to the Treg lineage by allowing for high levels of *Foxp3* mRNA and subsequent protein to be produced[18]. While FOXP3 is critical, studies where FOXP3 was introduced as a transgene into $CD4^+$ T cells did not fully recapitulate a full Treg phenotype, indicating there may be other transcription factors also involved in maintenance of Treg phenotype[19]. One such transcription factor may be Helios (IKZF2), which was has recently been reported to be involved in maintenance of Treg stability[20,21].

1.2.1 Treg development in the thymus and periphery

There are two types of $FOXP3^+$ Tregs: thymically-derived Tregs (tTregs) and peripherally-derived Tregs (pTregs)[22]. Both subsets of cells are phenotypically similar, and both are thought to have their respective roles in peripheral tolerance, however pTregs do not represent a population of stable Tregs and can downregulate FOXP3, leading to an acquisition of a phenotype and function reminiscent of conventional $CD4^+$ T helper cells[22]. There are no known surface antigens that can distinguish antigen-experienced tTregs from pTregs, however only tTregs contain a subset of CD45RA+ naïve Tregs, which maintain a stable demethylated TSDR Treg phenotype after TCR engagement and clonal expansion[22].

As their name suggests, pTregs are induced in the periphery to transiently express FOXP3 and exhibit suppressive properties[22]. While the pTreg population may be unstable and

transient, they have an important role in autoimmunity and gut tolerance[23]. pTregs may also be a vehicle by which a phenomenon described as infectious tolerance occurs[22] (discussed in Section 1.2.3). In vitro, these cells can be created through conventional $CD4^+$ T cell exposure to TGFβ, but whether these in vitro-generated Tregs are phenotypically identical to pTregs is unknown[22]. Because this Treg population is transient and outside the scope of this thesis, it will not be further discussed.

tTregs are thought to arise from several steps during T cell development in the thymus, and the affinity/specificity of their TCR is thought to play an essential role in their selection[5,24,25]. Indeed, tTreg TCRs have high affinity for self-peptides presented in MHC on epithelial cells and resident APCs in the thymus[5,24]. Mouse studies have shown that as the affinity between TCR-MHC increases, the propensity to differentiate into Tregs also increases[5]. An affinity threshold that determines Treg versus conventional T cell does not exist, as naïve $CD4^+$ T cells and Tregs do have some TCR repertoire overlap[5]. This high affinity TCR-MHC interaction event is a requirement that is an essential stage of Treg development[24]. Development of tTregs also requires other TCR-independent signals as well, such as co-receptor ligation[26] and cytokine signaling[24], but how these fit into a model of tTreg differentiation is unclear[24].

1.2.2 Treg activation and co-stimulation

Classical Treg stimulation mechanisms in the periphery are largely mediated by the same molecules that govern all $CD4^+$ T cells; however, ligation of the same co-receptor molecule in a Treg can deliver a different signal and transcriptional/translational response versus a conventional $CD4^+$ T cell. This implies that the underlying imprinted cellular “program”

ultimately determines the effect an individual signal will have on the cell, which can vary between cell types.

Tregs express an αβ T cell receptor (TCR), which determines their antigen-specificity and governs their suppressive function[27]. Indeed, mice lacking recombination activating gene (RAG), a protein essential for TCR rearrangement during T cell development, are deficient in Tregs[28]. High affinity detection of self-peptide-MHC complexes in the thymus governs differentiation of thymically-derived Tregs, generating a TCR repertoire distinct from that of conventional T cells, with some stochastic overlap[29-31]. Activation of Treg suppressor functions requires recognition of a cognate peptide-MHC Class II (MHCII) with its αβTCR[30,32,33] but once activated, Tregs can indirectly suppress bystander cells in an antigen non-specific manner[34]. Upon binding peptide-MHC, αβTCR heterodimers form the TCR complex by associating with the CD3 co-receptors, comprised of CD3γ, CD3δ, CD3ε, CD3ζ[35]. Unlike the αβTCR itself, the intracellular tails of CD3 co-receptors contain immunoreceptor tyrosine-based activation motifs (ITAMs), which start the signal cascade into the cell once phosphorylated by recruitment of the enzyme ZAP-70[35]. CD3γ,δ,ε subunits contain one ITAM motif, are structurally related to each other and form CD3εγ, CD3εδ heterodimers. CD3ζ is structurally unrelated to CD3γ,δ,ε and contains three ITAM motifs with no extracellular domain, enabling more interactions with ZAP-70 and a stronger activation signal[35]. TCR complex interaction with a peptide-MHC complex begins the formation of the immunological synapse, where interactions are stabilized through the recruitment of co-receptors (ex. CD4), co-stimulatory molecules (ex. CD28), additional TCR-MHC interactions, and rearrangement of cytoskeletal structures and organelles[35]. Formation of this complex dictates the strength and nature of the stimulating signal the T cell receives and therefore whether and how the cell responds to detection of this particular antigen.

Tregs express a number of co-receptor proteins that are generally classified as co-stimulatory and co-inhibitory molecules such as CD28 and PD-1, respectively[36]. However, classification of these molecules has been based primarily on the effects of these molecules in $CD4^+$ T cell studies, not Tregs. Given the specialized role and cellular programming of Tregs, stimulation of these molecules may result in a different cellular response versus conventional $CD4^+$ T cells. Thus, work to understand the role of each of these molecules in Tregs is still an active area of research in the literature. A major limitation of the studies performed thus far are that many are performed with mouse knockout models either using a pan-knockout or Treg-specific Cre/lox model. Using these models, it is difficult to conclude whether the manipulated molecule is critical for function within the periphery or for development in the thymus. Future studies of the role of these molecules in Treg activation in the periphery should ideally use an inducible (ie. taxomifen) Treg-specific Cre/lox mouse model or use CRISPR/Cas9 to interrogate the function in ex vivo human Tregs. Below is a summary of the current knowledge of selected co-receptor molecules as it relates to Tregs.

1.2.2.1 CD28 superfamily

CD28 superfamily members are a subgroup of the immunoglobulin superfamily and serve as critical regulators of immune cell response. Two co-stimulatory molecules, CD28 and ICOS, as well as two co-inhibitory molecules, CTLA-4 and PD-1, are reviewed below.

The best characterized co-stimulatory pathway in Tregs is CD28. Much like conventional T cells, signaling via CD28 occurs upon interaction with CD80/86 (B7-1/2) on antigen-presenting cells complementing TCR-mediated signals and promoting T cell activation, proliferation and survival[37]. CD28- and CD80/86-knockout mice are predisposed to autoimmune

diseases, with marked reduction in Treg populations, indicating that Tregs rely more on CD28 interactions during development and in the periphery than other T cells, which may receive sufficient pro-survival, proliferation and activation signals from alternative signaling pathways[37]. Indeed, CD28 co-stimulation was required for FOXP3 induction and Treg-differentiation in thymocytes during T cell development[38]. CD28 was shown to be important in the periphery in studies where mice were treated with CTLA-4Ig, which competitively inhibits CD28-CD80/86 activation signals, and a rapid reduction of the Treg population was observed within 9 days[39]. Other reports also show that the strength of CD28 signal may also play an important role in pTreg induction. In one such report, in vitro stimulation of $CD4^+CD25^-$ T cells with anti-CD3 and increasing amounts of anti-CD28 antibody resulted in a decrease in the number of induced Tregs by modulating Lck signaling[40]. Studies using CTLA-4Ig also noted that high-dose treatment of CTLA-4Ig prevented Treg proliferation and activity, while low dose CTLA-4Ig enriched for Tregs in vivo[41].

CD28 activation signals proceed via the PI3K/Akt/mTOR pathway, which activate metabolic pathways and play an important role in cell survival and fate[42-44]. In short, PI3K directly binds a YMNM motif in the CD28 cytoplasmic domain and then phosphorylates $PI(3,4)P_2$ to $PI(3,4,5)P_3$, starting a signaling cascade that results in the phosphorylation and activation of Akt, which positively regulates mammalian target of rapamycin 1 (mTORC1)[45]. In Tregs, mTOR signaling is somewhat paradoxical: mTORC1 signaling negatively regulates Treg differentiation but signaling via mTORC1 is important for Treg function. mTOR knockout mouse models resulted in the failure of CD4 T cells to differentiate into Th1, Th2, Th17 effector cells when stimulated and instead generated into $FOXP3^+$ Tregs[46]. Inhibition of mTOR in vitro results in preferential $FOXP3^+$ Treg induction and transcriptional profile; conversely,

constitutive PI3K signaling antagonizes FOXP3 induction[47]. Furthermore, culture of $CD4^+$ T cells with rapamycin, an mTORC1 inhibitor, reinforced a Treg phenotype through CD25 and FOXP3 upregulation, a strategy being used for in vitro-generation of Tregs for clinical application[42,48-50]. However, Tregs have high mTOR activity directly ex vivo and mTORC1 signaling is required for Treg suppressive function and production of metabolic intermediates that are required for expression of CTLA-4 and ICOS, two proteins important to Treg function[43]. Therefore, modulation of the mTOR axis may be important to regulate Treg abundance versus activity in a Treg-based therapy.

Another co-stimulatory molecule in the CD28 superfamily is inducible T cell co-stimulator (ICOS), which plays a non-redundant role to CD28 in T cell activation[51]. In conventional T cells, ICOS is known to promote T cell differentiation toward a T follicular helper phenotype, driving B cell stimulation and upregulation of IL-4, and therefore plays an important role in germinal centres within the lymph node[52,53]. ICOS signals via the PI3K/Akt pathway, giving positive co-stimulatory signals, but not via the NF-kB signaling pathway[51]. Despite signaling via PI3K/Akt, Tregs express higher basal levels of ICOS than Tconv and Tregs from ICOS-knockout mice have decreased FOXP3 expression, IL-10 production, in vitro suppressive ability as well as increased TSDR methylation and apoptosis, suggesting that ICOS plays an important role in Treg function and stability[54-56]. Furthermore, ICOS-knockout Tregs were unable to reverse colitis and, in a model of helminth infection, these mice had *increased* levels of IL-4 and IL-13 in serum, which was attributed to a blunted Treg response[54]. Studies from naïve mice show that populations of Tregs expressing high levels of ICOS were enriched for IL-10-producing cells[54]. In vivo blockade of ICOS/ICOS-L interactions inhibited production of IL-10 in an allergy-challenge model and caused exacerbation of type 1 diabetes in both NOD

and BDC2.5 mouse strains[57]. Recent adoptive transfer studies showed that ICOS blockade caused a decrease in the number of FOXP3$^+$ Tregs and caused acceleration of diabetes in NOD mice[55]. Although these studies have not been reported humans, some research suggest that ICOS may be important for human Treg function. For example, acute myeloid leukemia (AML) cells, which express ICOS-L, can cause expansion of Tregs and production of IL-10, measured both in vitro and ex vivo in the serum of AML patients[58]. These studies strongly suggest ICOS plays an important role in Treg IL-10 production, and therefore the ICOS/ICOS-L axis may be important to target for Treg therapeutics.

Cytotoxic T lymphocyte associated protein-4 (CTLA-4) is a molecule that downregulates immune responses and functions as an immune checkpoint to limit immune responses. On conventional T cells, CTLA-4 is upregulated on T cells upon activation[59]; in Tregs, CTLA-4 is expressed at resting state but is also upregulated upon Treg activation[60]. CTLA-4-knockout mouse models developed severe lymphoproliferative disease and uncontrolled autoimmunity[61]. At a molecular level, CTLA-4 is thought to disrupt downstream TCR/CD28 signaling, however the exact mechanism is unclear due to conflicting results in the literature. For example, one report suggested that CTLA-4 could disrupt T cell signaling far downstream the T cell signaling cascade by inhibiting ERK and JNK[62], but this was contested by later reports that CTLA-4 can directly disrupt ZAP-70 microcluster formation at the immune synapse[63], though this may not be essential to CTLA-4 function[64]. CTLA-4 action seems to primarily be based on activation of PP2A phosphatase, which inhibits numerous signaling cascades including transcriptional regulators ERK and JAK[65]. PKC-η has been shown to associate with the cytoplasmic tail of CTLA-4; Tregs without PKC-η were not able to suppress T cell proliferation, nor anti-tumor responses in mouse models[66]. However, mice lacking the cytoplasmic tail of CTLA-4 were still

able to control the lethal autoimmunity that CTLA-4-knockout mice experience[67], suggesting the function of the cytoplasmic tail may not be essential for CTLA-4 function and may play a more important role in cellular localization[68]. Indeed, transcriptional profiles of CTLA-4-sufficient and -deficient T cells showed little differences[69].

Programmed cell death protein-1 (PD-1) is an immune checkpoint molecule that negatively regulates immune responses through interaction with PD-L1 or PD-L2 on APCs. PD-L1 is expressed on several types of hematopoietic and non-hematopoietic cells and upregulated upon activation; PD-L2 is restricted to activated dendritic cell and macrophages[70]. Like CTLA-4, PD-1 is induced after T cell activation and Tregs express PD-1 at a resting state, but this expression level also increases after activation[71,72]. PD-1 interaction activates SHP-2 phosphatase and downregulation of Akt signaling, whereas CTLA-4 primarily activates PP2A phosphatase[65], suggesting that signaling downstream of PD-1 is distinct from CTLA-4. Furthermore, PD-1-knockout mice develop severe autoimmunity manifested as a lupus-like disease[73], unlike the uncontrolled lymphoproliferation observed in CTLA-4-knockout mice[74]. The PD-1/PD-L1 axis may play an important role in the development of pTregs and regulate the tolerance towards self-antigens[70]. Knockout of PD-1 and PD-L1 in mice did not affect the abundance of Tregs in the periphery, nor their suppressive function, but did blunt pTreg differentiation[75]. In another mouse study, PD-L1-deficient APCs failed to covert naïve T cells to pTregs and PD-L1 interaction caused sustained expression of FOXP3 and suppressive properties[76]. PD-L2 is important for maintenance of environmental and oral tolerance[70,77], but how PD-1/PD-L2 interactions affects Tregs is unknown. Collectively, these data indicate that PD-1 signaling may not play a role in circulating tTreg function, but may blunt the pTreg induction in the periphery.

1.2.2.2 TNFR superfamily

The tumor necrosis factor receptor (TNFR) superfamily is comprised of 27 members that bind tumor necrosis factor (TNF)-related proteins to modulate immune function. While some TNFR proteins are involved in apoptosis, others are involved in leukocyte proliferation, survival and differentiation[78]. Four of these TNFR superfamily receptors are reviewed below: 4-1BB, OX40, GITR and TNFR2.

4-1BB (CD137) is expressed on stimulated T cells, most resting Tregs and several other immune cells including dendritic cells, B cells, NK cells and granulocytes[78,79]. In T cells, 4-1BB signaling inhibits apoptosis and activates proliferation and activation pathways NF-κB, Akt, p38, MAPK and ERK[78,80]. 4-1BB-knockout mice had reduced memory $CD8^+$ T cells in a viral recall model, indicating its importance in $CD8^+$ T cell responses[81,82]. In Tregs, early in vitro studies reported that 4-1BB agonists and APCs expressing 4-1BBL promoted Treg proliferation and preserved their suppressive properties[83,84]. However, later studies using in vivo disease models showed that 4-1BB had a more nuanced role in modulating Treg responses, which may be dependent on the disease context. In disease models of autoimmunity, 4-1BB agonists expanded Tregs, thus protecting mice from diabetes[85], and ameliorating inflammatory bowel disease[86], experimental autoimmune encephalitis[87,88]. In contrast, in oncology, $4\text{-}1BB^+$ Tregs are enriched in the tumor microenvironment[89] and signals through 4-1BB were reported to directly inhibit Treg suppressive functions, enhancing anti-tumor responses[90]. Ligation of 4-1BB can also stimulate conventional $CD4^+$ cells to overcome Treg-mediated suppression via IL-2 production[91].

OX40, GITR and TNFR2 molecules are expressed at high levels on T cell precursors in the thymus[92,93] A comprehensive study of TNFR superfamily receptors revealed that stimulating the OX40, GITR, or TNFR2 pathway in thymocytes resulted in upregulation of STAT5, which is

required for IL-2 signaling, and development of $CD25^{+}FOXP3^{+}$ Tregs[92]. The effect was reversed if blocking antibodies were used, but there is some overlapping pathway redundancy. Stronger signaling via these pathways positively correlated with Treg differentiation of lower affinity TCR thymocytes in a dose-dependent manner. Thus, OX40, GITR and TNFR2 signaling is important in the thymic development of Tregs. 4-1BB is not expressed on thymocytes and therefore does not play an important role in this pathway[92].

In addition to thymocytes, OX40 (CD134) is also expressed on recently activated T cells[92], including Tregs, where it can be used as a biomarker of antigen-specific responses[94]. Mice and humans lacking OX40 have similar pools of circulating Tregs[95] but these cells are less suppressive and have impaired homing characteristics[96,97], providing support for its role in thymic development of Tregs. Reports on downstream effects of OX40 ligation in circulating Tregs are conflicting. Some studies show stimulation via OX40/OX40L axis represses expression of FOXP3[98], abrogates the ability of FOXP3+ cells to suppress effector T cell proliferation, cytokine production[95] and Treg-mediated tumor immunosuppression[99]. Further, in an allograft rejection model, blocking of OX40/OX40L signaling prevented skin rejection and supported Treg survival[100]. However, Ruby et al. showed that in an anti-inflammatory cytokine environment, OX40 stimulation can generate FOXP3+ cells in vitro[101]. Using an in vivo model of experimental autoimmune encephalitis, OX40 stimulation during disease priming, rather than disease onset, reduced disease severity and was associated with decreased pro-inflammatory serum cytokine levels and increased Tregs in secondary lymphoid organs[101]. This has since been challenged, as these OX40-induced Tregs were shown to be less suppressive without supplementing IL-2[102]. Signaling via OX40 triggers, STAT5, NF-κB and PI3K/Akt signaling pathways[78,102,103].

Glucocorticoid-induced tumor necrosis factor receptor (GITR; CD357)) binds GITRL, primarily expressed on APCs, and can be found on activated T cells, and resting state Tregs[78,104]. GITR stimulation has been reported to abrogate Treg-mediated suppression in vitro via active signaling into the cell[105,106]. In vivo, anti-GITR stimulating antibodies caused autoimmune gastritis and loss of suppressive function, but not abundance, of Tregs[105]. GITR-deficient mice are protected from experimental collagen-induced arthritis and colitis, suggesting that GITR signaling negatively affected Treg function[107,108]. However, GITR stimulation may also share the context dependent properties of OX40 as one study that injected GITRL-Ig into naïve mice found that Tregs were selectively enriched, but when injected into an established IBD model, that protective effect was lost and Tregs underwent apoptosis[109]. Downstream of GITR ligation, NF-κB and MAPK pathways, such as ERK, p38 and JNK, are activated[110].

Tumor necrosis factor receptor 2 (TNFR2; CD120b) binds tumor necrosis factor (TNFα) in the periphery and is expressed predominantly on endothelial cells, Tregs and thymocytes, as well as some specialized cells within the nervous system[78,111]. Accordingly, TNFR2 is thought to play a role in immune modulation and tissue regeneration. Unlike TNFR2, tumor necrosis factor receptor 1 (TNFR1) is expressed ubiquitously on all cells and is primarily concerned with pro-inflammatory response[111]. While TNFα can be expressed as membrane and soluble forms, TNFR2 can only be fully activated when recognizing membrane-bound TNFα, whilst TNFR1 can propagate signals in response to either membrane-bound or soluble TNFα[112]. The important role of TNFR2 in the development of thymic-derived Tregs has been addressed above. In the periphery, the role of TNFR2 in the immune system is of increasing interest as another immune checkpoint. TNFR2-knockout mice have depreciated ability to produce pTregs[113], while TNFR1-

knockout mice do not. TNFR2 agonists have been shown to increase Treg proliferation[114,115] and TNFR2 antagonist antibodies can deplete Treg populations in certain cancers where TNFR2$^+$ Tregs are enriched[116]. Interestingly, both TNFR2 agonist and antagonist antibodies have been used in HSCT applications, to manage graft-versus-host disease (GVHD) and graft-versus-leukemia effects, respectively[117]. In solid tumors, TNFR2$^+$ Tregs are enriched in the tumors of several types of cancer and represents a highly suppressive subset of Tregs[114]. At a molecular level, TNFR2 can trigger cell activation, proliferation and migration pathways, including NF-κB, AP-1 and PI3K/Akt[111]. Whether TNFα signaling benefits Treg function is hotly debated as some reports show that signaling via TNFR2 can increase the FOXP3 expression and suppressive capabilities of Tregs[114,115,118-120], while others report opposite findings[121-125].

1.2.3 Treg mechanisms of suppression

Tregs suppress the proliferation and function of many immune cells, even at very low Treg:effector cell ratios[16]. Many mechanisms of Treg-mediated suppression in the periphery have been described in the literature and several (but not all) are regulated by FOXP3[14,15]. As mentioned above, Treg suppressive functions requires Treg αβTCR recognition of a cognate peptide-MHC[30,32,33], but once activated Tregs can indirectly suppress bystander cells in an antigen non-specific manner[34]. Mechanisms of suppression can be categorized into two main groups: contact-dependent and contact-independent suppression.

Several Treg contact-dependent mechanisms involve the disruption of APC-mediated T cell priming. For example, CTLA-4 binds CD80/86 on APCs and has higher affinity for CD80/86 than CD28 and thus can inhibit signaling through competitive inhibition[126]. This limits the contact time between T cells and APCs by preventing stable immune synapse formation and

activation[127,128]. Tregs also use transendocytosis to pull the entire CD80/86 complex and surrounding supporting synaptic proteins off of the APC subsequent to CTLA-4 binding[129]. Mutations affecting CTLA-4 or blocking proteins in this pathway negatively affect Treg function[130,131]. Treg interactions can also elicit production of indoleamine 2,3-dioxygenase (IDO) from dendritic cells, which can further activate Tregs, drive pTreg-induction, and suppress NK and conventional T cells[132-135]. It has also been proposed that LAG-3, a CD4 homologue, can bind MHC Class II on immature dendritic cells, causing signaling that suppresses dendritic cell maturation[136].

Other contact-dependent mechanisms involve Treg disruption of the metabolic milieu or direct T cell contact. For example, Tregs can also cause apoptosis of $CD8^+$, but not $CD4^+$, T cells by ligation of CD95L (FasL) with CD95 (Fas) on Tregs[137]. Tregs also express CD39 and CD73, which can process pro-inflammatory extracellular adenosine triphosphate/diphosphate (ATP/ADP) to adenosine, which has anti-inflammatory properties[138,139].

A major mechanism of Treg suppression is via secretion of cytokines and cytolytic proteins. Tregs can produce membrane-bound and soluble forms of TGF-β1, which can suppress conventional T cell proliferation and IL-2 production, and upregulate inhibitors of cell cycling[140,141]. TGF-β1 can directly suppress APC-mediated T cell priming by inhibiting dendritic cell maturation and expression of MHC class II[140]. Membrane-bound TGF-β1 is also required for a phenomenon called infectious tolerance, where Tregs can endow conventional T cells with suppressive activity in the form of IL-10 or TGF-β production[141-143]. Some Tregs can also produce IL-10, which negatively regulates growth and differentiation of several immune cell types including B, NK, $CD4^+$ T, $CD8^+$ T cells, as well as APCs and innate immune cells[144]. This mechanism may only be important in certain contexts, such as the gut, as IL-10-knockout mice

are not susceptible to autoimmunity but are susceptible to colitis[144]. IL-10 and TGF-β are closely related and interdependent for optimal function: production of one of these cytokines can enhance the production of the other in a positive feedback loop[140]. Activated Tregs can also produce IL-35, an IL-12 family cytokine, which predominantly functions through direct suppression of T cell proliferation and effector functions[145]. Like NK cells and $CD8^+$ cytotoxic T cells, a subset of Tregs express and can target other immune cells for cytolysis using granzyme B[14,146]. CD25, the high affinity IL-2 receptor alpha chain, was initially proposed to be a mechanism of bystander T cell suppression by acting as an "IL-2 sink" where Tregs would deprive surrounding conventional T cells of IL-2 by preferentially absorbing IL-2 from the cytokine milieu[147], but this mechanism has been questioned[148,149].

Tregs have also been reported to have several other properties, both that aide in and are unrelated to suppression. Tregs can take on characteristics of other $CD4^+$ T helper (Th) cells[150,151] resulting in sub-specialization and enhanced suppression of the Th cell subset they mirror[152]. For example, Hoeppli et al. has shown that stable Th1-like Tregs can be generated in vitro and have enhanced suppressive function of and migration to Th1-inflammatory sites[153]. Non-suppressive functions of Tregs have also been proposed, for example, in tissue repair by Treg secretion of amphiregulin independent of TCR stimulation[154]. However, more work is required to understand the relevance of this finding to human Tregs[155].

1.3 Tregs as a target for novel therapeutic approaches

The immunosuppressive properties of Tregs make them attractive candidates for cellular therapy, particularly for application in conditions such as hematopoietic stem cell transplantation

(HSCT), solid organ transplantation (SOT) and autoimmunity. However, harnessing Tregs for this purpose has not been trivial due to limitations related to cell isolation and expansion.

1.3.1 Strategies to enhance Treg function in vivo

There are two main approaches to increase Treg numbers and function: in vivo "boosting" using small molecules or proteins, and adoptive cellular therapy. To date, the most successful strategy to “boost” Treg in vivo is the use of low-doses of IL-2. When given in limiting concentrations, IL-2 preferentially expands $CD25^{hi}$ Tregs without significantly affecting cells expressing low-levels of CD25, such as resting conventional T (Tconv) cells or natural killer (NK) cells. This concept was first tested for treatment of hepatitis-C-virus-induced vasculitis where low doses of IL-2 induced an increase in circulating Tregs and clinical improvements in 8 of 10 patients[156]. Subsequently, the beneficial effect of low dose IL-2 therapy was also observed in GVHD, alopecia areata, type 1 diabetes (T1D) and systemic lupus erythematosus[157-161]. However, a cautionary note is that in one study of T1D where IL-2 therapy was combined with rapamycin, there was an unexpected expansion of NK cells and worsening of disease[162]. Thus this approach may need further refinement to reduce the risk of expanding non-Tregs. Low dose IL-2 and other strategies for in vivo-boosting of Tregs are discussed extensively in Zhang et al. and Boyman et al[163,164].

With the early success of low dose IL-2 therapy as an approach to expand Tregs in vivo, there are now several efforts to improve upon this approach by modulating the way IL-2 interacts with its receptors. One strategy to modulate IL-2 is to use IL-2/anti-IL-2 monoclonal antibody (mAb) combination therapy to form “IL-2 complexes” that enhance the half-life of IL-2 after intravenous injection and provide preferential selection of certain immune cell subsets. For

example, IL-2 in complex with anti-IL-2 mAbs, JES6-1A12 (mouse) or 5344 (human), preferentially expand Tregs, but not other IL-2-dependent cells such as $CD8^+$ T and NK cells[165]. This approach enriches Tregs and treats disease in several different mouse models[164,165]. In 2015, Spangler et al. solved the crystal structure of IL-2/JES6-1A12, showing that this IL-2 complex preferentially binds cells with the trimeric IL-2R (CD25, CD122 and common gamma chain) and not dimeric complexes (CD122 and common gamma chain), thus selecting for Tregs because of their constitutive CD25 expression[166].

Another approach to modulate IL-2 is to directly mutate IL-2 itself to change how it interacts with its receptor complex. Specifically, IL-2 "muteins" have alterations in the CD25-binding domain, thus decrease affinity for CD25, and enabling preferential binding to dimeric IL-2R complexes and activation of NK and $CD8^+$ T cells[167-169]. There is also much commercial interest in making IL-2 muteins with the opposite effect: IL-2 muteins that preferentially activate Tregs have led to a $400 million investment from Eli Lilly to Nektar Therapeutics and $300M from Celgene to Delinia to develop this technology[170].

A final approach to modulate IL-2 signaling is to change IL-2R's affinity for IL-2. Specifically, it is well established that single nucleotide polymorphisms in the *CD25* locus are associated with autoimmunity[171-173]. Considering the power of CRISPR/Cas9 technology, in the future it could be possible to edit risk alleles of CD25 into protective alleles or otherwise engineer IL-2 signaling pathways to optimize therapeutic Treg function[174].

1.3.2 Adoptive transfer of Tregs as a cellular therapy

An alternate to in vivo-boosting is adoptive therapy with ex vivo-enriched, often expanded, Tregs. This method aims to overcome defective or low numbers of Tregs by transfer

of a large number of Tregs to reset the Treg:Tconv cell balance. Adoptive Treg therapy has been applied in the clinic for many years. The first successful study reported that chronic GVHD patients treated with Tregs had a significant reduction in clinical symptoms and immunosuppression[175]. Subsequently, Treg therapy has been tested in several other GVHD cohorts, overall showing that infusion of autologous or third party (partially HLA-matched) Tregs is well tolerated, does not inhibit graft-versus-leukemia, and may be protective from GVHD[176,177].

Adoptive transfer of Tregs has also been applied successfully in autoimmunity and organ transplantation. Children with T1D who received Tregs showed slowed disease progression and long term preservation of residual beta-cells[178,179]. Adoptive transfer of Tregs in adults with T1D is also well tolerated, with evidence that the cells persist long-term (> 1 year)[180]. A clinical trial of in vitro-expanded naïve Tregs is also underway in Crohn's Disease, the first application of $FOXP3^+$ Treg immunotherapy for inflammatory bowel disease (IBD) (ISRCTN97547683)[181]. In addition, several clinical trials are testing autologous polyclonal or antigen-expanded Tregs in kidney or liver transplantation; these trials are reviewed extensively in[182-184]. To date, all of these studies have shown that adoptive Treg therapy in humans is feasible and safe and initial data suggests that this approach may also be effective.

1.3.3 Isolation and in vitro expansion of polyclonal Tregs

A hurdle in Treg therapy is generating sufficient numbers for clinical application[184]. Since activated Tconv cells also express CD25 and FOXP3, and downregulate CD127, isolating Tregs on the basis of CD25 and CD127 alone introduces the risk of co-purifying and -expanding non-Tregs. One way to overcome this limitation is to isolate naive $CD45RA^+CD25^{hi}$ cells from

blood to enrich for a more homogeneous population[185,186]. However, this also significantly decreases the number of cells with which a culture can be started.

Another potential solution to this problem is to isolate Tregs from a third-party donor. Third party Tregs overcome the limitation of autologous Treg products in situations where timely delivery is required and allows for batch-preparation of Treg products and would streamline centralized manufacturing processes[187]. Since third party Tregs are likely HLA-mismatched, they are subject to immune-mediated rejection, which may limit treatment efficacy. Since large numbers of Tregs would be preferable for third-party approaches, apheresis and umbilical cord blood sources are not ideal because they would produce a limited number of Treg product and isolating a pure population of Tregs remains a challenge[188,189]. Another potential source for third-party Tregs, is to isolate Tregs directly from the thymus, a discarded product in pediatric heart surgeries, which generates a large number of highly-pure Treg cells[190]. In the future, it may be possible to generate stem cell-derived Tregs, which could provide an unlimited supply of identical Treg products[191]. Use of stem cell-derived products could be further manipulated to be immune agnostic through manipulation of HLA molecules to circumvent immune-mediated rejection.

1.3.4 Engineering "synthetic" Tregs using a transgene

An additional approach is to find a way to engineer the desired Treg product. Indeed, the possibility of engineering Tregs via over-expression of FOXP3 has been considered since its discovery, with multiple studies showing that viral-mediated over-expression of FOXP3 in mouse or human T cells can induce suppressive function[192]. Notably, in order to re-program

human T cells into Tregs, FOXP3 has to be expressed at high and stable levels[193]; Treg suppressive capacity can be quickly reversed upon removal of FOXP3[194].

Although FOXP3 is the master Treg transcription factor, evidence that its over-expression alone does not fully recapitulate the Treg gene signature led to the search for other co-factors and the discovery that co-expression of other transcription factors is important for full lineage specification[195]. A consideration is whether studies which found that FOXP3 expression alone is not sufficient to induce a complete Treg gene signature considered the time that may be required for epigenetic re-programming to take place. Epigenetic modification and the consequent change in expression of other transcription factors is necessary to stabilize Treg phenotype and function[196]. Since these epigenetic changes may require multiple rounds of cell division, re-programming Tconv cells into Tregs may not take place in short term culture. The first application of FOXP3-engineered Treg therapy will likely happen as gene therapy for IPEX. $CD4^+$ T cells from IPEX patients can be efficiently converted into functional and stable Tregs by FOXP3 gene transfer in vitro[197,198]. Testing these cells in vivo will rigorously determine if they have acquired sufficient Treg function to treat the severe autoimmunity in these patients.

1.3.5 Isolation and in vitro expansion of antigen-specific Tregs

Antigen-specific Tregs have the benefit of being directed towards desired therapeutic antigens, thus increasing their potency up to 100-fold compared to polyclonal Tregs[199]. Not only would fewer antigen-specific Tregs need to be infused, but they would also carry a lower risk of off-target suppression[199,200]. However, antigen-specific Tregs are extremely rare and must undergo significant in vitro expansion to achieve clinical doses because only up to ~10% of

Tregs are naturally alloAg-specific[201]. Despite this technical barrier, the testing of antigen-specific Tregs is already underway in the clinic in the context of organ transplantation[202].

1.3.6 Engineering Tregs to be antigen-specific using a transgene

Engineering antigen specific Tregs by genomic modification to confer expression of desired transgenic T cell receptors (TCR) or by chimeric antigen receptors (CARs) represents an exciting approach to solve the challenge of the rarity of antigen-specific Tregs[203] (Table 1.1). Attempts to re-program the specificity of Tregs have been underway for several years. The first application in human Tregs involved gene transfer of a melanoma-specific, MHC Class I-restricted, TCR[204]. These human TCR-transduced Tregs proliferated in response to antigen and suppressed antigen-specific Tconv cells in vitro and in vivo. Similarly, human Tregs transduced with an islet antigen-specific TCR suppressed antigen-stimulated T cell responses. However, they were less efficient than Tregs expressing a viral antigen-specific TCR[205], possibly due to Treg-specific TCR affinity requirements[206]. On the other hand, another study of human Tregs in which multiple class I-restricted TCRs recognizing the same peptide-MHC complex, but with affinities varying up to 3500-fold, were tested, found TCR affinity had no effect on antigen-specific suppressive function[207]. Thus, a consideration for future development of this approach is to find TCRs with an MHC restriction and specificity that would make them applicable in multiple patients, and which possess an optimal affinity for Tregs. TCRs which meet these requirements are most likely to be found in autoimmunity where there are well-known and relatively common MHC-peptide complexes that could be targeted.

Table 1.1 Comparison of the benefits and limitations of engineering Tregs to express a defined TCR or CAR.

TCR	CAR
Pros: ✓ "Natural" protein; engineered cells should not be immunogenic ✓ Recall responses of TCR-transgenic Tregs may be more effective than CAR Tregs ✓ Designed to detect intracellular antigens ✓ Low affinity but high antigen sensitivity; fewer number of antigens required for TCR activation than CAR activation	**Pros:** ✓ MHC-independent antigen detection of soluble or cell surface antigens ✓ Modular design enables more precise control over the type of antigen-stimulated response ✓ Hinge region provides flexibility, allowing CARs to bind antigen in a variety of orientations ✓ Higher antigen affinity than TCRs
Cons: - MHC-dependent peptide detection; each TCR complex has limited patient applicability - May require a DNA library of several TCR genes to adequately cover MHC/ peptide complexes for one disease - Mispairing with endogenous TCRs could create new specificities and reduce efficacy	**Cons:** - "Unnatural" peptide sequence; construct may be immunogenic and limit ability to administer repeat doses - Ability to detect cell-surface antigens may be blocked by the presence of competing soluble antigen

Also see [203].

1.4 Chimeric antigen receptors (CARs)

CARs were first described by Eshhar in 1993[208] and now being applied in humans for cancer immunotherapy[209-211]. CARs have been recognized as a breakthrough therapy by the Federal Drug Administration and research in this area has exploded since the first successful clinical application of a CD19 CAR CD8 T cell product was used for treatment of treat chronic lymphoid leukemia[212]. While CAR T cell therapy has been very effective for use in treating B cell cancers, it has had limited success in solid tumors and cancers where the tumor microenvironment is immunosuppressive and antigen selection is more nuanced[213]. Therefore, optimization and fine-tuning of CAR therapy has been the subject of much research. For example, to overcome an immunosuppressive tumor microenvironment, CAR T cells have been engineered to deliver "transgenic payloads", such as IL-12, which is then consumed in an autocrine mechanism, maintaining a high degree of T cell activation[214]. To protect from off-target toxicities, so-called logic-gated CARs have also been developed where expression of a CAR construct can be controlled through Boolean logic using a modified syn-Notch pathway[215].

CARs have a modular design, which allows for customization of specific regions (Figure 1.1): antigen-specificity domain, stalk region, transmembrane domain and signaling domains. For most CAR constructs, antigen specificity is conferred via a single chain antibody, which is a fusion of heavy and light chain variable regions. Use of single chain antibodies in CAR constructs give T cells the B cell-like ability to bind to antigen in an MHC-independent manner, enabling CAR T cells to engage extracellular antigens[203]. The stalk region of CAR constructs fine-tunes the overall signal strength of CAR-mediated stimulation and can play a role in CAR surface expression[203]. CAR transmembrane regions also play a role in expression of CAR on the surface of the cell[203]. The intracellular portion of the CAR contains modular signaling domain

regions, which tailor the desired response from the engineered cell through use of T cell signaling moieties[216].

1.4.1 Chimeric antigen receptors to induce operational tolerance

Over the last decade, a number of publications demonstrated the utility of CARs in Tregs[200]. Beginning with mouse models in 2008, Elinav et al. used Tregs from a mouse expressing a transgene for a hapten 2,4,6-trinitrophenol (TNP)-specific CAR[217]. They found that transgenic TNP-specific CAR Tregs mediated antigen-specific suppression of effector T cells in vitro as well as in vivo resistance to colitis. The same group then demonstrated that the TNP-CAR could be introduced into mouse Tregs using retroviral-mediated gene transfer, giving these cells the ability to protect from disease in vivo in a dose-dependent manner[218]. In a similar system, mouse CAR Tregs specific for a different model antigen, carcinoembryonic antigen (CEA), prevented disease in a model of colitis better than CAR Tregs specific for an irrelevant

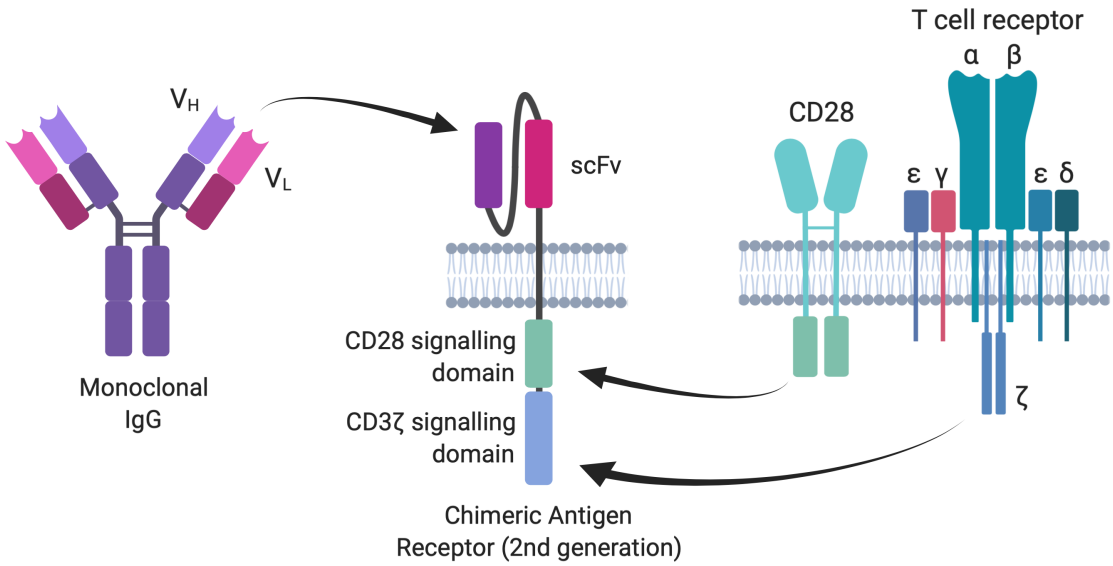

Figure 1.1 Schematic representation of a second-generation chimeric antigen receptor.
First-generation CAR constructs generally only contain the CD3z chain; third-generation CARs ligate an additional co-receptor signaling domain proximal to the membrane.

antigen. Importantly, these CEA-CAR Tregs homed to the location of inflammation and suppressed colitis in a potent, antigen-specific manner[219].

Apart from these studies in the context of IBD, there is currently only one other report of mouse CAR Tregs. Specifically, in 2012, Fransson et al. developed a CAR specific for myelin oligodendrocyte glycoprotein (MOG), the disease-causing agent for experimental autoimmune encephalomyelitis (EAE)[220]. In this study, instead of isolating $CD25^{+}FOXP3^{+}$ Tregs, lentivirus was used to ectopically express FOXP3 and enforce a Treg phenotype. The resultant MOG-specific CAR Tregs suppressed responder T cell expansion in vitro and reversed symptoms of EAE. Overall, these publications provided important proof-of-concept data supporting the development of CAR Tregs for use in human cells.

Several publications have demonstrated the application of CAR technology to human Tregs. Three reports investigated the utility of expressing a CAR specific for HLA-A*02:01 (A2) to test whether CAR Tregs could be a new approach to control alloreactive T cells that cause rejection in HSCT and solid organ transplantation[221-223]. The first publication showed that A2-CAR Tregs are activated and proliferate when stimulated through the CAR via co-culture with A2-expressing cells[221]. Additionally, A2-CAR Tregs prevented engraftment of $A2^{+}$ PBMCs and development of xenogeneic GVHD in a humanized mouse model. Two other groups confirmed this approach, showing that A2-CAR Tregs suppress alloimmune responses better than polyclonal Tregs in humanized mouse models of $A2^{+}$ skin xenografts[222,223]. HLA-A2 is an ideal antigen to target with CAR Tregs because it is broadly applicable in the transplant setting due to its high allelic frequency, meaning that ~25% of all organ transplants could potentially benefit from this therapy[221]. Moreover, HLAs in general are likely good targets for CAR Tregs since

they are a membrane bound protein specifically expressed on the transplanted tissues at a high antigen density.

Yoon et al. reported the characterization of human CAR Tregs that target factor VIII (FVIII), the protein lacking in hemophilia which is immunogenic in patients receiving FVIII replacement therapy[224]. Of specific interest from this study is the finding that a CAR specific for soluble antigens is suitable for use in Tregs, widening the possible antigen-targets that could be considered. This study also demonstrated that both T cell and antibody responses can be controlled by CAR Tregs. Also of note is that this study directly compared the effects of TCR versus CAR-engineered Tregs, finding that antibody recall responses were more effectively controlled by TCR-transgenic Tregs. More research is required to explore similarities and differences between TCR- and CAR-activated Tregs to better understand the affinity requirements and limitations of each approach[203].

Table 1.2 Summary of salient details from the current CAR Treg publications.
A summary of the key features of the types of CARs that have been tested in Tregs. All studies report superior effects of antigen-specific CAR Tregs compared to polyclonal or non-specific CAR Tregs.

Antigen & model disease	CAR structure	Species & expression system	Effects of CAR-Treg therapy and points of significance	Reference
TNP Colitis	Hinge: CD28 TM: CD28 Co-stim:CD28 ITAMs: FcRγ	Mouse Transgene	- Protect from TNBS colitis - Bystander suppression of oxazolone-induced colitis - CD28 signaling required for CAR Treg function - In vivo imaging of Treg trafficking to site of inflammation	(217)
TNP Colitis	Hinge: CD28 TM: CD28 Co-stim: CD28 ITAMs: FcRγ	Mouse Retrovirus	- Ex vivo expansion through cognate antigen - Protect from TNBS colitis	(218)
CEA Sarcoma	Hinge: IgG Fc* TM: CD28 Co-stim: CD28 ITAMs: CD3ζ	Human Retrovirus	- Suppression of CEA-specific anti-tumor response in humanized mouse model	(361)
MOG EAE	Hinge: IgG Fc* TM: CD3ζ Co-stim:CD28** ITAMs: CD3ζ	Mouse Lentivirus	- Dual expression system of FOXP3 and CAR - Reversal of EAE clinical symptoms, given at peak of disease	(220)
CEA Colitis	Hinge: IgG Fc* TM: unknown Co-stim: CD28 ITAMs: CD3ζ	Mouse Retrovirus	- Protect from CEA-CAR T effector cell induced colitis - In vivo imaging of Treg trafficking to site of inflammation - Presence of CAR-specific antibodies correlated with disappearance of CAR-Tregs	(219)
HLA-A2 Transplant rejection	Hinge: CD8α TM: CD28 Co-stim:CD28 ITAMs: CD3ζ	Human Lentivirus	- CAR-stimulated Tregs maintain stable phenotype - Suppression of alloantigen-specific T cells in vitro - Prevention of xenogeneic GVHD in vivo	(221)
HLA-A2 Transplant rejection	Hinge: CD28 TM: CD28 Co-stim: CD28 ITAMs: CD3ζ	Human, Lentivirus	- Prevention of skin allograft rejection in humanized mouse model - Partial effect of CAR-lacking CD28 and CD3ζ intracellular signaling domains	(223)
HLA-A2 Transplant rejection	Hinge: CD8α TM: CD8 Co-stim: CD28 ITAMs: CD3ζ	Human, Retrovirus	- Prevention of skin allograft rejection in humanized mouse models - CAR specificity tested against a panel of HLA-typed cells	(222)
Factor VIII Hemophilia A	Hinge: IgG Fc* TM: CD28 Co-stim: CD28 ITAMs: CD3ζ	Human, Retrovirus	- CAR directed against clinically-relevant soluble antigen - Suppression of recall antibody responses - Direct comparison between CAR and TCR engineered Tregs	(224)
CD19/EGFR Transplant rejection	Hinge/TM:unknown Co-stim: None, CD28 or 4-1BB ITAMs: None or CD3ζ	Human, Lentivirus	- 4-1BB CARs have diminished CAR-mediated suppression - CAR Tregs induce cell-mediated cytolysis via granzyme B - CAR Tregs can be detected at skin grafts and produce immunosuppressive cytokines in vivo	(248)

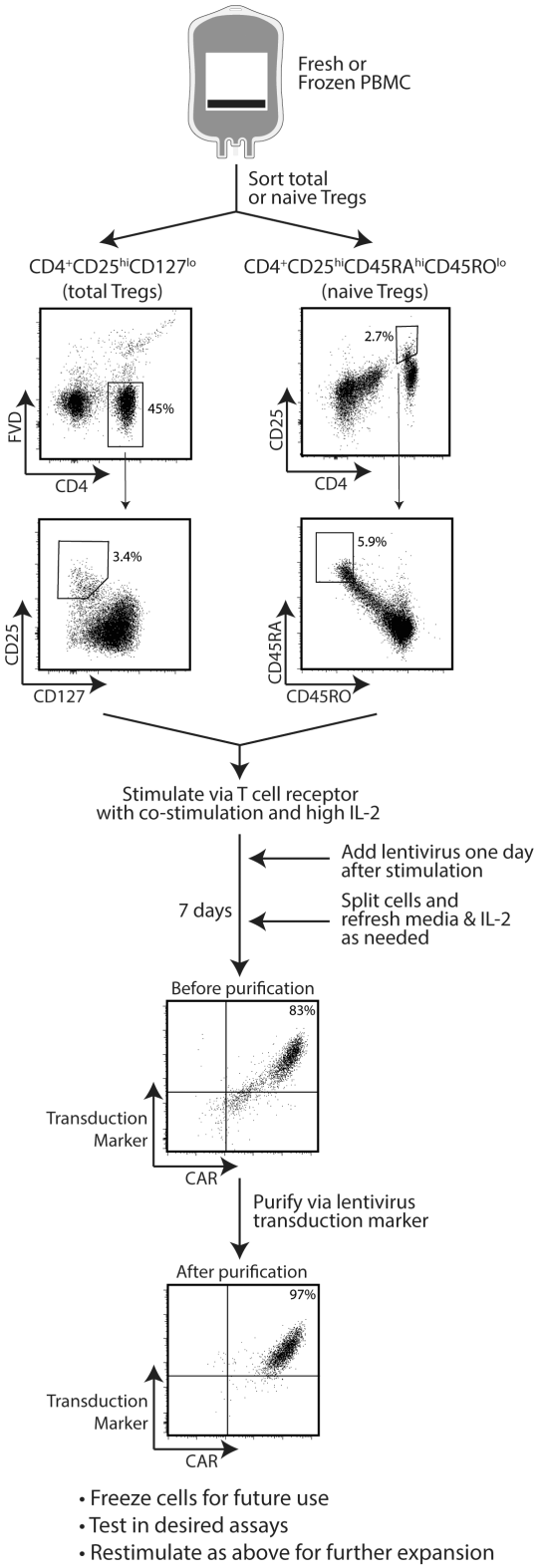

Figure 1.2 Example CAR Treg manufacturing pipeline.

1.4.1.1 Antibody humanization

CARs classically contain a single chain of antibody variable domains (scFv) derived from heavy and light chains of well-characterized, high affinity mouse monoclonal antibodies (mAbs), which face the extracellular space[225]. CARs derived from mouse scFvs can be highly effective[212,226-228], but carry the risk of immunogenicity, with sensitization possibly limiting therapeutic efficacy and repeat dosing[229-235]. Therapeutic mAb studies have shown that the structural residues in mouse variable regions are sufficient to elicit immune responses[236,237], leading to bioinformatic strategies to "humanize" mAbs[238-241] so that >90% of the structure originates from human, with only the Ag-binding complementarity-determining region (CDR) remaining from mouse. This approach can be highly successful, as evidenced by the numerous humanized mAbs in routine clinical use[242], but is empirical and can result in decreased affinity and loss or change of specificity[238,243]. The applicability of bioinformatic strategies developed to humanize mAbs to create humanized CARs is largely unknown.

1.4.1.2 Signaling domains in chimeric antigen receptors

CAR constructs initially described in the literature contained a single signaling moiety derived from CD3ζ, a component of the T cell receptor complex that contains three immunoreceptor tyrosine-based activation motifs[244]. While this construct activated T cells in vitro, they failed to produce a robust cytokine response and were prone to anergy[244]. Second-generation CAR constructs containing an additional co-stimulatory signaling domain were able to overcome the anergic properties associated with first generation CARs: the first of which was CD28, but 4-1BB, ICOS, DAP10 and OX-40 have also been reported in the literature. The addition of a CD28 co-stimulatory domain resulted in greater strength of signaling, potency and

efficacy in patients, when compared to CD3ζ alone[244]. These CD28 second-generation CARs were the first to be used the clinic and demonstrated strong efficacy at clearing malignant B cell leukemia[245] and 4-1BB second-generation CARs were also later used successfully in the clinic[212]. Studies comparing 4-1BB to CD28 showed that 4-1BB CAR T cells are more readily detected in patients long-term, form a larger central memory population, and exhibit less markers associated with exhaustion post-CAR stimulation[246]. Third-generation CARs, which contain two co-stimulatory domains in addition to CD3ζ, have also been developed and confer superior activation and proliferation compared with second-generation CARs, enabling further combinations of signaling domains to be tested[244]. While some limited comparisons of co-stimulatory domains have been performed, there have not been any exhaustive studies comparing co-stimulatory domains in CAR constructs. All initial reports in human Tregs used a second-generation CAR design including the CD28 co-stimulatory domain[221-223,247]. Recently, Boroughs et al. compared first-generation, CD28 and 4-1BB second-generation CAR Tregs and found that 4-1BB CAR Tregs were not as suppressive in vitro but did not compare the constructs in vivo[248].

1.5 Summary and synopsis of research questions

Initial reports of CAR Treg cell therapy in model systems showed that it is also a promising approach for treatment of solid organ transplant, hematopoietic stem cell transplant and autoimmunity[221-223]. Despite encouraging proof-of-principle studies, additional studies are required to prepare CAR Treg treatment for use in humans. Furthermore, once CAR Tregs are ready to be used in humans, it will be critical to track CAR Tregs in patients after the treatment is administered. Thus, my thesis work focuses on three main questions:

1. Can the single-chain antibody (scFv) be humanized to avoid potential immunogenic properties of a murine-derived scFv while maintaining specificity and function of CAR Tregs? *(Chapter 3)*
2. Can the signals given to Tregs be optimized by systematically changing CAR intracellular domains using signaling domains from known T cell co-receptors? *(Chapter 4)*
3. Can high-dimensional flow cytometry-based immunophenotyping be used to track Tregs effectively? *(Chapter 5)*

Engineering of antigen-specific Tregs via CAR-transduction is an effective approach using models of hematopoietic stem cell and solid organ transplantation in vitro and in vivo[221-223]. Taking lessons from monoclonal antibody and CAR therapy in oncology, to maximize persistence and efficacy of CAR Tregs in humans, we will need to minimize the immunogenic properties of the CAR transgene[249]. While the junctions between protein domains within the CAR sequence are unnatural and potentially immunogenic[250], the scFv sequence within the CAR is derived from mouse antibody sequences, which are known to potentiate strong immune responses in humans[249]. To optimally position CAR Tregs for long term survival in vivo, we sought to humanize CAR scFv sequence and generate a panel of humanized scFv sequences, which were then cloned into our existing CAR structure[221]. Publications detailing humanization of antibody sequences in the context of CARs are limited, so this work was non-trivial and an important addition to the CAR literature. My *hypothesis* for this work was that we could generate humanized CARs that are functionally equivalent to a murine-derived CAR in Tregs. My *rationale* was that methods to humanize monoclonal antibody sequences have been well-established and, given that the antibody in the CAR sequence only functions to detect the

antigen, an antibody sequence that delivers equivalent antigen detection should not affect the ability of the CAR to signal into the cell. In *Chapter 3*, I created a panel of humanized CARs based on sequences generated in silico and tested their functional characteristics in human Tregs in a series of in vitro and in vivo models.

Original CAR technologies were developed in conventional T cells using only a CD3ζ signaling domain, but since then researchers have added additional co-receptor signaling domains, such as 4-1BB and CD28, to augment activating signals and proliferation potential[216]. Comprehensive comparison of signaling domains in CARs have not been performed in either conventional T cells or Tregs. My *hypothesis* was that CAR signaling domains could be optimized for use in Tregs by swapping CD28 with intracellular domains from other co-receptor molecules that could provide a functional benefit to Tregs. My *rationale* was that since conventional T cells and Tregs have different signaling properties and a fundamentally different role in the immune system, therefore Tregs may require alternative pathways to achieve optimal function. In *Chapter 4*, I created and systematically tested of a battery of signaling domain CAR variants in human Tregs in several novel in vitro assays and an in vivo model of transplantation.

Once CAR Tregs are employed in the clinic setting, it will be important to track CAR Tregs in protocol blood samples as well as the composition of the patient's immune system. Interrogating the immune compartment in detail will be important to disseminate potential mechanisms of CAR Treg treatment efficacy and to identify potential improvements. Therefore, optimizing a high-dimensional flow cytometry-based method to track Tregs from patient samples is of high importance. Mass cytometry is a new technology that combines single cell fluidics from traditional fluorescence flow cytometry with the benefits of mass spectrometry, enabling simultaneous detection of over 50 parameters from a single sample with minimal

compensation[251]. Because mass cytometry is a new technology, adequate methods for intracellular detection of FOXP3, the Treg master transcription factor, have not yet been established. While methods for FOXP3 detection via fluorescence flow cytometry have been well-established, mass cytometers require a special staining method and existing commercially-available kits optimized fluorescence flow cytometry may have impurities that cause false-positive signals. My *hypothesis* was that detection of FOXP3 via mass cytometry could effectively be optimized using a custom saponin-based fixation and permeabilization method. My *rationale* was that saponin-based methods are used to detect FOXP3 in fluorescence flow cytometry and impurities could be controlled for using carefully screened reagents. In my final *Chapter 5*, I developed this saponin-based method, and tested its performance against two commercially available kits and provide an example analysis of Tregs from different tissue sources as a proof-of-principle study.

Chapter 2: Materials & Methods

2.1 Cloning and lentivirus generation

2.1.1 Generation of humanized HLA-A*02-specific CARs.

The humanized genes were codon optimized using the codon optimizer from Thermo Fisher Scientific Invitrogen GeneArt Gene Synthesis service using the settings for Homo sapiens. gBlocks® Gene Fragments were ordered from Integrated DNA Technologies (Coralville, Iowa) such that the 5' region of the CAR contained a Kozak sequence, and a 36 nucleotide overlap with a pcDNA3 plasmid. The 3' end contained a BamHI site and an overlap with a CD8 hinge sequence to facilitate Gibson assembly into the plasmid in frame with the CD8 hinge and CAR intracellular signaling domains.

The scFv variants were fused to a stalk region from human CD8α, the transmembrane and intracellular domains were from human CD28, and human CD3ζ as described[221,244]. The resulting cDNAs were cloned into a lentiviral vector encoding a truncated nerve-growth-factor receptor (ΔNGFR) as a marker. Surface expression was determined by flow cytometry with transiently transfected HEK 293T cells (jetPRIME®, Polyplus Transfection). Viral particles were produced as described[19].

2.1.2 Generation of HLA-expressing K562 cell lines.

CD64-expressing K562 cells (K562.64) were a gift from James Riley, University of Pennsylvania, Philadelphia, USA. cDNA for HLA-A*02:01 and A*24:02 were isolated from mRNA of peripheral blood mononuclear cells from a donor homozygous for A*02:01 or A*24:02, respectively, on the HLA-A locus using the primer sequences: 5’-TTTTCTAGACGCGTGCCACCATGGCCGTCATGGCGCC-3’ (forward) and 5’-

AAGTCGACGCTAGCTCACACTTTACAAGCTGTGAGAGACA-3' (reverse). The resulting sequence was confirmed by Sanger sequencing, aligned to the expected sequences from the IPD and IMGT/HLA Database[252] and transduced into K562 cells, respectively, using a lentiviral expression vector. To generate A25-, A68, or A69-K562 cells, HLA sequences for A*25:01, A*68:01, and A*69:01 were identified in the IPD and IMGT/HLA Database[252], codon optimized using the codon optimizer tool (set to Homo sapiens) from Thermo Fisher Scientific Invitrogen GeneArt Gene Synthesis service, then cloned into a lentiviral expression vector and transduced into K562 cells. The resulting K562 cell lines were then sorted on a FACSAria II (BD Biosciences) using anti-HLA-ABC (Thermo Fisher Scientific, 12-9983-41) to ensure equivalent surface expression of the transduced HLA and anti-HLA-A2 (BB7.2) (Thermo Fisher Scientific, 17-9876-42) to ensure purity.

2.1.3 Generation of signaling domain CAR variants

Sequences for the intracellular region of selected co-stimulatory or co-inhibitory molecules were identified in the Uniprot database[253], then codon optimized using the codon optimizer from Thermo Fisher Scientific Invitrogen GeneArt Gene Synthesis service using the settings for Homo sapiens. gBlocks® Gene Fragments were ordered from Integrated DNA Technologies (Coralville, Iowa) with appropriate unique restriction enzyme recognition sequences to clone onto our original BB7.2-CAR construct previously reported in[221] in place of the existing CD28 co-stimulatory domain. Unless overwise specified, all CAR constructs are on a lentivirus-compatible backbone containing a bicistronic promoter with the minimal-CMV promoter encoding truncated nerve-growth-factor receptor (ΔNGFR) as a transduction marker and an EF1α promoter encoding the CAR construct. From N- to C-terminal, the CAR construct

contained an scFv specific for HLA-A*02:01 (derived from BB7.2), a myc-tag, a stalk region from human CD8α, the specified human transmembrane and intracellular domain sequences, then human CD3ζ as described[244]. To observe the specific effect of the intracellular signaling domain, a first-generation CAR construct was generated which contains only the CD3ζ signaling moiety (denoted "CD3zeta"). Surface expression was determined by flow cytometry with transiently transfected HEK 293T cells (jetPRIME®, Polyplus Transfection). Viral particles were produced as described[193].

2.2 Isolation and culture of cells

2.2.1 Treg sorting, transduction, and expansion

$CD4^+$ T cells were isolated from HLA-$A2^-$ donors via RosetteSep (STEMCELL Technologies, 15062) and enriched for $CD25^+$ cells (Miltenyi, 130-092-983) prior to sorting live $CD4^+CD25^{hi}CD127^{lo}$ Tregs or $CD4^+CD127^{lo}CD25^{hi}$ $CD45RA^+$ Tregs using a MoFlo® Astrios (Beckman Coulter) or FACSAria II (BD Biosciences), respectively. In experiments where conventional T cells (Tconv) were used, the live $CD4^+CD25^{lo}CD127^{hi}$ fraction was also sorted. Sorted Tregs were stimulated with L cells and αCD3 mAb (OKT3, UBC AbLab; 100ng/mL) in Immunocult-XF T cell expansion media (STEMCELL Technologies, 10981) with 1000U/ml of IL-2 (Proleukin) or 100U/ml IL-2 for Tconv as described[221]. One day later, cells were transduced with lentivirus at a multiplicity of infection of 10 virus particles:1 cell. To generate polyclonal Treg controls, cells were transduced with a vector encoding either a HER2-CAR and the ΔNGFR marker (denoted "HER2 CAR"), or only ΔNGFR (denoted "NGFR"). The latter was used for in vivo skin transplant experiments to avoid HER2-mediated activation via HER2 expressed by human skin. At day 7, $NGFR^+$ cells were purified with magnetic selection (Miltenyi, 130-091-

330) then used in assays or re-stimulated with L cells as above and expanded for 5 days for in vivo experiments, unless otherwise specified. To test the effects of CAR or TCR-mediated stimulation, Tregs were cultured with limiting IL-2 (100U/mL) for 24 hours, then re-counted and co-cultured with irradiated anti-CD3/anti-CD28-loaded CD64-expressing K562 cells, HLA-A*24:02-, A*25:01, A*68:01, or A*69:01-expressing K562 cells, HLA-A*02:01-expressing K562 cells or HLA-A*02:01 FlowPRA Single Antigen beads (One Lambda, Thermo Fisher Scientific, custom order) at the specified ratios and timepoints.

2.3 Isolation, cryopreservation and thawing of mononuclear cells

Collection of human samples followed protocols approved by the University of British Columbia Clinical Research Ethics Board and Canadian Blood Services. Peripheral and umbilical cord blood mononuclear cells were isolated using density-dependent centrifugation with Lymphoprep (STEMCELL Technologies #07851) as per the manufacturer's recommendations. Peripheral blood cells were also incubated for 5 minutes in ammonium chloride (STEMCELL Technologies #07850) to lyse red blood cells. Thymus-derived $CD25^{+}CD8^{-}$ T cells were isolated from thymus tissue discarded in pediatric cardiac surgery as previously described[189]. Synovial fluid cells were isolated by pre-incubation with hyaluronidase (10U/mL; Sigma-Aldrich #H4272) for 20 min at 37°C before density-dependent centrifugation with Lymphoprep. Purified cells were cryopreserved at 5-50 × 10^6 cells/mL in 90% fetal bovine serum (FBS) (Gibco; ThermoFisher #16140089) and 10% DMSO (Sigma-Aldrich #C6414). Cells were thawed using warm complete media and DNase I (STEMCELL Technologies #07900), washed once with 1x PBS (Gibco; ThermoFisher #14190250) and counted prior to staining.

2.4 In vitro methods

2.4.1 Flow cytometry

All steps were performed in 96-well V-bottom plates and centrifuged in a swinging-bucket centrifuge. For phenotypic analysis, cells were stained with fixable viability dye (FVD, Thermo Fisher Scientific, 65-0865-14; Biolegend, 423102) and for surface markers before fixation and permeabilization using eBioscience FOXP3/Transcription Factor Staining Buffer Set (Thermo Fisher Scientific, 00-5523-00) and staining for intracellular proteins. In short, cells were stained with a fixable viability dye and for surface markers for 30 minutes at room temperature (RT) in 50μL 1x PBS (Gibco; ThermoFisher #14190250). Cells were washed, fixed, permeabilized and stained for FOXP3 in permeabilization buffer following the manufacturer's recommended times and volumes. After nuclear antigen staining, cells were washed and reconstituted in 1x PBS for data acquisition by a flow cytometer.

2.4.1.1 Staining methods specific to humanized CAR studies (Chapter 3)

Surface staining was performed for NGFR (Miltenyi, 130-091-885), CD3 (BD Biosciences, 564465), CD4 (Biolegend, 317410), CD25 (Miltenyi, 130-091-024), LAP (Thermo Fisher Scientific, 25-9829-42), CD69 (Biolegend, 310946), CD71 (BD Biosciences, 563768) and CD127 (Thermo Fisher Scientific, 48-1278-42). Tetramer staining was performed with HLA-A*02:01 monomers provided by the NIH Tetramer Core Facility (Emory University, Atlanta USA) made into tetramers with streptavidin-allophycocyanin (Prozyme, PJ27S). Intracellular staining was performed for CTLA-4 (Biolegend, 369606).

For in vivo experiments, 50μL of blood was collected weekly and at endpoints. Ammonium chloride was used for red blood cell lysis. Cells were resuspended in PBS with anti-mouse CD16/32 (Thermo Fisher Scientific, 14-0161-82) and stained for extracellular markers using fixable viability dye (FVD; Thermo Fisher Scientific, 65-0865-14), anti-mouse CD45 (Thermo Fisher Scientific, 25-0451-82), and anti-human CD45 (BD Biosciences, 560777), CD4 (Biolegend, 300554, 317434), CD8 (Thermo Fisher Scientific, 48-0087-42), anti-human CD271 (NGFR; BD Biosciences, 557196), HLA-A2 (BD Biosciences, 551285). Intracellular staining for FOXP3 (Thermo Fisher Scientific, 12-4777-42) was done with the eBioscience FOXP3/Transcription Factor Staining Buffer Set (Thermo Fisher Scientific, 00-5523-00). 10,000 counting beads were added to every sample (Thermo Fisher Scientific, 01-1234-42).

2.4.1.2 Staining methods specific to signaling domain CAR studies (Chapter 4)

Surface staining was performed for NGFR (Miltenyi, 130-091-885; BD Biosciences, 562122, 562562), myc (9E10 clone, UBC Ablab, Vancouver, Canada), CD4 (Biolegend, 317410, 300558), CD25 (Miltenyi, 130-091-024), LAP (Thermo Fisher Scientific, 25-9829-42), GARP (BD Biosciences, 563958), CD69 (Biolegend, 310945, 310931), CD71 (BD Biosciences, 563768) and CD127 (Thermo Fisher Scientific, 48-1278-42), CD39 (Biolegend, 328214), CD80 (BD Biosciences, 557226), CD11c (BD Biosciences, 555392), CD86 (BD Biosciences, 555660), CD83 (Biolegend, 305324), HLA-DR (Biolegend, 307646). Intracellular staining was performed for CTLA-4 (BD Biosciences, 563931), FOXP3 (Thermo Fisher Scientific, 25-4777-42, 12-4777-42), Helios (Biolegend, 137223) using the eBioscience FOXP3/Transcription Factor Staining Buffer Set (Thermo Fisher Scientific, 00-5523-00).

For in vivo experiments, 50µL of blood was collected weekly and at endpoints. Ammonium chloride was used for red blood cell lysis. Cells were resuspended in PBS with anti-mouse CD16/32 (Thermo Fisher Scientific, 14-0161-82) and stained for extracellular markers using fixable viability dye (FVD; Thermo Fisher Scientific, 65-0865-14), anti-mouse CD45 (Thermo Fisher Scientific, 56-0451-80), and anti-human CD45 (BD Biosciences, 560777), CD4 (Biolegend, 300554), CD8 (Thermo Fisher Scientific, 48-0087-42), anti-human CD271 (NGFR; BD Biosciences, 562562), HLA-A2 (Biolegend, 343306), myc (9E10 clone, UBC Ablab, Vancouver, Canada). Intracellular staining for FOXP3 (Thermo Fisher Scientific, 25-4777-42) and Helios (Biolegend, 137223) was done with the eBioscience FOXP3/Transcription Factor Staining Buffer Set (Thermo Fisher Scientific, 00-5523-00). 10,000 counting beads were added to every sample (Thermo Fisher Scientific, 01-1234-42).

For cytokine profile experiments, supernatants from stimulated CAR Tregs were taken diluted 2-fold before analysis via cytometric bead array (BD Biosciences, 560484) using manufacturer's recommendations.

2.4.1.3 Staining methods specific to mass cytometry studies (Chapter 5)

2.4.1.3.1 Whole blood reagents, stimulation, and staining protocol

Staphylococcal enterotoxin B (SEB) was from Sigma-Aldrich (St. Louis, USA; #S4881). Cytomegalovirus (CMV) pp65 antigen is a pool of 138 peptides (15mers with 11 aa overlap) from the 65 kDa phosphoprotein (pp65) of human CMV (JPT Peptide Technologies, Berlin, Germany; #PM-PP65-2). Aliquots of all antigens were stored at -80°C. The OX40 assay was performed as previously described[254,255] using either whole blood (diluted 1:1 with Iscove's Modified Dulbecco's Medium; IMDM, ThermoFisher Scientific, Waltham, USA) or PBMCs at 2

× 10^6 cells/mL, in IMDM supplemented with 5% human serum (NorthBio, Toronto, Canada). Cells were incubated with antigen for 44 hours at 37°C (5% CO_2). Antigen concentrations: SEB (1µg/mL), CMV pp65 (2µg/mL). Cells were stained for surface antigen markers in diluted whole blood as previously described[254,255]. For analysis by fluorescence flow cytometry, red blood cells were lysed with OptiLyse C (Beckman Coulter #A11895) and FOXP3 staining was performed using the BD Biosciences FOXP3 buffer kit (#56098). All flow cytometry reagents were used according to manufacturers' recommendations. An LSRFortessa X-20 flow cytometer (BD Biosciences) was used and analysis performed with FlowJo software (v10.3; Treestar Inc.). The optimal red blood cell lysis and FOXP3 staining protocol used for flow cytometry was incompatible with mass cytometry as it resulted in poor FOXP3 detection even after permeabilization using PFA/saponin as described above. Thus, for analysis via mass cytometry, cells were first subjected to ammonium chloride before washing and staining using the PFA/saponin-based protocol described in 2.4.2.1.

2.4.1.3.2 Antibodies used in mass cytometry studies

Table 2.1 Summary of fluorochrome-conjugated antibodies used for Figure 5.4A&B.

Fluor	Marker	Clone	Manufacturer	Catalog #
eFluor 780	Fixable Viability Dye	n/a	ThermoFisher	L34976
BV711	CD4	SK3	BD Biosciences	563028
BB515	CD25	2A3	BD Biosciences	564467
eFluor 450	CD127	eBioRDR5	ThermoFisher	48-1278-42
PE	FOXP3	PCH101	ThermoFisher	12-4776-41

Table 2.2 Summary of fluorochrome-conjugated antibodies used for Figure 5.4C.

Fluor	Marker	Clone	Manufacturer	Catalog #
eFluor 780	Fixable Viability Dye	n/a	ThermoFisher	L34976
APC	CD3	UCHT1	ThermoFisher	17-0038-42
BV711	CD4	SK3	BD Biosciences	563028
BB515	CD25	2A3	BD Biosciences	564467
eFluor 450	CD127	eBioRDR5	ThermoFisher	48-1278-42
PE	FOXP3	236A/E7	ThermoFisher	12-4777-42

Table 2.3 Summary of fluorochrome-conjugated antibodies used for Figure 5.3.

Panel	Fluor	Marker	Clone	Manufacturer	Catalog #
1	Alexa Fluor 700	CD4	RPA-T4	BD Biosciences	557922
1	APC	CD3	UCHT1	ThermoFisher	17-0038-42
1	eFluor 780	Fixable Viability Dye	n/a	ThermoFisher	L34976
1	PE-Cy7	CD25	M-A251	BD Biosciences	557741
1	FITC	HLA-DR	G46-6	BD Biosciences	555811
1	BV711	CD49d	9F10	BD Biosciences	563177
1	BV510	CD194 (CCR4)	L291H4	BioLegend	359416
1	BV421	CD152 (CTLA-4)	BNI3	BD Biosciences	562743
2	BV786	CD3	OKT3	BioLegend	317330
2	Alexa Fluor 700	CD4	RPA-T4	BD Biosciences	557922
2	PE-Cy7	CD25	M-A251	BD Biosciences	557741
2	APC	CD127	eBioRDR5	ThermoFisher	17-1278-41
2	FITC	CD45RA	HI100	ThermoFisher	11-0458-73
2	eFluor 450	CD45RO	UCHL1	ThermoFisher	48-0457-42
2	PerCP-eF710	CD279 (PD-1)	eBioJ105	ThermoFisher	46-2799-42
2	eFluor 780	Fixable Viability Dye	n/a	ThermoFisher	L34976
3	BV786	CD3	OKT3	BioLegend	317330
3	Alexa Fluor 700	CD4	RPA-T4	BD Biosciences	557922
3	PE-Cy7	CD25	M-A251	BD Biosciences	557741
3	APC	CD127	eBioRDR5	ThermoFisher	17-1278-41
3	FITC	CD95 (Fas)	DX2	BD Biosciences	555673
3	BV421	CD39	A1	BioLegend	328214
3	BV510	CD278 (ICOS)	C398.4A	BioLegend	313525
3	eFluor 780	Fixable Viability Dye	n/a	ThermoFisher	L34976

Table 2.4 Summary of fluorochrome-conjugated antibodies used for Figure 5.5.

Fluor	Marker	Clone	Manufacturer	Catalog #
BV786	CD3	OKT3	Biolegend	317330
PE-Cy7	CD4	SK3	BD Biosciences	557852
APC	CD25	2A3	BD Biosciences	340939
PE	CD134 (OX40)	ACT35	BD Biosciences	561700
Alexa Fluor 488	FOXP3	259D	BD Biosciences	560047

2.4.2 Mass cytometry

2.4.2.1 Saponin-based permeabilization and staining for mass cytometry

All steps were performed in 5mL polystyrene tubes (Corning Science #352054) and centrifuged in a swinging-bucket centrifuge. Cells were stained for surface markers for 30 minutes at room temperature (RT) in 100μL MaxPar Cell Staining Buffer (CSB; Fluidigm #201068). Cell-ID™ Cisplatin (Fluidigm #201064) was added in the last 5 minutes of surface marker staining to identify non-viable cells[256]. Cells were immediately topped up with 4mL serum-containing CSB, spun at 400x*g* for 5 minutes, then washed with 1mL CSB, spun at 400x*g* for 5 minutes, and fixed for 30 minutes RT with 1.6% paraformaldehyde (AlfaAesar #43368-9M diluted 10x in MaxPar Water (Fluidigm #201069)). Cells were spun at 800x*g* for 5 minutes, supernatant discarded, and washed once with 1mL 0.5% saponin (w/v; diluted in CSB; Sigma #S7900). Intracellular antigens were stained by adding antibodies in 100μL 0.5% saponin for 30 minutes at 4ºC. Cells were washed twice with 1mL CSB then reconstituted in 500μL Cell-ID™ Intercalator-Ir (Fluidigm #201192A) diluted 1:1000 in MaxPar Fix & Perm Buffer (Fluidigm #201067) and incubated overnight at 4ºC to identify nucleated cells. The next day, cells were washed once with 1mL CSB, then once with 2mL MaxPar Water. Cells were reconstituted in 0.1x EQ Four Element Beads (Fluidigm #201078; diluted in MaxPar Water) to enable post-acquisition data normalization and analyzed on a CyTOF2 at 400,000 cells/mL.

2.4.2.2 Permeabilization and staining using commercial reagents for mass cytometry

Staining with the eBioscience FOXP3 Staining Buffer Kit (ThermoFisher #00-5523-00) and Fluidigm MaxPar Human Regulatory T Cell Phenotyping Kit (Fluidigm #201319) was performed according to manufacturer's guidelines, substituting FBS-containing PBS buffer for CSB to adapt the protocol for mass cytometry analysis. In short, cells were stained for surface antigens as above, incubated in their respective fix/perm buffers, then washed and stained for nuclear antigens in the indicated permeabilization buffer following the manufacturer's recommended times and volumes. After nuclear antigen staining, cells were washed twice with CSB, reconstituted in intercalator solution and prepared for data acquisition as above.

2.4.2.3 Antibodies used in mass cytometry studies

Table 2.5 Summary of metal-conjugated antibodies used for Figure 5.1, Figure 5.2, Figure 5.3 and Figure 5.6.

Channel	Isotope	Marker	Clone	Manufacturer	Catalog #
141	Pr	CD49d	9F10	Fluidigm	3141004B
145	Nd	CD4	RPA-T4	Fluidigm	3145001B
149	Sm	CD194 (CCR4)	205410	Fluidigm	3149003A
151	Eu	CD278 (ICOS)	DX29	Fluidigm	3151008B
153	Eu	CD45RA	HI100	Fluidigm	3153001B
154	Sm	CD3	UCHT1	Fluidigm	3154003B
158	Gd	CD134 (OX40)	ACT35	Fluidigm	3158012B
160	Gd	CD39	A1	Fluidigm	3160004B
162	Dy	FOXP3	PCH101	Fluidigm	3162011A
164	Dy	CD95 (Fas)	DX2	Fluidigm	3164008B
165	Ho	CD45RO	UCHL1	Fluidigm	3165011B
169	Tm	CD25	2A3	Fluidigm	3169003B
170	Er	CD152 (CTLA-4)	14D3	Fluidigm	3170005B
174	Yb	HLA-DR	L243	Fluidigm	3174001B
175	Lu	CD279 (PD-1)	EH12.2H7	Fluidigm	3175008B
176	Yb	CD127	A019D5	Fluidigm	3176004B

Table 2.6 Summary of metal-conjugated antibodies used for Figure 5.4A-B.

Channel	Isotope	Marker	Clone	Manufacturer	Catalog #
115	In	CD45	HI30 (custom conjugate)	ThermoFisher Fluidigm Trace Sciences	14-0459-82 201300 n/a
145	Nd	CD4	RPA-T4	Fluidigm	3145001B
154	Sm	CD3	UCHT1	Fluidigm	3154003B
162	Dy	FOXP3	PCH101	Fluidigm	3162011A
169	Tm	CD25	2A3	Fluidigm	3169003B
176	Yb	CD127	eBioRDR5 (custom conjugate)	ThermoFisher Fluidigm	14-1278-82 201176B

Table 2.7 Summary of metal-conjugated antibodies used for Figure 5.4C.

Channel	Isotope	Marker	Clone	Manufacturer	Catalog #
115	In	CD45	HI30 (custom conjugate)	ThermoFisher Fluidigm Trace Sciences	14-0459-82 201300 n/a
145	Nd	CD4	RPA-T4	Fluidigm	3145001B
154	Sm	CD3	UCHT1	Fluidigm	3154003B
162	Dy	FOXP3	236A/E7 (custom conjugate)	ThermoFisher Fluidigm Trace Sciences	14-4777-82 201300 n/a
169	Tm	CD25	2A3	Fluidigm	3169003B
176	Yb	CD127	eBioRDR5	ThermoFisher Fluidigm	14-1278-82 201176B

Table 2.8 Summary of metal-conjugated antibodies used for Figure 5.5.

Channel	Isotope	Marker	Clone	Manufacturer	Catalog #
145	Nd	CD4	RPA-T4	Fluidigm	3145001B
154	Sm	CD3	UCHT1	Fluidigm	3154003B
158	Gd	CD134 (OX40)	ACT35	Fluidigm	3158012B
162	Dy	FOXP3	PCH101	Fluidigm	3162011A
169	Tm	CD25	2A3	Fluidigm	3169003B

2.4.3 HLA allele cross-reactivity assay

0.025× 10^6 CAR Tregs (prepared as above, after 7 days of culture) were incubated with individual FlowPRA Single Antigen beads panels (FL1HD01, FL1HD02, FL1HD03, FL1HD04, FL1HD06 and FL1HD08, One Lambda) and fixable viability dye (FVD; Thermo Fisher Scientific, 65-0865-14) for 30 minutes at room temperature. Samples were washed, fixed with 0.5% formaldehyde and analyzed via flow cytometry. Two hundred negative control beads were acquired per sample.

For analysis, single antigen beads were gated after exclusion of dead cells and doublets, and the number of beads for each HLA antigen was quantified within each distinct PE-intensity peak. To account for small variations in the absolute number of negative control beads collected in each sample, data were normalized by multiplying the number of beads of interest in each HLA-peak by 200, divided by the number of negative beads in the sample. Then, relative binding of A2-CAR Tregs compared to ΔNGFR CAR was obtained by dividing the average number of beads in the ΔNGFR specimen for a specific HLA minus the normalized number of beads in the A2-CAR Treg specimen for that same HLA by the average number of beads in the ΔNGFR specimen, times 100.

2.4.4 Suppression of mixed lymphocyte reactions (MLRs)

Adherent cells from PBMCs from HLA-$A2^+$ healthy donors were differentiated into monocyte-derived dendritic cells as described[257]. For MLRs, HLA-$A2^-$ PBMC responder cells were labeled with cell proliferation dye eF450 (Thermo Fisher Scientific, 65-0842-85), then plated with 5x10^4 HLA-$A2^+$ monocyte-derived dendritic cells and increasing ratios of expanded ΔNGFR- or hA2-CAR-expressing Tregs labelled with cell proliferation dye e670 (Thermo Fisher

Scientific, 65-0840-90). After 6 days, division of HLA-A2$^-$ CD4$^+$ responder T cells was measured by flow cytometry. Percent suppression was calculated based on the proliferation index of a given cell combination and ratio versus the positive control (HLA-A2$^+$ monocyte-derived dendritic cells with HLA-A2- CD4$^+$ responder T cells only) as described [258]. Data were normalized by first calculating percent suppression as follows: $\%\ suppression = 100 - 100 \times \frac{proliferation\ index\ (sample)}{proliferation\ index\ (DC+responder\ control)}$, then normalizing the resulting values from 0-100%, according to the formula for each independent experiment: $normalized\ \%\ suppression = 100 \times \frac{\%\ suppression\ (sample)}{\%\ suppression\ (DC+responder\ control)}$

2.4.5 Histology

Human skin grafts and surrounding mouse skin were harvested 28 days post-cell injection, fixed overnight at 4°C in 10% formalin (1:10 v/v ratio of tissue to formalin), and stored in 70% ethanol before paraffin-embedding. Paraffin sections (5-µm thickness) and H&E staining were prepared by BCCHR Histology Services (Vancouver, British Columbia, Canada). For immunostaining, sections were deparaffinized and rehydrated using a series of xylene washes (×3), graded alcohol solutions (2× 100% ethanol, 1× 95% ethanol and 1× 70% ethanol), and 1×PBS. Heat-induced epitope retrieval (HIER) was performed on slides using a microwave to reach 93-95°C (5 min, high power followed by 20 min, low power) in 10 mM sodium citrate buffer (0.5% Tween-20, pH 6.0). Following HIER, slides were washed using running tap water, deionized water and PBS. Sections were incubated with DAKO® Protein Block, Serum-Free (Dako, Burlington, Canada, X0909) to limit non-specific antibody staining. Sections were then incubated at 4°C overnight with the following primary antibodies: FOXP3 (Invitrogen, clone PCH101, 14-4776-82), CD45 (eBioscience, clone H130, 17-0459), Ki67 (eBioscience, clone

20Raji, 17-5699), Involucrin (Abcam, ab53112). The following day, sections were gently rinsed with PBS several times, then stained for 1 hour at room temperature with the following secondary antibodies: donkey anti-rat 488 (Life Tech, A11006), goat anti-mouse APC (Invitrogen, 1834696), donkey anti-rabbit 488 (Life Tech, A21206). Finally, sections were counterstained with 4',6-diamidino-2-phenylindole (DAPI) to identify cell nuclei and mounted using VECTASHIELD® Mounting Medium with DAPI (Vector Laboratories, Burlingame, California, USA, H-1200). All antibodies were diluted in Antibody Diluent (Dako, Burlington, Canada, S3022). Images were captured using the Olympus BX61 Fluorescence and Bright Field Automated Upright Microscope with QImaging Retiga Exi camera and Olympus DP71 color camera. Quantitative analysis of fluorescence images performed using Fiji with Olympus viewer Plugin[259,260]. Immunofluorescence images were quantified by counting the number of indicated cells in several different fields of view from one section.

H&E-stained slides were evaluated by a blinded clinical pathologist using a scoring system defined by 8 factors each graded from 0 to 3-4; Lerner grade (0, 1 - focal or diffuse vacuolar degeneration, 2 - dyskeratosis, 3 - clefts in basal or superficial layers, 4 - frank loss of epidermis), spongiosis (0, 1 - basal layer only, 2 - up to half way, 3 - full thickness), necrotic keratinocytes (0, 1 - rare (1/hpf), 2 - occasional (2-3/hpf), 3 - many (>4/hpf)), necrotic keratinocyte location (0, 1 - basal only, 2 - up to upper half, 3 - full thickness), satellitetosis (0, 1 - 1 only, 2 - 2-3/hpf, 3 - >4/hpf), exocytosis (0, 1 - focal, 2 - <50% biopsy, 3 - >50% biopsy), adnexal involvement (0, 1 - minor involvement of any adnexa, 2 - marked involvement of <50% adnexa, 3 - marked involvement of > 50% adnexa) and lymphoid cuffs in dermis (0, 1 - slight, 2 - abundant, 3 - band like) [261-263].

2.4.6 qPCR

RNA was harvested from human skin samples according to the manufacturer's instructions (RNeasy Plus Mini Kit; Qiagen) and converted to complementary DNA (cDNA). qPCR was performed using SYBR-green (Biorad) and primers for *IL17, IL6, IL1B, DEFB4, IFNg, TNFa, 18S* ribosomal RNA. Melt curve and SYBR-green emission data were collected. Relative concentrations were calculated using a standard curve and values were normalized to amplification products of *18S* ribosomal RNA. Log_2(RQ) values for each sample were obtained using the double delta Ct (ΔΔCt) method[264]. Each sample's ΔCt value was obtained by calculating averaged Ct (gene of interest) – Ct (housekeeping gene). To obtain ΔΔCt, the ΔCt of the control sample was subtracted from the ΔCt of the treated sample. Fold gene expression was then calculated by $2^{-(\Delta\Delta Ct)}$.

2.4.7 Suppression of pre-stimulated $CD3^+$ T cells

Allogeneic HLA-$A2^-$ $CD3^+$ responder cells were thawed and labeled with cell proliferation dye eF450 (Thermo Fisher Scientific, 65-0842-85), then plated with anti-CD3/CD28 Dynabeads (Thermo Fisher Scientific, 11141D) at ratio of 1:2 (bead to cell) in X-Vivo 15 medium (Lonza, 04-744Q) supplemented with 5% human serum (Wisent Bio Products, 022210), 1% glutamax (Gibco, 35050-061), 1% penicillin/streptomycin (Gibco, 15140-122), herein referred to as "XH medium", with 100U/mL IL-2 (Proleukin). Simultaneously, 2 x 10^5 CAR Tregs were labeled with cell proliferation dye eF670 (Thermo Fisher Scientific, 65-0840-85), then plated with 2 x 10^5 HLA-A*02:01 FlowPRA Single Antigen beads (One Lambda, Thermo Fisher Scientific) in XH medium with 100U/mL IL-2. A polyclonal Treg control (NGFR) and a no Treg control was included in each experimental replicate. After 24-hour

incubation, half of the volume of Tregs + beads was serially diluted in fresh XH medium with 100U/mL IL-2. Dynabeads were removed from CD3/28-stimulated CD3+ responder cells by resuspension and 3-5-minute incubation on a magnet (STEMCELL Technologies, 18103). Bead-free responder cells were then resuspended in fresh XH media + 100U/mL IL-2 and 0.5 x 10^5 cells were plated on top of each well. Resulting co-culture was incubated for 3 additional days, then analyzed by flow cytometry. Percent suppression was calculated based on the division index of a given cell combination and ratio versus the positive control (HLA-A2- $CD3^+$ responder T cells only) as described [258]. Percent suppression was calculated as follows: $\% \, suppression = 100 - 100 \times \frac{division\ index\ (sample)}{division\ index\ (responder\ only\ control)}$.

2.4.8 Suppression of co-stimulatory molecules on matured antigen-presenting cells

$CD14^+$ monocytes were isolated (STEMCELL Technologies, 18058) from frozen HLA-$A2^+$ human PBMC, then cultured in X-Vivo15 medium supplemented with 5% human serum (Wisent Bio Products, 022210), 1% glutamax (Gibco, 35050-061), 1% penicillin/streptomycin (Gibco, 15140-122), 1mM sodium pyruvate (STEMCELL Technologies, 07000), herein referred to as "DC medium", and 100ng/mL IL-4 (STEMCELL Technologies, 78045.1), 50ng/mL GM-CSF (STEMCELL Technologies, 78015) for 5 days (media and cytokines refreshed on day 3). Cells were then matured using DC medium containing a cytokine cocktail of 100ng/mL IL-4, 50ng/mL GM-CSF, 10ng/mL TNFa (Thermo Fisher Scientific, 14-8329-63), 1ug/mL PGE-2 (Sigma, P6532), 10ng/mL IL-1b (STEMCELL Technologies, 780341) and 100ng/mL IL-6 (Thermo Fisher Scientific, 14-8069-80) for 2 additional days. In the last 24 hours of culture, 1000U/mL IFN-gamma (Thermo Fisher Scientific, 34-8319-82) was added. Matured "dendritic

cells" were resuspended in DC medium with a final concentration of 50U/mL IL-2 and co-cultured with CAR Tregs at a ratio of 1 dendritic cell to 5 CAR Tregs for 4 days then analyzed by flow cytometry.

2.4.9 Generation and analysis of stimulated CAR Tregs for RNA sequencing

NGFR-purified CAR Tregs and CAR Tconv cells (2.5×10^5) were stimulated using 1.25×10^5 HLA-A*02:01 FlowPRA Single Antigen beads or 2.5×10^5 anti-CD3/CD28 Dynabeads for 24 hours in Immunocult-XF T cell media (STEMCELL Technologies, 10981). Approximately 0.5×10^5 cells were taken for flow cytometry analysis and the remaining cells were processed for total RNA (New England Biolabs, T2010S) using the optional protocol to omit small RNAs. RNA was quantified using fluorometer (Thermo Fisher Scientific, Q32855) and quality (RNA Integrity Number) determined using Bioanalyzer analysis (Agilent, 5067-1513). All RNA used had an RNA integrity number > 8.0.

mRNA enrichment and library preparations were performed with a NEBNext Poly(A) mRNA Magnetic Isolation Module and a NEBNext Ultra II Directional RNA Library Prep Kit for Illumina (both New England Biolabs). Paired-end libraries were sequenced (43 x 43 bp reads) on a NextSeq 500 (Illumina). The accession number for the RNA-sequencing data in GEO is: GSE136432

Reads that mapped to the transgene were removed using the data processing method outlined in (Figure 2.1). The read sequences were aligned to both the GRCh37/hg19 reference genome using STAR (v2.5.0a) and the transgene sequences using Burrows-Wheeler Aligner (v0.7.10). Cross-referencing the alignment files (.bam) from both reference genome and transgene sequences allowed for reads that mapped to the transgene sequences to be filtered out

from further analysis by using unique identifiers for each read. In R, raw count matrices were generated using HTSeq (v0.11.2), then scale factors were calculated to take into account differences in library sizes using edgeR (v3.24.3) and normalization was performed using limma (v3.38.3) as in[265]. Log(CPM) and visualization was performed using: ggplot2 (3.1.1), RColorBrewer (v1.1.2), tibble (2.1.1), pheatmap (v1.0.12), stats (v3.5.1), and gplots (v3.0.1.1). The code used for data analysis is available on GitHub: https://github.com/najdawson/sigDom-RNAseq-git/

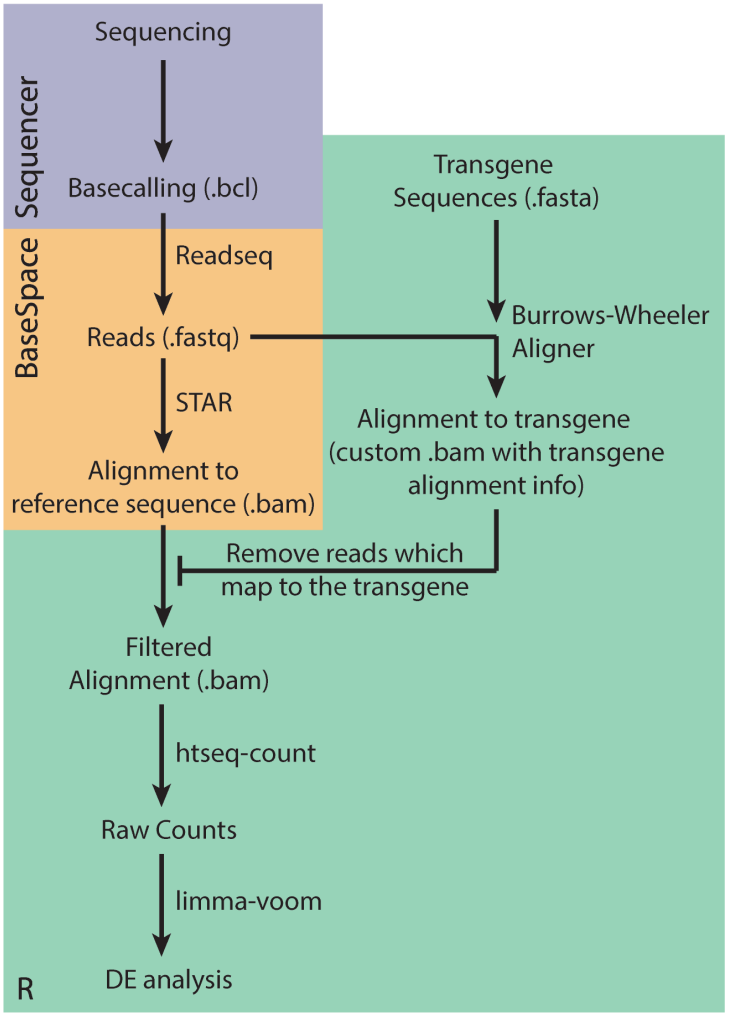

Figure 2.1 Schematic of RNA-sequencing pre-processing strategy to remove transgene reads.

2.5 In vivo methods

2.5.1 Xenogeneic graft-versus-host disease

8- to 12-week-old female NSG mice (The Jackson Laboratory, Maine USA; bred in house) received whole-body irradiation (150 cGy, RS-2000 Pro Biological System) 1 day before injection of either: (1) 8 x 10^6 HLA-$A2^+$ PBMCs with or without 4 x 10^6 hA2-CAR Tregs, for humanized CAR experiments or; (2) 10 x 10^6 HLA-$A2^+$ PBMCs with or without 5 x 10^6 (high ratio) or 2.5 x 10^6 (low ratio) CAR Tregs, for signaling domain CAR experiments, intravenously into the tail vein. Saline-injected and PBMC-only mice served as controls. In signaling domain CAR experiments, CD28wt CAR conditions were included in every experimental cohort. GVHD was scored based on weight, fur texture, posture, activity level, and skin integrity, with 0 to 2 points per category as described[266,267]. Peripheral blood from the saphenous vein was centrifuged; then erythrocytes were lysed and leukocytes were measured by flow cytometry.

2.5.2 Luciferase

To evaluate Treg homing towards HLA-A2-expressing mouse skin grafts in vivo, sorted Tregs ($CD4^+CD25^{hi}CD127^{lo}$) were stimulated with L-cells as described above. The next day, cells were transduced with HER2-CAR, mA2-CAR or H1k2 hA2-CAR lentivirus at a MOI of 10 and 8h later with luciferase-GFP-lentivirus at an MOI of 5. The lentiviral plasmid encoding a beetle luciferase-GFP-fusion protein (pELNS.CBG-T2A-GFP (CBR)) was kindly provided by Dr. David Barrett (The Children's Hospital of Philadelphia)[268]. After 7 days of culture, double-transduced $GFP^+\Delta NGFR^+$ Tregs expressing the CAR and luciferase were sorted before restimulation with L-cells as described above. On day 12 of the culture, 1-3 x10^6 luciferase-CAR Tregs and 6x10^6 human allogeneic HLA-$A2^-$ PBMCs were injected intravenously into skin-

transplanted NSG mice. For bioluminescent imaging, D-luciferin potassium salt (150mg/kg, Gold Bio) was injected intraperitoneally immediately before anesthesia with isoflurane and images were acquired within 15-20min on Ami-X (Spectral Instruments Imaging). Data were analyzed with AmiView software (Spectral Instruments Imaging, version 1.7.06) and the luminescent signal was quantified as the ratio of photons/sec/cm^2/steradian in the HLA-$A2^+$ over the HLA-$A2^-$ skin graft. At experimental endpoints, skin-draining axillar lymph nodes and spleen were harvested, placed on a 70μm cell strainer (BD Falcon), then fragmented and filtered through using the plunger of a 1cc syringe. Cells were then stained for flow cytometry.

2.5.3 Skin transplantation

To evaluate A2-CAR Treg homing and capacity to inhibit skin rejection, 8- to 12-week-old female NSG mice (The Jackson Laboratory, bred in house) were transplanted with skin from transgenic HLA-$A2^+$ NSG mice (The Jackson Laboratory, bred in house) and NSG skin (HLA-A2 negative). For mouse skin transplants, skin was cut into circular pieces utilizing 8mm biopsy punch and skin was placed onto fresh plates with PBS and kept at 4-8°C until transplanted (~1–4 hr). HLA-A2 expression of human skin was assessed by flow cytometry and qPCR. Split-thickness skin explants were generated by trimming fat and rinsing with sterile PBS then cut into 1 cm^2 pieces, placed onto fresh plates with PBS and kept at low temperature (4-8°C) until transplanted (~1–4 hr). For both mouse and human skin transplants, previously shaved mice were anesthetized, dorsal skin was cut near the shoulder and mouse skin of similar size was removed, then grafts were placed on the exposed area and stabilized with steri-strips (3M, Nexcare). Grafts were covered with a Vaseline gauze and wrapped with a 2 cm wide CoFlex bandage (3M, Nexcare) to secure graft for up to 14 days prior to cell injection.

2.6 Statistical tests

All statistics were done using Prism versions 7.0b or 8.1.1. IBM*SPSS Statistics Version 24.0.0.0 was used for in vivo humanized CAR luciferase experiment (Figure 3.14). For human skin transplant study, normality was not assumed. For all other studies, normality was assumed. Corrections for multiple comparisons were made as described in each figure.

2.6.1 Analysis of mass cytometry data

Mass cytometry data were first normalized using bead standards as described in[269] using Normalizer (v0.3; Nolan lab, Stanford University), then analyzed using FlowJo software (v10.3; Tree Star Inc.) and Prism statistical software (v7.0c; GraphPad Software). Cells were identified as bead$^-$cisplatin$^-$DNA1$^+$DNA2$^+$ singlets. For comparison of Tregs from different sources, data from n=3-4 donors per cell source were pooled using the Cytobank FCS file concatenation tool (https://support.cytobank.org/hc/en-us/articles/206336147-FCS-file-concatenation-tool) and R statistical software (v3.3.2). ACCENSE analysis was performed on the pooled samples from each source using ACCENSE v0.5.0-beta[270]. Heat map analysis was performed using FlowJo software (v10.3; Treestar Inc.) and R statistical software (v3.3.2).

2.7 Study approval

For human PBMCs used for in vitro and skin homing in vivo experiments, healthy volunteers gave written informed consent according to protocols approved by the University of British Columbia Clinical Research Ethics Board (UBC-CREB) and Canadian Blood Services. For in vivo xenoGvHD and human skin transplant studies, commercial leukapheresis blood products were purchased from StemCell Technologies (Vancouver, Canada) excluding all

variants of following HLA alleles: A*02, A*68, A*69. Samples of human skin discarded from plastic surgery were obtained from the Harvard Skin Resource Centre, Skin Works or the Cambie Surgery Clinic according to UBC-CREB-approved protocols. Animal protocols were approved by the UBC Animal Care Committee.

Chapter 3: Systematic testing and specificity mapping of alloantigen-specific chimeric antigen receptors in T regulatory cells

3.1 Introduction

Using our previously described HLA-A*02:01-specific CAR, which was derived from the scFv of the mouse BB7.2 mAb[221], we report an effective way to generate multiple humanized CARs. In addition to systematic testing for in vitro and in vivo function in Tregs, we developed a new methodology to comprehensively determine HLA-specificity. This approach can be used as a platform to generate a series of HLA-specific CARs to advance the use of CAR Tregs as a widely-applicable therapy to prevent allograft rejection.

In addition to immunogenicity, a specific consideration for alloantigen-specific mAbs is that because many HLA alleles differ by only a few amino acids[271], there is often cross-reactivity with closely-related HLA proteins, with anti-HLA mAbs recognizing multiple alleles within an evolutionarily-related family. Cross-reactivity of anti-HLA mAbs/CARs could be problematic for a CAR Treg approach as exquisite specificity for the donor organ is needed to prevent the risk of systemic CAR Treg activation by cross-reactive HLA alleles expressed by the recipient.

3.2 Results

3.2.1 Design, expression and Treg activation potential of a panel of humanized A2-CARs

The amino acid sequence of the variable regions of the heavy and light chains from the mouse BB7.2 mAb were aligned to the human immunoglobulin sequences obtained from the international ImMunoGeneTics information system® database using IgBLAST (National Center

for Biotechnology Information). The V-gene delimitation system was set to the Kabat sequences to obtain the Kabat defined CDRs[272]. In addition, the Chothia definition[273] was determined.

A number of different human germline genes were identified as possible framework sequences, and we selected those that were most homologous to the mouse sequence and which encoded CDRs with similar lengths as those in BB7.2 for CDR grafting. The human CDRs from these candidate human germline genes were replaced with the mouse counterpart CDRs from BB7.2 using the Chothia and Kabat numbering systems[272,273]. Ultimately, 6 humanized heavy chains based on 4 human germline V-genes, and 5 humanized light chains based on 5 human germline V-genes were generated, resulting in 18 humanized CARs generated by combining different humanized heavy and light chains (Figure 3.1).

Humanization can affect Ag specificity[238,243] so we first transiently transfected the humanized A2-CARs (hA2-CAR) into 293T cells and used HLA-A*02:01 tetramers to quantify Ag binding by flow cytometry. Of the 18 hA2-CAR constructs tested, only 10 were expressed and bound to the A*02:01 tetramer (Figure 3.2, Table 3.2). To test expression and function of these 10 hA2-CARs in Tregs, $CD4^{+}CD25^{hi}CD127^{lo}$ cells were transduced with the

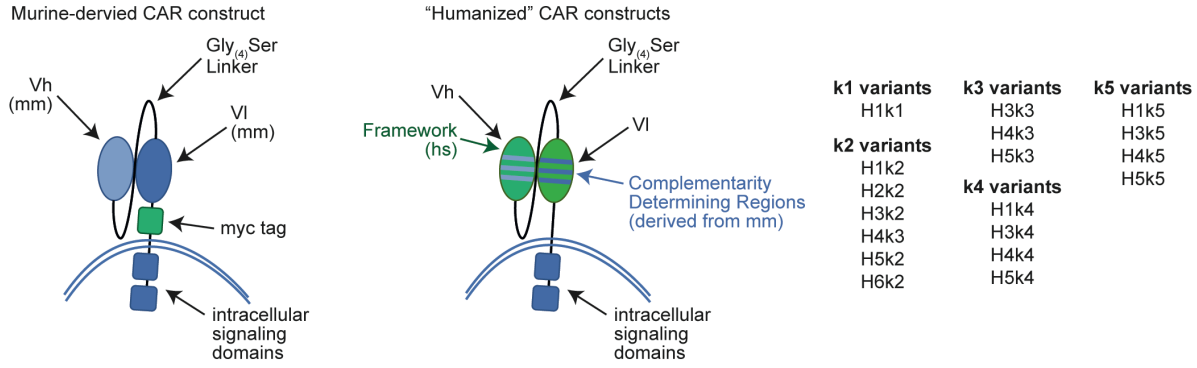

Figure 3.1 Schematic of humanized CAR construction.
Schematic representation of CAR humanization. CDRs from the BB7.2-derived scFv were determined using Kabat or Chothia definitions for each heavy and light chain and grafted onto suitable human framework sequences.

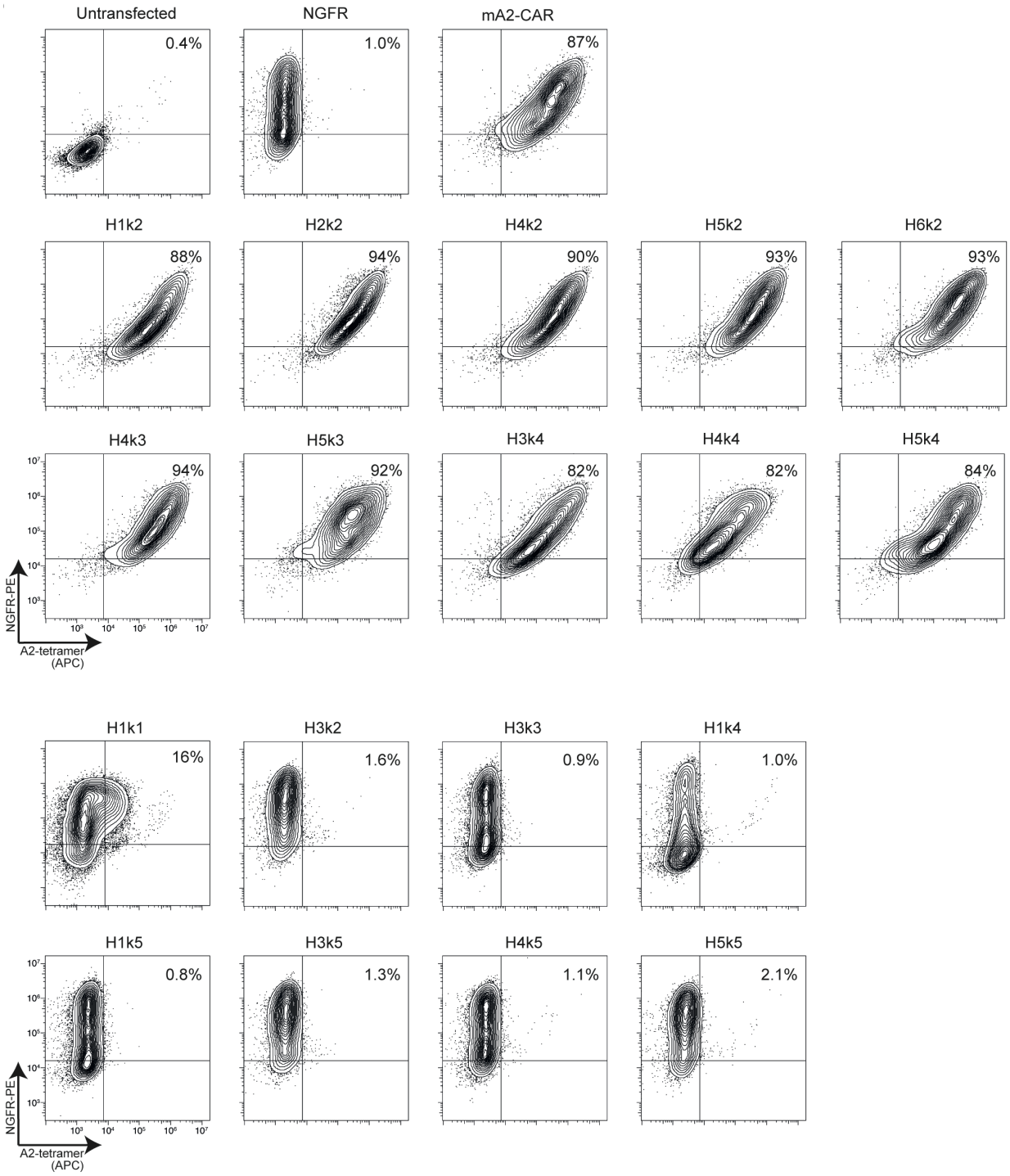

Figure 3.2 Cell surface expression and tetramer binding of hA2 CARs in 293T cells.
293T cells were transiently transfected with the indicated constructs. 48 hours later, expression and tetramer binding were analysed by flow cytometry. Gated on live cells (FvD-). Representative flow plots are shown for constructs which do (top) or do not (bottom) retain their ability to bind to HLA-A*02:01. Data are representative of two independent experiments.

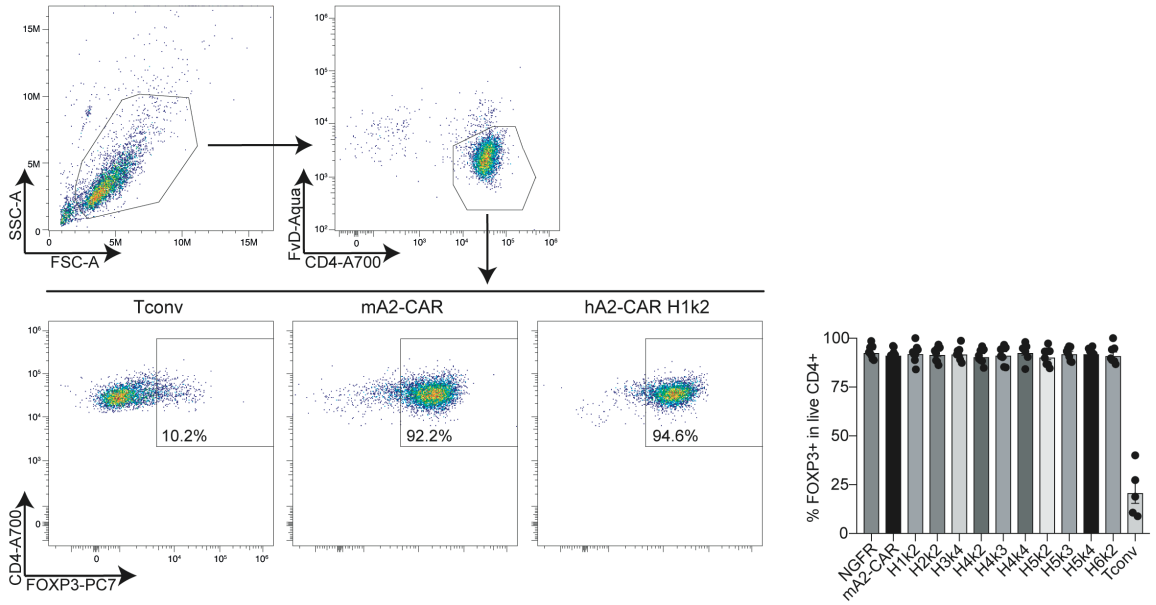

Figure 3.3 FOXP3 expression on m/hA2-CAR Tregs after 7 days in vitro expansion.
CAR Tregs and untransduced Tconv cells were expanded on irradiated feeder cells with OKT3 and 1000U/mL or 100U/mL IL-2 for Tregs and Tconv, respectively, for 7 days then purified using anti-NGFR magnetic beads on MACS column. The purified cells were stained for FOXP3 prior to use in in vitro and in vivo experiments. Representative (left) and summary (right) data are shown. Mean ± SEM. n=5-9 pooled from at least 5 independent experiments.

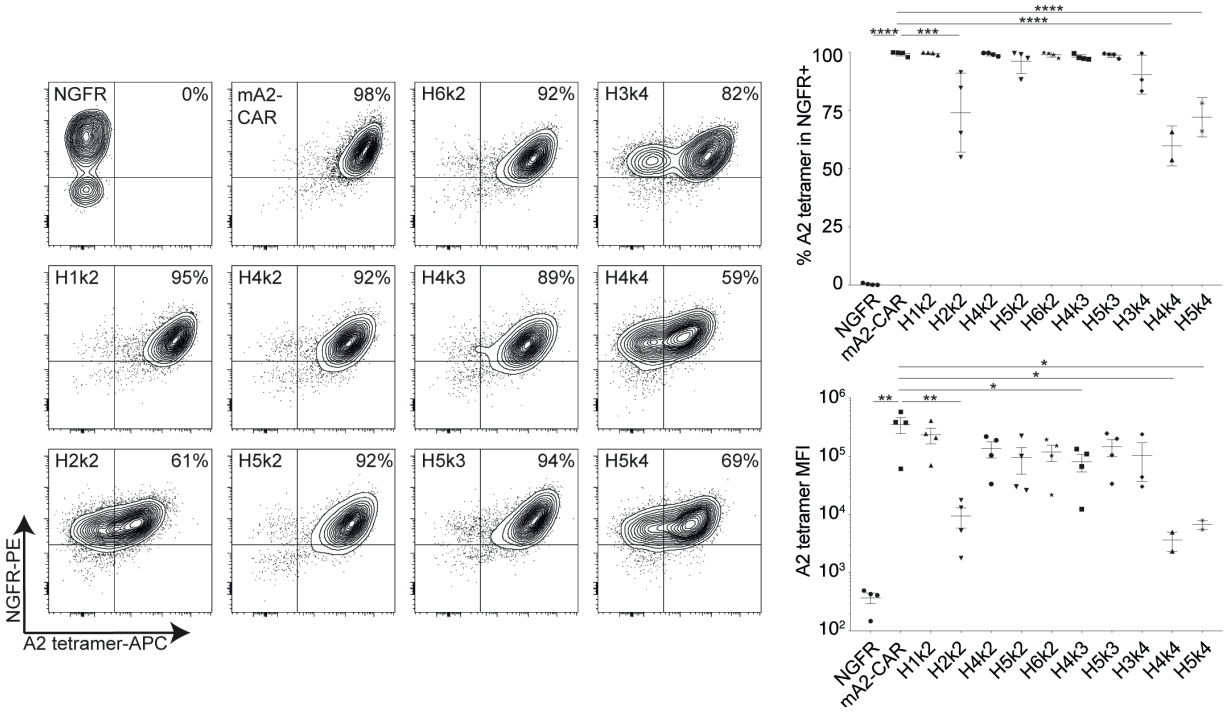

Figure 3.4 Expression of a panel of hA2-CARs on human Tregs.
Tregs were transduced with lentivirus encoding the indicated constructs. After 7 days of expansion the ability of NGFR+ cells to bind to HLA-A*02:01 tetramers was measured by flow cytometry Left: representative flow cytometry plots. Right: summarized data of percent or mean fluorescence intensity of A*02:01-tetramer binding. Data are n=2-4 for each construct pooled from at least two independent experiments. Mean ± SEM. * $p < 0.05$, ** $p < 0.01$, *** $p < 0.001$, **** $p < 0.0001$.

hA2-CARs, the original mouse (m)A2-CAR[221], or a vector only control encoding the ΔNGFR transduction marker but no CAR. Following transduction and expansion, CAR Tregs were

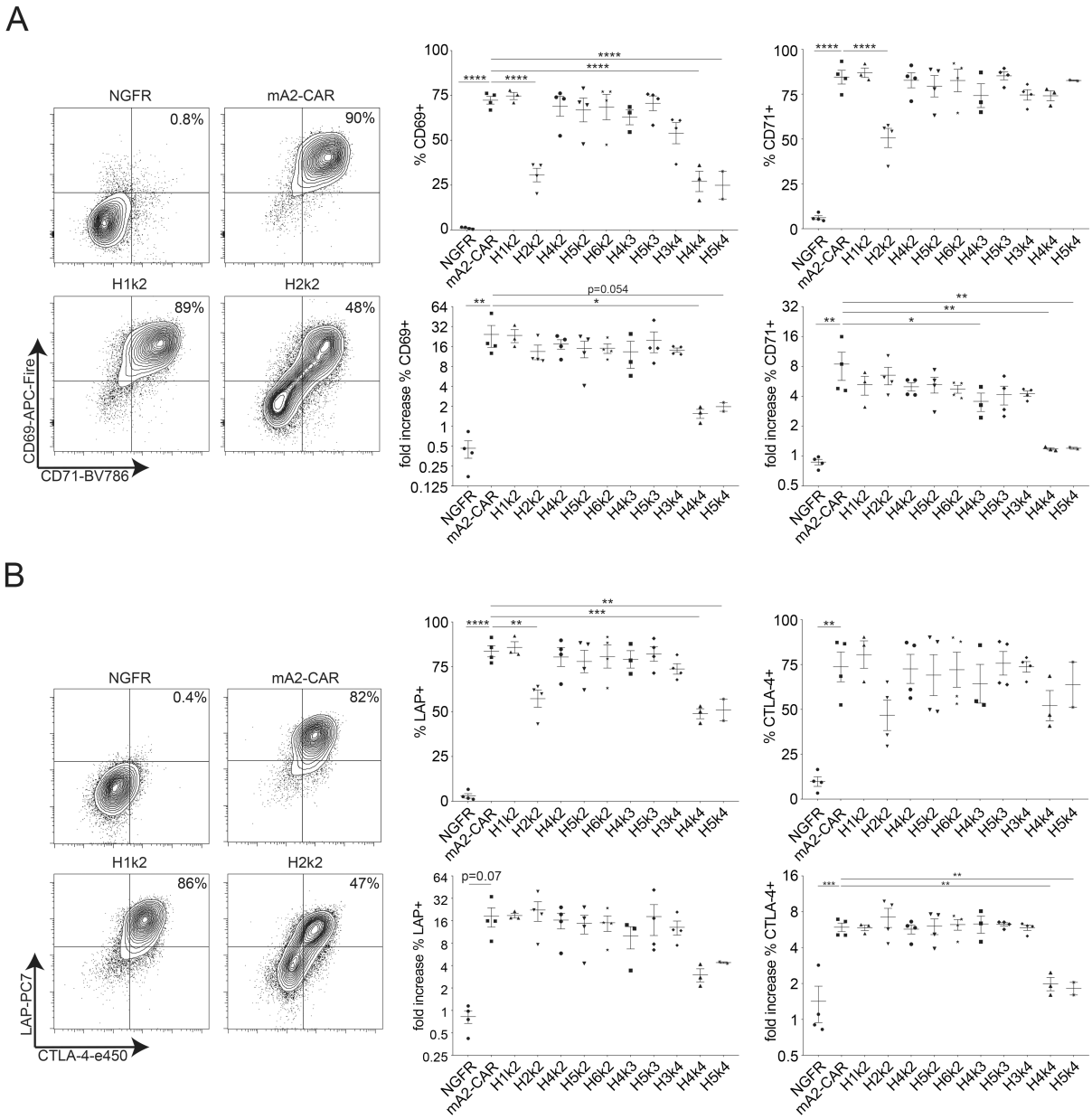

Figure 3.5 In vitro function of a panel of hA2-CARs on human Tregs (CAR stimulation).
(A&B) ΔNGFR control/CAR Tregs were co-cultured with a 2:1 (Tregs: K562) ratio of HLA-A2-expressing K562 cells. After 16 hours, expression of CD69, CD71, CTLA-4 and LAP were measured by flow cytometry. Live CD4+ cells are shown. **(A)** Percent positive and fold increase over baseline (no K562; Supplemental Data 3B) expression of CD69 and CD71. **(B)** Percent positive and fold increase over baseline (no K562; Supplemental Data 3B) expression of CTLA-4 and LAP. Data are n=2-4 for each construct pooled from at least two independent experiments. One-way ANOVA and Holm-Sidak's post-test comparing all constructs to mA2-CAR Tregs. Mean ± SEM. * $p < 0.05$, ** $p < 0.01$, *** $p < 0.001$, **** $p < 0.0001$.

confirmed to retain high expression of FOXP3 (Figure 3.3). CAR cell surface expression and specificity was tested by staining with an A*02:01 tetramer revealing strong, uniform binding to 7 and low, bimodal binding to 3 (H2k2, H4k4 and H5k4) hA2-CARs (Figure 3.4). In addition, although the H4k3 hA2-CAR was expressed on a similar proportion of Tregs, it was expressed at a lower MFI than the mA2-CAR.

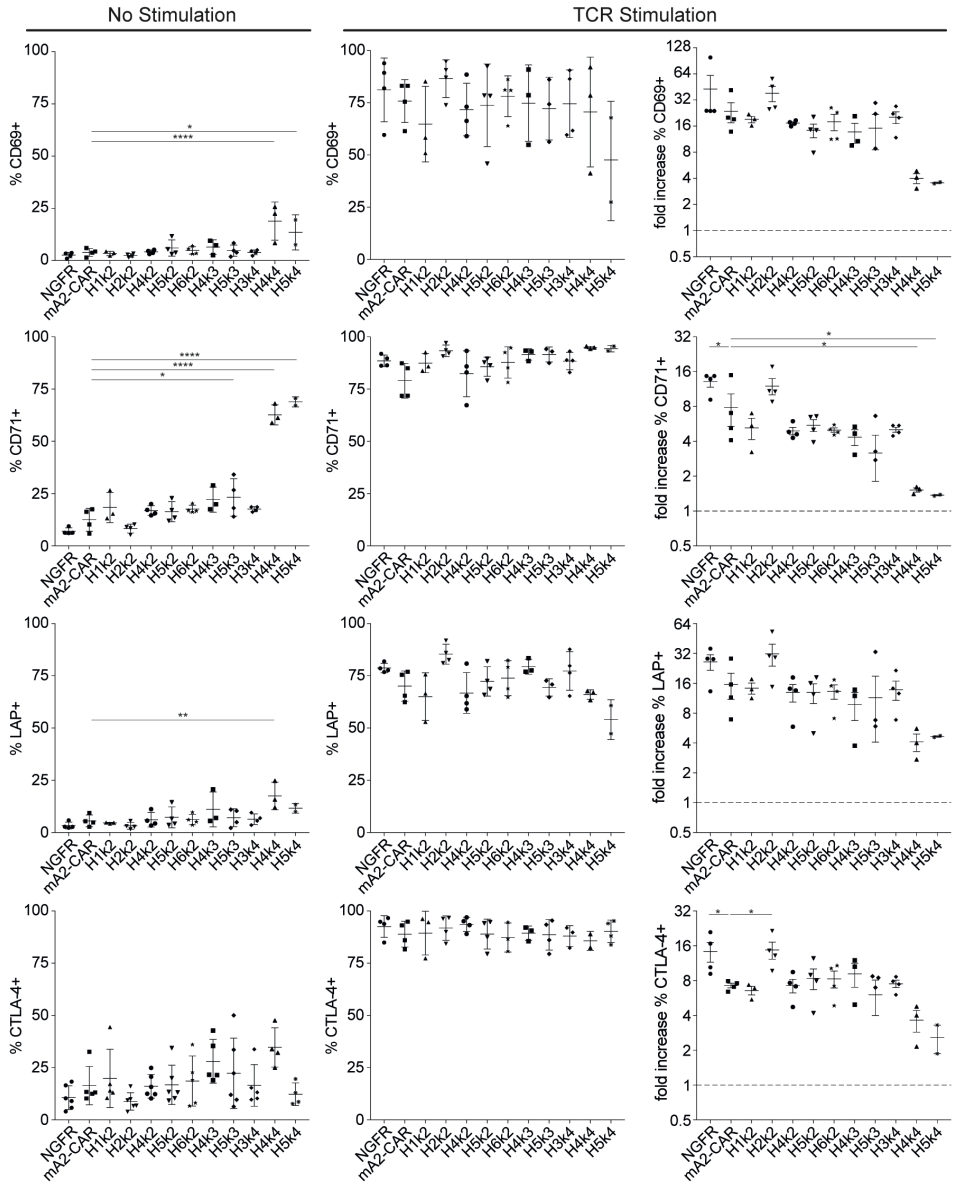

Figure 3.6 In vitro function of a panel of hA2-CARs on human Tregs (Resting & TCR stimulation). In tandem with the experiment shown in Figure 3.5, ΔNGFR control/CAR Tregs were co-cultured for 16 hours with either no stimulation or a 2:1 (Tregs: K562) ratio of CD64-expressing K562 cells loaded with anti-CD3 and anti-CD28 monoclonal antibodies (TCR stimulation). Expression of CD69, CD71, CTLA-4 and LAP were measured by flow cytometry. Live CD4+ cells are shown. Fold increase of each activation marker over baseline (no stimulation, left panels) was calculated (right panels). Data are n=2-4 for each construct from at least two independent experiments. Mean ± SEM. One-way ANOVA and Holm-Sidak's multiple comparisons test comparing all constructs to mA2-CAR Tregs. * $p < 0.05$, ** $p < 0.01$, **** $p < 0.0001$.

We next tested the ability of the 10 hA2-CAR variants to activate Tregs. Tregs expressing one of the 10 hA2-CAR variants, mA2-CAR, or ΔNGFR alone were stimulated via the CAR (Figure 3.5), left unstimulated, or stimulated via TCR (Figure 3.6). Stimulation of m/hA2-CAR-Tregs with A2-expressing artificial antigen presenting cells (APCs) resulted in high expression of both CD69 and CD71 for most constructs, with the exception of the 3 poorly-expressed CARs (Figure 3.5A). Specifically, H2k2 showed low basal activation and a moderate increase in CD69 and CD71 expression after CAR stimulation, whereas H4k4 and H5k4 showed high basal activation and no increase in CD69 and CD71 expression when stimulated through the CAR (Figure 3.5A, Figure 3.6).

Upregulation of proteins associated with Treg function (Cytotoxic T-lymphocyte-associated protein 4 (CTLA-4) and the latency-associated peptide (LAP)) displayed a similar pattern, with low CAR-stimulated expression of CTLA-4 and LAP for H2k2, H4k4 and H5k4 (Figure 3.5B). Similar to CD69 and CD71, H4k4 and H5k4 had low CAR-stimulated upregulation of CTLA-4 and LAP compared to unstimulated controls. These data suggest that the impaired activation capacity of H4k4 and H5k4, but not H2k2, may be driven by tonic CAR signaling, an interpretation supported by evidence that TCR-mediated activation is also hampered in cells expressing these constructs (Figure 3.6).

3.2.2 Alloantigen specificity mapping of hA2-CAR constructs

T cell alloAg-specificity is traditionally tested by in vitro stimulation with peripheral blood mononuclear cells (PBMC) of known haplotypes. This approach, however, is cumbersome and imprecise as it requires an extensive bank of viable, haplotyped PBMCs and specificity towards individual HLA alleles cannot be determined in isolation. We sought to develop a more

feasible, comprehensive and accurate way to assess the cross-reactivity of alloAg-specific CARs. Specifically, we hypothesized that the One Lambda Flow Panel Reactive Antibody (FlowPRA) single antigen beads previously developed to measure serum alloantibody titers[274], which consist of fluorescently-labeled beads coupled to single HLA Ags, could be adapted to measure alloAg-

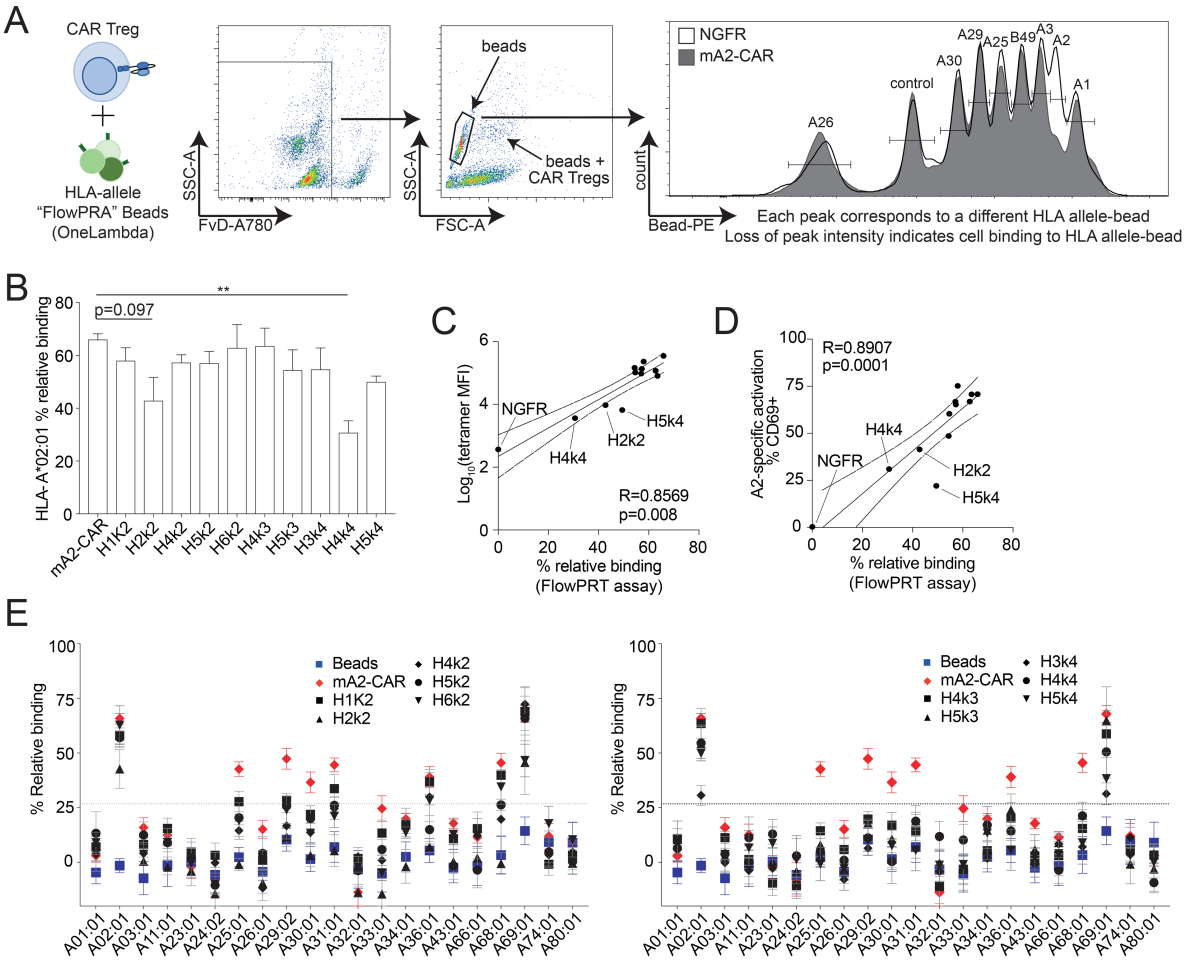

Figure 3.7 Cross-reactivity of humanized anti-HLA-A2 CARs with common HLA-A allelic variants. **(A)** Schematic diagram of experimental set up and gating strategy for the FlowPRT cell assay. ΔNGFR or CAR Tregs were incubated with a cocktail of single HLA FlowPRA beads for 30 min, and bead-CAR Treg interactions were quantified as the loss of beads in a bead singlet gate based on FSC/SSC profile. **(B)** Binding to HLA-A*02:01-coated beads for each m/hA2-CAR Treg relative to binding of a ΔNGFR Treg control. Statistical significance determined by one-way ANOVA (p=0.0140) and Holm-Sidak post-test comparing to mA2-CAR, mean ± SEM, ** $p < 0.01$. **(C&D)** Correlation between the mean of HLA-A*02:01 binding measured by the FlowPRT cell assay and either **(C)** HLA-A*02:01-tetramer MFI evaluated by flow cytometry or **(D)** the increase in proportion of CD69+ cells 16h after co-culture with HLA-A*02:01 versus negative control HLA-A*24:01 K562 cells. **(E)** Percent binding of each m/hA2-CAR Treg to the indicated HLA-A alleles after normalization to an ΔNGFR Treg control from the same donor. Dotted line represents two standard deviations from the mean of the bead-only control. A summary of statistical results in E can be found in Supplemental Table 1. n=3-6 from at least 3 independent experiments.

directed CAR Treg specificity. Tregs expressing the m/hA2-CARs, or ΔNGFR were incubated with a mixture of FlowPRA single antigen beads, then analyzed by flow cytometry using FSC/SSC to identify beads, cells, and bead/cell conjugates (hereafter called the FlowPRT cell assay). Since the number of beads bound per cell and cells bound per bead could not be controlled, the amount of CAR Treg binding to beads was assessed by comparing the number of unbound beads in samples incubated with CAR Tregs to the number in samples incubated with the ΔNGFR Treg control (see Methods for formula calculation, Figure 3.7A) with Tregs in excess to beads.

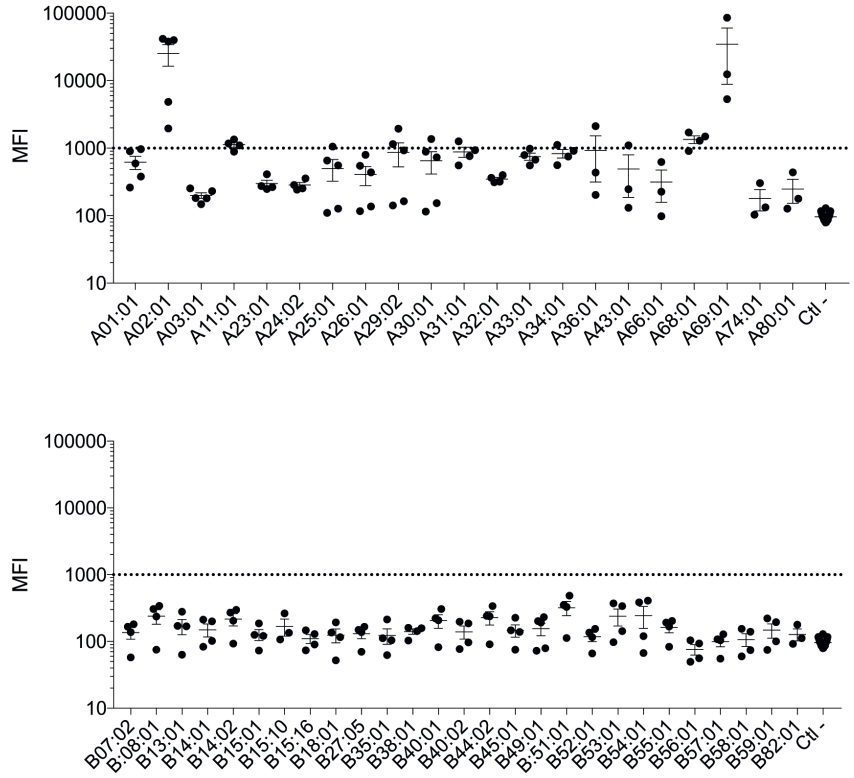

Figure 3.8 Cross-reactivity of BB7.2 mAb with HLA-A and HLA-B allelic variants.
FlowPRA beads were incubated with APC-conjugated BB7.2 monoclonal antibody (Thermo Fisher Scientific, 17-9876-41) as recommended by manufacturer, and then analyzed by flow cytometry. Mean fluorescence intensity (MFI) of the reporter anti-FITC human IgG antibody is shown. Higher MFI indicates binding to the indicated HLA alleles. n=3-5 from 2-3 independent experiments.

To validate the methodology, the relative binding of each m/hA2-CAR construct to HLA-A*02:01 as determined by the FlowPRT cell assay (Figure 3.7B) was compared to the MFI of tetramer binding (Figure 3.7C). This analysis revealed a strong, direct correlation between the two methods of detecting A*02:01 binding. The data also revealed a lower ability of H2k2 and H4k4 to bind to A*02:01 and a trend to low binding with H5k4, consistent with their low expression and activation capacity. We further asked if the amount of A*02:01 binding, as determined by the FlowPRT cell assay, correlated with the biological effect of exposure to A*02:01. Indeed, we found there was a direct correlation between the amount of A*02:01 binding quantified by the FlowPRT cell assay and stimulation of Treg activation, as judged by CD69 upregulation following exposure to A*02:01-expressing APCs (Figure 3.7D). These data demonstrate the utility of the FlowPRT cell method to measure the ability of alloAg-specific CARs to bind to different HLA alleles.

We next examined the degree of m/hA2-CAR Treg cross-reactivity to alleles of HLA-A and HLA-B. BB7.2 has been reported to bind to HLA-A*23:01, A*24:02, and A*69:01[275]. When we tested BB7.2 binding in the single antigen FlowPRA assay, we confirmed high binding to A*69:01 but could not confirm cross-reactivity to A*23:01 or A*24:02 (Figure 3.8). We next tested the relative ability of the m/hA2-CAR Tregs to bind to various HLA-A alleles. We found the mA2-CAR-Tregs bound significantly to A*03:01, A*25:01, A*29:02, A*30:01. A*31:01, A*33:01, A*36:01, A*68:01 and A*69:01 (Figure 3.7E, Table 3.1). In contrast, all variants of hA2-CAR Tregs displayed reduced cross reactivity compared to mA2-CAR Tregs. As expected, all CAR constructs bound to A*69:01, a variant of A*02:01 differing by only 6 amino acids, which is also bound by BB7.2. None of the CAR-constructs displayed any significant binding to HLA-B (Figure 3.9).

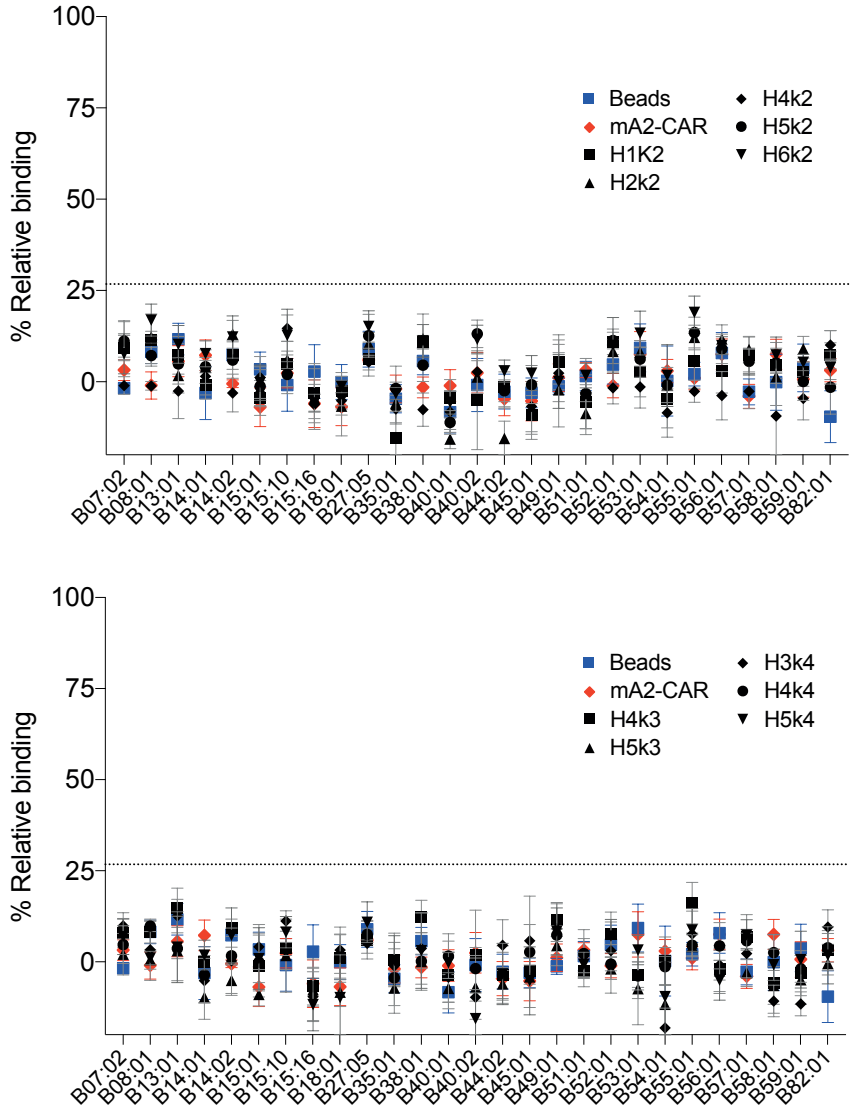

Figure 3.9 Cross-reactivity of m/hA2 CARs with common HLA-B allelic variants.
NGFR control, m/hA2-CAR Tregs were incubated with HLA-B single antigen FlowPRA beads, analyzed and normalized as in Figure 3.7. Results shown are n=2-6 from at least 2 independent experiments.

Table 3.1 Summary of p values from Figures 3.7 & 3.9

HLA-A*02:01		HLA-A*69:01		HLA-A*03:01		HLA-A*33:01	
mA2-CAR	0.0001	mA2-CAR	0.0001	mA2-CAR	0.0315	mA2-CAR	0.0019
H4k4	0.0006	H4k2	0.0001	**HLA-A*25:01**		**HLA-A*36:01**	
H4k2	0.0001	H5k2	0.0001	mA2-CAR	0.0001	mA2-CAR	0.0035
H5k2	0.0001	H1k2	0.0001	H1k2	0.0130	H1k2	0.0082
H1k2	0.0001	H3k4	0.0013	**HLA-A*29:02**		**HLA-A*68:01**	
H3k4	0.0001	H2k2	0.0084	mA2-CAR	0.0001	mA2-CAR	0.0001
H2k2	0.0001	H5k3	0.0001	**HLA-A*30:01**		H1k2	0.0001
H5k3	0.0001	H4k3	0.0001	mA2-CAR	0.0001	H5k2	0.0337
H4k3	0.0001	H6k2	0.0060	**HLA-A*31:01**		H6k2	0.0009
H6k2	0.0001			mA2-CAR	0.0001		
H5k4	0.0001			H1k2	0.0077		

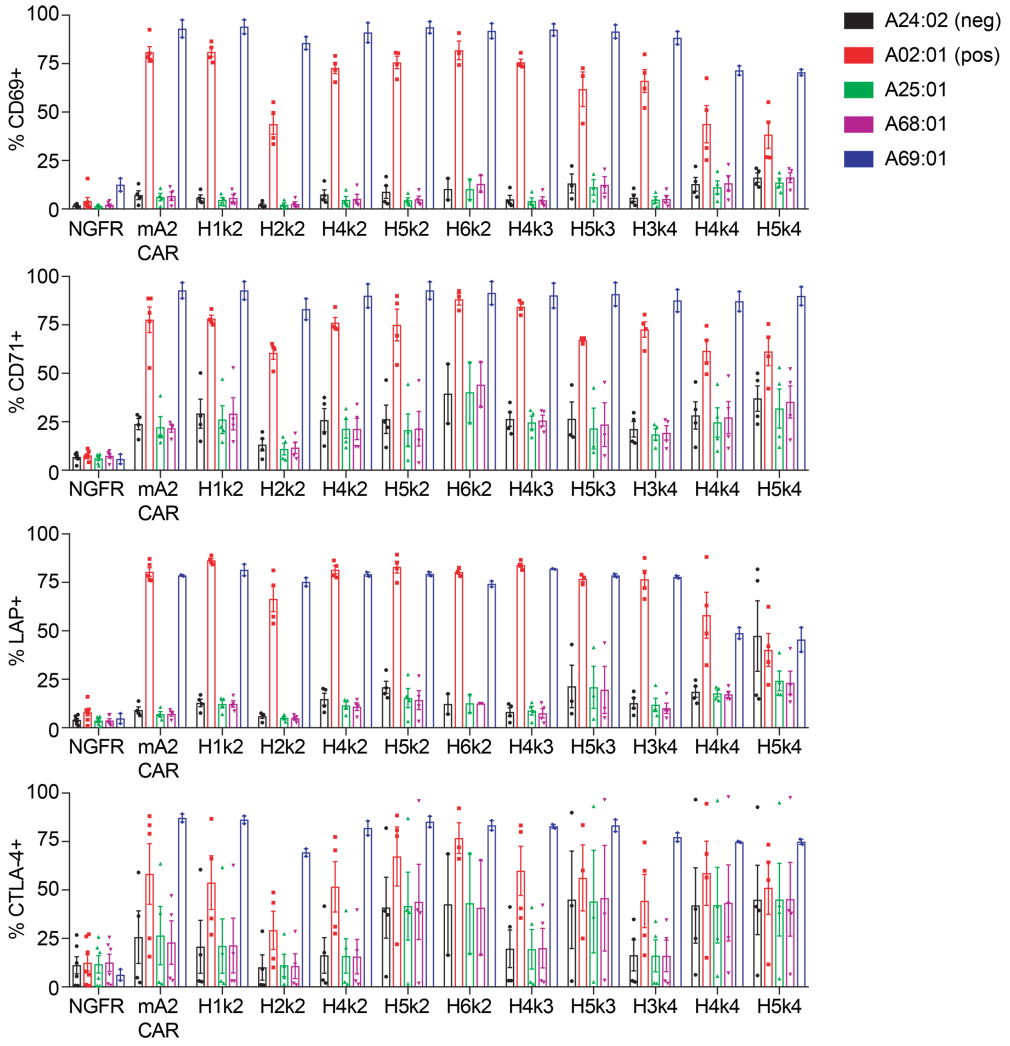

Figure 3.10 Functional cross-reactivity of a panel of hA2-CAR constructs in human Tregs.
ΔNGFR or m/hA2-CAR Tregs were co-cultured with K562 cells transduced to express the indicated HLA-A alleles. After 16 hours, expression of CD69, CD71, LAP and CTLA-4 were measured on live $CD4^+$ T cells. n=2-6 pooled from at least 2 independent experiments, mean ± SEM.

The relationship between the degree of CAR-Treg Ag binding and biological activity is unknown. To define the biological significance of HLA cross reactivity we generated APCs expressing HLA-A*24:02, A*25:01, A*68:01 or A*69:01. We found that only co-culture with HLA-A*02:01- or HLA-A*69:01- expressing cells resulted in significant activation of m/hCAR-Tregs, as judged by upregulated expression of CD69, CD71, LAP, CTLA-4 (Figure 3.10) or CD40L (data not shown). The lack of stimulation by HLA-A*24:02, A*25:01, or A*68:01-expressing K562 cells was not due to poor HLA-expression (Figure 3.11). These data suggested that effective CAR-mediated activation of Tregs requires high affinity and/or avidity interactions. Accordingly, while some hA2-CARs showed binding to A*25:01 and A*68:01 in the FlowPRT assay, the strength of binding was insufficient for cellular activation.

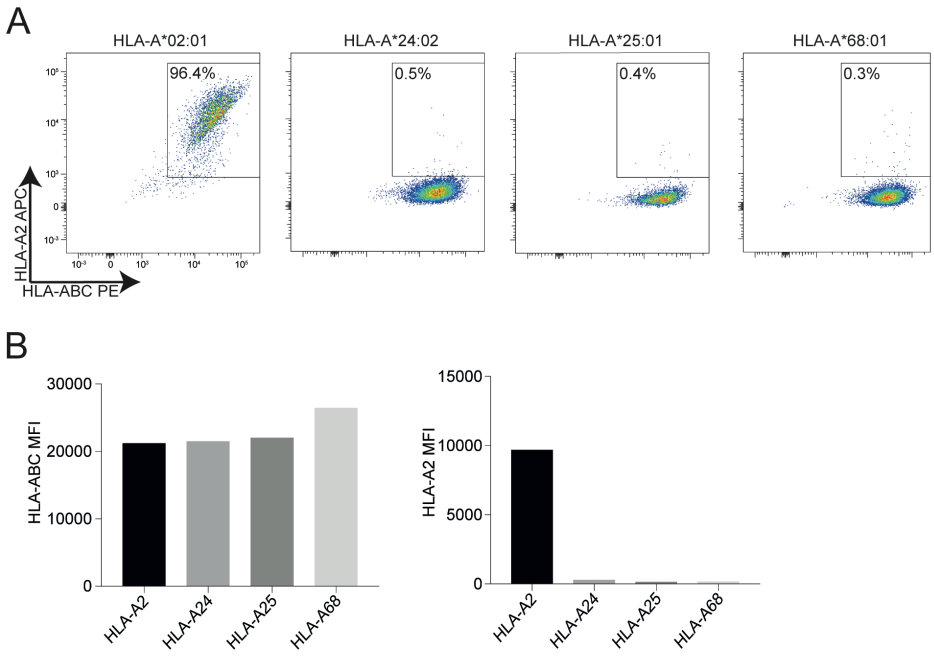

Figure 3.11 Characterization of K562 cells expressing HLA-A allelic variants.
(A) Representative flow cytometry plots from staining HLA-A2, A24, A25 and A68-expressing K562s (from left to right) with anti-HLA-ABC or anti-HLA-A2 (BB7.2 clone) mAbs. Gated on live cells. **(B)** Mean fluorescence intensity of HLA-ABC (left) and HLA-A2 (right) for each K562 cell line.

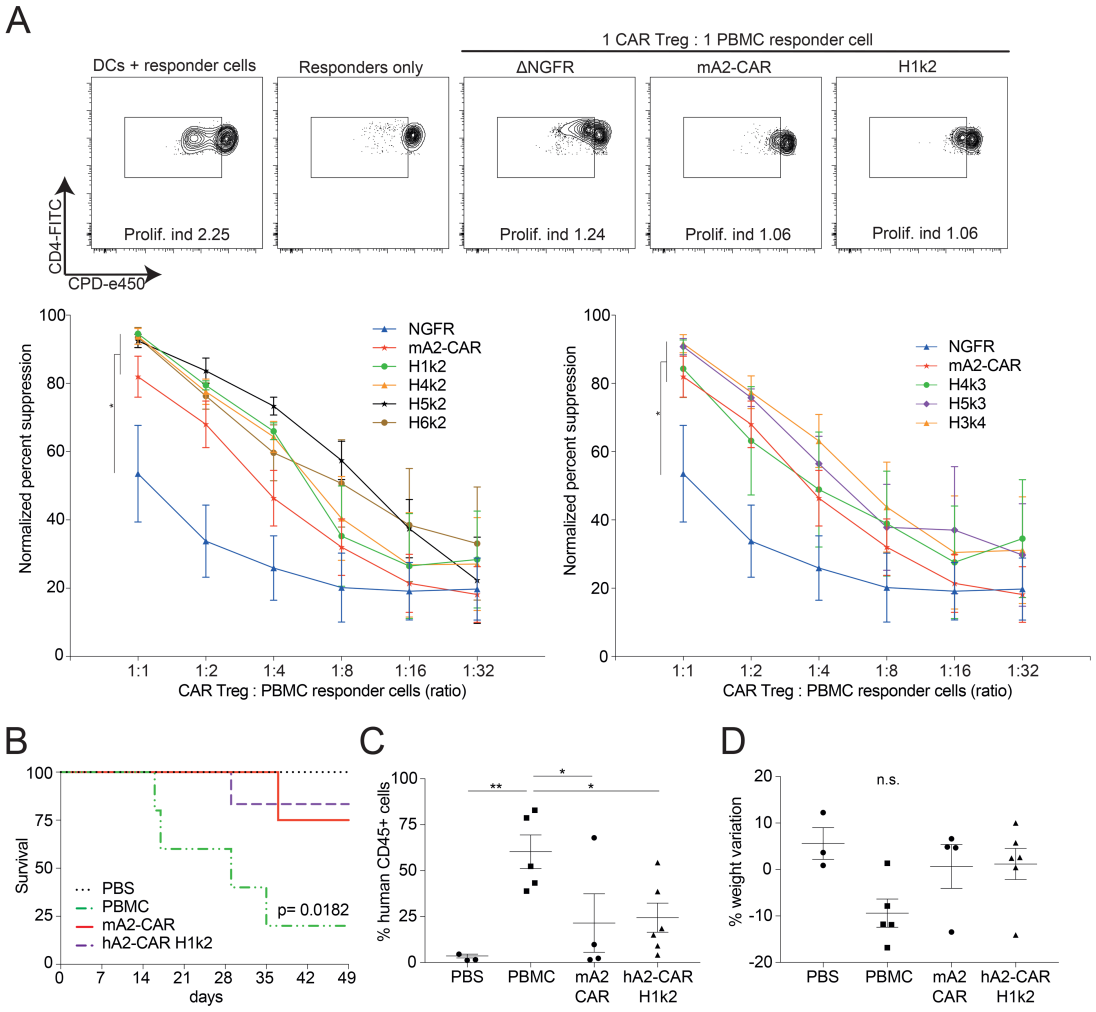

Figure 3.12 hA2-CAR Tregs are suppressive in vitro and in a model of xenogeneic GvHD in vivo. **(A)** Cell Proliferation Dye (CPD)-e450-labelled HLA-A2^{neg} CD4^{+} "responder" T cells were stimulated with a 1:1 ratio of mature HLA-A2^{+} dendritic cells in the absence/presence of varying ratios of the indicated CPD-e660-labelled control or m/hA2-CAR Tregs. After 6 days the amount of proliferation of the responder CPD-e450-labelled CD4^{+} responder T cells was measured by flow cytometry. Top: representative data and gating strategy, with proliferation index. Bottom: average data for n=3-7 pooled from at least 3 independent experiments. Statistics were performed using a two-way ANOVA with Holm-Sidak post-test versus a ΔNGFR Treg control. * $p < 0.05$, mean ± SEM. **(B-D)** Irradiated NSG mice were injected with either: PBS (n=3); HLA-A*02:01^{pos} PBMCs alone (n=5); HLA-A*02:01^{pos} PBMCs and a 1:2 ratio of H1k2 hA2-CAR Tregs (n=6) or mA2-CAR Tregs (n=4) pooled from two independent experiments. **(B)** Survival curve, log-rank (Mantel-Cox) test. **(C)** Human CD45^{+} engraftment upon experimental or humane endpoint (gating strategy in Supplemental Figure 7A). **(D)** Percent of weight change at sacrifice relative to experiment start (day 49 or earlier). Statistical significance determined using a one-way ANOVA and Holm-Sidak post-test, mean ± SEM. * $p \leq 0.05$, ** $p \leq 0.01$

3.2.3 hA2-CAR Tregs are suppressive in vitro and in vivo

We used mixed lymphocyte reactions (MLRs) with A*02:01 expressing dendritic cells to test the ability of the hA2-CAR constructs to stimulate Treg suppressive function. The three poorly functional constructs were excluded (H2k2, H4k4 and H5k4). Proliferation of third-party HLA-A*02:01^{neg} PBMCs were stimulated by co-culture with mature HLA-A*02:01^{pos} monocyte-derived dendritic cells in the absence or presence of increasing ratios of m/hA2-CAR or control Tregs. Both mA2- and hA2-CAR-expressing Tregs were significantly better at suppressing alloAg-stimulated proliferation of CD4^{+} T cells in comparison to control Tregs transduced with the ΔNGFR control up to a ratio of 1:16 Treg:PBMC (Figure 3.12A). To confirm the functional capacity of hA2-CAR Tregs *in vivo*, we used a model of xenogeneic GvHD in which we previously showed that HLA-A2-specific CAR Tregs were more potent than non-specific (polyclonal) CAR Treg controls[221]. Using this model, we compared one of the six hA2-CAR which displayed optimal characteristics (Table 3.2), H1k2, to the original mA2-CAR construct. HLA-A*02:01^{pos} PBMCs were injected into NSG mice with or without H1k2-CAR Tregs, or mA2-CAR Tregs as a positive control. Mice that received mA2- or hA2-CAR-expressing Tregs had significantly improved survival and reduced human CD45^{+} cell engraftment and weight loss compared with those that did not receive CAR Tregs (Figure 3.12B-D). While the biological

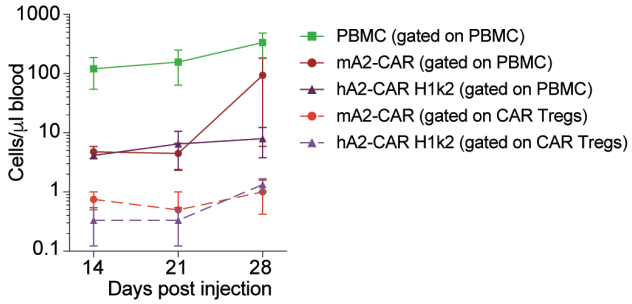

Figure 3.13 In-vivo CAR Treg tracking after adoptive transfer in a xenogeneic GVHD mouse model.
Irradiated NSG mice were injected with cells as described in Figure 3.12. Absolute number of PBMC and CAR Treg engraftment per µL of blood over time. Number of PBMCs were calculated as hCD45^{+} minus CAR Treg counts.

effect of the Tregs was observed, as we previously observed[221] we did not detect circulating m/hA2-CAR Tregs, measured from 14 days post injection (Figure 3.13).

3.2.4 hA2-CAR Tregs traffic to HLA-A2$^+$ skin grafts in vivo

For effective suppression of allograft rejection, Tregs need to migrate to the allograft and control local immunity[276,277]. To test how CAR-directed specificity affected Treg trafficking, we performed side-by-side skin transplants from NSG or NSG-A*02:01-transgenic mice onto NSG mice (Figure 3.14A). After graft recovery, PBMCs were injected in the absence or presence of m/hA2-CAR Tregs or with HER2-CAR Tregs as a non-specific polyclonal Treg control[221]. In addition to the CAR, Tregs were co-transduced with a lentivirus encoding a luciferase-GFP fusion protein. Bioluminescent imaging was performed after D-luciferin injection up to 21 days post-Treg injection[268]. In contrast to polyclonal HER2-CAR Tregs, which trafficked equally to A2-negative and -positive skin, m/hA2-CAR Tregs rapidly trafficked to the A2-expressing skin. In addition, m/hA2-CAR Tregs persisted longer than non-specific HER2-CAR Tregs. Whereas HER2-CAR Tregs were undetectable by day 7-14, a strong m/hA2-CAR Treg signal remained within the A2-positive skin throughout the experiment (Figure 3.14B). Quantification of the ratio of luminescence in the A2-positive versus A2-negative graft revealed significant Ag-driven trafficking of both H1k2 and mA2-CAR Tregs to the A2-expressing graft (Figure 3.14C&D).

In addition to graft-localized m/hA2-CAR Tregs, we noted an adjacent signal consistent with the location of a local draining lymph node. The timing of when this signal was first detected was variable, ranging from 7-14 days (Figure 3.14B) and in some mice waned over time (Figure 3.15). In a subset or animals, flow cytometric analysis of skin graft draining lymph nodes

revealed a significant proportion of hCD4^{+}FOXP3^{+}ΔNGFR^{+}A2-tetramer^{+} CAR Tregs. In contrast, very few of these cells were detected in the spleen (Figure 3.16).

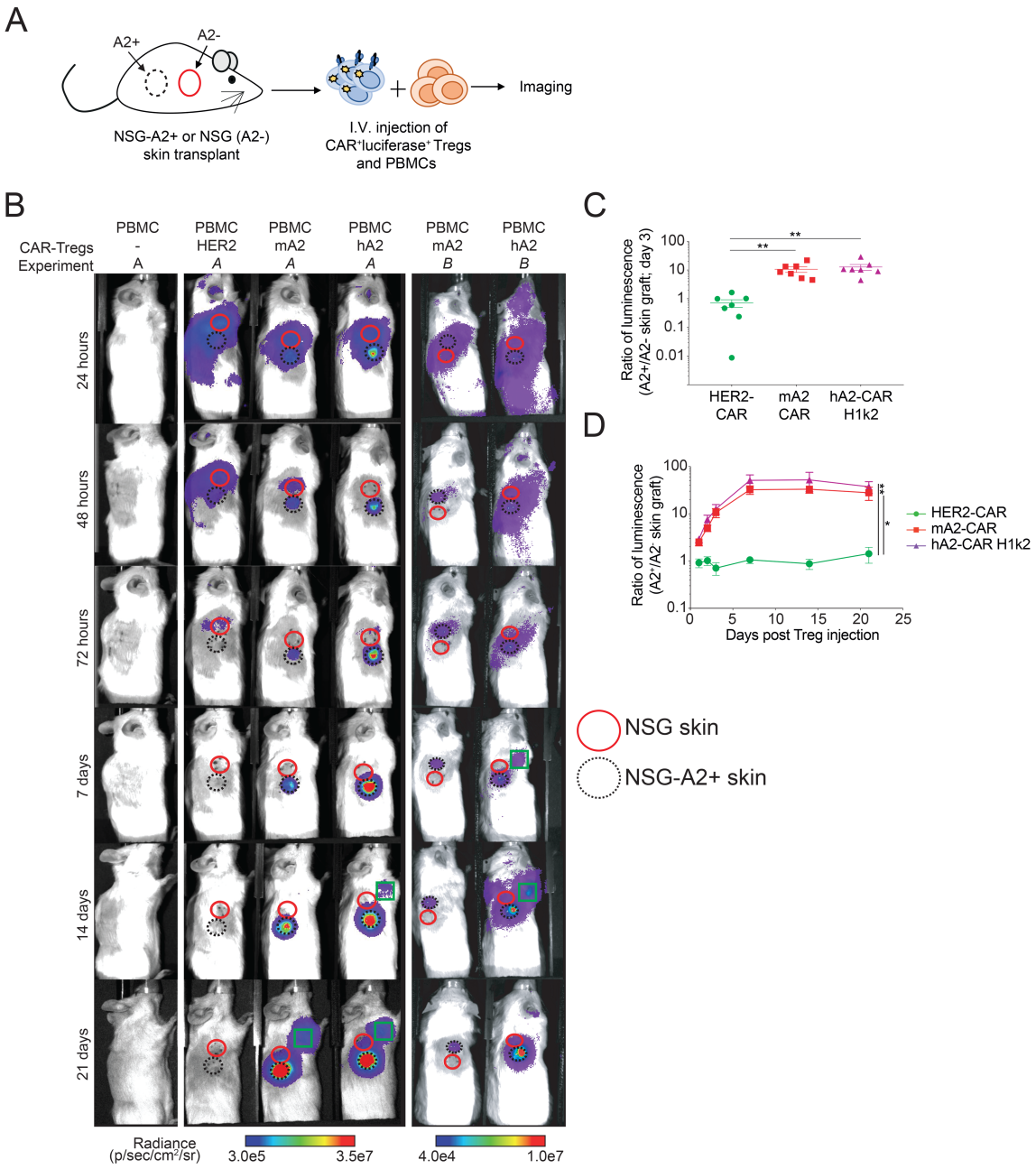

Figure 3.14 Expression of m/hA2 CARs endows Tregs with rapid and persistent homing to HLA-A2:01+ skin allografts.

Tregs were co-transduced with lentivirus encoding luciferase and either a control HER2-CAR, mA2-CAR or hA2-CAR (H1k2) and expanded for 7 days. Dual transduced cells were FACS-sorted, expanded for 5 more days, then injected into NSG mice which had previously been transplanted with juxtaposed skin transplants from both NSG and NSG-HLA-A*02:01 transgenic mice. **(A)** Schematic representation of the experimental setup. **(B)** Representative luciferase imaging of skin grafts at the indicated timepoints after Treg injection. Red closed circle denotes location of NSG skin graft; black dotted circle denotes location of A2-NSG skin graft; green square denotes potential location of draining lymph node. Amount of luciferase radiance was quantified using the average amount of photons/sec/cm2/steradian and plotted as a ratio between **(C)** the HLA-A*02:01-NSG and NSG skin grafts 72 hours after Treg injection or **(D)** over time. n=6-7 per group pooled from three independents experiments, mean ± SEM. Repeated measures ANOVA with Bonferroni correction. * $p < 0.05$, ** $p < 0.01$.

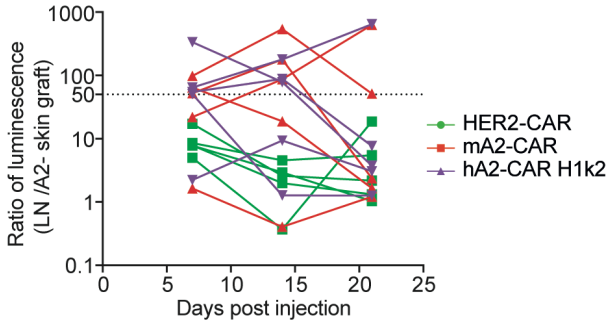

Figure 3.15 Variable kinetics of lymph node homing in CAR+luciferase+ Tregs in vivo.
Tregs were co-transduced with lentivirus containing luciferase and either HER2-CAR, mA2-CAR or hA2-CAR constructs, expanded and injected into transplanted NSG mice as in Figure 3.14. Amount of luciferase radiance was quantified using the average amount of photons/sec/cm^2/steradian and plotted as a ratio between the suspected draining lymph node area and NSG skin grafts over time.

3.2.5 hA2-CAR Tregs prevent human skin allograft rejection

To evaluate the immunoregulatory potential of hA2-CAR Tregs in a solid organ transplant model, we used a humanized model of skin transplantation in which NSG mice were transplanted with human HLA-A2^{pos} skin grafts. After 6 weeks, mice were injected with HLA-

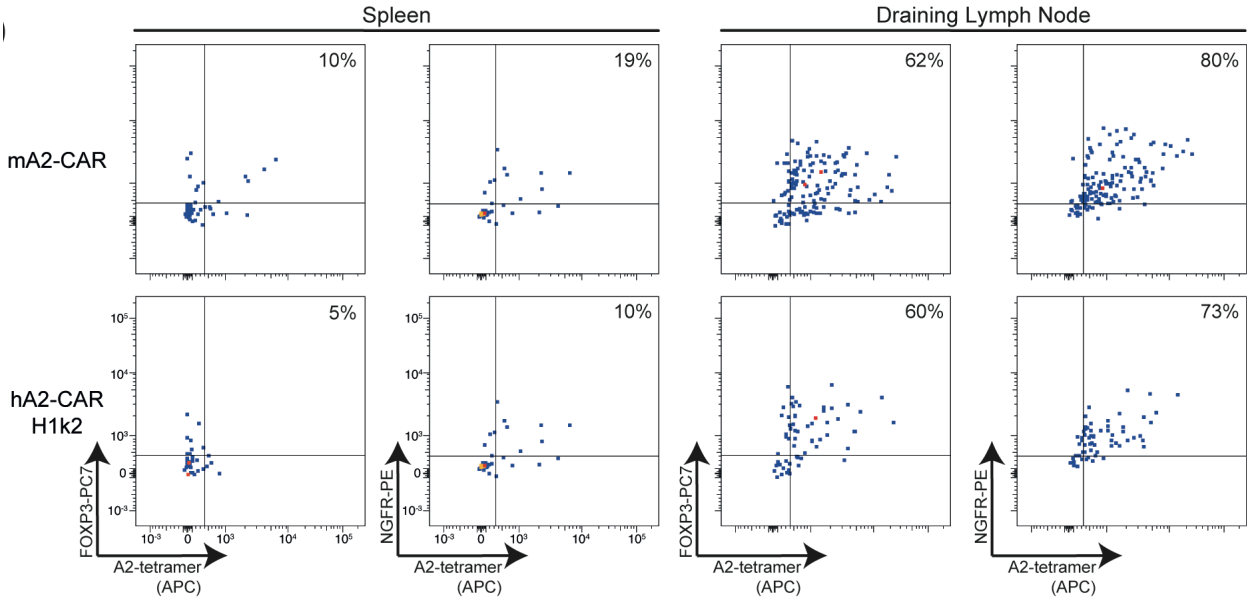

Figure 3.16 Phenotype of lymph node-homing m/hA2-CAR Tregs.
Tregs were co-transduced with lentivirus containing luciferase and either mA2-CAR or hA2-CAR constructs, expanded and injected into transplanted NSG mice as in Figure 3.14. Flow cytometry plots showing staining for m/hA2-CAR Tregs in the spleen and draining lymph node upon experiment endpoint (day 23). n=1 per group from one independent experiment.

$A2^{neg}$ PBMCs with or without autologous ΔNGFR Tregs or H1k2 hA2-CAR Tregs. Four weeks after cell injection, mice were sacrificed, and the skin graft was collected for evaluation of pathology and inflammatory cytokine expression. All mice maintained stable body weight, indicating a lack of xenogeneic GvHD (Figure 3.18A), with evidence of human leukocyte engraftment in blood and spleen (Figure 3.18B). H&E sections were evaluated for rejection by a blinded pathologist using a 25-point scale, revealing a significant decrease in the cumulative pathological rejection score in mice that received H1k2 hA2-CAR or ΔNGFR Tregs versus PBMCs alone (Figure 3.18C). Immunostaining revealed that, in comparison to mice receiving PBMCs alone, mice receiving PBMCs and H1k2 hA2-CAR Tregs had a significant reduction in $Ki67^{+}$ keratinocytes, and a trend towards less involucrin destruction (Figure 3.18D). qPCR quantification also showed a general reduction in inflammatory cytokines within the grafts of ΔNGFR Treg or H1k2 hA2-CAR Treg-treated mice (Figure 3.18E).

Consistent with data from the xenogeneic GvHD model, while PBMCs were detectable in blood, CAR Tregs were not (Figure 3.17). However, immunostaining revealed that in comparison to mice receiving PBMCs alone, mice receiving ΔNGFR Tregs or H1k2 hA2-CAR Tregs had a trend towards higher proportions of $FOXP3^{+}$ cells in the graft (Figure 3.18F). The presence of $FOXP3^{+}$ cells was unique to the transplanted skin graft as they were undetectable in the intestine, liver or lung (Figure 3.18G). These data suggest that, as for the model with A2 transgenic NSG skin, H1k2 hA2-CAR Tregs specifically traffic to human $A2^{+}$ skin allograft, where they persisted.

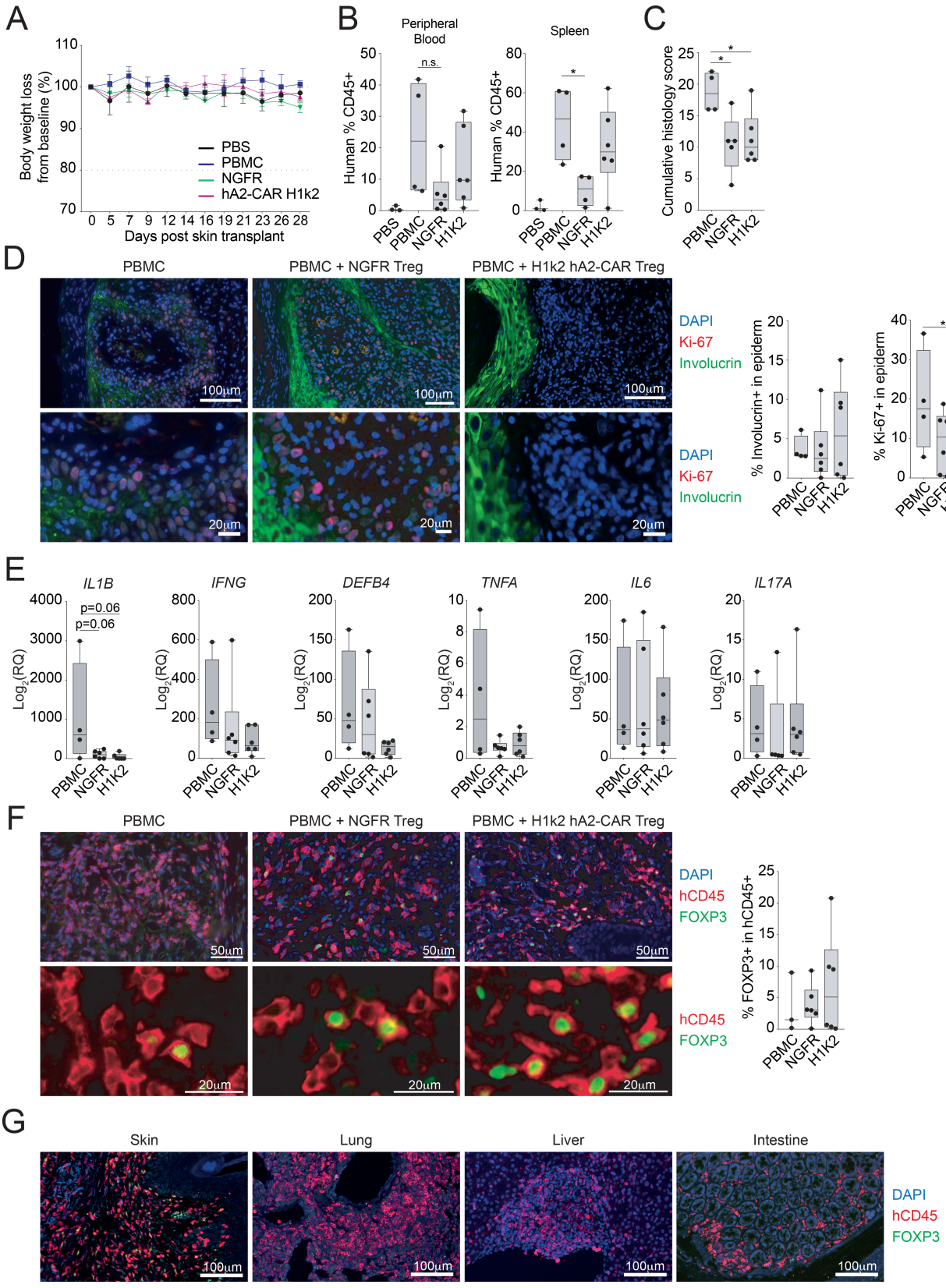
A
Body weight loss from baseline (%)
Days post skin transplant
PBS
PBMC
NGFR
hA2-CAR H1k2
B
Peripheral Blood
Spleen
Human % CD45+
n.s.
PBS
PBMC
NGFR
H1K2
C
Cumulative histology score
D
PBMC
PBMC + NGFR Treg
PBMC + H1k2 hA2-CAR Treg
DAPI
Ki-67
Involucrin
% Involucrin+ in epiderm
% Ki-67+ in epiderm
100µm
20µm
E
IL1B
IFNG
DEFB4
TNFA
IL6
IL17A
Log2(RQ)
p=0.06
p=0.06
F
hCD45
FOXP3
% FOXP3+ in hCD45+
50µm
20µm
G
Skin
Lung
Liver
Intestine
100µm

Figure 3.18 hA2-CAR-Tregs diminish human skin allograft rejection.
NSG mice were transplanted with HLA-A*02:01^{+} human skin and injected six weeks later with either: PBS (n=3); HLA-A*02:01^{neg} PBMCs alone (n=4) or with a 2:1 ratio of autologous H1k2 hA2-CAR Tregs (n=6). PBMC/hA2-CAR Tregs were from two individual donors, tested in one experiment. Mice were monitored thrice weekly and sacrificed 28 days after cell injection for mRNA and histology assessment. **(A)** Body weight was monitored thrice weekly and **(B)** the proportion of human CD45^{+} cells in the blood (left) and spleen (right) was measured at day 28. **(C)** Cumulative histological score of transplanted skin sections as determined by H&E stain. **(D)** Transplanted skin grafts were immunostained at experiment endpoint to quantify the amount of involucrin expression and proportion of Ki-67^{+} cells in the epidermis. **(E)** mRNA expression of the indicated genes within transplanted skin sections was determined by qRT-PCR. **(F)** Transplanted skin grafts were immunostained at experiment endpoint to quantify the proportion of FOXP3+ cells within human CD45+ cells. **(G)** Transplanted skin grafts, intestine, lung and liver sections were immunostained at the experiment endpoint to show the proportion of FOXP3+ cells within human CD45+ cells in each tissue. Each data point represents one mouse. Box-whisker plots show mean ± range. Statistical significance determined by two-tailed Mann-Whitney test comparing PBMC to H1k2. For immunofluorescence quantifications in D&F, each data point represents the average cell number seen in several fields of view from one section/mouse. * $p < 0.05$

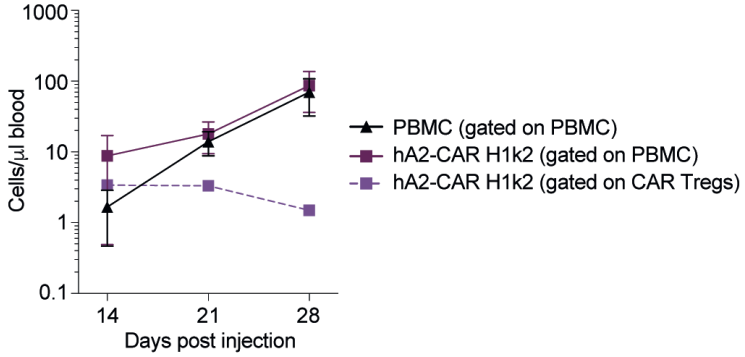

Figure 3.17 Flow cytometric tracking of hA2 CAR Tregs in the human skin transplant model.
NSG mice were transplanted with human HLA-A*02^{+} skin and injected with cells as described in Figure 3.18. Absolute number of PBMCs and CAR Treg engraftment per µL of blood over time. Number of PBMCs were calculated as hCD45+ minus total CAR Treg counts.

3.3 Discussion

Mouse-derived CARs can be highly effective, but T cells expressing humanized or fully-human CARs have increased cell persistence and efficacy[278], and have decreased side-effects[229,231-234,279]. To date, there has been no comprehensive investigation of the applicability of bioinformatic methods for humanizing mAbs for use in CAR constructs. Herein, we describe a method to generate a panel of humanized CARs and illustrate the importance of testing multiple versions with a series of assays to identify constructs with optimal specificity and activation capacity, and in vivo function. We also developed a new way to systematically test the specificity of CARs for alloAgs, creating a new platform to comprehensively identify constructs with defined allele specificity.

Of the 18 in silico-generated hA2-CARs generated, 10 of 18 constructs maintained specificity for HLA-A*02:01, as judged by tetramer staining in 293T cells. These data are consistent with reports that humanization of scFvs can alter affinity and/or Ag-specificity[280,281]. Notably, 3 constructs (H2k2, H4K4 and H5k4) bound to tetramer in 293T cells but, when expressed in human Tregs, displayed a significantly reduced ability to bind to A*02:01, both in terms of percent tetramer^{+} cells and MFI. Their bimodal expression pattern suggestive of receptor internalization, high basal activation levels, and failure to become further activated in the presence of CAR or TCR stimulation, suggest that these CARs may induce "tonic" activation in Tregs. Interestingly, evidence of functional tonic activation was not uniformly revealed with all activation markers tested. Specifically, for all three constructs it was clearly evident with CD69 and LAP, not clearly present for CTLA-4, and for CD71 only evident with H2k2. Thus, when screening a panel of CARs, expression and specificity must be tested in T cells, and multiple activation markers should be screened to identify constructs with high, uniform

Table 3.2 Summary of hA2-CAR Treg construct performance in various in vitro assays.
✓ indicates a successful or favourable result; X indicates a failed or undesirable result; − indicates an experiment not performed.

hA2-CAR variant	HLA-A*02:01 binding (293Ts)	HLA-A*02:01 binding (Tregs)	HLA-A*02:01-mediated activation	Cross-reactivity to other HLA-A alleles	Antigen-specific suppression (MLR)
H1k1	X	–	–	–	–
H1k2	✓	✓	✓	✓	✓
H2k2	✓	X	X	✓	–
H3k2	X	–	–	–	–
H4k2	✓	✓	✓	✓	✓
H5k2	✓	✓	✓	✓	✓
H6k2	✓	✓	✓	✓	✓
H3k3	X	–	–	–	–
H4k3	✓	X	✓	✓	✓
H5k3	✓	✓	✓	✓	✓
H1k4	X	–	–	–	–
H3k4	✓	✓	✓	✓	✓
H4k4	✓	X	X	✓	–
H5k4	✓	X	X	✓	–
H1k5	X	–	–	–	–
H3k5	X	–	–	–	–
H4k5	X	–	–	–	–
H5k5	X	–	–	–	–

expression without evidence for tonic signaling.

There are limited previous reports of humanized CARs[281-283]. Sun et al described a humanized anti-HER2 CAR for use in breast cancer, but comparisons with the original murine construct were not reported[282]. Johnson et al humanized a CAR specific for the variant III mutation of the epidermal growth factor receptor (EGFRvIII)[281]. Of 8 humanized constructs, only two remained EGFRvIII specific and these had lower affinity than the original mouse CAR. We show here that sequence and structure-based approaches to antibody humanization can be used to generate humanized CARs[284-286], with empirical testing of multiple framework regions required to identify those with preserved expression and specificity without tonic signaling.

In the context of transplantation, knowledge of alloAg-specificity is required to ensure specific targeting to allogeneic cells, tissues and/or organs. The traditional way to measure T cell

alloreactivity is imprecise and non-quantitative as it involves functional MLRs with large banks of haplotyped PBMCs. We developed and validated a new way to test the specificity of alloAg-directed CARs using commercially-available reagents in common use to measure alloAg-specific Abs in serum. Surprisingly, we discovered that in comparison to the mA2-CAR, CAR humanization decreased cross-reactivity to several HLA-A allelic variants. All constructs also bound to A*69:01, and those containing k2 also to A*68:01. This cross-reactivity is likely due to a shared eplet (138MT), an antibody-accessible polymorphic region of HLA defined by molecular modeling[287]. Notably, the level of cross-reactivity towards A*25:01 or A*68:01 was not sufficient to stimulate m/hCAR Treg activation, suggesting that a relatively high level of binding is required for a functional effect. This possibility is supported by data derived from analysis of A*02:01, where the FlowPRT cell assay revealed a direct correlation between the relative binding of the CARs to A*02:01 beads and induction of CD69. Nevertheless, lack of an effect on Treg activation marker expression does not exclude the possibility that there could be biological effects mediated by cross-reactive HLAs since CAR-mediated T cell activation depends on both the scFv affinity and avidity/antigen density, parameters which may not be fully recapitulated in this in vitro system[288].

The optimal CAR affinity for activation of Treg suppression is unknown. In terms of TCR affinity, it is known that TCR affinities for the same peptide-MHC complex can vary up to 3,500-fold in Tregs but ultimately, affinity has no effect on antigen-driven suppressive function[207]. However, work from the CAR oncology field has shown that the structure and composition of the immunological synapses derived from CAR-peptide versus TCR-MHC/peptide interactions are fundamentally different[289]. We found that CARs with the lowest tetramer binding (percent and MFI) had high apparent constitutive activity in some cases (H4k4,

H5k4) but not others (H2k2), with a positive correlation between Ag binding and activation. Overall, more studies are required to determine the optimal Treg-specific synapse properties.

The homing of Tregs to allografts is key for their ability to induce tolerance to the grafts (reviewed in [276]). Here we found that m/hA2-CAR expression endowed Tregs with the ability to rapidly and specifically traffic to A2-expressing allografts. After trafficking to the $A2^+$ graft, m/hA2-CAR Tregs (or their progeny), but not polyclonal Tregs, remained for at least 21 days. Other groups have also observed that continual Ag exposure enables long-term CAR Treg persistence, for example with CD19 CAR cytotoxic T cells[230,290] and murine CAR Treg models of colitis[291] and islet transplantation[292]. The Ag-driven persistence of Tregs is also supported by our findings in xenogeneic GvHD, where poor A2-CAR Treg persistence is correlated with diminished A2-positive immune cell engraftment[221]. Interestingly, polyclonal HER2-CAR Tregs also showed a directed pattern of trafficking toward the allografts but were equally distributed between the A2-positive and -negative grafts. These polyclonal Tregs may be migrating in response to the inflammatory signals emanating from post-operative skin, because in unmanipulated immunodeficient mice, human T cells typically traffic to the lung[293]. We also detected CAR Tregs in the draining lymph nodes in some mice. Since a two-step migratory process from graft to lymph node has previously been reported to be necessary for tolerance induction[294], a more detailed investigation of CAR Treg trafficking is warranted.

Infusion of autologous hA2-CAR Tregs inhibited human skin allograft rejection as judged by an improved pathological score, a lower proportion of proliferating keratinocytes and a trend towards diminished involucrin destruction. Consistent with previous reports in this model [222,223] we noted modest differences between hA2-CAR Tregs and polyclonal (ΔNGFR) Tregs. A consideration is that we used a relatively high Treg:PBMC ratio of 1:2. For comparison,

Boardman et al and Noyan et al, who used lower A2-CAR Tregs:PBMC ratios (1:5 and 1:7.5 ratios of respectively)[222,223], also did not observe significant differences between polyclonal and A2-CAR Tregs in terms of skin rejection. It is possible that in this model the intrinsic alloreactivity of polyclonal Tregs may be sufficient for a therapeutic effect even at relatively low Treg:PBMC ratios.

Importantly, A2-CAR Tregs did not make rejection worse in any reported studies[221-223], arguing against the possibility that post-in vivo injection the cells acquired cytotoxic function either via Treg instability or outgrowth of contaminating conventional CAR-T cells. To mitigate the risk of manufacturing CAR Tregs which were contaminated with low proportions of conventional T cells, for all in vivo studies we used naïve $CD45RA^{+}CD25^{hi}$ Tregs as our starting population since, in comparison to the $CD45RA^{-}$ memory Treg fraction, post expansion these cells maintain a more consistent Treg phenotype[186,295]. Nevertheless, the long terms effects of repeated CAR stimulation on Tregs is unknown. Future work in immunocompetent mouse models will be needed to address this question, as well as the question of how these cells may be affected by standard immunosuppression regimens that would be used in transplanted patients.

Collectively, these data provide a simple platform for CAR humanization and highlight the critical importance of testing several CARs in multiple assays to define optimal constructs for use in Tregs. Specifically, expressing/binding data in 293T cells was not entirely indicative of the construct properties in Tregs, as evidenced in the low expression of H2k2 and bimodal expression patterns of the H4k4 and H5k4 variants. Furthermore, deficits in hA2-CAR Treg activation capacity were only revealed by testing multiple activation parameters. Consistent with the concept that Tregs require a strong Ag-receptor signal, there was a direct correlation between strength of HLA binding and expression of activation and Treg functional markers. Evidence that

hA2-CAR-engineered alloAg-specific Tregs persisted at the allograft, migrated to draining lymph nodes and suppressed rejection sets the stage for testing their ability to regulate allograft rejection in humans.

Chapter 4: Functional effects of chimeric antigen receptor co-receptor signaling domains in human Tregs

4.1 Introduction

Regulatory T cells (Tregs) are a promising adoptive cell therapy to prevent or treat undesired immune responses, with several clinical trials completed or ongoing (reviewed in [182]). To date, most of these trials have used polyclonal Tregs with unknown antigen (Ag) specificity, but work in mouse models has shown that Ag-specific Tregs are significantly more potent in a variety of disease contexts[199]. We and others developed an approach to generate Ag-specific Tregs using chimeric antigen receptor (CAR) technology to create synthetic receptors which combine extracellular antigen binding domains and intracellular signaling domains[296]. In comparison to Ag-non-specific cells, the resulting CAR Tregs have enhanced potency, as demonstrated in a variety of models, including colitis[217,219,291], experimental autoimmune encephalomyelitis[220], transplantation[221-223,247,297], and immunity to therapeutic proteins[224,298].

The majority of CAR Treg studies to date have used the so-called "second generation" CAR design, which includes a single membrane proximal co-stimulatory domain, followed by CD3ζ. Due to the extensive evidence for the important role of CD28 co-stimulation in Tregs[37], the majority of CAR Treg studies selected this protein as the source of co-stimulation. However, as with conventional T cells (Tconvs), Tregs express a number of co-receptors that provide co-stimulatory or co-inhibitory signals (reviewed in [299]), the functional relevance of which may differ from that in Tconvs and vary depending on the tissue/disease context. An additional consideration is that the vast majority of studies which defined co-receptor function in Tregs used genetic-deletion models in which receptors of interest were absent throughout Treg

development, thus making it difficult to infer function in the fully differentiated cells which would be used for CAR engineering.

Extensive research in the context of oncology has sought to optimize CAR design to deliver potent and persistent Tconvs[244]. Much of this work focused on comparing co-receptor signaling domains, revealing a key role for co-stimulation in CAR function. For example, comparisons of CD28- to 4-1BB-based second generation CARs in $CD8^+$ T cells, revealed that 4-1BB-based CAR T cells are more persistent and resistant to exhaustion, and express a memory-T-cell like pattern of gene expression[300,301] whereas CD28-based CAR T cells have a more acute anti-tumor effect (reviewed in [302]). These findings led to intense research to define the optimal contexts in which to use 4-1BB- versus CD28-based CAR T cells, with both versions are now in clinical use with Kymriah® encoding CD28 and Yescarta® 4-1BB[303].

The functional effects of CARs encoding other co-receptor domains has also been examined in Tconvs. For example, in comparison to CD28 and 4-1BB, expression of an ICOS-based CAR results in higher secretion of Th17-associated cytokines and longer in vivo persistence in a xenograft tumor model[304,305]. The effects of CARs encoding co-inhibitory receptors have also been explored. Expression of second-generation CARs encoding PD-1 or CTLA-4 together with CD28- or 4-1BB-encoding CARs is an effective approach to limit toxicity by restricting off-target T cell stimulation[306]. Thus the function, potency and persistence of CAR-engineered Tconvs can be tailored by choice of co-stimulatory domain.

How Tregs would be affected by CARs encoding co-stimulatory domains other than CD28 or 4-1BB was unknown[248,307]. Seeking to identify CARs that could modulate Tregs by altering their stability, cytokine production, survival and/or other properties of therapeutic

benefit, we sought to comprehensively compare the *in vitro* and *in vivo* function of CAR Tregs expressing second-generation CARs encoding one of 10 different co-stimulatory domains.

4.2 Results

4.2.1 Generation, cell surface expression and selection of signaling-domain CAR variants

We selected 9 co-receptor proteins to test in a CAR format in comparison to an existing CAR which encodes an intracellular CD28 domain, an extracellular single chain antibody (scFv) specific was specific for HLA-A2, and stimulates potent Treg suppression in vitro and in vivo[221,247]. Co-receptors were selected from CD28 or TNFR family proteins (Figure 4.1) since these are functionally-relevant in T cells and in some cases had already been successfully used as CARs in Tconvs. Within the CD28 family, in addition to the CD28 wild type (wt) protein, which is known to be important for Treg activation and proliferation[308-310] we selected: CD28(Y173F), a point mutant with diminished PI3K pathway activity which may be beneficial for Treg function[311]; ICOS, which is important in Treg survival and may be involved in IL-10 production[54-56]; CTLA-4, which is essential for Treg function[37,312]; CTLA-4(Y165G), a point mutant which increases cell surface expression[313]; and PD-1, which is essential for generation and maintenance of peripherally-induced Tregs[75]. Within the TNFR family, we selected: 4-1BB as this co-receptor is beneficial for the longevity of CAR T cells[300,301] and in models of autoimmunity is beneficial for Tregs[299]; OX40 and GITR, which promote Tregs in certain contexts[299]; and TNFR2 which stimulates Treg proliferation and suppression[314,315].

Sequences for the intracellular signaling portions of these proteins were identified in the UniProt database[253], placed C-terminal to the anti-HLA-A2-specific scFv and a c-Myc epitope tag, and cloned into a bi-directional lentiviral vector encoding ΔNGFR as a transduction marker[221]. Because the choice of transmembrane domain can affect CAR expression[316,317], two

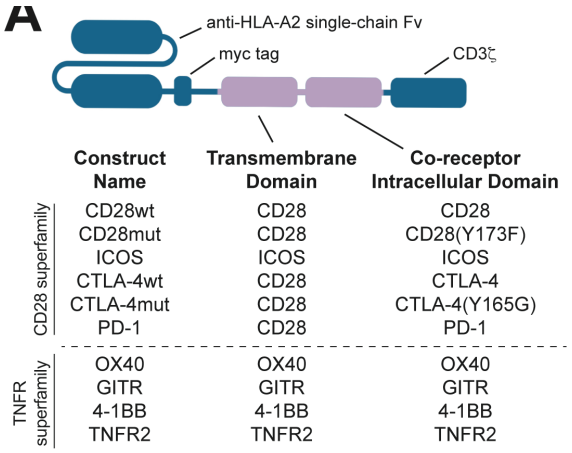

Figure 4.1 Design of signaling domain CAR variants.
CARs consisting of an extracellular anti-HLA-A2 scFv, myc tag and CD8α stalk, followed by various transmembrane and co-receptor domains, and CD3ζ were cloned. The indicated constructs were selected on the basis of cell surface expression in transiently transfected 293T cells (Figure 4.2).

versions were created for several of constructs: one using the transmembrane domain from CD28 and the other using the transmembrane domain from the co-receptor being tested. Cell surface expression was first tested in 293T cells by quantifying the proportion and intensity of Myc-expressing cells within the ΔNGFR-positive population (Figure 4.2A). Most CAR constructs had similar levels of expression with the CD28 or native transmembrane domains (PD-1, ICOS, OX40, 4-1BB, TNFR2), but the expression of CTLA-4mut and GITR was significantly higher with the CD28 or native domain, respectively. To test if changing the scFv affected expression patterns, some of the co-stimulatory domains were also tested in the context of a CAR encoding an anti-HER2 scFv revealing no significant differences in comparison to the HLA-A2-based CAR (Figure 4.2B). On the basis of these data, for all the CD28 family co-receptors, with the exception of ICOS, the CD28 transmembrane domain was selected, and for all the TNFR family co-receptors the native transmembrane domain was selected.

To test expression in human Tregs, $CD25^{hi}CD127^{lo}CD4^{+}$ cells were sorted from peripheral blood, activated via their TCR and transduced with lentivirus encoding one of the 10

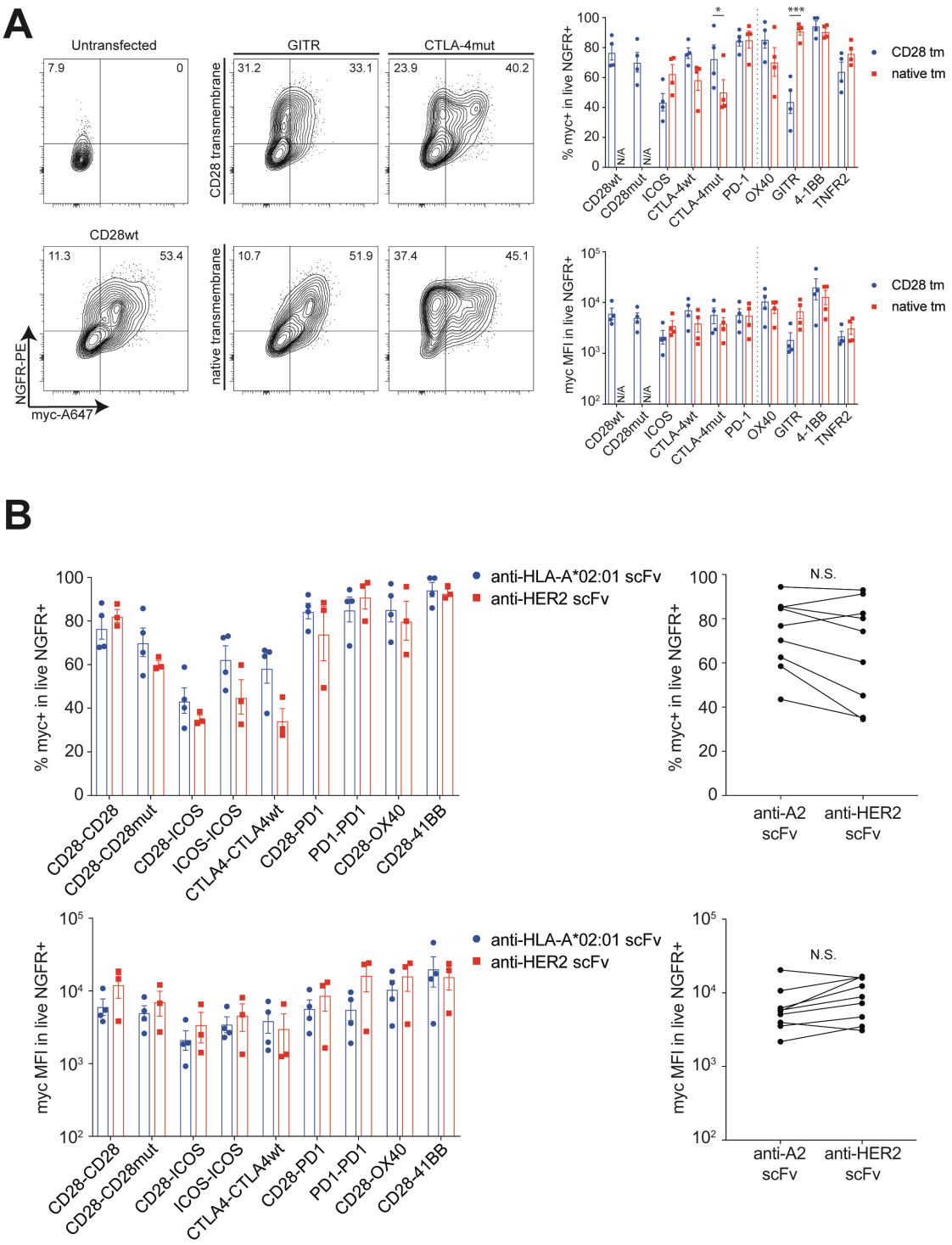

Figure 4.2 Surface expression of signaling domain CAR variants with different transmembrane domains or scFvs. **(A)** Anti-HLA-A2 CARs variants were generated differing in their co-stimulatory domain with either their original (or "native") transmembrane domain or a CD28 transmembrane domain. These constructs were transiently transfected into 293T cells and assessed by flow cytometry 48 hours after transfection for their surface expression of the CAR, denoted by myc-tag detection, and the transduction marker, truncated NGFR (CD271). Left: representative flow cytometry plots. Right: summarized data of percent of mean fluorescence intensity of myc-tag detection in the live NGFR+ fraction. Data are n=3-4, pooled from at least three independent experiments. **(B)** Selected constructs from (A) were also cloned onto an anti-HER2 scFv, then transfected into transiently transfected into 293T cells and assessed by flow cytometry 48 hours after transfection for their surface expression of the CAR, denoted by myc-tag detection, and the transduction marker, truncated NGFR (CD271). Top: percent myc positive cells in live NGFR+ cells. Bottom: mean fluorescence intensity of myc in live NGFR+ cells. Individual data (left) and summarized data (right) are shown. Statistics show one-way ANOVA with Holm-Sidak post-test comparing each transmembrane variant or scFv pair. Mean ± SEM. * $p < 0.05$, ** $p < 0.01$, *** $p < 0.001$. "n.s." denotes not significant.

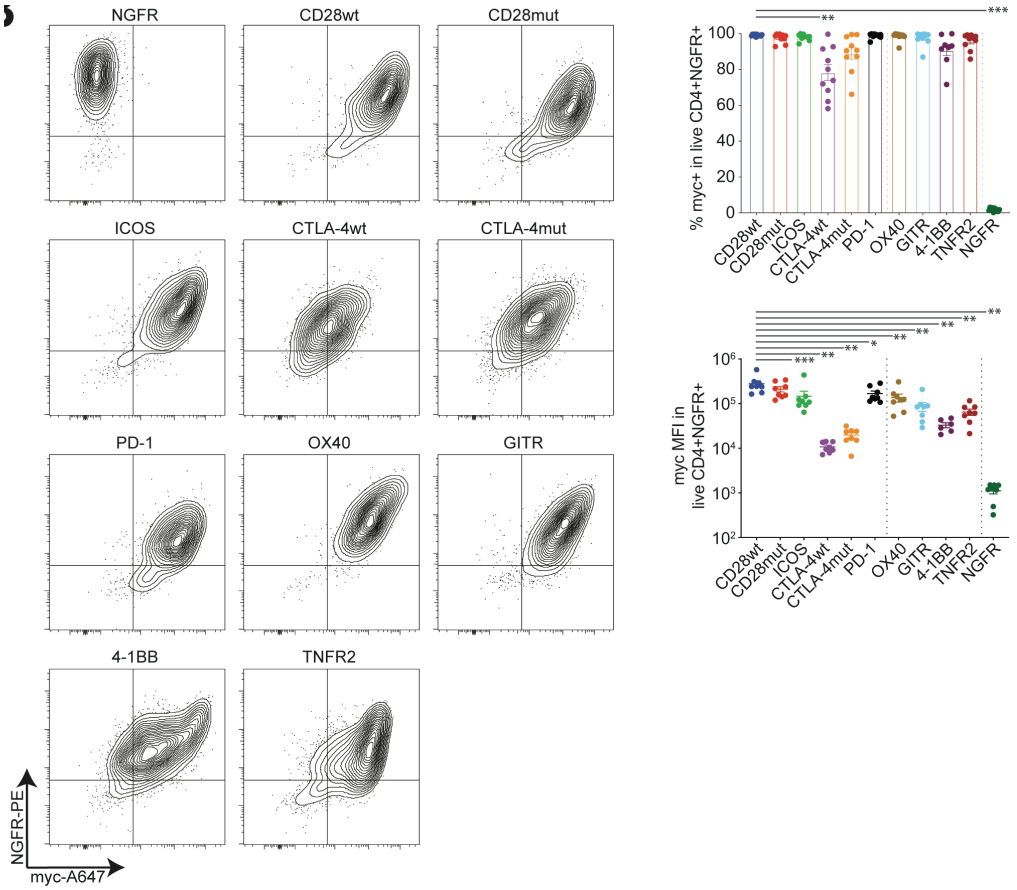

Figure 4.4 Surface expression of signaling domain CAR variants.
CD4$^+$CD25$^+$CD127$^-$ human Tregs were sorted and transduced using lentivirus generated from the constructs in Figure 4.1. After 7 days, transduced cells were purified based on the basis of NGFR expression and analyzed by flow cytometry. Shown are representative and averaged data depicted as the proportion or mean fluorescence intensity (MFI) of myc$^+$ cells within live, CD4$^+$ΔNGFR$^+$ cells. n=6-8 from at least four independent experiments. Statistics show one-way ANOVA with a Holm-Sidak post-test to compare all constructs to CD28wt. Mean ± SEM, * $p < 0.05$, ** $p < 0.01$, *** $p < 0.001$.

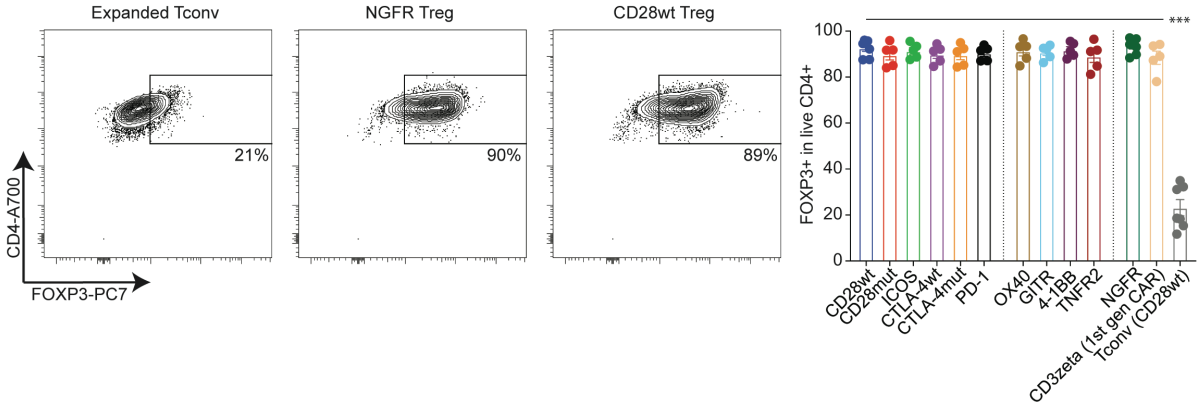

Figure 4.3 FOXP3 and Helios expression of CAR Tregs after 7-day expansion and purification.
CAR Tregs were transduced, expanded, purified as in Figure 1b, then analyzed by flow cytometry for FOXP3 and Helios purity. Left: representative flow plots. Right: summarized data of percent FOXP3 and Helios expression within live CD4+ cells. Data are n=5-6 donors, pooled from at least 3 independent experiments. Statistics show one-way ANOVA with a Holm-Sidak post-test to compare all constructs to CD28wt. Mean ± SEM. *** $p < 0.001$.

signaling domain variant A2-CARs (Figure 4.4 and Figure 4.3), or an empty vector control. After 7 days, successfully transduced $\Delta NGFR^+$ cells were isolated and CAR expression was determined on the basis of the proportion and mean fluorescence intensity (MFI) of myc expression. In terms of proportion, within the CD28 family, only the CTLA-4wt (but notably not the CTLA-4mut) variant had significantly lower A2-CAR expression in comparison to the CD28wt construct; within the TNFR2 series, there were no significant differences. In terms of MFI, differences in expression intensity were seen, with the CD28wt and CD28mut constructs consistently having the highest level of expression.

4.2.2 Wild type CD28 signaling is required for optimal Treg suppression in vivo

To test the function of the signaling domain A2-CAR variants with human Tregs, we used the well-established, xenogeneic graft-versus-host disease (GVHD) model in which A2-CAR Tregs prevent GVHD via suppressed proliferation/engraftment of co-injected allogeneic HLA-$A2^+$ PBMCs[221]. $CD25^{hi}CD127^{lo}CD4^+$ Tregs were sorted, stimulated, transduced and purified as described above, and expanded further by TCR-restimulation for 5 additional days. Immunodeficient NGS mice were irradiated, then injected with 10^6 HLA-$A2^+$ PBMCs in the absence or presence of $5x10^6$ (high ratio) or 2.5 $x10^6$ (low ratio) of the indicated type of Treg (Figure 4.5A). The positive control was Tregs transduced with the CD28wt A2-CAR, and negative controls were Tregs transduced with an antigen irrelevant HER2-CAR, or a first-generation A2-specific CAR lacking a co-receptor signaling domain. Survival and GVHD score were monitored over time. As expected, mice which received CD28wt A2-CAR Tregs at either a high or low ratio were significantly more protected from GVHD in comparison to the negative controls (Figure 4.5B and Figure 4.6).

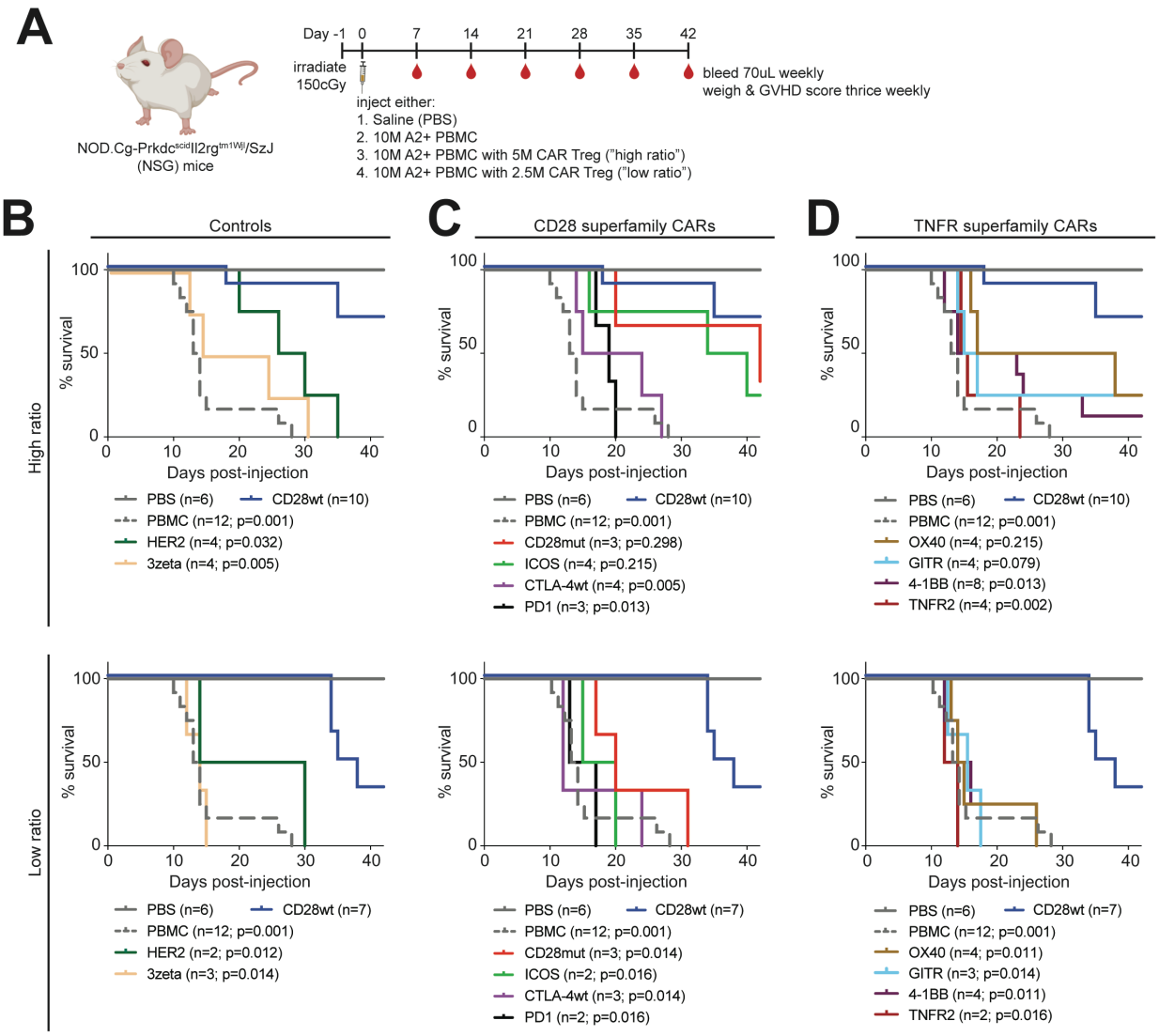

Figure 4.5 In vivo suppression of xenogenic graft-versus-host disease by signaling domain CAR variant Tregs. 8 to 12-week old female NSG mice were irradiated one day before injection with PBS, or 10^7 HLA-A2$^+$ PBMC in the absence or presence of 2.5 or 5.0 x10^6 of the indicated type of CAR-Treg. Mice were weighed and scored for GVHD thrice weekly and bled weekly for flow cytometry analysis. **(A)** Schematic design of the experiment. **(B-D)** Survival curves. **(B)** Positive (CD28wt) and negative (HER2, CD3zeta) controls. **(C)** CARs with signaling domains from the CD28 superfamily. **(D)** CARs with signaling domains from the TNFR superfamily. Top: Mice receiving a high ratio of Treg:PBMC (1:2). Bottom: Mice receiving a low ratio of Treg:PBMC (1:4). Data from PBS, PBMC and CD28wt Treg mice are repeated in each panel. Statistics show adjusted p values corrected for multiple comparisons for pair-wise log-rank Mantel-Cox tests, comparing the survival curve for all constructs to CD28wt.

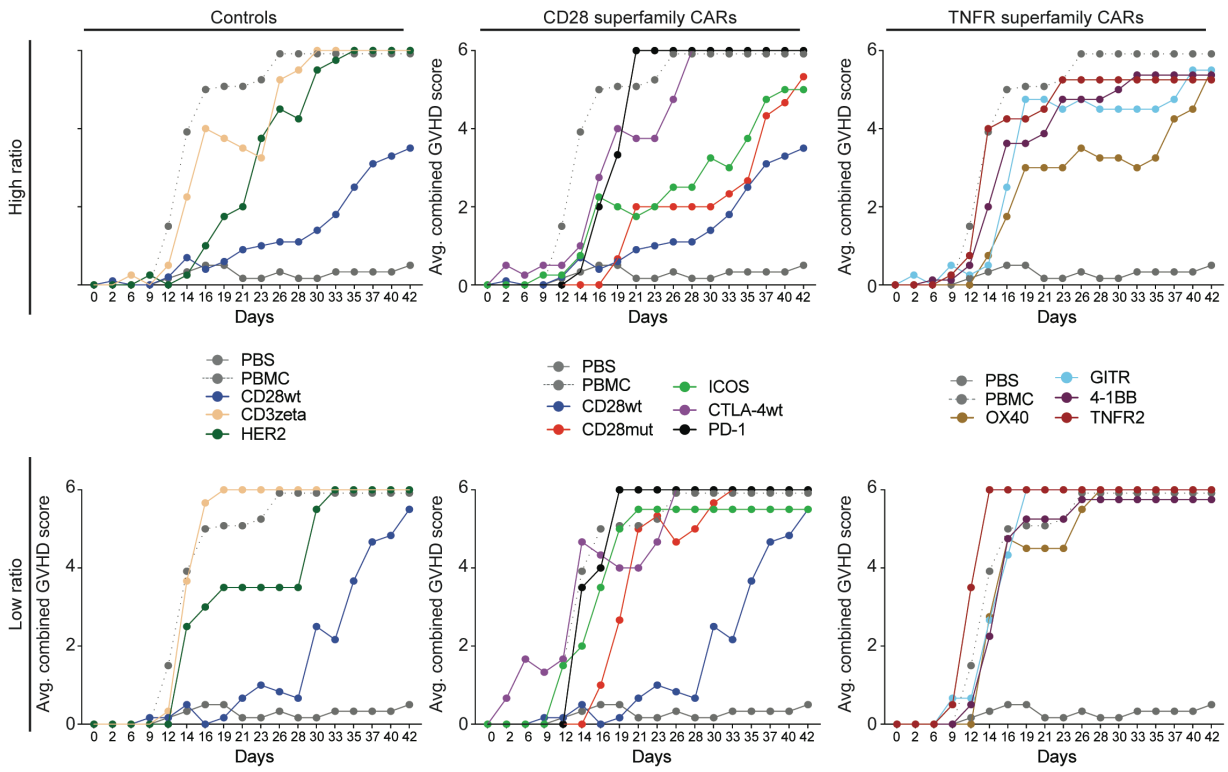

Figure 4.6 GVHD score for mice in xenoGVHD model.
Mice were scored on a scale from 0-3 for the following factors: weight loss, skin inflammation, fur maintenance, pain, deteriorating posture. If a score of 3 in any category or a combined score of 6 occurred, the mouse was sacrificed. Plotted are the average rolling combined GVHD score for each experimental group, split by CAR signaling domain superfamily and Treg:PBMC ratio. If a mouse was sacrificed for a score of 3 in one category, a value of 6 was assigned. Numbers of replicates are as in Figure 4.5, pooled from three independent experiments. Mean without error is shown.

Surprisingly, CD28wt A2-CAR Tregs also provided superior protection in comparison to all the other co-receptors tested. Although at a high ratio CARs encoding CD28mut or ICOS domains were not significantly different from the CD28wt constructs, at low ratios there was a clear and significant benefit for the CD28wt A2-CAR Tregs (Figure 4.5C). Similarly, at both high and low ratios CARs encoding TNFR family co-receptors were ineffective at promoting CAR Treg function; at low ratios survival and GVHD scores that were even lower than for those in mice injected with antigen-non-specific HER2-CAR Tregs (Figure 4.5D). The effects on in vivo survival and GVHD scores were mirrored by engraftment and proliferation of human HLA-

$A2^+$ cells: mice which received CD28wt A2-CAR Tregs consistently had the slowest increase in human $CD45^+$ cell engraftment (Figure A.1 and Figure 4.7) and, in the high ratio mice, lower proportions of circulating HLA-$A2^+$ cells at day 7 (Figure 4.8).

We previously found that circulating CAR Tregs are difficult to detect >7 days after injection[247]. Since CARs encoding TNFR family domains increase CAR T cell longevity[300,301], CAR Treg engraftment and stability was analyzed as the proportion of Myc^+ cells within the $hCD45^+$ gate. At day 7, there was large variation in the frequency (Figure 4.9A) and absolute number (Figure 4.10A) of CAR Tregs between the constructs, but a clear and significant survival advantage for the CD28wt-CAR Tregs. Indeed, at day 14 only mice that received CD28wt-CAR Tregs (Figure 4.10B) had detectable circulating cells.

Further characterization of CAR Tregs in mice in which they were detectable also revealed variation in the maintenance of the expected $FOXP3^+$ phenotype, with the CD28wt-CAR Tregs having the most consistent and high proportion of FOXP3-expressing cells (Figure 4.9B and Figure 4.10C). It has been reported that one property of CAR Tconv is their ability to acquire their target antigen through a process called trogocytosis[318]. In all samples where myc+ CAR T cells were detected, none were HLA-A2+, suggesting that at least in this model and at this time point, trogocytosis does not occur (Figure 4.10D).

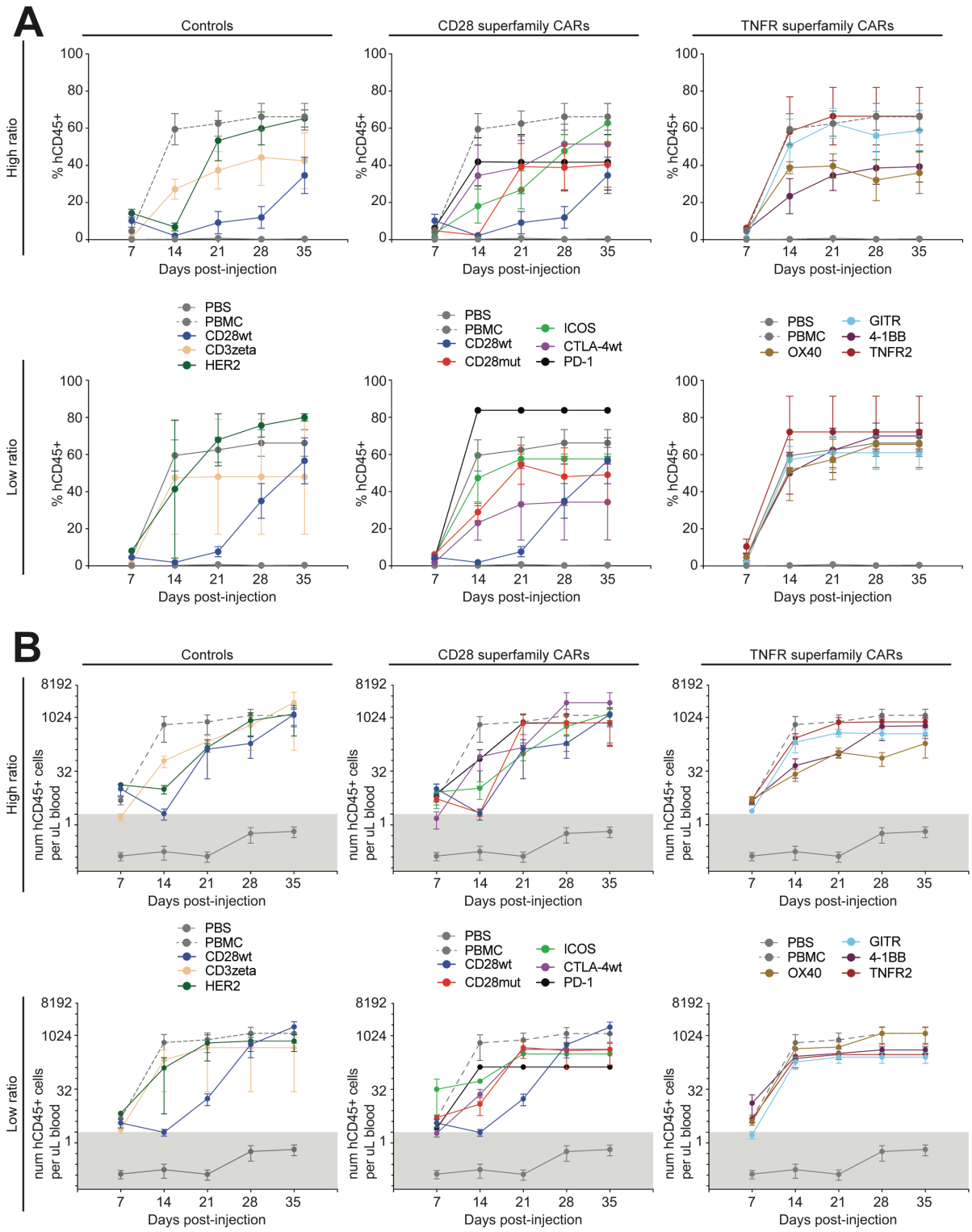

Figure 4.7 hCD45 engraftment in xenoGVHD model.
Mice were bled weekly and at experimental endpoint as per Figure 4.5. Flow cytometry analysis of blood was performed to determine the blood composition. **(A)** Percent of hCD45 engraftment is shown over time, split by Treg:PBMC ratio and CAR signaling domain superfamily. **(B)** Absolute number of hCD45 cells per uL of blood is shown over time. Mean ± SEM.

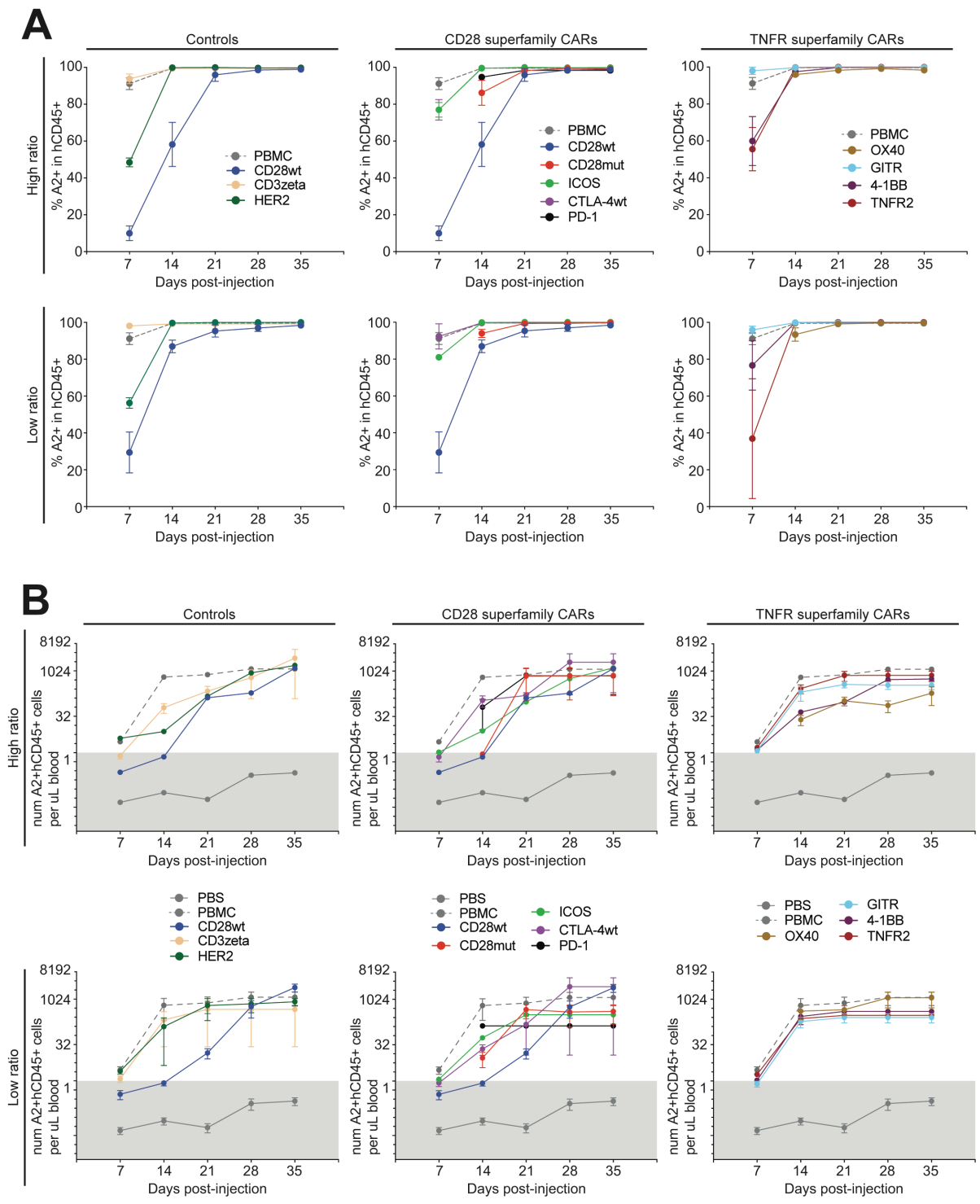

Figure 4.8 HLA-A2+ cell engraftment in xenoGVHD model.
Mice were bled weekly and at experimental endpoint as per Figure 4.5. **(A)** Proportion of A2+ cells in hCD45 subset is shown over time, split by Treg:PBMC ratio and CAR signaling domain superfamily. **(B)** Absolute number of A2+hCD45+ cells per uL of blood is shown over time. Mean ± SEM.

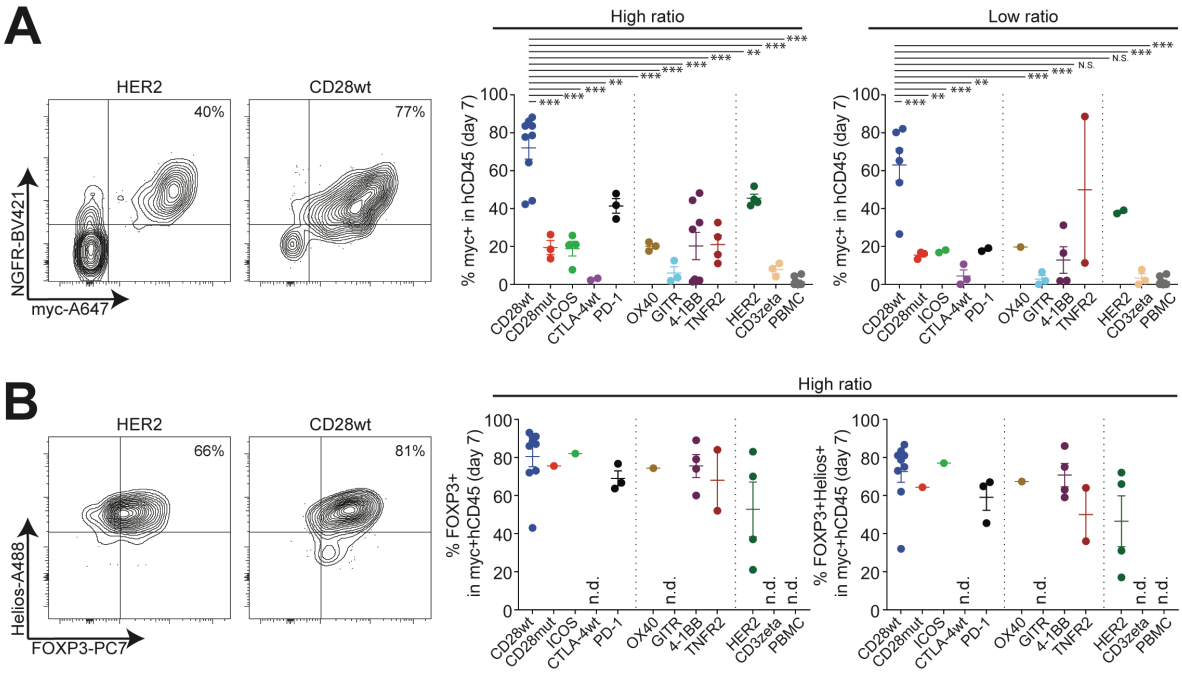

Figure 4.9 In vivo persistence of signaling-domain CAR-variant Tregs in a xenogenic graft-versus-host disease model.

Seven days post-cell injection as in Figure 4.5, the proportion of **(A)** CAR-expressing (myc+) cells within hCD45+ cells and, for mice with sufficient cells, **(B)** FOXP3+ (left) and FOXP3+Helios+ (right) cells within CAR-expressing (myc+) hCD45+ cells was determined. Representative and averaged data are shown. The number of individual mice in each group tested over three independent experiments are indicated on the Figure. Statistics show one-way ANOVA with Holm-Sidak post-test comparing all constructs with at least two data points to CD28wt. Mean ± SEM. * $p < 0.05$, ** $p < 0.01$, *** $p < 0.001$. "n.s." denotes not significant. "n.d." denotes no data where insufficient events to plot a result.

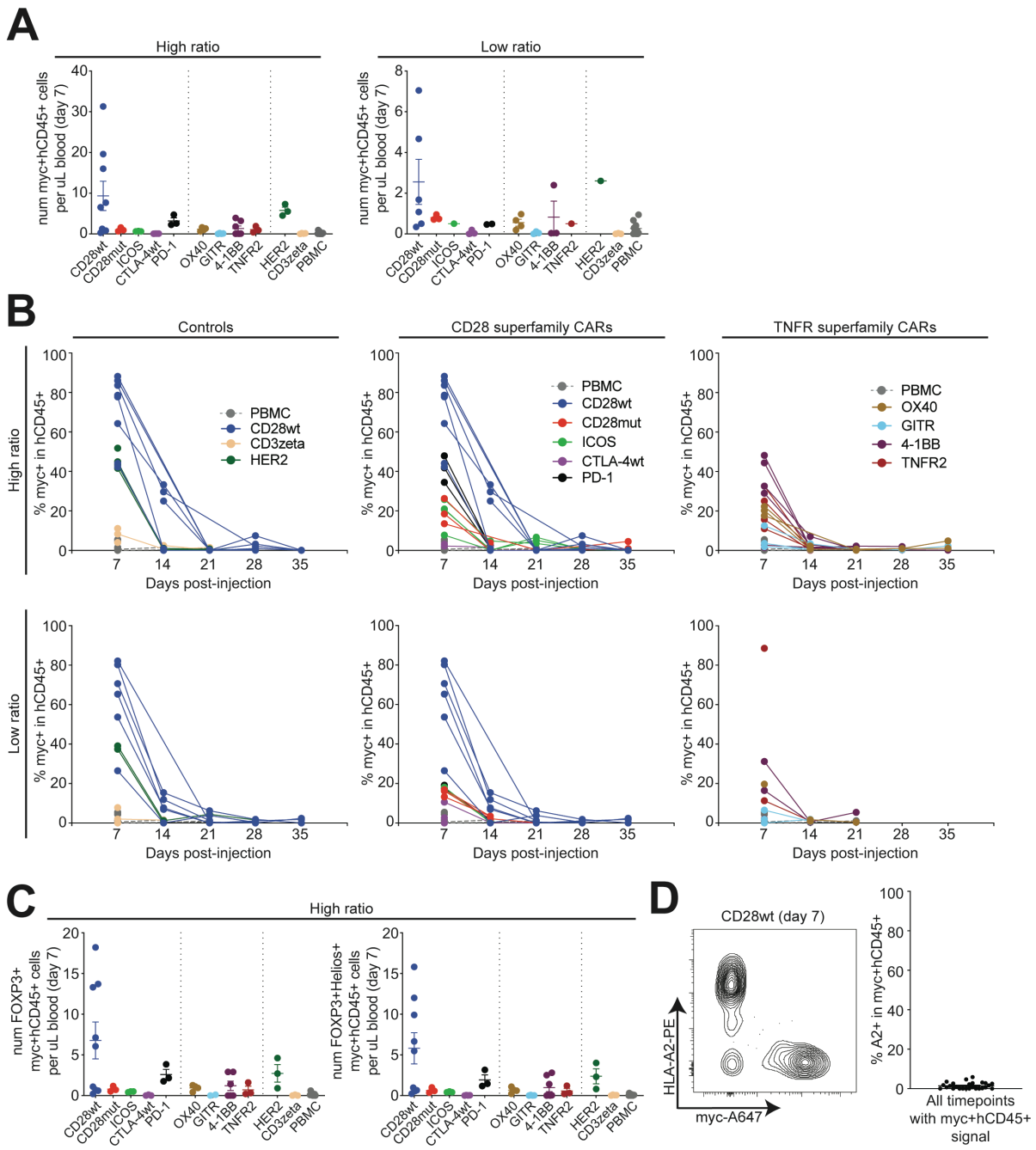

Figure 4.10 Characterization of myc+hCD45+ CAR Tregs in xenoGVHD model.
Mice were bled on day 7 as per Figure 4.5. **(A)** Proportion of myc+ cells in hCD45 subset is shown over time, split by Treg:PBMC ratio and CAR signaling domain superfamily. **(B)** Absolute number of myc+hCD45+ cells per uL of blood was determined on day 7 post-cell injection. Left: high Treg:PBMC ratio mice are shown. Right: low Treg:PBMC ratio mice are shown. **(C)** Absolute number of FOXP3+ myc+hCD45+ (left) FOXP3+Helios+myc+hCD45+ (right) cells per uL of blood was determined on day 7 post-cell injection. High Treg:PBMC ratio is shown. **(D)** Comparison of HLA-A2- and myc-expressing cells. Left: example flow plot of mutually-exclusive HLA-A2 and myc staining. Right: Summary data is shown. Each dot is the average A2+ expression of the myc+hCD45+ population at a single timepoint. Mean ± SEM.

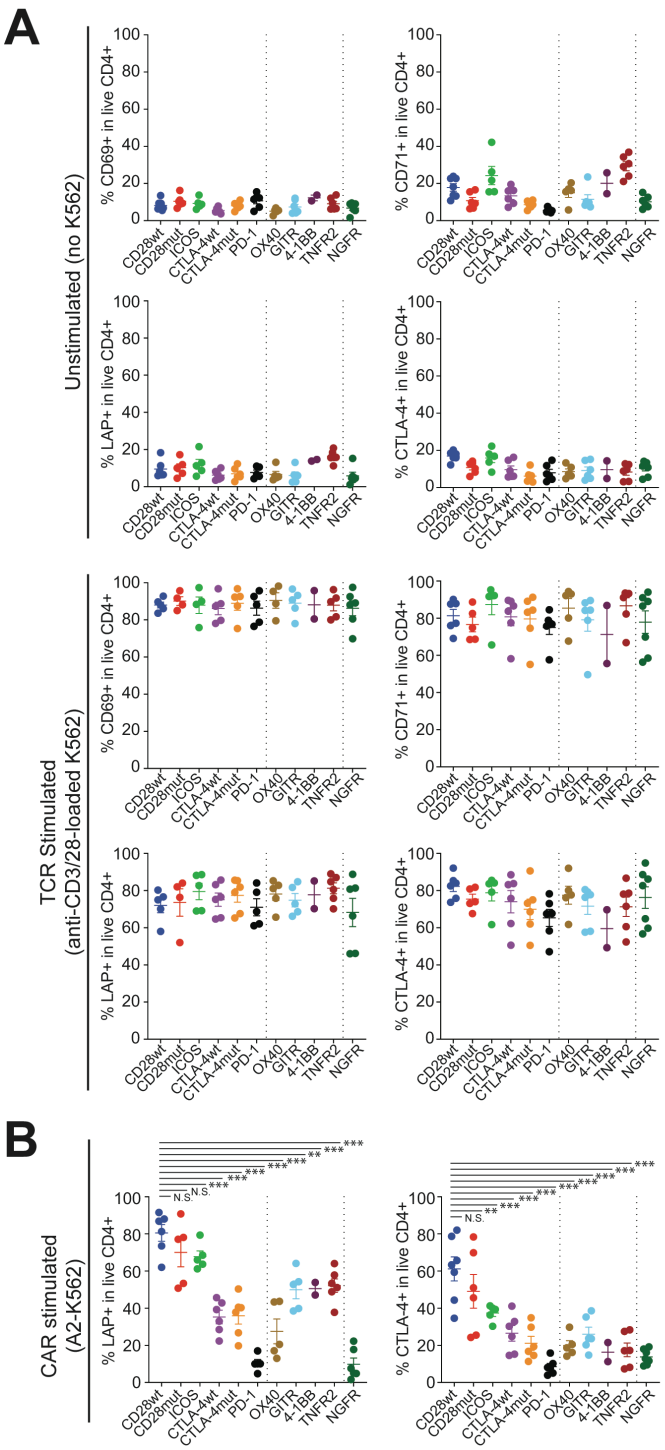

Figure 4.11 Resting state and TCR-activation of signaling domain CAR variants in human Tregs. Human Tregs were transduced and expanded, rested overnight in low IL-2 conditions, then co-cultured with either **(A)** no K562 cells (unstimulated), irradiated anti-CD3/CD28-loaded K562 cells expressing CD64 (TCR-stimulated) or **(B)** HLA-A2-expressing K562 cells (CAR-stimulated) at a ratio of 1 K562 to 2 CAR Tregs. After 24 hours, percent CD69, CD71, LAP and CTLA-4 positive in live CD4 cells was determined. Summary data is shown. Data are n=2-7 donors, pooled from at least two independent experiments. Mean ± SEM. * $p < 0.05$, ** $p < 0.01$, *** $p < 0.001$. "n.s." denotes not significant.

4.2.3 Signaling domain CAR variants differ in their ability to activate Tregs and stimulate cytokine production

The in vitro phenotypic and/or functional features of CAR Tregs that correlate/predict in vivo function are unknown. This series of signaling domain CAR variants provided an ideal opportunity to further explore this question as they had a range of effect in vivo, from highly effective (CD28wt), to moderately effective (e.g. CD28mut and ICOS) to ineffective (TNFR2). We first asked whether the CARs might differ in their ability to stimulate Treg activation. Signaling domain CAR-Treg variants were rested overnight, then stimulated with HLA-A2-expressing K562 cells, and after 24h analyzed by flow cytometry for expression of the activation markers CD69 and CD71. In the absence of stimulation there were no significant differences in expression, demonstrating a lack of tonic signaling (Figure 4.11A). Importantly, the presence of each CAR variant did not affect the ability of CAR Tregs to be activated via the TCR. There was a large variation in the capacity of the different CARs to activate Tregs, with CD28wt and CD28mut stimulating the highest and PD-1 stimulating the lowest expression of both markers (Figure 4.12A).

We next asked how the signaling domain CAR variants affected expression of key Treg-specific effector molecules, including LAP (inactive form of TGF-β), GARP (receptor for LAP), CD39 (ATP/ADP ectonucleoside) and CTLA-4. CAR Tregs were stimulated with HLA-A2-K562 cells for 24h (Figure 4.11B) or 72h (Figure 4.12B) then analyzed by flow cytometry. Similar to results with CD69 and CD71, CD28wt- and CD28mut-CARs stimulated the highest expression of GARP, LAP and CTLA-4. Interestingly, several CARs, even those that were non-functional in vivo (e.g. 4-1BB and TNFR2), stimulated higher expression of CD39, between TCR and CAR stimulation revealed an interesting difference in kinetics: in response to CD28wt

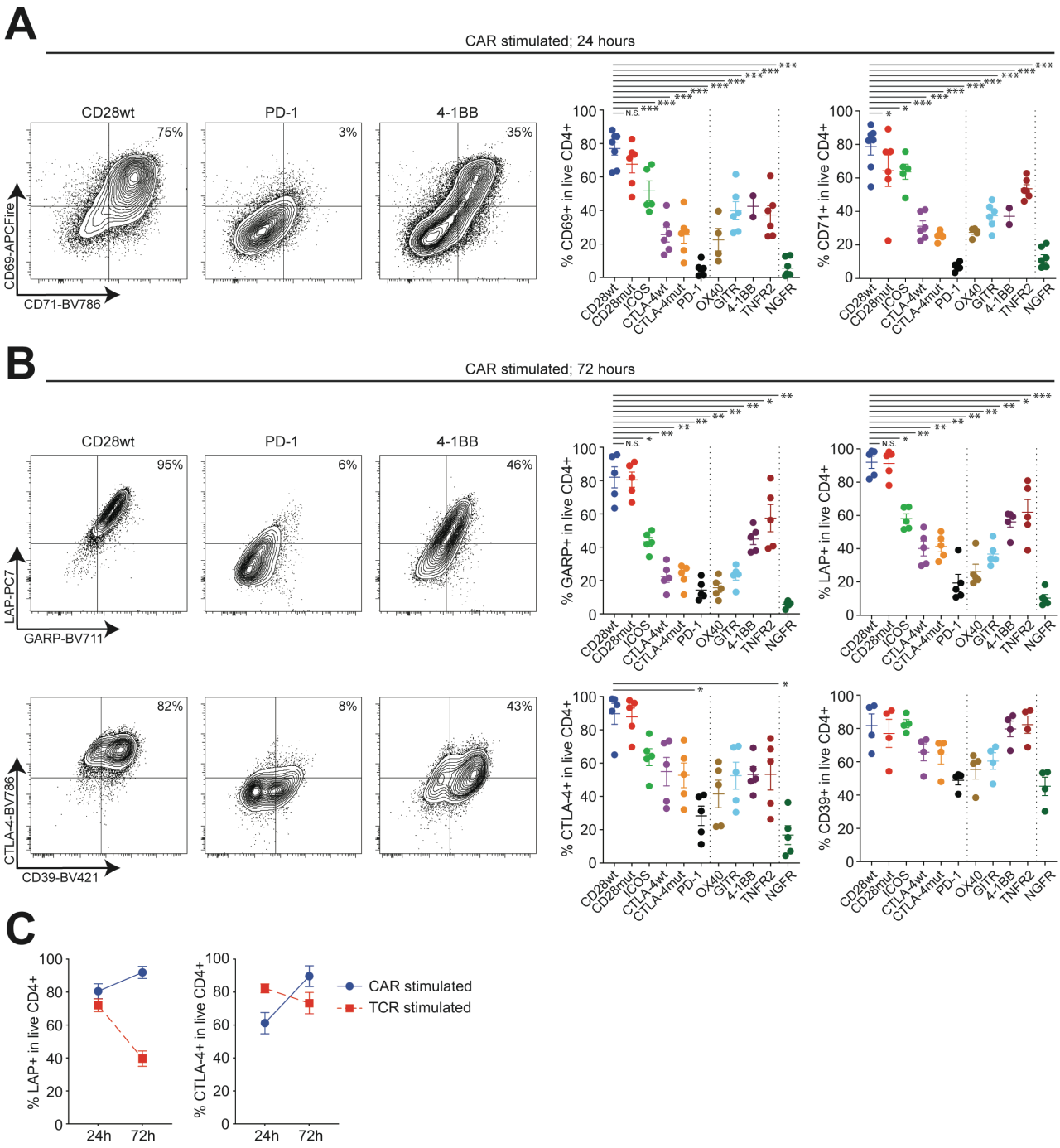

Figure 4.12 Signaling domain CAR variant-mediated expression of activation makers and suppressive proteins. Human Tregs were transduced and expanded, rested overnight in low IL-2 conditions, then co-cultured with irradiated K562 cells expressing HLA-A2 at a ratio of 1 K562 to 2 CAR Tregs. After 24 **(A)** or 72 **(B)** hours expression of the indicated protein was determined by flow cytometry. n=2-7 donors from a minimum of least two independent experiments. Statistics show one-way ANOVA with Holm-Sidak post-test comparing all constructs to CD28wt. **(C)** Kinetics of LAP+ (left) and CTLA-4+ (right) expression on CAR- or TCR-stimulated CD28wt-CAR Tregs from experiments in (A) and (B). Mean ± SEM. * $p < 0.05$, ** $p < 0.01$, *** $p < 0.001$. "n.s." denotes not significant.

A2-CAR, but not TCR, stimulation, expression of LAP and CTLA-4 was reinforced over time (Figure 4.12C).

To ask how the cytokine profile of CAR-stimulated Tregs varied with co-receptor domains, supernatants were collected from cells stimulated via HLA-A2 for 72h and analyzed by cytometric bead assay. In comparison to Tconvs expressing a CD28wt CAR, all Tregs exhibited a low level of cytokine production, either when stimulated through the CAR (Figure 4.13) or TCR (Figure 4.14). None of the CAR Tregs produced detectable amounts of IL-2, IL-4 or TNF

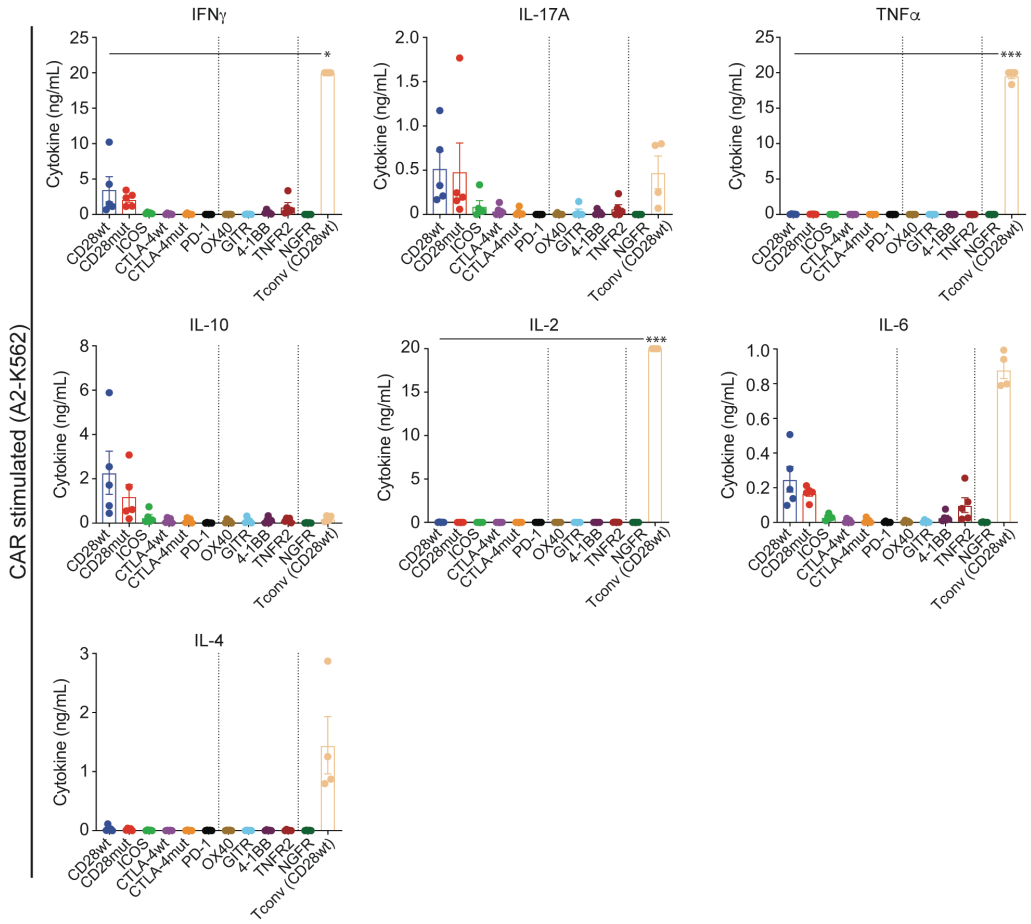

Figure 4.13 Cytokine profile of signaling-domain CAR-variant Tregs (CAR-stimulated).
CAR Tregs were transduced with the indicated CAR and conventional T cells (Tconv, CD4+CD25-CD127+ cells) were transduced with the CD28wt-CAR. Cells were expanded, purified and co-cultured with HLA-A2-expressing K562 cells and after 72 hours supernatants were collected. Amounts of the indicated cytokines were determined by cytometric bead array. Results for all examined cytokines are expressed as a concentration in the supernatant. n=4-5 from at least two independent experiments. Statistics show one-way ANOVA with Holm-Sidak post-test comparing all constructs to CD28wt-Tregs. Mean ± SEM. * $p < 0.05$, ** $p < 0.01$, *** $p < 0.001$.

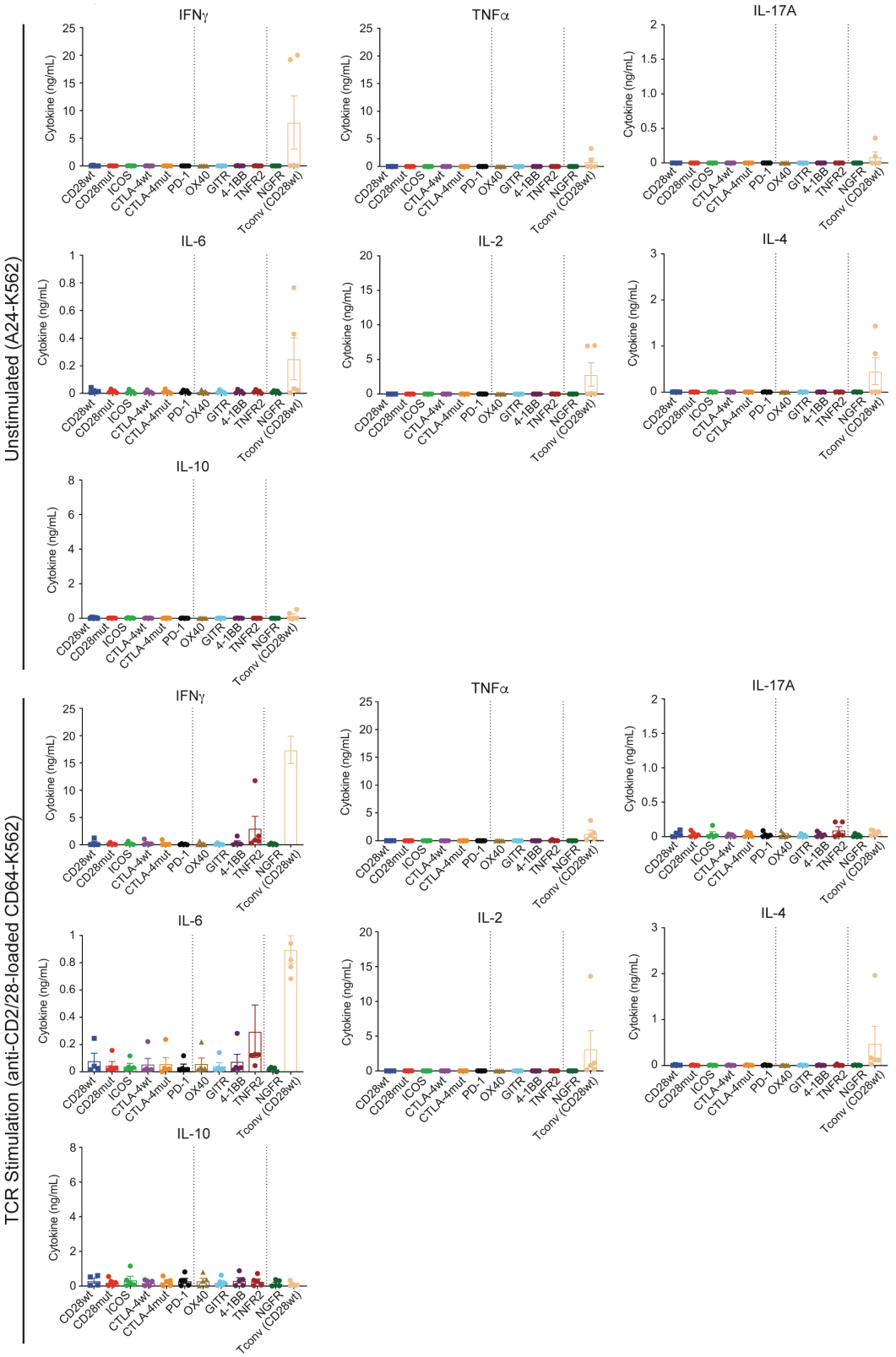

Figure 4.14 Cytokine profile of signaling-domain CAR-variant Tregs (Resting and TCR-stimulated). Experiment co-cultures were set up as in Supplemental Figure 3. After 72 hours, supernatants from co-cultures were diluted 2-fold before being analyzed by cytometric bead array on a flow cytometer. Results for all examined cytokines are expressed as a concentration in the supernatant. Unstimulated (top) and TCR-stimulated (bottom) conditions are shown. Data are n=4-5 donors, pooled from at least two independent experiments.

-α when stimulated with A2 or the TCR. The CD28wt- and CD28mut-CAR Tregs did produce detectable levels of IFN-γ, IL-17A, IL-10 and IL-6 when stimulated via the CAR (but not TCR), but the amounts produced were significantly lower than those from the Tconv control. Notably, contrary to our prediction and a previous report in Tconvs[304], the ICOS-encoding CAR did not stimulate production of IL-10 or IL-17A.

4.2.4 4-1BB and TNFR2 encoding CARs destabilize Tregs

Since 4-1BB is an effective co-stimulatory domain in conventional CAR T cells[319,320], and TNFR2 signaling is well-known to positively affect Tregs[297,314], we were surprised to find that not only did these two CARs not perform as well as the CD28wt-CAR, but that they were significantly worse than the antigen-non-specific HER2-CAR control at protecting mice from GVHD (Figure 4.5). To further investigate the mechanistic basis for this finding we carried out in vitro assays to more extensively investigate the long terms effects of CAR-stimulated Treg activation. Tregs expressing one of the signaling domain variants, or control CARs, were stimulated with beads coated with HLA-A2, with 100U/mL exogenous IL-2, then cell number, expression of FOXP3 and Helios, and the amount of methylation in the Treg-specific demethylation region (TSDR) were monitored for 12 days (Figure 4.15A). Using this system, we found that most CAR constructs did not stimulate Treg proliferation (Figure 4.15B) with only CD28wt, 4-1BB or TNFR2 encoding CARs able to stimulate a significant amount of proliferation in comparison to ΔNGFR control Tregs. Notably, the TNFR2-CAR stimulated significantly more proliferation than the 4-1BB- or CD28wt-CARs, with an average of >16-fold expansion over 12 days. Interestingly, this was the first in vitro assay in which we observed a clear difference between the CD28mut- and CD28wt-CARs, suggesting that this tyrosine residue

(Y173) in CD28 is essential for stimulating Treg proliferation and that this an important property for in vivo function.

Whereas analysis of FOXP3 expression showed no significant difference between the groups, Helios expression revealed significant differences which directly correlated with proliferation. Specifically, only 4-1BB and TNFR2 encoding constructs lost significant amounts of Helios expression (Figure 4.15C). Since Helios expression is thought to be associated with Treg lineage stability[321-324] we next asked whether Tregs expressing 4-1BB and TNFR2 encoding CARs differed in their lineage stability. Accordingly, for these three constructs, we analyzed the methylation status of 8 CpG islands within the Treg-specific demethylated region (TSDR)[17,325] of the *FOXP3* gene (Figure 4.15D). We found that before stimulation via the CAR (day 0) the 3 types of CAR Tregs did not differ in the amount of TSDR methylation, with an almost completely demethylated TSDR. However, after 12 days of stimulation with HLA-A2-coated beads, Tregs expressing the TNFR2-CAR had a marked, ~50% increase in methylation. Tregs expressing the 4-1BB-CAR exhibited an intermediate phenotype, trending toward a more highly methylated TSDR region in comparison to CD28wt-CAR expressing cells. Interestingly, expression of Helios, but not of FOXP3, and TSDR methylation had a strong negative correlation (Figure 4.15E). These data indicate that loss of Helios expression is more highly correlated with Treg lineage instability than is FOXP3.

We next asked if the basis for the differential proliferative capacity between the CD28wt, 4-1BB and TNFR2 encoding CARs, and the other constructs could be due to differences in the proportions of naive versus memory cells. The various CAR Tregs were stimulated via HLA-A2 for 7 days, then analyzed for expression of CCR7 and CD45RA in order to quantify naive, central memory, effector memory, and $CD45RA^{+}$ effector memory cells. Most CARs, including

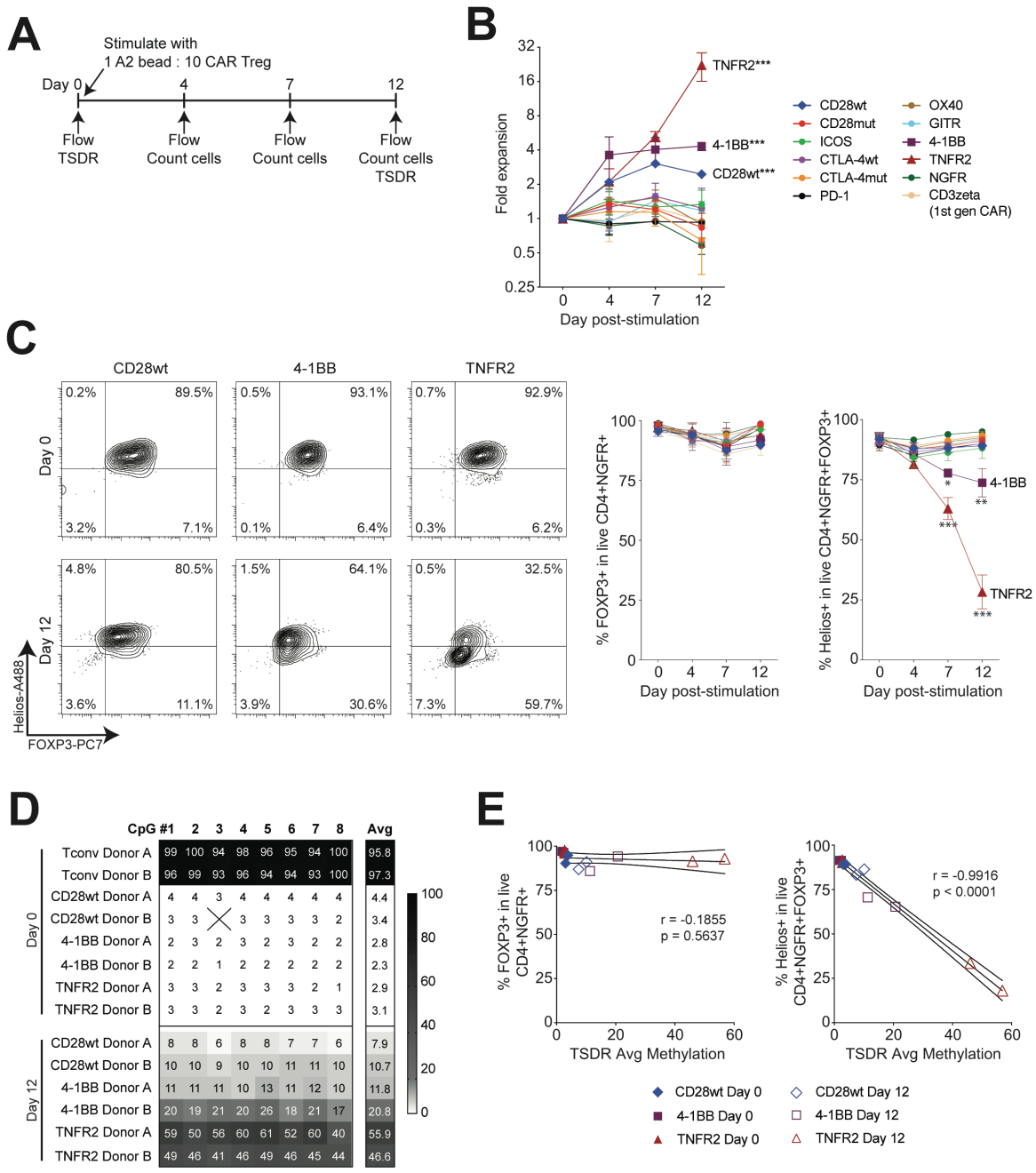

Figure 4.15 Effects of prolonged stimulation of signaling domain CAR variants on Treg stability.
Naïve Tregs (CD4+CD25+CD127-CD45RA+) were sorted, transduced with the indicated signaling-domain CAR variants and expanded for 7 days. After resting overnight in low amounts of IL-2, CAR Tregs were stimulated with beads coated with HLA-A2 at a ratio of 1 bead to 10 CAR Tregs for 12 days. Cells were counted and analyzed via flow cytometry on day 4, 7 and 12. **(A)** Schematic diagram of experiment setup. **(B)** Cell expansion over time. Statistics show overall effects two-way ANOVA with Holm-Sidak post-test comparing all constructs to the NGFR group. **(C)** Flow cytometry analysis of FOXP3 and Helios within live CD4+NGFR+ cells before (day 0) or 12 days after bead stimulation. Representative and averaged data for proportion of FOXP3+ cells within live CD4+NGFR+ and Helios+ cells within live CD4+NGFR+FOXP3+ cells. Data for (A-C) are n=2-3 donors, pooled from at least two independent experiments. Statistics show two-way ANOVA with Holm-Sidak post-test comparing all constructs at each timepoint to CD28wt. **(D)** Pyrosequencing of cells lysed on day 0 and day 12 showing percent methylation of eight CpGs from CNS2 within the *FOXP3* locus known as the Treg-specific demethylated region (TSDR). **(E)** Correlation of average TSDR methylation and percent FOXP3+ or percent Helios+ from (C). For (D-E), n=2 male samples tested from one experiment. Pearson r statistic and two-tailed p value shown. Mean ± SEM. * $p < 0.05$, ** $p < 0.01$, *** $p < 0.001$.

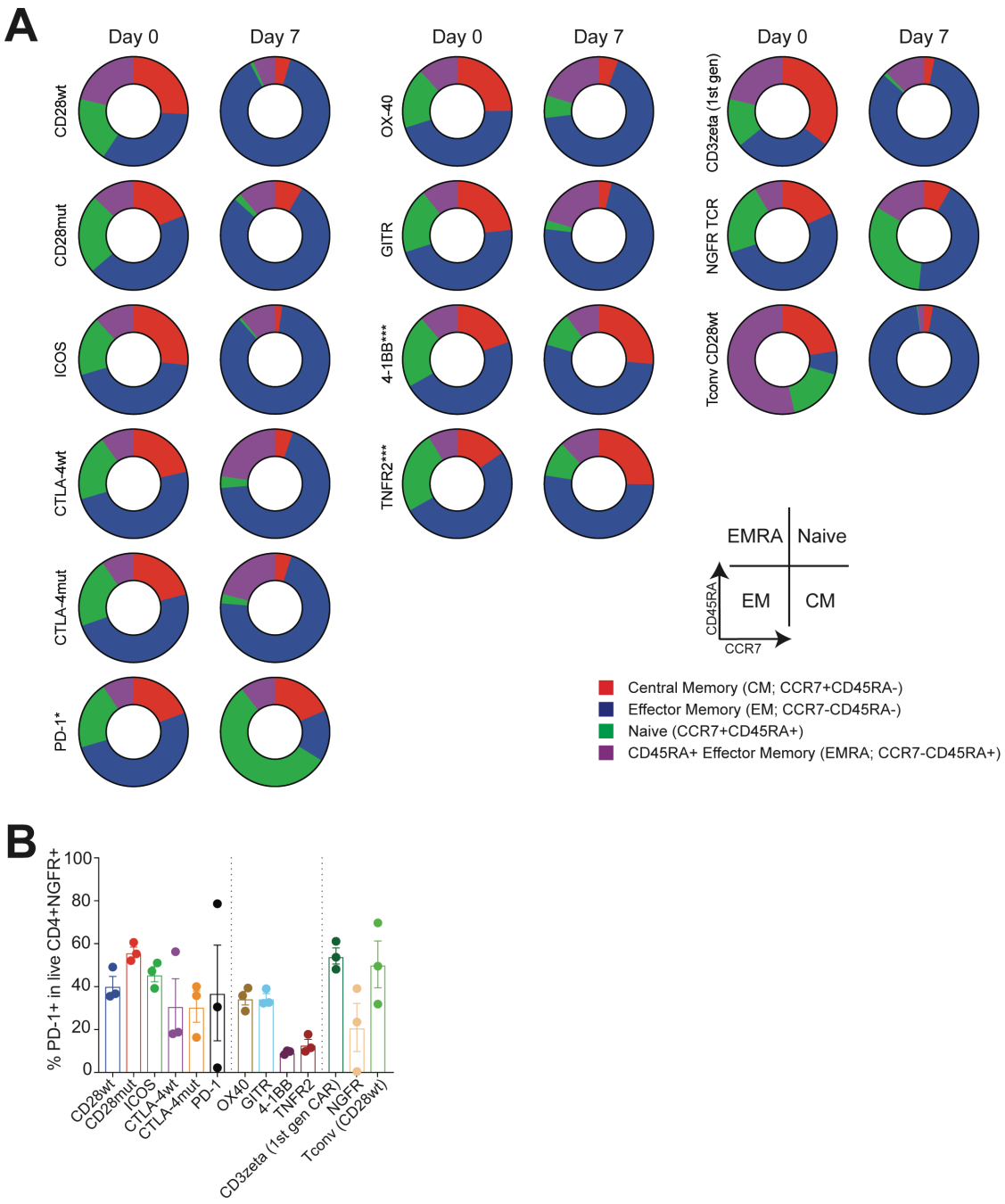

Figure 4.16 Memory subset and exhaustion of signaling variant CAR Tregs after 7-day CAR-mediated expansion.

Signaling variant CAR Tregs derived from naïve Tregs were produced as in Figure 5, then co-cultured for 7 days with irradiated K562 cells expressing HLA-A2 at a ratio of 1 K562 cell to 2 CAR Tregs. **(A)** Using flow cytometry analysis of CD45RA and CCR7 expression in live CD4+NGFR+ cells, memory subset polarization after CAR stimulation was determined. Average subset values are shown for baseline (day 0) and day 7. Statistics show a one-way ANOVA with Holm-Sidak post-test comparing proportion of central memory cells (CD45RA-CCR7+) from CD28wt to all other groups. **(B)** PD-1 expression of CD4+NGFR+ cells. Data are n=3-4 donors, pooled from at least 2 independent experiments. *** $p < 0.001$.

the CD28wt, promoted expansion of Tregs with an effector memory phenotype, with the exception of the 4-1BB- and TNFR2-encoding CARs which preserved high proportions of central memory cells and the PD-1-encoding CAR which had an enhanced proportion of naive cells (Figure 4.16A). By corollary, Tregs stimulated with 4-1BB and TNFR2 CARs also had a trend toward lower PD-1 expression, a cell surface molecular often inversely associated with cell expansion potential (Figure 4.16B).

Overall, these data suggest that the functional in vivo CAR Tregs must be able to proliferate and acquire an effector memory phenotype, but that excessive and rapid proliferation is detrimental, leading to instability and an unfavorable central memory phenotype.

4.2.5 Suppression of antigen presenting cells is a better predictor of CAR Treg in vivo function than suppression of T cells

Tregs suppress many different types of immune cells via different mechanisms, with a growing appreciation for the important role of CTLA-4 mediated suppression of dendritic cells[312] in addition to classical direct suppression of T cell proliferation. We next sought to measure the suppressive capacity of the signaling-domain CAR variants towards these two different cell types. To measure direct suppression of T cells we set up an assay in which A2-negative T cells were pre-stimulated with anti-CD3/28 beads for one day, then the beads removed, and the cells were cultured for 72h in the absence or presence of the various signaling-domain A2-CAR Tregs, which had been previously stimulated with A2-coated beads (Figure 4.17A). Consistent with the in vivo data (Figure 4.5), CD28wt-CAR Tregs suppressed both $CD4^+$ and $CD8^+$ T cells more potently than all other CAR constructs (Figure 4.17B&C). However, distinct from the in vivo data, most CAR variants, including 4-1BB and TNFR2, were superior to the control

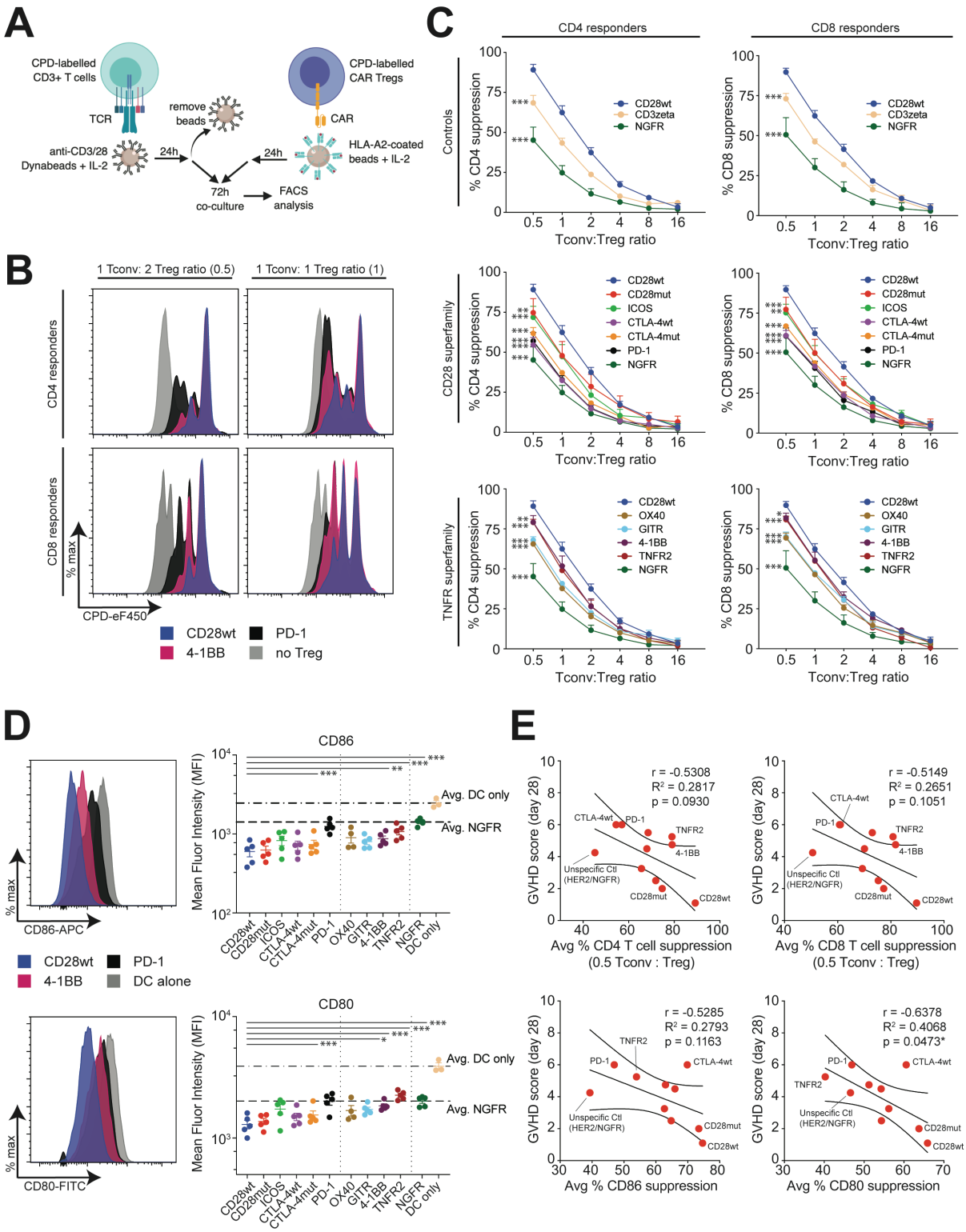

Figure 4.17 Suppressive properties of signaling-domain CAR Treg variants.

(A-C) In vitro indirect T cell suppression assay. Cell-proliferation dye (CPD) 450-labelled responder HLA-A2^{neg}CD3+ T cells were pre-stimulated for one day with anti-CD3/CD28 dynabeads and IL-2 before being co-cultured without or with different ratios of cell-proliferation dye 670-labelled CAR Tregs. The CAR Tregs were pre-stimulated with HLA-A2-coated beads and IL-2. After co-culture for 72h, division of gated CPD-450^{+} CD4^{+} or CD8^{+} responder T cells was determined by flow cytometry. **(A)** Schematic diagram of experiment setup.

continued on next page

(B) Percent suppression was calculated using the ratio of the division index of the experimental condition over wells with no Tregs added. Representative (B) and averaged (C) data are shown. The NGFR and CD28wt Treg groups are repeated in the various graphs. n=3, averaged from two independent experiments. Statistics show overall effects two-way ANOVA with Holm-Sidak post-test comparing all constructs to CD28wt. **(D)** In vitro suppression of co-stimulatory molecule expression on dendritic cells. HLA-A2+ monocyte-derived dendritic cells were matured then co-cultured with the indicated type of CAR Treg (ratio of 1 dendritic cell to 2 CAR Tregs) for 72 hours. Flow cytometry analysis of mean fluorescence intensity of CD86 and CD80 on gated dendritic cells with representative and averages data shown. n=3-5, pooled from at least three independent experiments. Statistics show one-way ANOVA with Holm-Sidak post-test comparing all constructs to CD28wt. Mean ± SEM. **(E)** Correlation analyses comparing day 28 GVHD score to suppression of CD4 or CD8 T cell proliferation, or suppression of CD86 or CD80 co-stimulatory molecule expression on DCs. Suppression of CD86/CD80 expression was calculated using the ratio of MFI of the experimental condition over MFI of the control without Tregs (DC only). Statistics shown are Pearson correlation coefficient showing a line of best fit with 95% confidence intervals. * $p < 0.05$, ** $p < 0.01$, *** $p < 0.001$.

transduced ΔNGFR Tregs at suppressing T cell proliferation.

We then tested the ability of the various CAR Tregs suppress dendritic cells (DCs) on the basis of reduced expression of CD80 and CD86[326,327]. HLA-A2$^+$CD14$^+$ monocytes were cultured for 7 days in IL-4 and GM-CSF and matured for the last 2 days in a pro-inflammatory cytokine cocktail as described[327]. Matured DCs were then co-cultured with CAR Tregs to test their ability to suppress expression of co-stimulatory ligands on DCs. We found once again that the most potent effect was mediated by the CD28wt-CAR, and that in this case the 4-1BB and TNFR2 encoding CARs had a significantly lower ability to cause diminished expression of CD80 (Figure 4.17D). Expression of CD83 or HLA-DR were unaffected by CAR Tregs (Figure 4.18).

Since in vitro suppression assays are often used to predict in vivo Treg function, we sought to determine if this was an accurate assumption by carrying out correlation analyses. We used the day 28 GVHD score from our in vivo experiments as a surrogate of in vivo suppressive function and asked how well survival correlated with T cell and/or DC suppression assays (Figure 4.17E). While there was a trend towards a correlation between suppression of CD4$^+$ and CD8$^+$ T cell proliferation and CD86 expression and in vivo GVHD score, the only significant correlation was with suppression of CD80.

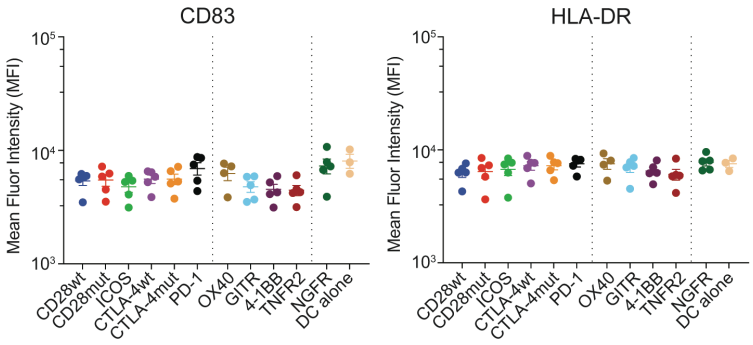

Figure 4.18 Summarized data for co-stimulatory molecules CD83 and HLA-DR from DC suppression assay.
In vitro suppression assay of co-stimulatory molecule expression on dendritic cells was set up as in Figure 4.17. Data are n=3-5 donors, pooled from at least three independent experiments. Mean ± SEM.

4.2.6 Gene expression analysis reveals CD28wt-CAR Treg are enriched in cell cycle and proliferation pathways compared to poorly functioning CAR Tregs

Finally, we asked how the various signaling domain CAR variants differed in their modulation of Treg gene expression. CAR Tregs were expanded, purified as described above before co-culture with A2-coated beads for 24h then lysed for RNA sequencing. Controls consisted of ΔNGFR-transduced Tregs or Tconv either unstimulated or αCD3/28-stimulated with beads. Paired-end libraries were created from isolated RNA and sequences on a NextSeq 500 Illumina sequencer. Reads that mapped to the transgene sequences were filtered out to enable comparisons between groups and CAR- versus TCR-stimulation (Figure 2.1). Differential expression analysis was performed on the raw counts from filtered, aligned sequences, which were scaled for library size. Within the Treg groups a number of differentially expressed transcripts were identified, with a heatmap depicting the top 50 differentially expressed genes shown in Figure 4.19. Strong patterns emerged, with clear similarities between unstimulated and PD-1-CAR Tregs, and CD28wt-, CD28mut- and TCR-stimulated Tregs.

Guided by the results from the xenoGVHD study (Figure 4.5), we then asked if there were differences in the transcriptional profile between the CAR Tregs that performed the poorest - defined as groups where none of the mice survived to endpoints (CTLA-4wt and CTLA-4mut, PD-1, TNFR2, CD3zeta) versus the optimal CD28wt-CAR (Figure 4.20A, Table B.1). We found that CD28wt-CAR Tregs were highly enriched for several genes targeted by transcription factors associated with cell proliferation and DNA replication, such as the MCM complex, MYB and E2F4. NFKB1 and RELA transcription factor targets were also elevated, indicating that the NF-κB signaling pathway may be important for cell cycling and proliferation secondary to CAR

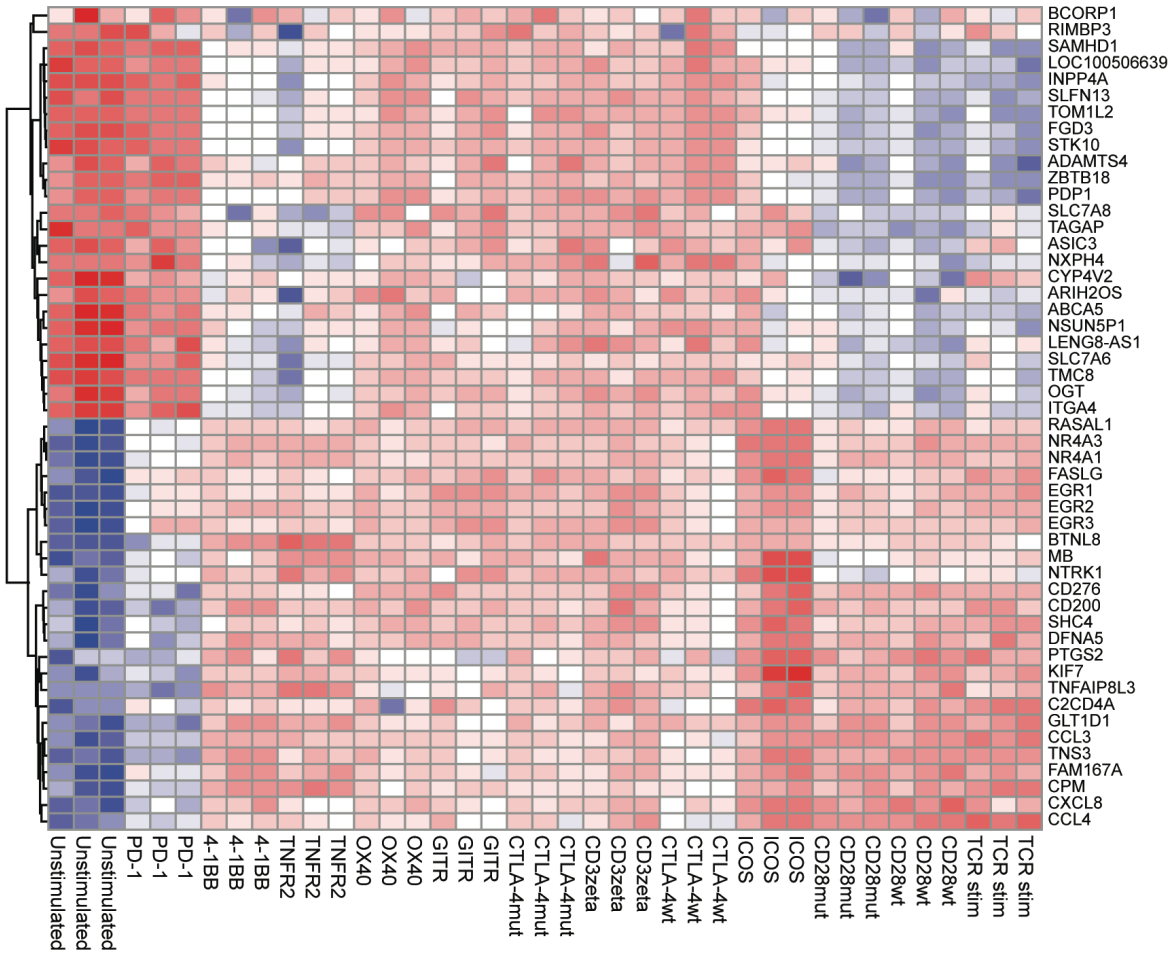

Figure 4.19 Effects of signaling domain CAR variants on the Treg transcriptome.
Purified CAR Tregs were stimulated with HLA-A2-coated beads (CAR stimulated) or anti-CD3/CD28 coated Dynabeads (TCR stimulated) for 16 hours, then processed for RNA sequencing. Reads that mapped to transgene sequences were filtered out as described in Figure 2.1. Heatmap showing the top 50 differentially expressed genes compared with unstimulated Tregs.

activation. Pathway analysis showed that CD28wt-CAR Tregs also had elevated transcripts associated with mTORC1 signaling, G2M checkpoint and myc targets, supporting the concept that cell cycling is an important component of CAR Treg function.

CD28wt-, 4-1BB- and TNFR2-CAR Tregs all proliferated in response to A2, but only CD28wt-CAR Tregs maintained Helios expression (Figure 4.15), so we queried how the transcriptional profile of 4-1BB- and TNFR2-CAR Tregs differed from that of the CD28wt-CAR (Figure 4.20B, Table B.2). We found that in comparison to the 4-1BB- and TNFR2-CARs, the

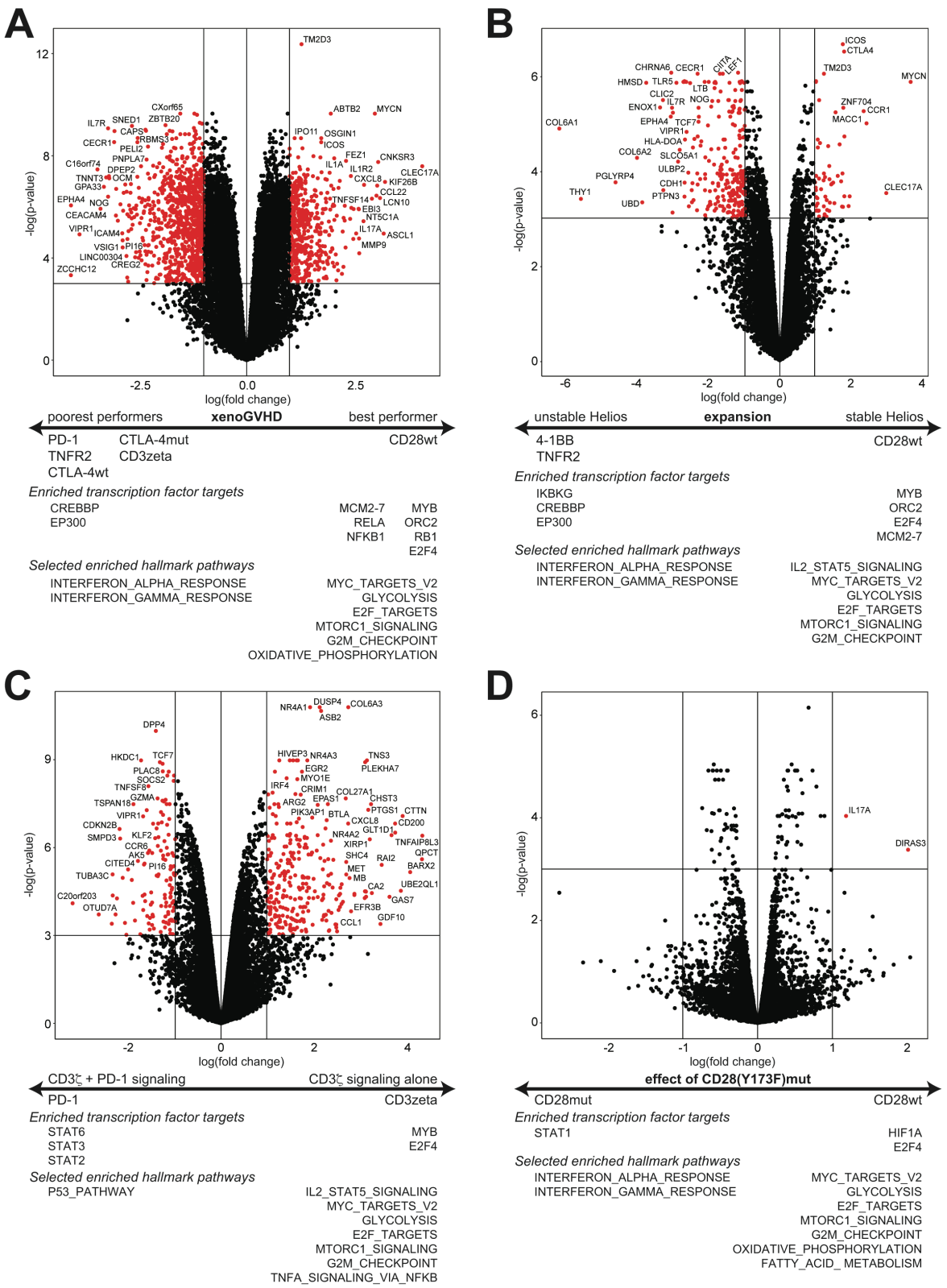

Figure 4.20 Effects of signaling domain CAR variants on the Treg transcriptome.
CAR Tregs were prepared and stimulated as in Figure 4.19. **(A)** Differentially expressed genes between CD28wt and PD-1, TNFR2, CTLA-4wt, CTLA-4mut, CD3zeta to highlight differences in the transcriptome between CD28wt-CAR Tregs and the CAR Treg groups for which no mice remained at the experimental endpoint (day 42) of the xenoGVHD study. **(B)** Differentially expressed genes between CD28wt-CAR Tregs and 4-1BB/TNFR2-CAR Tregs to highlight differences in gene

continued on next page

expression between constructs that all stimulated proliferation, but for which the 4-1BB and TNFR2 domains promoted Treg instability. **(C)** Differentially expressed genes between CD3zeta- (first-generation CAR) and PD1-CAR Tregs to highlight the negative effects of PD-1 signaling on CD3zeta signaling in Tregs. **(D)** Differentially expressed genes between CD28wt- and CD28mut-CAR Tregs to highlight the transcriptome differences caused when stimulated via mutated CD28(Y173F) in Tregs. Volcano plots (above) and selected results from enrichment analysis of transcription factor targets and hallmark pathways (below). Full lists of differentially-expressed transcription factor targets and hallmark pathways with normalized enrichment scores and adjusted p values are found in Table B.1-4. Full lists of differentially-expressed genes are available as online supplemental resources. n=3 from two independent experiments.

CD28wt-CAR had higher expression of ICOS and CTLA-4, but lower IL7R (CD127). As in Figure 4.20A, pathway analysis revealed that the CD28wt-CAR Tregs had elevated transcription factor targets and pathways associated with cell cycle and division. On the other hand, 4-1BB- and TNFR2-CARs were elevated in inflammatory cytokine response pathways (IFN and TNF) and similar to findings in Figure 4.20A, were enriched in CREBBP and EP300 transcription factor targets. IKBKG transcription factor targets were also elevated in 4-1BB and TNFR2 samples, a transcription factor associated with suppression of the NF-κB pathway.

Interestingly, we noticed that the top differentially expressed genes in the PD-1-CAR Tregs were more similar to unstimulated cells than the CD3zeta-CAR (Figure 4.20C). We therefore performed an enrichment analysis to determine the pathways stimulated by PD-1 that override CD3ζ activating signals (Figure 4.20C, Table B.3). In accordance with an activated phenotype, CD3zeta-CAR Tregs had higher expression of transcripts associated with cell cycling and proliferation. We found that the PD-1-CAR was enriched for genes associated with the p53 tumor suppressor gene pathway, providing a potential mechanism for how inhibitory PD-1 signaling functions in Tregs.

Since the CD28mut-CAR Tregs failed to proliferate after CAR stimulation in vitro and, in comparison to CD28wt-CAR Tregs, had a diminished function in vivo, we next interrogated the transcriptional differences between these two cell types (Figure 4.20D, Table B.4). These data showed that there were only two differentially expressed genes, *IL17A* and *DIRAS3*, but that

the CD28wt-CAR Tregs were enriched in pathways related to cell cycle and metabolism. These data indicate that the functional differences between these CARs is likely related to differences in post-transcriptional events (e.g. protein phosphorylation) which are not evident from short term gene expression analysis.

4.2.7 Differences in CAR- versus TCR-stimulated gene expression in Tregs and Tconv cells

To date there has been no analysis of how CAR-stimulated gene expression in Tregs compares to TCR stimulation, or of that in CAR Tconv cells. We this also compared the transcriptional profiles of CD28wt-CAR versus αCD3/28-stimulated Tregs (Figure 4.21A, Table B.5), finding an overall similar pattern of gene expression, with only a handful of differentially expressed genes. Gene set enrichment analyses revealed that both stimuli upregulated transcripts associated with proliferation, but that the CD28wt-CAR stimulated Tregs were enriched gene associated with response to pro-inflammatory cytokines. These data indicate that, at least for the anti-A2 scFv, stimulation via the CD28wt-CAR in Tregs faithfully replicates endogenous TCR/CD28 signaling activated by αCD3/28 crosslinking. We repeated this analysis using CAR Tconv cells and noted an enrichment of pro-inflammatory cytokines, e.g. *IL2, IL13, and IL5*, and genes associated with cytokine response in CAR-stimulated versus TCR-stimulated cells (Figure 4.21B, Table B.6). Conversely, TCR-stimulated cells were enriched for genes associated with proliferation and DNA replication. Interestingly, like Tregs, CAR-stimulation in Tconvs had upregulated transcripts associated with NF-κB-related transcription factors, e.g. NFKB1, REL and RELA, which could be due to differences in the immunological synapse between CAR- and TCR-ligation[289].

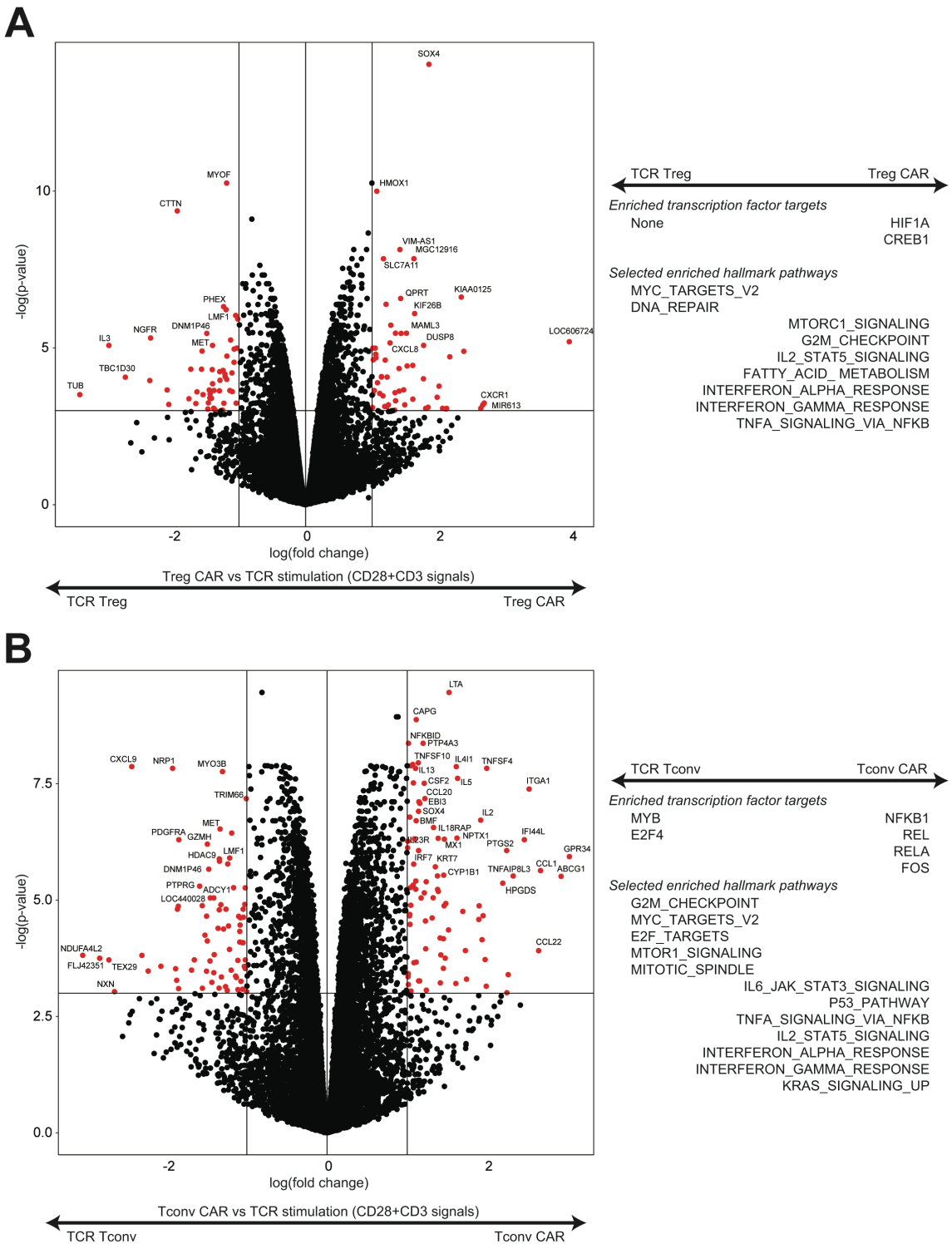

Figure 4.21 Transcriptome analysis comparing CAR and TCR stimulation in human Tregs and Tconv. Purified ΔNGFR/CAR Tregs or Tconv were stimulated with anti-CD3/CD28-dynabeads or HLA-A2-coated beads for 16 hours, then processed for RNA sequencing. Reads that mapped to transgene sequences were filtered out as described in the Methods to specifically observe effects of CAR stimulation. **(A)** Differentially expressed genes between CAR- and TCR-stimulated Tregs. **(B)** Differentially expressed genes between CAR- and TCR-stimulated Tconv. (Left) Volcano plots. (Right) Selected results from enrichment analysis of transcription factor targets and hallmark pathways. Full lists, normalized enrichment scores and adjusted p values are found in Table B.5-6.

To further understand the biology of CD28wt-CAR Tregs we also compared gene expression stimulated by the CD28wt-CAR expressed in Treg versus Tconvs (Figure 4.22, Table B.7). These data revealed a large number of differentially expressed genes, many of which were consistent with the expected Treg and Tconv phenotypes. For example, The CD28wt-CAR Tregs were enriched for *FOXP3*, *IKZF2* (Helios) as well as for numerous genes associated with suppressive Tregs, such as *CTLA4*, *FCRL3*, *LRRC32* (*GARP*), and *TIGIT*[328,329]. CAR Tregs also exhibited upregulated transcription of genes associated with TGFβ, IL2/STAT5, and NF-κB signaling. Tconv expressed a number of effector cytokines, e.g. *IL2*, *IL5*, *IFNG*, *IL13*, and *IL9*. Interestingly, this comparison showed that CD28wt-CAR Tconvs were enriched for many of the same proliferation-related transcription factor targets that were evidence in the CD28wt-CAR Tregs when compared to poorly functional CAR Tregs. These data suggest that although proliferation is an important feature of functional CAR Tregs, it is at a lower level than in CAR Tconvs.

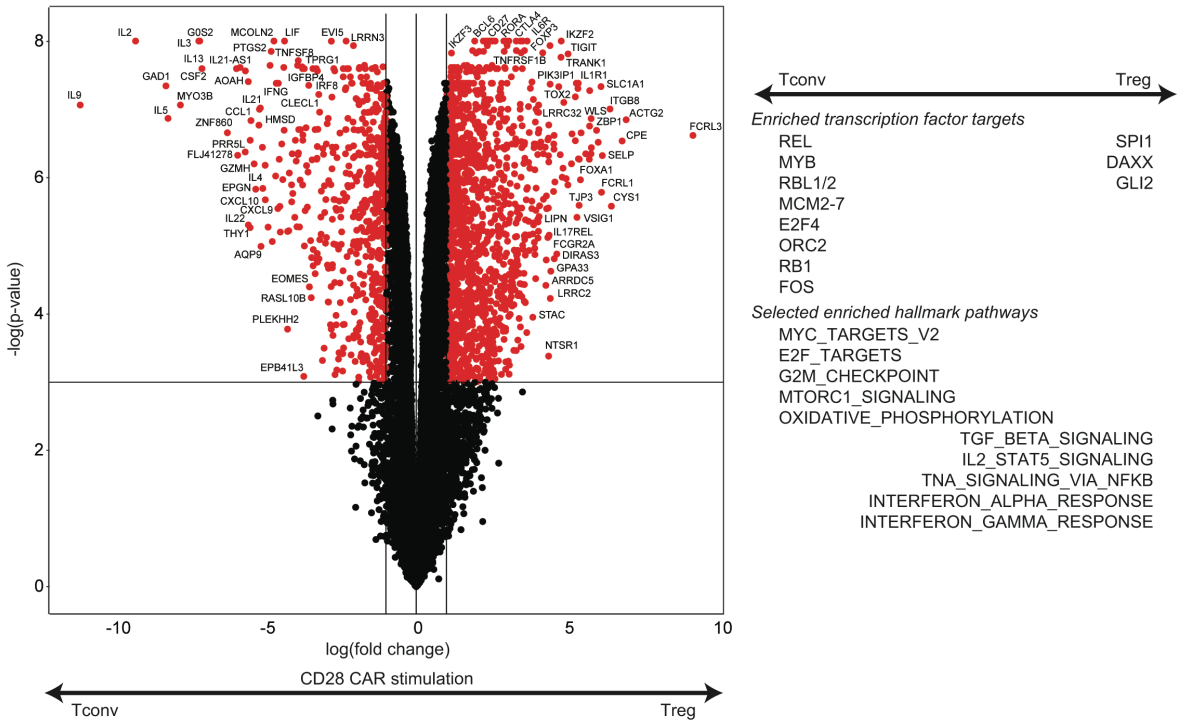

Figure 4.22 Transcriptome analysis of CD28wt-CAR in human Tregs and Tconv.
Purified CAR Tregs or CAR Tconv were stimulated with HLA-A2-coated beads for 16 hours, then processed for RNA sequencing. Reads that mapped to transgene sequences were filtered out as described in the Methods to specifically observe effects of CAR stimulation. Differentially expressed genes between Tregs and Tconv expressing a CD28 CAR to highlight differences in transcription program between CAR Tregs and CAR Tconv. (Left) Volcano plots. (Right) Selected results from enrichment analysis of transcription factor targets and hallmark pathways. Full lists, normalized enrichment scores and adjusted p values are found in Table B.7.

4.3 Discussion

Here we report the first comprehensive comparison of co-receptor signaling domains CAR variants in Tregs, revealing key features of CAR Treg biology and discovering in vitro assays which do, or do not, correlate with in vivo function. Surprisingly, and distinct from findings with CAR Tconvs, we found that inclusion of the wild type CD28 co-stimulatory domain was essential for potent function. No other CD28-family member tested could substitute for CD28, even a version of CD28 with a single point mutation was inferior. Moreover, CARs encoding domains from TNFR family members were unable to confer a significant protective effect in comparison to antigen-non-specific control Tregs. These data show that Tregs and Tconv cells have distinct requirements for optimal CAR-mediated suppression/effector function and reveal new aspects of Treg biology that can be used to further optimize CAR design.

Importantly, no single in vitro assay was predictive of the in vivo effect of CAR Tregs. Of particular note was the limited correlation between in vivo function and three assays which are commonly used to gauge human Treg function: CAR-mediated stimulation of activation/functional markers, proliferation, and in vitro suppression of T cells. Rather, the in vitro assay that most strongly correlated with GVHD score at day 28 was suppression of CD80 on mature DCs co-stimulatory molecule suppression assay. These data support the notion that APCs play a key role in mediating and propagating Treg suppression. Notably, CD80 has a higher affinity for CTLA-4 than does CD86[312], consistent with the finding that CD28wt-CAR Tregs had high and prolonged CTLA-4 expression. Our data also indicate that strong CAR-stimulated proliferation is essential for in vivo function, but that this must not be at the expense of lineage stability.

It has been shown previously that the level of CAR expression affects function[305], leading to the possibility that some of our findings could be related to the observed differences in mean fluorescence intensity of CAR expression. Indeed, all but the CD28mut-CAR had a significantly lower MFI in comparison to the CD28wt-CAR, as well as diminished abilities to stimulate expression of key Treg effector proteins (*i.e*. LAP, GARP and CTLA-4). However, it seems unlikely differences in expression would be the sole explanation for the observed differences. Many CARs were capable of stimulating in vitro suppression of T cell proliferation and dendritic cell expression of CD80/86 and, despite being expressed at the same level as the CD28wt-CAR, the CD28mut-CAR was unable to proliferate in response to A2-mediated stimulation in vitro. Moreover, although the ICOS- and OX40-CARs were expressed at significantly lower levels than the CD28wt-CAR, at high ratios they both provided a survival benefit in vivo in comparison to mice treated HER2-CAR Tregs.

We were surprised to find such a clear difference between the CD28wt-CAR and all other CAR constructs tested in the in vivo xenogeneic GVHD model, an effect that was particularly striking at low Treg:PBMC ratios. Although all of the in vitro assays trended towards the superiority of the CD28wt-CAR, no single in vitro assay could have predicted this in vivo outcome. The CD28wt-CAR Tregs clearly survived better in vivo and indeed, at day 7, this group had a significantly higher absolute number of $CAR^{+}FOXP3^{+}Helios^{+}$ cells in circulation compared to all the other groups. The observed survival advantage of the CD28wt-CAR Tregs in vivo is supported by the transcriptome analysis which showed an enrichment for many cell cycle/proliferation/DNA replication related pathways (e.g. ORC, MYC and the MCM complex), as well as the ability to proliferate in response to A2 in vitro. However, the simple ability to

stimulate proliferation is clearly not sufficient because the proliferative signals activated by the 4-1BB and TNFR2-CARs led to loss of TSDR methylation and Helios expression.

Notably, the distinction between the downstream effects of CD28wt- and 4-1BB/TNFR2-CAR-stimulated proliferation was evident on the basis of Helios but not FOXP3 expression. Helios is dispensable for Treg development but required for Treg stability and suppressive function; mice without Helios^{+} Tregs are unable to control peripheral immune effector cells or prevent colitis[321-324]. It is possible that this observation could also be explained by preferential expansion of contaminating non-Treg cells, but this seems unlikely given that TSDR analysis prior to CAR stimulation showed all cell populations had an almost completely demethylated TSDR.

Interestingly, transcriptome analysis revealed a strong enrichment in the NF-κB pathway/target genes in CD28wt-CAR Tregs. This finding is consistent with the fact that CD28 co-stimulation activates the NF-κB pathway via Protein kinase C[330,331] and that both p65 (Rela) and c-Rel (Rel) have important roles in Treg development, maintenance, and function[332-335]. We also detected a decrease in the level of CREBBP (CBP) and EP300 (p300) transcriptional targets. The CBP/p300 complex contains a bromodomain that binds acetylated histones on the *FOXP3* promoter, a process shown to be critical for promotion of Treg development and stability[336-338], However, we do not detect a destabilization of FOXP3, nor defects in other Treg functional properties, so the observed changes in gene expression related to this pathway are not sufficiently strong to result in a functional Treg defect.

Based on the extensive evidence for the benefit of 4-1BB encoding CARs in anti-tumour directed CAR T cells, we were surprised to find that inclusion of this domain provided no apparent benefit for Tregs. This finding is consistent with a recent report from Boroughs et al

who used a CD19 CAR system to compare the function of first generation, CD28 or 4-1BB encoding CARs in Tregs[248]. They found that a 4-1BB CD19-CAR stimulated expression of CTLA-4 and LAP but had diminished suppressive function in vitro. Previous reports on the function of 4-1BB in Tregs have been conflicting with some evidence showing promotion of Treg proliferation and suppression[83,86,87], and other showing that 4-1BB signaling inhibits Treg suppression[89,90,339]. We were also surprised to find no benefit for inclusion of a TNFR2 domain, given the extensive evidence for the beneficial effect of TNFR2 ligation on Treg proliferation in other systems[119,277,340]. Although both 4-1BB- and TNFR2-CAR Tregs proliferated in response to A2 in vitro, they did not have a survival advantage in vivo. Relative to the CD28wt-CAR, 4-1BB- and TNFR2-CAR Tregs upregulated transcriptional pathways involved in type I and type II interferon response and TNFα signaling, and down regulated those associated with IL2/STAT5 signaling, glycolysis and mTORC1 signaling, findings consistent with the observed destabilized Treg phenotype. Moreover, 4-1BB and TNFR2 had higher relative expression of IKBKG targets, which is involved in the negative regulation of NF-κB signaling, further suggesting that this axis is important in CAR Treg function.

Both GITR and OX40 have well-established roles in Treg development in the thymus[92], but their role in the periphery is unclear and nuanced. Some reports show that stimulation via OX40 or GITR decreases Treg suppressive capability[95,98,99,102,105,108] with others reporting a benefit for Treg proliferation and function[100,109], possibly related to the kinetics of receptor stimulation. We found that although the GITR- and OX40-CAR Tregs provided an intermediate survival benefit at the high Treg:PBMC ratio in vivo, neither construct was able to stimulate proliferation or strong activation. Poor proliferation with the OX40-CAR is consistent with the

finding that stimulation of Treg expansion via anti-CD3 and anti-OX40 antibodies is inferior to treatment with anti-CD3 and anti-CD28 antibodies[341].

Focusing on CARs encoding inhibitory co-receptors, inclusion of PD-1 completely blocked CD3ζ-mediated activation of Tregs, with no A2-stimulated expression of activation markers or effector molecules, proliferation or suppression. Transcriptome analysis comparing the PD-1-CAR to a first generation CD3ζ-CAR revealed that PD-1 signaling in Tregs resulted in upregulated p53 signaling, a pathway strongly associated with cell cycle arrest[342]. While a strong association between PD-1 signaling and development of peripherally-induced Tregs has been established[75], whether or not there is a functional role for PD-1 signaling in thymic-derived Tregs, and by extension CAR Tregs, is unclear. Our data show that signaling via PD-1 has a similar function in Tregs as it does in Tconv cells, i.e. PD-1 signaling inhibits Tregs. In terms of CTLA-4, although clearly required for Treg function[312], the role for intrinsic signaling versus extrinsic effects is unclear[68]. Our data confirm that the point mutation Y165G improves cell surface expression[313] and show that CTLA-4 intrinsic signaling is not beneficial for Tregs.

A notable limitation of our study is the paucity of models in which to test human Treg function in vivo. We elected to use the well-established xenoGVHD model because it is a system in which the advantage of CAR Tregs has previously been observed[221,247] and it is significantly more high throughput than other humanized mouse models and thus amenable to testing multiple CAR Treg groups in parallel. Mechanistically, it is known that the suppressive effects of Tregs in this model are at least partially due to TGF-β[343] and CTLA-4 signaling[344], two pathways that are strongly stimulated by the CD28wt-CAR. However, we acknowledge that this model does not recapitulate a normal immune response, since there is poor engraftment of human APCs, the lack of a lymph node network, and only select cross-reactivity of mouse homing stimuli/receptors to

support human T cell trafficking. In the context of a complete immune system, different CAR-stimulated effects may be observed, a possibility that will require further study in systems without the limitations of the xenoGVHD model.

Collectively, our findings support the use of CD28wt-based CAR for use in Treg therapies. Future studies could seek to future optimize the signaling moieties by using a third-generation CAR in combination with CD28 or adding additional signals that reinforce Treg identity. Our extensive analysis of the in vitro and in vivo properties and effects of signaling-domain CAR variants provides a platform from which to design future studies and also leads to significant insight into the essential properties of engineered Treg therapies.

Chapter 5: An optimized method to measure human FOXP3+ regulatory T cells from multiple tissue types using mass cytometry

5.1 Introduction

High-dimensional phenotyping with mass cytometry has revealed new cell populations and functions as well as immunological networks[251] but its use to measure transcription factors, which are difficult to detect due to intranuclear localization and DNA association, has been limited. High and stable expression of the transcription factor FOXP3 defines regulatory T cells (Tregs)[345] so robust methodology to detect FOXP3 is essential for mass cytometry-based analysis of Tregs in health, disease and/or in response to therapy.

Mass cytometry is a new technology that combines single cell fluidics from traditional fluorescence flow cytometry with the benefits of mass spectrometry, enabling simultaneous detection of over 50 parameters from a single sample with minimal compensation[251]. Several studies have analyzed human Tregs using mass cytometry. Mason et al analyzed pre-sorted $CD4^+CD25^+CD127^-$ Tregs but without FOXP3 staining in their mass cytometry panel[254]. In unfractionated peripheral blood, changes in FOXP3 expression following low-dose IL-2 therapy for graft-versus-host disease[255], in aplastic anemia[346], or with cytotoxic protein co-expression patterns[347] have been reported. In tissue, mass cytometry was used to phenotype circulating versus tumor-infiltrating $FOXP3^+$ Tregs in glioblastoma multiforme[348] or hepatocellular carcinoma[349]. However, none of these studies reported validation of the FOXP3 staining protocol or compared results to "gold-standard" flow cytometry data. Using flow cytometry as a benchmark, we sought to optimize mass cytometry FOXP3 staining for detection of polyclonal and antigen-specific human Tregs from peripheral blood and other tissues.

5.2 Results

5.2.1 Custom fixation and permeabilization protocol yields optimal FOXP3 staining

To develop an optimal protocol to detect FOXP3 by mass cytometry, we aimed for clear resolution of $FOXP3^+$ Tregs, minimal staining of conventional T cells (Tconvs), and uncompromised detection of cell surface proteins necessary to identify Tregs/or and other cell types. We tested three buffer sets: the FOXP3 mass cytometry staining kit from Fluidigm; the commonly-used eBioscience FOXP3 fix/perm buffer set developed for flow cytometry[350], and a custom buffer system using paraformaldehyde (PFA)-based fixation and saponin-based membrane permeabilization (termed PFA/saponin; see Methods). For all samples and buffers, FOXP3 gates were set on the basis of staining in live $CD4^{neg}$ cells (Figure C.1). We found that all three buffer systems resulted in similar proportions of $FOXP3^+$ cells within the $CD4^+CD25^+CD127^-$ gate, which is the widely accepted combination of Treg-defining cell surface molecules in humans (Figure 5.1A, Figure C.1)[345,351,352]. These data were confirmed by determining the proportion of $CD25^+CD127^-$ cells within the $CD4^+FOXP3^+$ gate (Figure 5.1B). In the majority of samples, a proportion of Tconvs ($CD4^+CD25^-CD127^+$) displayed background FOXP3 staining using the eBioscience, but not Fluidigm or PFA/saponin, protocol (Figure 5.1A).

Since fixation methods can destroy or alter epitopes[353,354], we determined the effect of each FOXP3 staining protocol on detection of a range of T cell surface markers. The Fluidigm buffers had the greatest negative effect on several Treg-defining cell surface markers including CD3, CD4, and CD25, resulting in poor resolution of $CD3^+CD4^+$ cells as well as $CD25^+CD127^-$ cells (Figure 5.2A). In contrast, PFA/saponin and

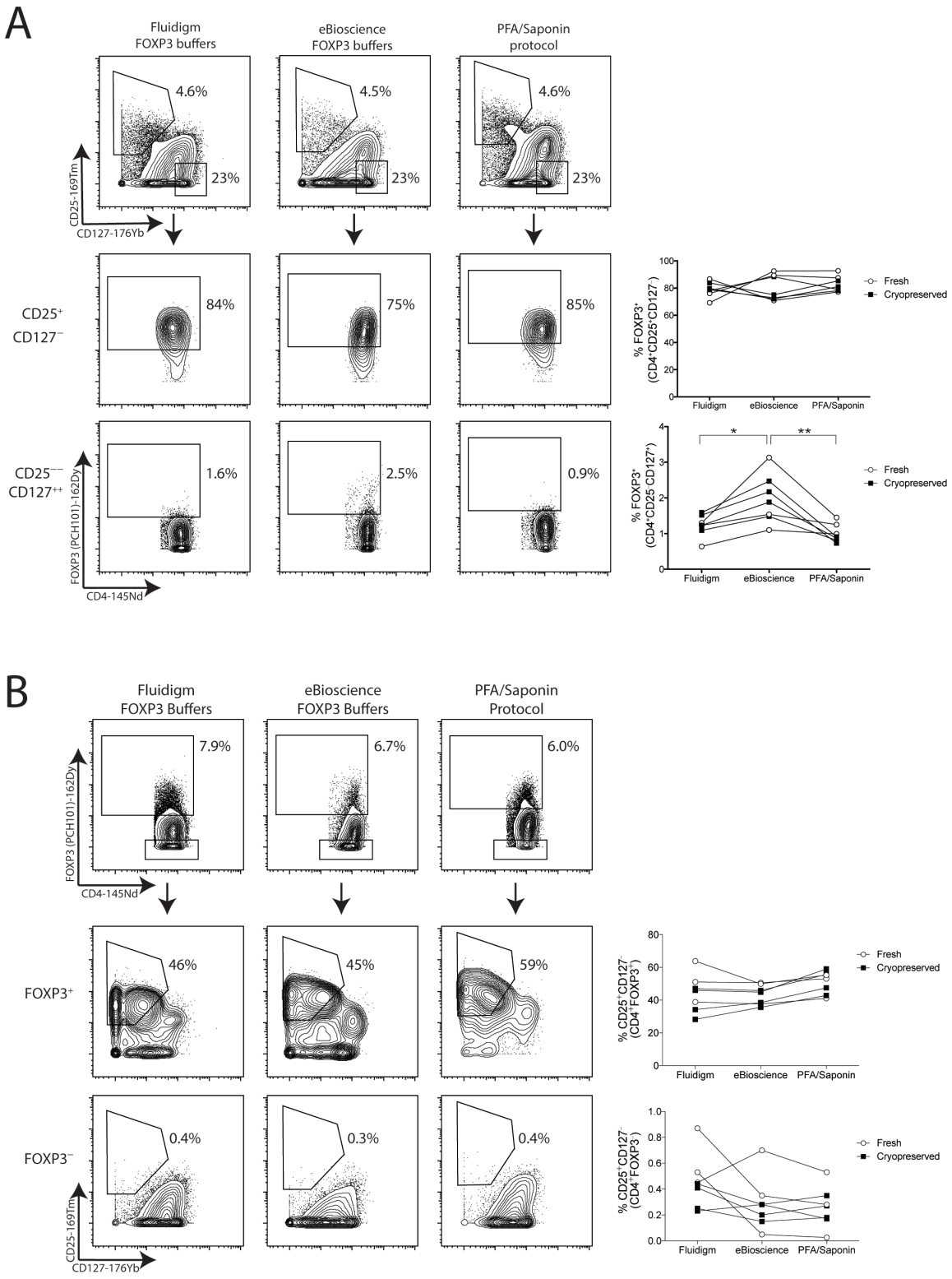

Figure 5.1 Development of a FOXP3 staining protocol for mass cytometry and comparison to flow cytometry. **(A)** Fresh or thawed PBMCs (n=7) were stained using the Fluidigm or eBioscience FOXP3 Staining Kit or fixed in PFA and stained in saponin. Cisplatin^{-}bead^{-}DNA1^{+}DNA2^{+}CD3^{+}CD4^{+} single cells were gated as CD25^{+}CD127^{-} or CD25^{--}CD127^{++} cells and analyzed for FOXP3 (gating in Appendix A). **(B)** Viable (cisplatin–) bead–DNA1^{+}DNA2^{+}CD3^{+}CD4^{+} single cells were gated as FOXP3+ or FOXP3– cells (gates set as in A) and the proportions of CD25^{+}CD127^{-} cells within the parent population were determined. Each line is data from one individual (n=7) pooled from three independent experiments. Statistical significance was determined for with a one-way ANOVA with a Tukey multiple comparisons post-test. * $p < 0.05$, ** $p < 0.01$, **** $p < 0.0001$

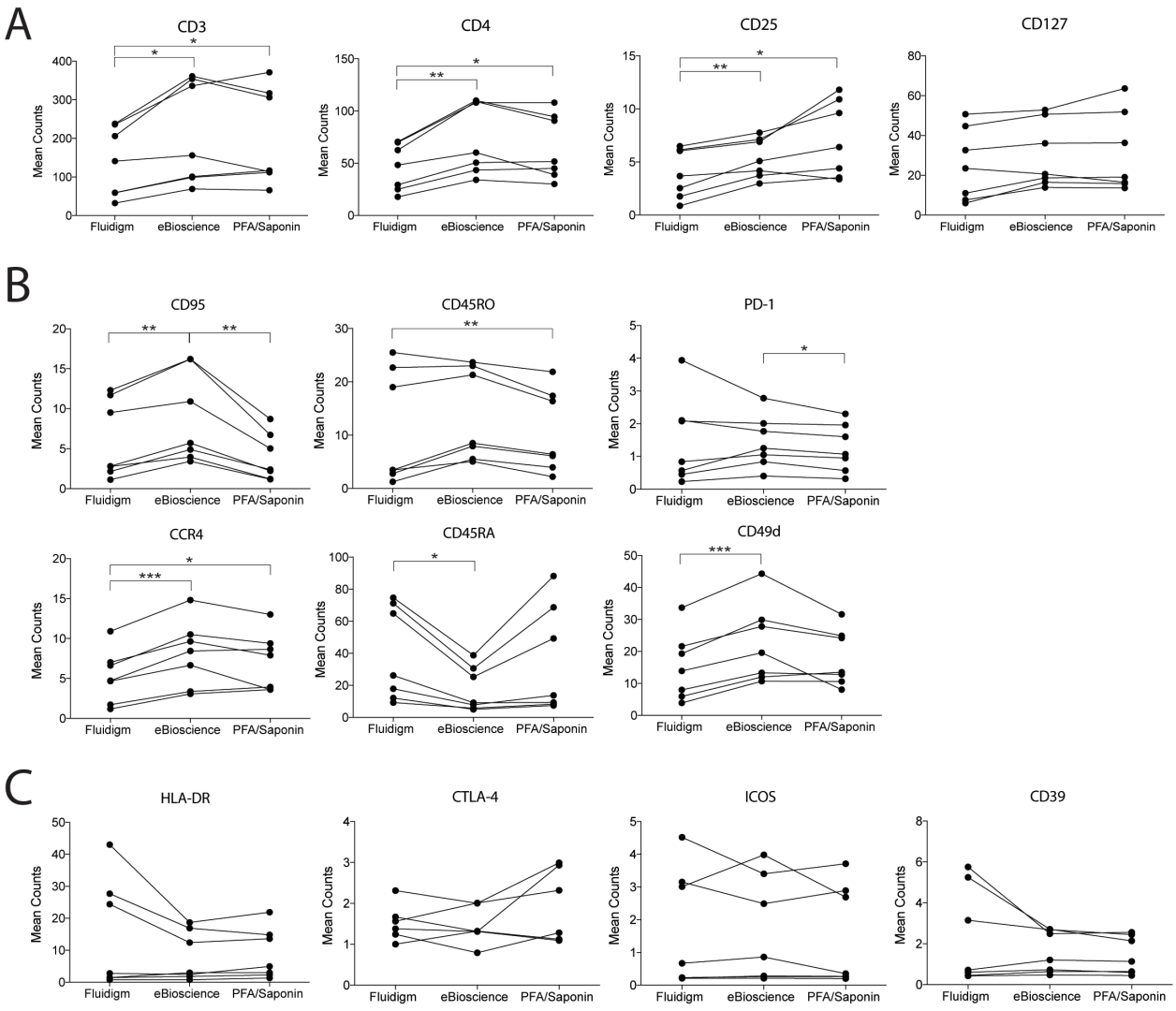

Figure 5.2 Mean count detection of extracellular and intracellular molecules on CD4 T cells using different fix/perm buffers on mass cytometry.
PBMC were prepared using various fixation/permeabilization methods as in Figure 1A and analyzed on a mass cytometer. Shown are the mean counts of each target within the viable ($cisplatin^-$)$bead^-DNA1^+DNA2^+CD3^+CD4^+$ single cell gate for each fixation method. Data from n=7 individual donors are shown. Treg-relevant cell surface markers that are used to define Tregs are shown in **(A)**. Markers that were **(B)** or were not **(C)** differentially affected by different fixation methods. In all graphs, each line is data from one individual with data collected in three independent experiments. Statistical significance was determined for with a one-way ANOVA with a Tukey multiple comparisons post-test. * $p < 0.05$, ** $p < 0.01$, *** $p < 0.001$

eBioscience buffers showed equivalent and optimal detection of CD3, CD4, and CD25, supporting their use for detection of $CD4^+CD25^+CD127^-$ Tregs. Evaluation of other Treg-associated cell surface markers revealed that no single fixation method was optimal for detection

of all markers tested. Although each method had its respective limitations (Figure 5.2B&C), the PFA/saponin protocol was optimal for detection of Tregs by mass cytometry because it neither caused background staining of FOXP3 in Tconvs nor diminished detection of Treg-defining cell surface molecules. These data highlight the importance of determining the impact of fixation methods used to measure nuclear proteins on detection of other cytoplasmic or cell surface markers of interest.

5.2.2 FOXP3 detection via mass cytometry is inferior to fluorescence flow cytometry

Having identified an optimal method for staining FOXP3 via mass cytometry, we next compared mass cytometry data obtained using the PFA/saponin protocol to fluorescence flow cytometry. Since human immune cells are often analyzed after cryopreservation, we compared ex vivo or cryopreserved cells on both platforms. We found that cell surface marker detection was similar on both platforms for most antigens tested (Figure 5.3A-E), with the notable exception of significantly lower proportions of CCR4-expressing $CD3^+CD4^+$ T cells in mass cytometry. This difference was likely due to differential CCR4 clone sensitivity (Figure 5.3F), highlighting the need for careful antibody clone selection to achieve optimal resolution in mass (and flow) cytometry.

For both ex vivo and cryopreserved samples, the proportion of FOXP3-expressing cells (PCH101 clone) detected via mass cytometry was significantly lower than via flow cytometry (Figure 5.4A-B, Figure C.1). However, within each platform, there were no significant differences in the proportion of $FOXP3^+$ cells detected in ex vivo versus cryopreserved samples (Figure 5.4B). To determine if reduced detection of FOXP3 in mass cytometry was a limitation of the PCH101 clone, the experiment was repeated with the FOXP3 clone 236A/E7, with similar

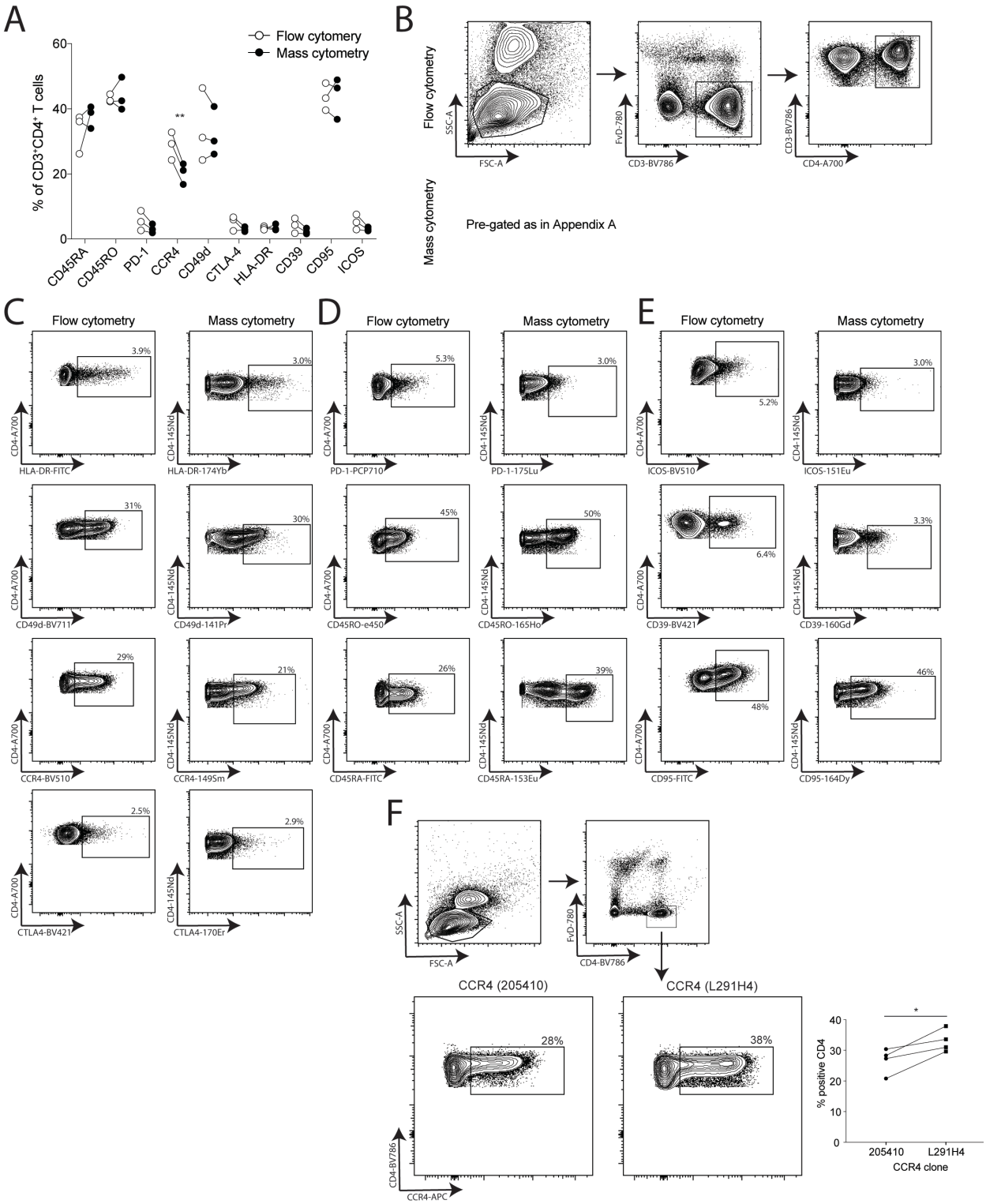

Figure 5.3 Comparison of cell surface molecule detection using PFA/saponin-mass cytometry or fluorescence flow cytometry.

Ex vivo or cryopreserved PBMC were stained using the PFA/saponin method described in Figure 5.1, then stained with fluorescent-tagged antibodies or metal-tagged antibodies and analyzed by flow or mass cytometry. **(A)** Shown are paired data (n=3) for each marker tested. ***continued on next page***

(B) Example pre-gating strategies for flow and mass cytometry. **(C-E)** Representative plots for each marker tested are shown from panel 1 **(C),** panel 2 **(D),** and panel 3 **(E).** Flow and mass cytometry panels and antibody information are in Methods. (F) Flow cytometry comparison of CCR4 clones used in panel 1 (C) on mass cytometry (205410) and flow cytometry (L291H4). Shown is example gating and representative plots (left) and summary data from n=4 donors (right). Data shown are from one independent experiment. Gates were manually drawn in FlowJo v10.3 and analyzed in Prism v7.0c using a two-tailed paired t-test. * $p < 0.05$, ** $p < 0.01$

results (Figure 5.4C). This reduced sensitivity may be due to chemical properties of fluorophores versus metals, possibly resulting in a differential ability of metal- versus fluorochrome-conjugated antibodies to pass through the nuclear membrane. Additionally, even the most sensitive metals (eg. 162Dy) are less sensitive than the brightest fluorophores (eg. PE)[355,356].

It is often desirable to detect antigen-specific Tregs, so we assessed the ability of the PFA/saponin protocol to enumerate FOXP3$^+$ Tregs within a population of antigen-specific CD4$^+$ T cells. Blood was stimulated with the indicated antigen for 44 hours and antigen-specific CD4$^+$

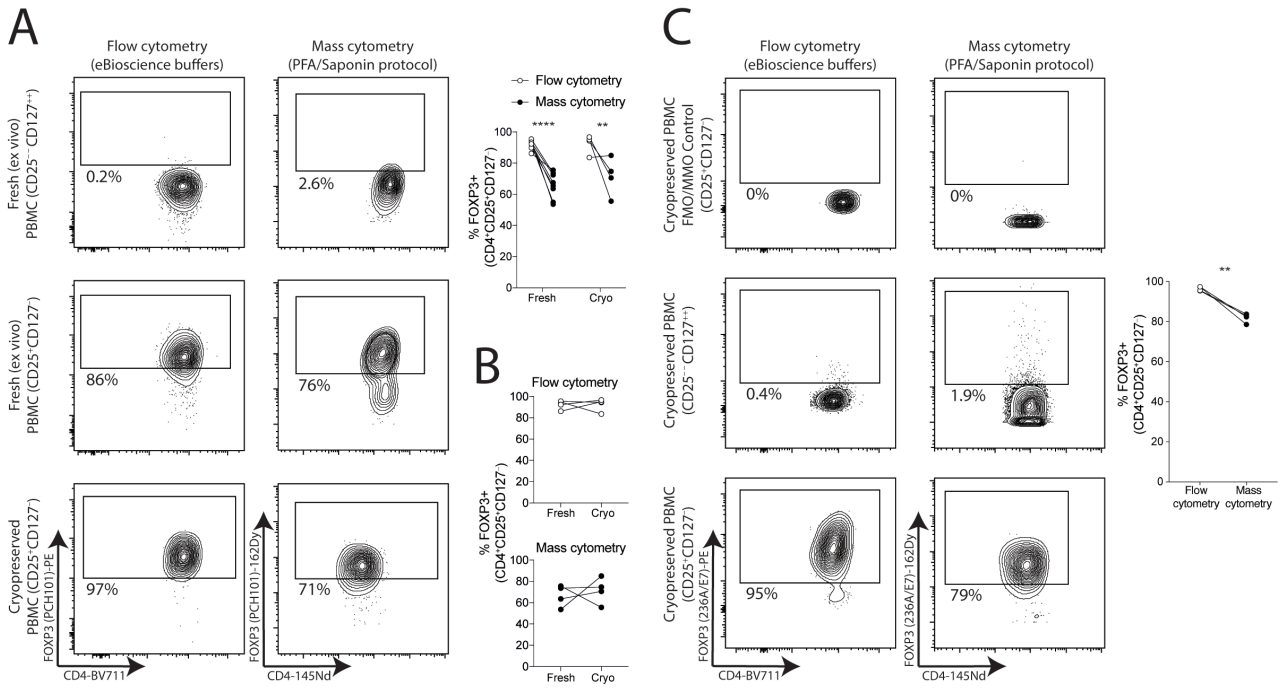

Figure 5.4 Comparison of FOXP3 detection using PFA/saponin-mass cytometry or fluorescence flow cytometry. (A&B) PBMCs (n=4-8) were analyzed by flow or mass cytometry (PFA/saponin fixation) before/after cryopreservation. The PCH101 anti-FOXP3 gate was set on cisplatin$^-$bead$^-$DNA1$^+$DNA2$^+$CD3$^+$CD4$^-$ single cells. **(C)** Cryopreserved PBMCs (n=4) were stained as in (A&B) using 236A/E7 anti-FOXP3 or a fluorescence/metal minus one (FMO/MMO) control. Each line is data from one individual with data collected in at least one independent experiment. Statistical significance was determined with two-tailed paired t tests. * $p < 0.05$, ** $p < 0.01$, **** $p < 0.0001$

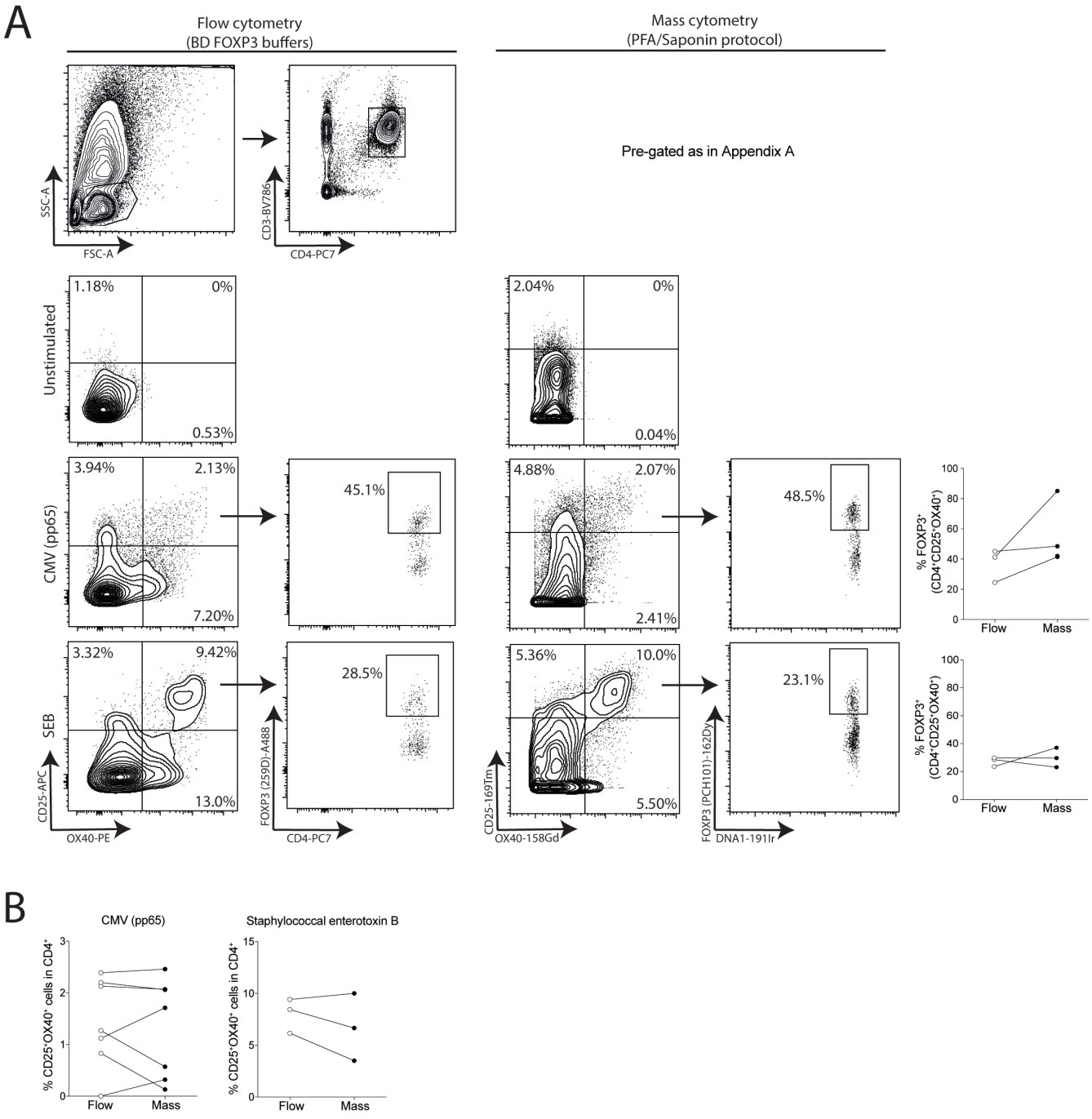

Figure 5.5 Detection of antigen-specific Tregs by mass cytometry.
Unfractionated blood was stimulated with a pool of pp65 CMV peptides or staphylococcal enterotoxin B (SEB) for 44 hours, then stained for surface markers with fluorescent antibodies or with metal-tagged antibodies. Samples were red blood cell lysed and intracellular antigens were stained with BD FOXP3 staining buffers or the aforementioned PFA/saponin protocol for flow or mass cytometry, respectively. **(A)** Example gating of viable $CD4^+$ cells; CD25/OX40 gate based on an unstimulated control (top). Representative and summarized (n=3, far right) data, n=3 individual donors from a single independent experiment. **(B)** Summary data of the total proportion of antigen-specific CD4+ T cells comparing fluorescence flow cytometry to mass cytometry. Percentage of $CD4^+CD25^+OX40^+$ (antigen-specific helper T cells) was compared across cytometry platforms. Statistical significance determined using a two-tailed paired t-test. Shown are representative and individual data for n=3-7 donors pooled from at least two independent experiments.

T cells were detected by induced co-expression of CD25 and OX40[94] by flow or mass cytometry using optimal methods (Figure 5.5). The proportion of antigen-specific $CD4^+$ responder cells detected by mass cytometry was similar to flow cytometry and, since Tregs comprise a substantial proportion of recall responses[357], both mass cytometry and flow cytometry detected a clear population of antigen-specific $FOXP3^+$ cells. Notably, in contrast to ex vivo cells, the proportion of $FOXP3^+$ cells detected by mass cytometry was similar to that detected with flow cytometry.

5.2.3 ACCENSE analysis reveals distinct Treg phenotypes in steady state and diseased tissues

We next tested the applicability of PFA/saponin-based FOXP3 staining to detect $CD4^+CD25^+CD127^-$ Tregs in samples other than peripheral blood via mass cytometry. Mononuclear cells from umbilical cord blood, CD8-depleted thymocytes, or synovial fluid from juvenile idiopathic arthritis (JIA) patients were stained with a panel of T cell and Treg-related markers, including FOXP3. Data were analyzed with ACCENSE[358], which compares cells on a two-dimensional plot while maintaining single cell resolution and complexity, and then further identifies statistically significant subpopulations (Figure 5.6A). The relative expression of each marker within the 25 ACCENSE-defined populations, as well as their relative abundance within each tissue, was determined (Figure 5.6B). Strikingly, Tregs preferentially clustered into ACCENSE populations by tissue source. For example, Treg populations in cord blood were uniquely identified by high CD45RA, whereas Treg populations in JIA synovial fluid were defined by high expression of multiple activation/effector molecules and enriched for high PD-1. Despite strong tissue-specific segregation, a few populations were shared between tissues. For

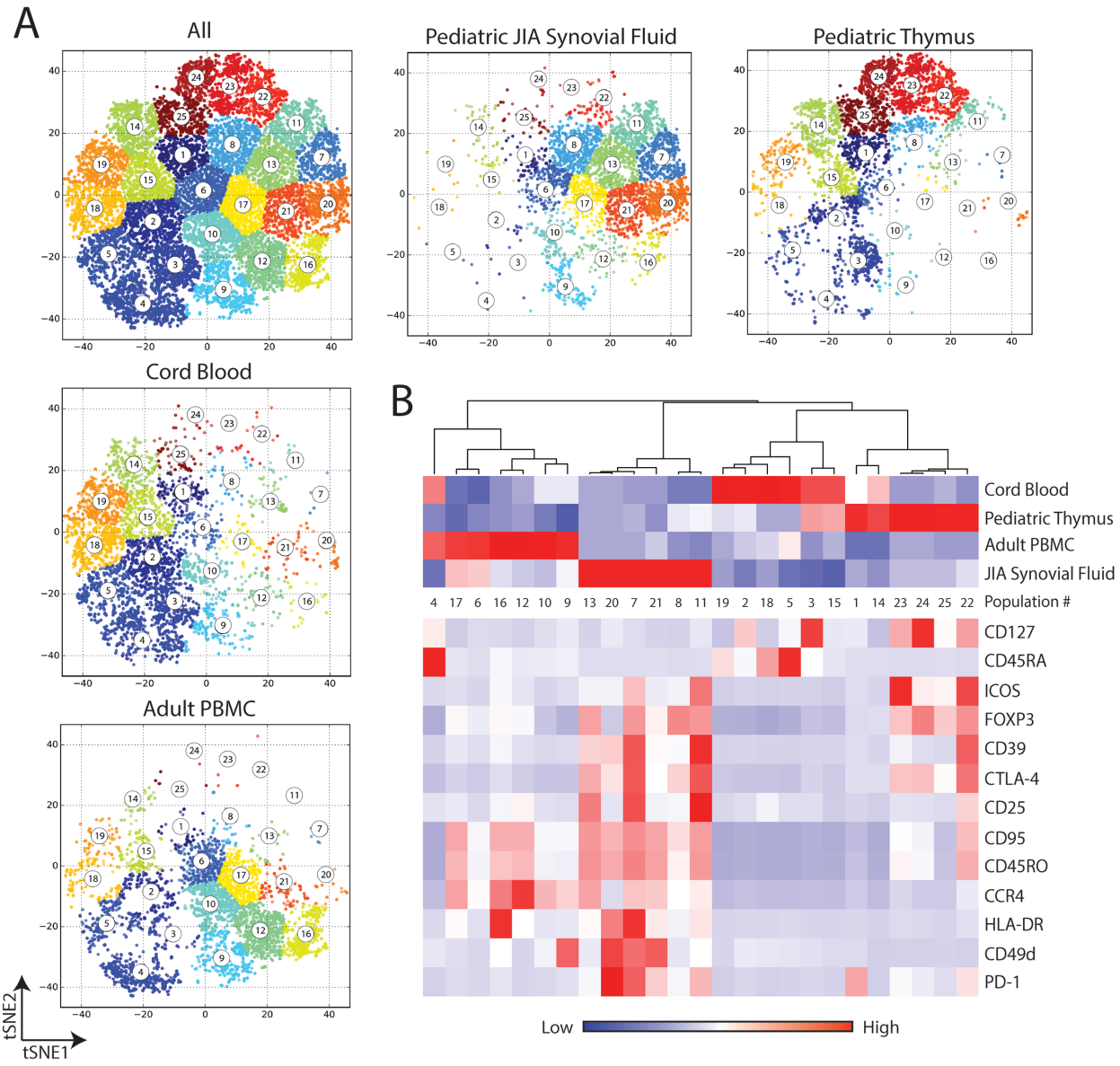

Figure 5.6 ACCENSE analysis of Tregs in peripheral blood, cord blood, thymus and JIA synovial fluid. **(A)** Cryopreserved mononuclear cells from the indicated tissues were stained with the PFA/saponin method and analyzed by mass cytometry (n=3-4 per tissue). Data from cisplatin$^-$bead$^-$DNA1$^+$DNA2$^+$CD3$^+$CD4$^+$CD25$^+$CD127$^-$ single cells from each tissue were pooled and analyzed using ACCENSE v0.5.0-beta (Barnes-Hut-SNE dimension reduction and k-means significance of 10^{-8}). **(B)** Heat map analysis of mean count expression of each protein included in the ACCENSE analysis; populations were clustered by tissue frequency. Average marker expression and population frequencies were normalized using Z-score analysis to highlight the range of markers expressed in different populations and emphasize which tissues were enriched for each ACCENSE population. Data represent two independent experiments.

instance, a subset of CD45RA$^+$ Tregs (population 4) was found in peripheral blood and cord blood, and populations 3 (CD127$^+$) and 15 (low for all markers) were present in cord blood and thymus. Overall, these results support a growing body of evidence indicating that Tregs acquire unique tissue-specific phenotypes and that phenotypes in peripheral blood may not reflect those of tissue-resident cells[359,360].

5.3 Discussion

In conclusion, we developed an optimal protocol to detect FOXP3 expression by mass cytometry, tested its suitability for ex vivo and cryopreserved samples, and showed its utility across a broad range of immune cell sources. We have further shown that antigen-specific FOXP3$^+$ Tregs can be detected by mass cytometry in whole blood. An important consideration is that, at least in ex vivo peripheral blood samples, mass cytometry is significantly less sensitive than fluorescence flow cytometry at detecting FOXP3 expression. Overall, our optimized PFA/saponin protocol is the best-validated method described to date to detect FOXP3 expression by mass cytometry without compromising detection of cell surface markers. This method will enhance high-dimensional studies of Treg phenotype, cellular networks and enable tracking of FOXP3$^+$ Tregs in longitudinal clinical studies.

Chapter 6: Conclusion

6.1 Summary of major findings

The study of humanized CAR Tregs represents the most comprehensive comparison and screening of humanized CARs to date in the literature. First, constructs were screened for their ability to retain antigen binding, then their specificity and function in vitro and in vivo. This was the first study to show specific homing of CAR constructs and show that our humanized CAR constructs had improved specificity versus the murine CAR construct. My original *hypothesis* for this work was that we could generate humanized CARs that were functionally equivalent to a murine-derived CAR in Tregs. While some humanized CAR constructs showed deficiencies in functional tests performed, several humanized CARs maintained similar function and characteristics of the original murine construct, providing support for this hypothesis. The main limitation of this study is that long-term effects of CAR Tregs in vivo could not be evaluated. The humanized mouse models that were employed for these studies involved co-injection of PBMCs to provide survival signals, in particular IL-2, for Treg survival. The injected PBMCs eventually cause GVHD in the mice, thus limiting the length of the study since experimental readouts can be confounded once GVHD occurs. Further studies with syngeneic mouse models will be required to address questions relating to the molecular mechanism and long-term effects of CAR Tregs in vivo.

Modulating CAR Treg signaling by alteration of the intracellular signaling moieties was the most ambitious and thorough comparison thus far in both oncology and tolerance literature. My original *hypothesis* was that CAR signaling domains could be optimized for use in Tregs by swapping CD28 with intracellular domains from other co-receptor molecules that could provide a functional benefit to Tregs. CD28wt provided a clear benefit over all the signaling domain

variants tested in both the xenoGVHD and in vitro suppression assays. Although constructs encoding, CD28wt, 4-1BB or TNFR2 CARs all supported CAR-mediated proliferation, only cells expressing the CD28wt construct maintained a Treg phenotype. Collectively, these data indicate that CD28 is the optimal signaling domain for Tregs in the context of a second-generation CAR construct, which is contrary to our original hypothesis. Due to the limitations of humanized mouse models discussed above, these studies do not account for possible long-term differences in vivo. However, on the basis of the in vitro results suggesting that the majority of the constructs tested do not proliferate after CAR stimulation, I would predict that these CARs will not perform as well as CD28 in fully mouse models.

In my final chapter, I outlined the optimization of FOXP3 staining via mass cytometry by comparing the performance of several fixation/permeabilization buffers. Further, I compared the method to traditional fluorescence flow cytometry and applied the method to Tregs staining of several different tissues including whole blood, synovial fluid and umbilical cord blood. My original *hypothesis* was that detection of FOXP3 via mass cytometry could effectively be optimized using a custom saponin-based fixation and permeabilization method. I was able to support this hypothesis using thorough testing of this method in several applications, but the resolution of $FOXP3^+$ cells was never as sensitive as traditional fluorescence flow cytometry. While these studies support the use of mass cytometry to detect $FOXP3^+$ Tregs, in studies where the $FOXP3^+$ population is of critical importance, a more sensitive method should be employed.

6.2 Future Directions

Many clinical trials with low-dose IL-2 therapies, expanded polyclonal and antigen-specific Tregs for use in autoimmune diseases, HSCT and solid organ transplantation are underway[202,361,362]. While initial reports from these trials show that the treatments are well tolerated, the aggregate safety and efficacy data from each approach will greatly inform future studies. Notably, possible long-term effects, in particular the potential risk of cancer and infection, of these treatments will not be known for a significant period of time. Many of the fundamental properties of Tregs are similar to Tconv cells so it may be possible to predict some aspects of in vivo Treg behavior on the basis of findings from CAR Tconv cells used in the oncology field. However, Tregs also have many unique properties, such as their strict dependence on other cells for IL-2 and constitutive expression of inhibitory proteins such as CTLA-4 and TGF-β.

Thus, there is a need for more detailed studies in animal models to fully appreciate the similarities and differences between the two cell types. For example, will CAR Tregs be able to persist long-term through repeated stimulations? Tregs have different activation requirements than Tconv cells[206,222], meaning that optimal proliferation and long-term persistence may require Treg-specific CAR design. Will CAR Tregs induce long-term tolerance, and if yes, what molecular mechanisms will be necessary? CAR-activated Tregs upregulate CTLA-4, LAP, GARP and CD39[247,363], but it is unknown which pathway(s) are necessary for CAR Treg-mediated suppression. Further, what is the primary target of CAR Treg-mediated suppression? While CAR Tregs can traffic to the site of inflammation and secondary lymphoid organs, it is unknown whether CAR Tregs suppress immune cells at those sites and which are essential. Are molecular mechanisms of suppression different at the site of the graft versus secondary lymphoid

organs? Dissecting the mechanisms important to CAR Treg function may also provide clues as to their primary mode and location of immune suppression. Many of these questions are ideally suited for study in models of transplantation where similar questions with polyclonal or transgenic Tregs have been addressed[199].

Further studies could be performed to alter the structure of the CAR construct to optimize CAR Treg treatment. Given the clear result that CD28 signaling is critical for CAR function and maintenance of Treg stability, CD28 must be a part of the CAR structure. However, the use of third-generation CARs could be used to further tailor the signal as CD28 and an additional co-receptor signal may provide additional benefit versus CD28 alone. In oncology, third generation CARs further augmented cytolytic and proliferative abilities of the CAR T cell compared to second-generation CARs. Other changes could be made to the CAR transgene, and such changes could be guided by answering some of the questions posed above. For example, additional signaling domains could be added to simulate detection of cytokines or force secretion of cytokines (ex. TGFβ), but which improvement is best will informed by the mechanistic studies in the full murine models discussed above.

In the near future, there may be a rapid transition from the rather crude current approaches with unmodified IL-2 and/or polyclonal Tregs to engineered approaches that enable precise control over the desired immunosuppressive effects[364]. It is likely that, as for low-dose IL-2 and polyclonal Treg therapy, transplantation will lead the way in testing these new engineered approaches. HSCT is a setting with a wealth of experience in using engineered T cells for cancer and it would be a natural transition to test engineered Tregs in this context. Moreover, in solid organ transplantation allogeneic HLA antigens represent an ideal target for antigen-specific Tregs because they are only expressed on the transplanted issue, minimizing the

risk of off-target suppression[365]. Additionally, since solid organ transplant donors and recipients are usually not HLA-matched, there is a large pool of patients that could benefit from this treatment. CAR targets for autoimmunity will be more difficult to identify because there are few truly organ and/or cell-specific antigens that would be suitable CAR targets. This challenge is similar to that faced in oncology, where off-target effects of CAR-T cells can have devastating consequences[211,366]. The use of CAR Tregs in autoimmunity may require logic-gated CARs to be more specific to the targeted tissue[215]. The field of engineered Tregs will continue to benefit greatly from the huge resources being invested into solving this problem in oncology[209,210,367], creating an ideal landscape to support the rapid development of this next generation of Treg therapies.

Bibliography

1. Spits, H. Development of alphabeta T cells in the human thymus. *Nat. Rev. Immun.* **2,** 760–772 (2002).
2. Zhu, J. & Paul, W. E. CD4 T cells: fates, functions, and faults. *Blood* **112,** 1557–1569 (2008).
3. Zúñiga-Pflücker, J. C. T-cell development made simple. *Nat. Rev. Immun.* **4,** 67–72 (2004).
4. Koch, U. & Radtke, F. Mechanisms of T cell development and transformation. *Annu. Rev. Cell Dev. Biol.* **27,** 539–562 (2011).
5. Klein, L., Kyewski, B., Allen, P. M. & Hogquist, K. A. Positive and negative selection of the T cell repertoire: what thymocytes see (and don't see). *Nat. Rev. Immun.* **14,** 377–391 (2014).
6. Perry, J. S. A. *et al.* Distinct Contributions of Aire and Antigen-Presenting-Cell Subsets to the Generation of Self-Tolerance in the Thymus. *Immunity* **41,** 414–426 (2014).
7. Bird, L. Tolerance: AIREs and graces. *Nat. Rev. Immun.* **14,** 714–715 (2014).
8. Fooksman, D. R. *et al.* Functional anatomy of T cell activation and synapse formation. *Annu. Rev. Immunol.* **28,** 79–105 (2010).
9. Pennock, N. D. *et al.* T cell responses: naive to memory and everything in between. *Adv Physiol Educ* **37,** 273–283 (2013).
10. Farber, D. L., Yudanin, N. A. & Restifo, N. P. Human memory T cells: generation, compartmentalization and homeostasis. *Nat. Rev. Immun.* **14,** 24–35 (2014).
11. Billingham, R. E., Brent, L., Medawar, P. B. & Sparrow, E. M. Quantitative studies on tissue transplantation immunity. I. The survival times of skin homografts exchanged between members of different inbred strains of mice. *Proc. R. Soc. Lond., B, Biol. Sci.* **143,** 43–58 (1954).
12. Gershon, R. K. & Kondo, K. Cell interactions in the induction of tolerance: the role of thymic lymphocytes. *Immunology* **18,** 723–737 (1970).
13. Bacchetta, R. *et al.* Defective regulatory and effector T cell functions in patients with FOXP3 mutations. *J. Clin. Invest.* **116,** 1713–1722 (2006).
14. Vignali, D. A., Collison, L. W. & Workman, C. J. How regulatory T cells work. *Nat. Rev. Immun.* **8,** 523–532 (2008).
15. Sakaguchi, S., Miyara, M., Costantino, C. M. & Hafler, D. A. FOXP3+ regulatory T cells in the human immune system. *Nat. Rev. Immun.* **10,** 490–500 (2010).
16. Lu, L., Barbi, J. & Pan, F. The regulation of immune tolerance by FOXP3. *Nat. Rev. Immun.* **37,** 129 (2017).
17. Baron, U. *et al.* DNA demethylation in the human FOXP3 locus discriminates regulatory T cells from activated FOXP3+ conventional T cells. *Eur. J. Immunol.* **37,** 2378–2389 (2007).
18. Polansky, J. K. *et al.* DNA methylation controls Foxp3 gene expression. *Eur. J. Immunol.* **38,** 1654–1663 (2008).
19. Allan, S. E. *et al.* Generation of potent and stable human CD4+ T regulatory cells by activation-independent expression of FOXP3. *Mol. Ther.* **16,** 194–202 (2008).

20. Nakagawa, H. *et al.* Instability of Helios-deficient Tregs is associated with conversion to a T-effector phenotype and enhanced antitumor immunity. *Proc. Natl. Acad. Sci. U.S.A.* **113,** 6248–6253 (2016).
21. Kim, H.-J. *et al.* Stable inhibitory activity of regulatory T cells requires the transcription factor Helios. *Science* **350,** 334–339 (2015).
22. Shevach, E. M. & Thornton, A. M. tTregs, pTregs, and iTregs: similarities and differences. *Immunol. Rev.* **259,** 88–102 (2014).
23. Yadav, M., Stephan, S. & Bluestone, J. A. Peripherally induced tregs - role in immune homeostasis and autoimmunity. *Front Immunol* **4,** 232 (2013).
24. Hsieh, C.-S., Lee, H.-M. & Lio, C.-W. J. Selection of regulatory T cells in the thymus. *Nat. Rev. Immun.* (2012). doi:10.1038/nri3155
25. Caramalho, Í., Nunes-Cabaço, H., Foxall, R. B. & Sousa, A. E. Regulatory T-Cell Development in the Human Thymus. *Front Immunol* **6,** 395 (2015).
26. Mahmud, S. A. *et al.* Costimulation via the tumor-necrosis factor receptor superfamily couples TCR signal strength to the thymic differentiation of regulatory T cells. *Nat Immunol* **15,** 473–481 (2014).
27. Pacholczyk, R. & Kern, J. The T-cell receptor repertoire of regulatory T cells. *Immunology* **125,** 450–458 (2008).
28. Itoh, M. *et al.* Thymus and autoimmunity: production of CD25+CD4+ naturally anergic and suppressive T cells as a key function of the thymus in maintaining immunologic self-tolerance. *J. Immunol.* **162,** 5317–5326 (1999).
29. Jordan, M. S. *et al.* Thymic selection of CD4+CD25+ regulatory T cells induced by an agonist self-peptide. *Nat Immunol* **2,** 301–306 (2001).
30. Apostolou, I., Sarukhan, A., Klein, L. & Boehmer, von, H. Origin of regulatory T cells with known specificity for antigen. *Nat Immunol* **3,** 756–763 (2002).
31. Lee, H.-M., Bautista, J. L., Scott-Browne, J., Mohan, J. F. & Hsieh, C.-S. A broad range of self-reactivity drives thymic regulatory T cell selection to limit responses to self. *Immunity* **37,** 475–486 (2012).
32. Takahashi, T. *et al.* Immunologic self-tolerance maintained by CD25+CD4+ naturally anergic and suppressive T cells: induction of autoimmune disease by breaking their anergic/suppressive state. *Int. Immunol.* **10,** 1969–1980 (1998).
33. Thornton, A. M. & Shevach, E. M. CD4+CD25+ immunoregulatory T cells suppress polyclonal T cell activation in vitro by inhibiting interleukin 2 production. *Journal of Experimental Medicine* **188,** 287–296 (1998).
34. Klein, L., Khazaie, K. & Boehmer, von, H. In vivo dynamics of antigen-specific regulatory T cells not predicted from behavior in vitro. *Proc Natl Acad Sci USA* **100,** 8886–8891 (2003).
35. Alcover, A., Alarcón, B. & Di Bartolo, V. Cell Biology of T Cell Receptor Expression and Regulation. *Annu. Rev. Immunol.* **36,** 103–125 (2018).
36. Kumar, P., Bhattacharya, P. & Prabhakar, B. S. A comprehensive review on the role of co-signaling receptors and Treg homeostasis in autoimmunity and tumor immunity. *J. Autoimmun.* **95,** 77–99 (2018).
37. Esensten, J. H., Helou, Y. A., Chopra, G., Weiss, A. & Bluestone, J. A. CD28 Costimulation: From Mechanism to Therapy. *Immunity* **44,** 973–988 (2016).

38. Tai, X., Cowan, M., Feigenbaum, L. & Singer, A. CD28 costimulation of developing thymocytes induces Foxp3 expression and regulatory T cell differentiation independently of interleukin 2. *Nat Immunol* **6,** 152–162 (2005).
39. Vogel, I. *et al.* CD28/CTLA-4/B7 costimulatory pathway blockade affects regulatory T-cell function in autoimmunity. *Eur. J. Immunol.* **45,** 1832–1841 (2015).
40. Semple, K. *et al.* Strong CD28 costimulation suppresses induction of regulatory T cells from naive precursors through Lck signaling. *Blood* **117,** 3096–3103 (2011).
41. Schwarz, C. *et al.* The Immunosuppressive Effect of CTLA4 Immunoglobulin Is Dependent on Regulatory T Cells at Low But Not High Doses. *Am. J. Transplant.* **16,** 3404–3415 (2016).
42. Procaccini, C. *et al.* An oscillatory switch in mTOR kinase activity sets regulatory T cell responsiveness. *Immunity* **33,** 929–941 (2010).
43. Zeng, H. *et al.* mTORC1 couples immune signals and metabolic programming to establish T(reg)-cell function. *Nature* **499,** 485–490 (2013).
44. Saxton, R. A. & Sabatini, D. M. mTOR Signaling in Growth, Metabolism, and Disease. *Cell* **168,** 960–976 (2017).
45. Pompura, S. L. & Dominguez-Villar, M. The PI3K/AKT signaling pathway in regulatory T-cell development, stability, and function. *Journal of Leukocyte Biology* **103,** 1065–1076 (2018).
46. Delgoffe, G. M. *et al.* The mTOR kinase differentially regulates effector and regulatory T cell lineage commitment. *Immunity* **30,** 832–844 (2009).
47. Sauer, S. *et al.* T cell receptor signaling controls Foxp3 expression via PI3K, Akt, and mTOR. *Proc. Natl. Acad. Sci. U.S.A.* **105,** 7797–7802 (2008).
48. Battaglia, M., Stabilini, A. & Tresoldi, E. Expanding human T regulatory cells with the mTOR-inhibitor rapamycin. *Methods Mol. Biol.* **821,** 279–293 (2012).
49. Battaglia, M., Stabilini, A. & Roncarolo, M. G. Rapamycin selectively expands CD4+CD25+FoxP3+ regulatory T cells. *Blood* **105,** 4743–4748 (2005).
50. Battaglia, M. *et al.* Rapamycin promotes expansion of functional CD4+CD25+FOXP3+ regulatory T cells of both healthy subjects and type 1 diabetic patients. *J. Immunol.* **177,** 8338–8347 (2006).
51. Wikenheiser, D. J. & Stumhofer, J. S. ICOS Co-Stimulation: Friend or Foe? *Front Immunol* **7,** 304 (2016).
52. Crotty, S. Follicular helper CD4 T cells (TFH). *Annu. Rev. Immunol.* **29,** 621–663 (2011).
53. Chen, L. & Flies, D. B. Molecular mechanisms of T cell co-stimulation and co-inhibition. *Nat. Rev. Immun.* **13,** 227–242 (2013).
54. Redpath, S. A. *et al.* ICOS controls Foxp3(+) regulatory T-cell expansion, maintenance and IL-10 production during helminth infection. *Eur. J. Immunol.* **43,** 705–715 (2013).
55. Landuyt, A. E., Klocke, B. J., Colvin, T. B., Schoeb, T. R. & Maynard, C. L. Cutting Edge: ICOS-Deficient Regulatory T Cells Display Normal Induction of Il10 but Readily Downregulate Expression of Foxp3. *The Journal of Immunology* **202,** 1039–1044 (2019).
56. Kornete, M., Sgouroudis, E. & Piccirillo, C. A. ICOS-dependent homeostasis and function of Foxp3+ regulatory T cells in islets of nonobese diabetic mice. *The Journal of Immunology* **188,** 1064–1074 (2012).

57. Kohyama, M. *et al.* Inducible costimulator-dependent IL-10 production by regulatory T cells specific for self-antigen. *Proc Natl Acad Sci USA* **101,** 4192–4197 (2004).
58. Han, Y. *et al.* Acute Myeloid Leukemia Cells Express ICOS Ligand to Promote the Expansion of Regulatory T Cells. *Front Immunol* **9,** 2227 (2018).
59. Linsley, P. S. *et al.* Coexpression and functional cooperation of CTLA-4 and CD28 on activated T lymphocytes. *Journal of Experimental Medicine* **176,** 1595–1604 (1992).
60. Takahashi, T. *et al.* Immunologic self-tolerance maintained by CD25(+)CD4(+) regulatory T cells constitutively expressing cytotoxic T lymphocyte-associated antigen 4. *Journal of Experimental Medicine* **192,** 303–310 (2000).
61. Chambers, C. A., Sullivan, T. J. & Allison, J. P. Lymphoproliferation in CTLA-4-deficient mice is mediated by costimulation-dependent activation of CD4+ T cells. *Immunity* **7,** 885–895 (1997).
62. Calvo, C. R., Amsen, D. & Kruisbeek, A. M. Cytotoxic T lymphocyte antigen 4 (CTLA-4) interferes with extracellular signal-regulated kinase (ERK) and Jun NH2-terminal kinase (JNK) activation, but does not affect phosphorylation of T cell receptor zeta and ZAP70. *Journal of Experimental Medicine* **186,** 1645–1653 (1997).
63. Schneider, H., Smith, X., Liu, H., Bismuth, G. & Rudd, C. E. CTLA-4 disrupts ZAP70 microcluster formation with reduced T cell/APC dwell times and calcium mobilization. *Eur. J. Immunol.* **38,** 40–47 (2008).
64. Schneider, H., da Rocha Dias, S., Hu, H. & Rudd, C. E. A regulatory role for cytoplasmic YVKM motif in CTLA-4 inhibition of TCR signaling. *Eur. J. Immunol.* **31,** 2042–2050 (2001).
65. Parry, R. V. *et al.* CTLA-4 and PD-1 receptors inhibit T-cell activation by distinct mechanisms. *Molecular and Cellular Biology* **25,** 9543–9553 (2005).
66. Kong, K.-F. *et al.* Protein kinase C-η controls CTLA-4–mediated regulatory T cell function. *Nat Immunol* **15,** 465–472 (2014).
67. Masteller, E. L., Chuang, E., Mullen, A. C., Reiner, S. L. & Thompson, C. B. Structural analysis of CTLA-4 function in vivo. *J. Immunol.* **164,** 5319–5327 (2000).
68. Walker, L. S. K. & Sansom, D. M. Confusing signals: Recent progress in CTLA-4 biology. *Trends in Immunology* **36,** 63–70 (2015).
69. Friedline, R. H. *et al.* CD4+ regulatory T cells require CTLA-4 for the maintenance of systemic tolerance. *J. Exp. Med.* **206,** 421–434 (2009).
70. Fife, B. T. & Pauken, K. E. The role of the PD-1 pathway in autoimmunity and peripheral tolerance. *Ann. N. Y. Acad. Sci.* **1217,** 45–59 (2011).
71. Riley, J. L. PD-1 signaling in primary T cells. *Immunol. Rev.* **229,** 114–125 (2009).
72. Francisco, L. M., Sage, P. T. & Sharpe, A. H. The PD-1 pathway in tolerance and autoimmunity. *Immunol. Rev.* **236,** 219–242 (2010).
73. Nishimura, H., Nose, M., Hiai, H., Minato, N. & Honjo, T. Development of lupus-like autoimmune diseases by disruption of the PD-1 gene encoding an ITIM motif-carrying immunoreceptor. *Immunity* **11,** 141–151 (1999).
74. Intlekofer, A. M. & Thompson, C. B. At the bench: preclinical rationale for CTLA-4 and PD-1 blockade as cancer immunotherapy. *Journal of Leukocyte Biology* **94,** 25–39 (2013).
75. Chen, X. *et al.* PD-1 regulates extrathymic regulatory T-cell differentiation. *Eur. J. Immunol.* **44,** 2603–2616 (2014).

76. Francisco, L. M. *et al.* PD-L1 regulates the development, maintenance, and function of induced regulatory T cells. *J. Exp. Med.* **206,** 3015–3029 (2009).
77. Zhang, Y. *et al.* Regulation of T cell activation and tolerance by PDL2. *Proc Natl Acad Sci USA* **103,** 11695–11700 (2006).
78. Ward-Kavanagh, L. K., Lin, W. W., Šedý, J. R. & Ware, C. F. The TNF Receptor Superfamily in Co-stimulating and Co-inhibitory Responses. *Immunity* **44,** 1005–1019 (2016).
79. Chester, C., Sanmamed, M. F., Wang, J. & Melero, I. Immunotherapy targeting 4-1BB: mechanistic rationale, clinical results, and future strategies. *Blood* **131,** 49–57 (2018).
80. Sanchez Paulete, A. R. *et al.* Deciphering cd137 (4-1bb) signaling in T-cell costimulation for translation into successful cancer immunotherapy. *Eur. J. Immunol.* n/a–n/a (2016). doi:10.1002/eji.201445388
81. Humphreys, I. R. *et al.* Biphasic role of 4-1BB in the regulation of mouse cytomegalovirus-specific CD8(+) T cells. *Eur. J. Immunol.* **40,** 2762–2768 (2010).
82. Middendorp, S. *et al.* Mice deficient for CD137 ligand are predisposed to develop germinal center-derived B-cell lymphoma. *Blood* **114,** 2280–2289 (2009).
83. Zhang, P. *et al.* Agonistic Anti-4-1BB Antibody Promotes the Expansion of Natural Regulatory T Cells While Maintaining Foxp3 Expression. *Scand. J. Immunol.* **66,** 435–440 (2007).
84. Hippen, K. L. *et al.* Umbilical cord blood regulatory T-cell expansion and functional effects of tumor necrosis factor receptor family members OX40 and 4-1BB expressed on artificial antigen-presenting cells. *Blood* **112,** 2847–2857 (2008).
85. Irie, J., Wu, Y., Kachapati, K., Mittler, R. S. & Ridgway, W. M. Modulating protective and pathogenic CD4+ subsets via CD137 in type 1 diabetes. *Diabetes* **56,** 186–196 (2007).
86. Lee, J. *et al.* Administration of agonistic anti-4-1BB monoclonal antibody leads to the amelioration of inflammatory bowel disease. *Immunol. Lett.* **101,** 210–216 (2005).
87. Sun, Y. *et al.* Administration of agonistic anti-4-1BB monoclonal antibody leads to the amelioration of experimental autoimmune encephalomyelitis. *J. Immunol.* **168,** 1457–1465 (2002).
88. Kim, Y. H. *et al.* 4-1BB triggering ameliorates experimental autoimmune encephalomyelitis by modulating the balance between Th17 and regulatory T cells. *The Journal of Immunology* **187,** 1120–1128 (2011).
89. Buchan, S. L. *et al.* Antibodies to Costimulatory Receptor 4-1BB Enhance Anti-tumor Immunity via T Regulatory Cell Depletion and Promotion of CD8 T Cell Effector Function. *Immunity* **49,** 958–970.e7 (2018).
90. Smith, S. E., Hoelzinger, D. B., Dominguez, A. L., Van Snick, J. & Lustgarten, J. Signals through 4-1BB inhibit T regulatory cells by blocking IL-9 production enhancing antitumor responses. *Cancer Immunol. Immunother.* **60,** 1775–1787 (2011).
91. Barsoumian, H. B., Yolcu, E. S. & Shirwan, H. 4-1BB Signaling in Conventional T Cells Drives IL-2 Production That Overcomes CD4+CD25+FoxP3+ T Regulatory Cell Suppression. *PLoS ONE* **11,** e0153088 (2016).
92. Mahmud, S. A. *et al.* Costimulation via the tumor-necrosis factor receptor superfamily couples TCR signal strength to the thymic differentiation of regulatory T cells. *Nat Immunol* **15,** 473–481 (2014).

93. Kumar, P. *et al.* Critical role of OX40 signaling in the TCR-independent phase of human and murine thymic Treg generation. *Cellular and Molecular Immunology* **16,** 138–153 (2019).
94. Zaunders, J. J. *et al.* High levels of human antigen-specific CD4+ T cells in peripheral blood revealed by stimulated coexpression of CD25 and CD134 (OX40). *The Journal of Immunology* **183,** 2827–2836 (2009).
95. Vu, M. D. *et al.* OX40 costimulation turns off Foxp3+ Tregs. *Blood* **110,** 2501–2510 (2007).
96. Griseri, T., Asquith, M., Thompson, C. & Powrie, F. OX40 is required for regulatory T cell-mediated control of colitis. *J. Exp. Med.* **207,** 699–709 (2010).
97. Piconese, S. *et al.* A non-redundant role for OX40 in the competitive fitness of Treg in response to IL-2. *Eur. J. Immunol.* **40,** 2902–2913 (2010).
98. Zhang, X. *et al.* OX40 Costimulation Inhibits Foxp3 Expression and Treg Induction via BATF3-Dependent and Independent Mechanisms. *Cell Rep* **24,** 607–618 (2018).
99. Kitamura, N. *et al.* OX40 costimulation can abrogate Foxp3+ regulatory T cell-mediated suppression of antitumor immunity. *Int. J. Cancer* **125,** 630–638 (2009).
100. Kinnear, G., Wood, K. J., Fallah-Arani, F. & Jones, N. D. A diametric role for OX40 in the response of effector/memory CD4+ T cells and regulatory T cells to alloantigen. *The Journal of Immunology* **191,** 1465–1475 (2013).
101. Ruby, C. E. *et al.* Cutting Edge: OX40 agonists can drive regulatory T cell expansion if the cytokine milieu is right. *The Journal of Immunology* **183,** 4853–4857 (2009).
102. Xiao, X. *et al.* New insights on OX40 in the control of T cell immunity and immune tolerance in vivo. *The Journal of Immunology* **188,** 892–901 (2012).
103. Kawamata, S., Hori, T., Imura, A., Takaori-Kondo, A. & Uchiyama, T. Activation of OX40 signal transduction pathways leads to tumor necrosis factor receptor-associated factor (TRAF) 2- and TRAF5-mediated NF-kappaB activation. *Journal of Biological Chemistry* **273,** 5808–5814 (1998).
104. Tone, M. *et al.* Mouse glucocorticoid-induced tumor necrosis factor receptor ligand is costimulatory for T cells. *Proc Natl Acad Sci USA* **100,** 15059–15064 (2003).
105. Shimizu, J., Yamazaki, S., Takahashi, T., Ishida, Y. & Sakaguchi, S. Stimulation of CD25(+)CD4(+) regulatory T cells through GITR breaks immunological self-tolerance. *Nat Immunol* **3,** 135–142 (2002).
106. McHugh, R. S. *et al.* CD4(+)CD25(+) immunoregulatory T cells: gene expression analysis reveals a functional role for the glucocorticoid-induced TNF receptor. *Immunity* **16,** 311–323 (2002).
107. Cuzzocrea, S. *et al.* Glucocorticoid-induced TNF receptor family gene (GITR) knockout mice exhibit a resistance to splanchnic artery occlusion (SAO) shock. *Journal of Leukocyte Biology* **76,** 933–940 (2004).
108. Cuzzocrea, S. *et al.* Role of glucocorticoid-induced TNF receptor family gene (GITR) in collagen-induced arthritis. *FASEB J.* **19,** 1253–1265 (2005).
109. Ephrem, A. *et al.* Modulation of Treg cells/T effector function by GITR signaling is context-dependent. *Eur. J. Immunol.* **43,** 2421–2429 (2013).
110. Knee, D. A., Hewes, B. & Brogdon, J. L. Rationale for anti-GITR cancer immunotherapy. *Eur. J. Cancer* **67,** 1–10 (2016).

111. Yang, S., Wang, J., Brand, D. D. & Zheng, S. G. Role of TNF-TNF Receptor 2 Signal in Regulatory T Cells and Its Therapeutic Implications. *Front Immunol* **9,** 784 (2018).
112. Grell, M. *et al.* The transmembrane form of tumor necrosis factor is the prime activating ligand of the 80 kDa tumor necrosis factor receptor. *Cell* **83,** 793–802 (1995).
113. Yang, S. *et al.* Differential roles of TNFα-TNFR1 and TNFα-TNFR2 in the differentiation and function of CD4+Foxp3+ induced Treg cells in vitro and in vivo periphery in autoimmune diseases. *Cell Death Dis* **10,** 27 (2019).
114. Chen, X. *et al.* Cutting edge: expression of TNFR2 defines a maximally suppressive subset of mouse CD4+CD25+FoxP3+ T regulatory cells: applicability to tumor-infiltrating T regulatory cells. *J. Immunol.* **180,** 6467–6471 (2008).
115. Chen, X., Bäumel, M., Männel, D. N., Howard, O. M. Z. & Oppenheim, J. J. Interaction of TNF with TNF receptor type 2 promotes expansion and function of mouse CD4+CD25+ T regulatory cells. *J. Immunol.* **179,** 154–161 (2007).
116. Torrey, H. *et al.* Targeted killing of TNFR2-expressing tumor cells and Tregs by TNFR2 antagonistic antibodies in advanced Sézary syndrome. *Leukemia* **33,** 1206–1218 (2019).
117. Cohen, J. L. & Wood, K. J. TNFR2: The new Treg switch? *Oncoimmunology* **7,** e1373236 (2017).
118. Atretkhany, K.-S. N. *et al.* Intrinsic TNFR2 signaling in T regulatory cells provides protection in CNS autoimmunity. *Proc. Natl. Acad. Sci. U.S.A.* **115,** 13051–13056 (2018).
119. He, X. *et al.* A TNFR2-Agonist Facilitates High Purity Expansion of Human Low Purity Treg Cells. *PLoS ONE* **11,** e0156311 (2016).
120. Grinberg-Bleyer, Y. *et al.* Pathogenic T cells have a paradoxical protective effect in murine autoimmune diabetes by boosting Tregs. *J. Clin. Invest.* **120,** 4558–4568 (2010).
121. Nie, H. *et al.* Phosphorylation of FOXP3 controls regulatory T cell function and is inhibited by TNF-alpha; in rheumatoid arthritis. *Nature Medicine* **19,** 1–9 (2013).
122. Valencia, X. *et al.* TNF downmodulates the function of human CD4+CD25hi T-regulatory cells. *Blood* **108,** 253–261 (2006).
123. Stoop, J. N. *et al.* Tumor necrosis factor alpha inhibits the suppressive effect of regulatory T cells on the hepatitis B virus-specific immune response. *Hepatology* **46,** 699–705 (2007).
124. Zanin-Zhorov, A. *et al.* Protein kinase C-theta mediates negative feedback on regulatory T cell function. *Science* **328,** 372–376 (2010).
125. Nagar, M. *et al.* TNF activates a NF-kappaB-regulated cellular program in human CD45RA- regulatory T cells that modulates their suppressive function. *The Journal of Immunology* **184,** 3570–3581 (2010).
126. Linsley, P. S. *et al.* CTLA-4 is a second receptor for the B cell activation antigen B7. *Journal of Experimental Medicine* **174,** 561–569 (1991).
127. Schneider, H. *et al.* Reversal of the TCR stop signal by CTLA-4. *Science* **313,** 1972–1975 (2006).
128. Miska, J. *et al.* Real-time immune cell interactions in target tissue during autoimmune-induced damage and graft tolerance. *J. Exp. Med.* **211,** 441–456 (2014).
129. Hou, T. Z. *et al.* A transendocytosis model of CTLA-4 function predicts its suppressive behavior on regulatory T cells. *The Journal of Immunology* **194,** 2148–2159 (2015).

130. Hou, T. Z. *et al.* Identifying functional defects in patients with immune dysregulation due to LRBA and CTLA-4 mutations. *Blood* **129,** 1458–1468 (2017).
131. Hou, T. Z. *et al.* A transendocytosis model of CTLA-4 function predicts its suppressive behavior on regulatory T cells. *The Journal of Immunology* **194,** 2148–2159 (2015).
132. Baban, B. *et al.* IDO activates regulatory T cells and blocks their conversion into Th17-like T cells. *The Journal of Immunology* **183,** 2475–2483 (2009).
133. Prendergast, G. C. *et al.* Indoleamine 2,3-dioxygenase pathways of pathogenic inflammation and immune escape in cancer. *Cancer Immunol. Immunother.* **63,** 721–735 (2014).
134. Munn, D. H. Indoleamine 2,3-dioxygenase, Tregs and cancer. *Curr. Med. Chem.* **18,** 2240–2246 (2011).
135. Sharma, M. D. *et al.* Indoleamine 2,3-dioxygenase controls conversion of Foxp3+ Tregs to TH17-like cells in tumor-draining lymph nodes. *Blood* **113,** 6102–6111 (2009).
136. Huang, C.-T. *et al.* Role of LAG-3 in regulatory T cells. *Immunity* **21,** 503–513 (2004).
137. Strauss, L., Bergmann, C. & Whiteside, T. L. Human circulating CD4+CD25highFoxp3+ regulatory T cells kill autologous CD8+ but not CD4+ responder cells by Fas-mediated apoptosis. *The Journal of Immunology* **182,** 1469–1480 (2009).
138. Mandapathil, M. *et al.* Generation and accumulation of immunosuppressive adenosine by human CD4+CD25highFOXP3+ regulatory T cells. *J. Biol. Chem.* **285,** 7176–7186 (2010).
139. Antonioli, L., Pacher, P., Vizi, E. S. & Haskó, G. CD39 and CD73 in immunity and inflammation. *Trends Mol Med* **19,** 355–367 (2013).
140. Levings, M. K., Bacchetta, R., Schulz, U. & Roncarolo, M.-G. The Role of IL-10 and TGF-β in the Differentiation and Effector Function of T Regulatory Cells. *Int Arch Allergy Immunol* **129,** 263–276 (2002).
141. Andersson, J. *et al.* CD4+ FoxP3+ regulatory T cells confer infectious tolerance in a TGF-beta-dependent manner. *J. Exp. Med.* **205,** 1975–1981 (2008).
142. Jonuleit, H. *et al.* Infectious tolerance: human CD25(+) regulatory T cells convey suppressor activity to conventional CD4(+) T helper cells. *Journal of Experimental Medicine* **196,** 255–260 (2002).
143. Dieckmann, D., Bruett, C. H., Ploettner, H., Lutz, M. B. & Schuler, G. Human CD4(+)CD25(+) regulatory, contact-dependent T cells induce interleukin 10-producing, contact-independent type 1-like regulatory T cells [corrected]. *Journal of Experimental Medicine* **196,** 247–253 (2002).
144. Schmidt, A., Oberle, N. & Krammer, P. H. Molecular mechanisms of treg-mediated T cell suppression. *Front Immunol* **3,** 51 (2012).
145. Olson, B. M., Sullivan, J. A. & Burlingham, W. J. Interleukin 35: a key mediator of suppression and the propagation of infectious tolerance. *Front Immunol* **4,** 315 (2013).
146. Cao, X. *et al.* Granzyme B and perforin are important for regulatory T cell-mediated suppression of tumor clearance. *Immunity* **27,** 635–646 (2007).
147. Pandiyan, P., Zheng, L., Ishihara, S., Reed, J. & Lenardo, M. J. CD4+CD25+Foxp3+ regulatory T cells induce cytokine deprivation-mediated apoptosis of effector CD4+ T cells. *Nat Immunol* **8,** 1353–1362 (2007).

148. Chinen, T. *et al.* An essential role for the IL-2 receptor in Treg cell function. *Nat Immunol* **17,** 1322–1333 (2016).
149. Oberle, N., Eberhardt, N., Falk, C. S., Krammer, P. H. & Suri-Payer, E. Rapid suppression of cytokine transcription in human CD4+CD25 T cells by CD4+Foxp3+ regulatory T cells: independence of IL-2 consumption, TGF-beta, and various inhibitors of TCR signaling. *J. Immunol.* **179,** 3578–3587 (2007).
150. Duhen, T., Duhen, R., Lanzavecchia, A., Sallusto, F. & Campbell, D. J. Functionally distinct subsets of human FOXP3+ Treg cells that phenotypically mirror effector Th cells. *Blood* **119,** 4430–4440 (2012).
151. Halim, L. *et al.* An Atlas of Human Regulatory T Helper-like Cells Reveals Features of Th2-like Tregs that Support a Tumorigenic Environment. *Cell Rep* **20,** 757–770 (2017).
152. Campbell, D. J. Control of Regulatory T Cell Migration, Function, and Homeostasis. *The Journal of Immunology* **195,** 2507–2513 (2015).
153. Hoeppli, R. E. *et al.* Tailoring the homing capacity of human Tregs for directed migration to sites of Th1-inflammation or intestinal regions. *Am. J. Transplant.* **19,** 62–76 (2019).
154. Arpaia, N. *et al.* A Distinct Function of Regulatory T Cells in Tissue Protection. *Cell* **162,** 1078–1089 (2015).
155. Lam, A. J. *et al.* Innate Control of Tissue-Reparative Human Regulatory T Cells. *The Journal of Immunology* **202,** 2195–2209 (2019).
156. Saadoun, D. *et al.* Regulatory T-cell responses to low-dose interleukin-2 in HCV-induced vasculitis. *N Engl J Med* **365,** 2067–2077 (2011).
157. Klatzmann, D. & Abbas, A. K. The promise of low-dose interleukin-2 therapy for autoimmune and inflammatory diseases. *Nat. Rev. Immun.* **15,** 283–294 (2015).
158. Matsuoka, K.-I. *et al.* Low-dose interleukin-2 therapy restores regulatory T cell homeostasis in patients with chronic graft-versus-host disease. *Science Translational Medicine* **5,** 179ra43–179ra43 (2013).
159. Mizui, M. & Tsokos, G. C. Low-Dose IL-2 in the Treatment of Lupus. *Current Rheumatology Reports* 1–7 (2016). doi:10.1007/s11926-016-0617-5
160. Pham, M. N., Herrath, Von, M. G. & Vela, J. L. Antigen-Specific Regulatory T Cells and Low Dose of IL-2 in Treatment of Type 1 Diabetes. *Front Immunol* **6,** 1007–9 (2016).
161. Todd, J. A. *et al.* Regulatory T Cell Responses in Participants with Type 1 Diabetes after a Single Dose of Interleukin-2: A Non-Randomised, Open Label, Adaptive Dose-Finding Trial. *PLoS Med* **13,** e1002139–33 (2016).
162. Long, S. A. *et al.* Rapamycin/IL-2 combination therapy in patients with type 1 diabetes augments Tregs yet transiently impairs beta-cell function. *Diabetes* **61,** 2340–2348 (2012).
163. Zhang, D. *et al.* Manipulating regulatory T cells: a promising strategy to treat autoimmunity. *Immunotherapy* **7,** 1201–1211 (2015).
164. Boyman, O., Kolios, A. G. A. & Raeber, M. E. Modulation of T cell responses by IL-2 and IL-2 complexes. *Clinical and Experimental Rheumatology* **33,** S54–S57 (2015).
165. Arenas-Ramirez, N., Woytschak, J. & Boyman, O. Interleukin-2: Biology, Design and Application. *Trends in Immunology* **36,** 763–777 (2015).

166. Spangler, J. B. *et al.* Antibodies to Interleukin-2 Elicit Selective T Cell Subset Potentiation through Distinct Conformational Mechanisms. *Immunity* **42,** 815–825 (2015).
167. Carmenate, T. *et al.* Human IL-2 Mutein with Higher Antitumor Efficacy Than Wild Type IL-2. *Journal of Immunology* **190,** 6230–6238 (2013).
168. Rojas, G., Carmenate, T. & Leon, K. Molecular dissection of the interactions of an antitumor interleukin-2-derived mutein on a phage display-based platform. *J. Mol. Recognit.* **28,** 261–268 (2015).
169. Mitra, S. *et al.* Interleukin-2 Activity Can Be Fine Tuned with Engineered Receptor Signaling Clamps. *Immunity* **42,** 826–838 (2015).
170. Ledford, H. Drug companies flock to supercharged T-cells in fight against autoimmune disease. *Nature News* (2017). doi:10.1038/nature.2017.22393
171. Alcina, A. *et al.* IL2RA/CD25 gene polymorphisms: uneven association with multiple sclerosis (MS) and type 1 diabetes (T1D). *PLoS ONE* **4,** e4137 (2009).
172. Hinks, A. *et al.* Association of the IL2RA/CD25 gene with juvenile idiopathic arthritis. *Arthritis Rheum.* **60,** 251–257 (2009).
173. Sebode, M. *et al.* Reduced FOXP3(+) regulatory T cells in patients with primary sclerosing cholangitis are associated with IL2RA gene polymorphisms. *J. Hepatol.* **60,** 1010–1016 (2014).
174. Simeonov, D. R., Gowen, B. G., Boontanrart, M. & Roth, T. Discovery of an autoimmunity-associated IL2RA enhancer by unbiased targeting of transcriptional activation. *bioRxiv* (2016). doi:10.1101/091843
175. Trzonkowski, P. *et al.* First-in-man clinical results of the treatment of patients with graft versus host disease with human ex vivo expanded CD4+CD25+CD127- T regulatory cells. *Clin. Immunol.* **133,** 22–26 (2009).
176. Brunstein, C. G. *et al.* Infusion of ex vivo expanded T regulatory cells in adults transplanted with umbilical cord blood: safety profile and detection kinetics. *Blood* **117,** 1061–1070 (2011).
177. Brunstein, C. G. *et al.* Umbilical cord blood-derived T regulatory cells to prevent GVHD: kinetics, toxicity profile, and clinical effect. *Blood* **127,** 1044–1051 (2016).
178. Marek-Trzonkowska, N. *et al.* Administration of CD4+CD25highCD127- regulatory T cells preserves beta-cell function in type 1 diabetes in children. *Diabetes Care* **35,** 1817–1820 (2012).
179. Marek-Trzonkowska, N. *et al.* Factors affecting long-term efficacy of T regulatory cell-based therapy in type 1 diabetes. *J Transl Med* **14,** 332 (2016).
180. Bluestone, J. A. *et al.* Type 1 diabetes immunotherapy using polyclonal regulatory T cells. *Science Translational Medicine* **7,** 315ra189–315ra189 (2015).
181. Canavan, J. B. *et al.* Developing in vitro expanded CD45RA+ regulatory T cells as an adoptive cell therapy for Crohn's disease. *Gut* **65,** 584–594 (2016).
182. Gliwinski, M., Iwaszkiewicz-Grzes, D. & Trzonkowski, P. Cell-Based Therapies with T Regulatory Cells. *BioDrugs* **31,** 335–347 (2017).
183. Romano, M., Tung, S. L., Smyth, L. A. & Lombardi, G. Treg therapy in transplantation: a general overview. *Transpl Int* **30,** 745–753 (2017).
184. Trzonkowski, P. *et al.* Hurdles in therapy with regulatory T cells. *Science Translational Medicine* **7,** 304ps18 (2015).

185. Rossetti, M. *et al.* Ex vivo-expanded but not in vitro-induced human regulatory T cells are candidates for cell therapy in autoimmune diseases thanks to stable demethylation of the FOXP3 regulatory T cell-specific demethylated region. *The Journal of Immunology* **194,** 113–124 (2015).
186. Hoffmann, P. *et al.* Only the CD45RA+ subpopulation of CD4+CD25high T cells gives rise to homogeneous regulatory T-cell lines upon in vitro expansion. *Blood* **108,** 4260–4267 (2006).
187. Sicard, A., Levings, M. K. & Scott, D. W. Engineering therapeutic T cells to suppress alloimmune responses using TCRs, CARs, or BARs. *Am. J. Transplant.* **18,** 1305–1311 (2018).
188. Dijke, I. E. *et al.* Discarded Human Thymus Is a Novel Source of Stable and Long-Lived Therapeutic Regulatory T Cells. *Am. J. Transplant.* **16,** 58–71 (2016).
189. Dijke, I. E. *et al.* Discarded Human Thymus Is a Novel Source of Stable and Long-Lived Therapeutic Regulatory T Cells. *Am. J. Transplant.* **16,** 58–71 (2016).
190. Dijke, I. E. *et al.* Discarded Human Thymus Is a Novel Source of Stable and Long-Lived Therapeutic Regulatory T Cells. *Am. J. Transplant.* (2015). doi:10.1111/ajt.13456
191. Haque, M. *et al.* Stem cell-derived tissue-associated regulatory T cells suppress the activity of pathogenic cells in autoimmune diabetes. *JCI Insight* **4,** 1273 (2019).
192. McMurchy, A. N. & Levings, M. K. In vitro generation of human T regulatory cells: generation, culture, and analysis of FOXP3-transduced T cells. *Methods Mol. Biol.* **946,** 115–132 (2013).
193. Allan, S. E. *et al.* Generation of potent and stable human CD4+ T regulatory cells by activation-independent expression of FOXP3. *Mol. Ther.* **16,** 194–202 (2008).
194. Amendola, M. *et al.* Regulated and multiple miRNA and siRNA delivery into primary cells by a lentiviral platform. *Mol. Ther.* **17,** 1039–1052 (2009).
195. Fu, W. *et al.* A multiply redundant genetic switch 'locks in' the transcriptional signature of regulatory T cells. *Nat Immunol* **13,** 972–980 (2012).
196. Vent-Schmidt, J., Han, J. M., Macdonald, K. G. & Levings, M. K. The Role of FOXP3 in Regulating Immune Responses. *Int Rev Immunol* **33,** 110–128 (2014).
197. Passerini, L. *et al.* $CD4^+$ T cells from IPEX patients convert into functional and stable regulatory T cells by FOXP3 gene transfer. *Science Translational Medicine* **5,** 215ra174–215ra174 (2013).
198. Passerini, L., Santoni de Sio, F. R., Porteus, M. H. & Bacchetta, R. Gene/cell therapy approaches for Immune Dysregulation Polyendocrinopathy Enteropathy X-linked syndrome. *Curr Gene Ther* **14,** 422–428 (2014).
199. Hoeppli, R. E., MacDonald, K. G., Levings, M. K. & Cook, L. How antigen specificity directs regulatory T-cell function: self, foreign and engineered specificity. *HLA* **88,** 3–13 (2016).
200. Dawson, N. A. J. & Levings, M. K. Antigen-specific regulatory T cells: are police CARs the answer? *Transl Res* 1–6 (2017). doi:10.1016/j.trsl.2017.06.009
201. Tang, Q. & Lee, K. Regulatory T-cell therapy for transplantation: how many cells do we need? *Current Opinion in Organ Transplantation* **17,** 349–354 (2012).
202. Tang, Q. & Vincenti, F. Transplant trials with Tregs: perils and promises. *J. Clin. Invest.* **127,** 2505–2512 (2017).

203. Harris, D. T. & Kranz, D. M. Adoptive T Cell Therapies: A Comparison of T Cell Receptors and Chimeric Antigen Receptors. *Trends in Pharmacological Sciences* (2015). doi:10.1016/j.tips.2015.11.004
204. Brusko, T. M. *et al.* Human antigen-specific regulatory T cells generated by T cell receptor gene transfer. *PLoS ONE* **5,** e11726 (2010).
205. Hull, C. M. *et al.* Generation of human islet-specific regulatory T cells by TCR gene transfer. *J. Autoimmun.* **79,** 63–73 (2017).
206. Tsang, J. Y. S. *et al.* The potency of allospecific Tregs cells appears to correlate with T cell receptor functional avidity. *Am. J. Transplant.* **11,** 1610–1620 (2011).
207. Plesa, G. *et al.* TCR affinity and specificity requirements for human regulatory T-cell function. *Blood* **119,** 3420–3430 (2012).
208. Eshhar, Z., Waks, T., Gross, G. & Schindler, D. G. Specific activation and targeting of cytotoxic lymphocytes through chimeric single chains consisting of antibody-binding domains and the gamma or zeta subunits of the immunoglobulin and T-cell receptors. *Proc Natl Acad Sci USA* **90,** 720–724 (1993).
209. Maus, M. V. & June, C. H. Making Better Chimeric Antigen Receptors for Adoptive T-cell Therapy. *Clinical cancer research : an official journal of the American Association for Cancer Research* **22,** 1875–1884 (2016).
210. Esensten, J. H., Bluestone, J. A. & Lim, W. A. Engineering Therapeutic T Cells: From Synthetic Biology to Clinical Trials. *Annu Rev Pathol* **12,** 305–330 (2017).
211. Sadelain, M. Chimeric antigen receptors: driving immunology towards synthetic biology. *Curr. Opin. Immunol.* **41,** 68–76 (2016).
212. Porter, D. L., Levine, B. L., Kalos, M., Bagg, A. & June, C. H. Chimeric antigen receptor-modified T cells in chronic lymphoid leukemia. *N Engl J Med* **365,** 725–733 (2011).
213. Haji-Fatahaliha, M. *et al.* CAR-modified T-cell therapy for cancer: an updated review. *Artif Cells Nanomed Biotechnol* **44,** 1339–1349 (2016).
214. Chmielewski, M. & Abken, H. TRUCKs: the fourth generation of CARs. *Expert Opinion on Biological Therapy* **15,** 1145–1154 (2015).
215. Roybal, K. T. *et al.* Precision Tumor Recognition by T Cells With Combinatorial Antigen-Sensing Circuits. *Cell* **164,** 770–779 (2016).
216. Chang, Z. L. & Chen, Y. Y. CARs: Synthetic Immunoreceptors for Cancer Therapy and Beyond. *Trends Mol Med* **23,** 430–450 (2017).
217. Elinav, E., Waks, T. & Eshhar, Z. Redirection of regulatory T cells with predetermined specificity for the treatment of experimental colitis in mice. *Gastroenterology* **134,** 2014–2024 (2008).
218. Elinav, E., Adam, N., Waks, T. & Eshhar, Z. Amelioration of colitis by genetically engineered murine regulatory T cells redirected by antigen-specific chimeric receptor. *Gastroenterology* **136,** 1721–1731 (2009).
219. Blat, D., Zigmond, E., Alteber, Z., Waks, T. & Eshhar, Z. Suppression of murine colitis and its associated cancer by carcinoembryonic antigen-specific regulatory T cells. *Mol. Ther.* **22,** 1018–1028 (2014).
220. Fransson, M. *et al.* CAR/FoxP3-engineered T regulatory cells target the CNS and suppress EAE upon intranasal delivery. *Journal of neuroinflammation* **9,** 112 (2012).

221. MacDonald, K. G. *et al.* Alloantigen-specific regulatory T cells generated with a chimeric antigen receptor. *J. Clin. Invest.* **126,** 1413–1424 (2016).
222. Noyan, F. *et al.* Prevention of Allograft Rejection by Use of Regulatory T Cells With an MHC-Specific Chimeric Antigen Receptor. *Am. J. Transplant.* **17,** 917–930 (2017).
223. Boardman, D. A. *et al.* Expression of a Chimeric Antigen Receptor Specific for Donor HLA Class I Enhances the Potency of Human Regulatory T Cells in Preventing Human Skin Transplant Rejection. *Am. J. Transplant.* **17,** 931–943 (2017).
224. Yoon, J. *et al.* FVIII-specific human chimeric antigen receptor T-regulatory cells suppress T- and B-cell responses to FVIII. *Blood* **129,** 238–245 (2017).
225. Wu, Y., Jiang, S. & Ying, T. From therapeutic antibodies to chimeric antigen receptors (CARs): making better CARs based on antigen-binding domain. *Expert Opinion on Biological Therapy* **16,** 1469–1478 (2016).
226. Lee, D. W. *et al.* T cells expressing CD19 chimeric antigen receptors for acute lymphoblastic leukaemia in children and young adults: a phase 1 dose-escalation trial. *Lancet* **385,** 517–528 (2015).
227. Maude, S. L. *et al.* Chimeric antigen receptor T cells for sustained remissions in leukemia. *N Engl J Med* **371,** 1507–1517 (2014).
228. Grupp, S. A. *et al.* Chimeric antigen receptor-modified T cells for acute lymphoid leukemia. *N Engl J Med* **368,** 1509–1518 (2013).
229. Hege, K. M. *et al.* Safety, tumor trafficking and immunogenicity of chimeric antigen receptor (CAR)-T cells specific for TAG-72 in colorectal cancer. *Journal for immunotherapy of cancer* **5,** 22 (2017).
230. Lamers, C. H. *et al.* Parallel detection of transduced T lymphocytes after immunogene therapy of renal cell cancer by flow cytometry and real-time polymerase chain reaction: implications for loss of transgene expression. *Hum Gene Ther* **16,** 1452–1462 (2005).
231. Kershaw, M. H. *et al.* A phase I study on adoptive immunotherapy using gene-modified T cells for ovarian cancer. *Clinical cancer research : an official journal of the American Association for Cancer Research* **12,** 6106–6115 (2006).
232. Turtle, C. J. *et al.* CD19 CAR-T cells of defined CD4+:CD8+ composition in adult B cell ALL patients. *J. Clin. Invest.* **126,** 2123–2138 (2016).
233. Maude, S. L. *et al.* Efficacy of Humanized CD19-Targeted Chimeric Antigen Receptor (CAR)-Modified T Cells in Children and Young Adults with Relapsed/Refractory Acute Lymphoblastic Leukemia. *Blood* **128,** 217–217 (2016).
234. Maus, M. V. *et al.* T cells expressing chimeric antigen receptors can cause anaphylaxis in humans. *Cancer Immunol Res* **1,** 26–31 (2013).
235. Lamers, C. H. *et al.* Immune responses to transgene and retroviral vector in patients treated with ex vivo-engineered T cells. *Blood* **117,** 72–82 (2011).
236. Hwang, W. Y. & Foote, J. Immunogenicity of engineered antibodies. *Methods* **36,** 3–10 (2005).
237. Hansel, T. T., Kropshofer, H., Singer, T., Mitchell, J. A. & George, A. J. The safety and side effects of monoclonal antibodies. *Nat Rev Drug Discov* **9,** 325–338 (2010).
238. Jones, P. T., Dear, P. H., Foote, J., Neuberger, M. S. & Winter, G. Replacing the complementarity-determining regions in a human antibody with those from a mouse. *Nature* **321,** 522–525 (1986).

239. Verhoeyen, M., Milstein, C. & Winter, G. Reshaping human antibodies: grafting an antilysozyme activity. *Science* **239,** 1534–1536 (1988).
240. Queen, C. *et al.* A humanized antibody that binds to the interleukin 2 receptor. *Proc Natl Acad Sci USA* **86,** 10029–10033 (1989).
241. Kashmiri, S. V., De Pascalis, R., Gonzales, N. R. & Schlom, J. SDR grafting--a new approach to antibody humanization. *Methods* **36,** 25–34 (2005).
242. Suzuki, M., Kato, C. & Kato, A. Therapeutic antibodies: their mechanisms of action and the pathological findings they induce in toxicity studies. *J Toxicol Pathol* **28,** 133–139 (2015).
243. Riechmann, L., Clark, M., Waldmann, H. & Winter, G. Reshaping human antibodies for therapy. *Nature* **332,** 323–327 (1988).
244. Sadelain, M., Brentjens, R. & Riviere, I. The basic principles of chimeric antigen receptor design. *Cancer discovery* **3,** 388–398 (2013).
245. Brentjens, R. J. *et al.* CD19-targeted T cells rapidly induce molecular remissions in adults with chemotherapy-refractory acute lymphoblastic leukemia. *Science Translational Medicine* **5,** 177ra38–177ra38 (2013).
246. Long, A. H. *et al.* 4-1BB costimulation ameliorates T cell exhaustion induced by tonic signaling of chimeric antigen receptors. *Nature Medicine* **21,** 581–590 (2015).
247. Dawson, N. A. *et al.* Systematic testing and specificity mapping of alloantigen-specific chimeric antigen receptors in regulatory T cells. *JCI Insight* **4,** (2019).
248. Boroughs, A. C. *et al.* Chimeric antigen receptor costimulation domains modulate human regulatory T cell function. *JCI Insight* **4,** 5426 (2019).
249. Waldmann, H. Human Monoclonal Antibodies: The Benefits of Humanization. *Methods Mol. Biol.* **1904,** 1–10 (2019).
250. Sommermeyer, D. *et al.* Fully human CD19-specific chimeric antigen receptors for T-cell therapy. *Leukemia* **31,** 2191–2199 (2017).
251. Spitzer, M. H. & Nolan, G. P. Mass Cytometry: Single Cells, Many Features. *Cell* **165,** 780–791 (2016).
252. Robinson, J. *et al.* The IPD and IMGT/HLA database: allele variant databases. *Nucleic Acids Res.* **43,** D423–31 (2015).
253. The UniProt Consortium. UniProt: a worldwide hub of protein knowledge. *Nucleic Acids Res.* **47,** D506–D515 (2018).
254. Mason, G. M. *et al.* Phenotypic Complexity of the Human Regulatory T Cell Compartment Revealed by Mass Cytometry. *The Journal of Immunology* **195,** 2030–2037 (2015).
255. Hirakawa, M. *et al.* Low-dose IL-2 selectively activates subsets of CD4(+) Tregs and NK cells. *JCI Insight* **1,** e89278 (2016).
256. Fienberg, H. G., Simonds, E. F., Fantl, W. J., Nolan, G. P. & Bodenmiller, B. A platinum-based covalent viability reagent for single-cell mass cytometry. *Cytometry A* **81,** 467–475 (2012).
257. Lamarche, C. *et al.* Clinical-Scale Rapid Autologous BK Virus-Specific T Cell Line Generation From Kidney Transplant Recipients With Active Viremia for Adoptive Immunotherapy. *Transplantation* **101,** 2713–2721 (2017).
258. McMurchy, A. N. & Levings, M. K. Suppression assays with human T regulatory cells: a technical guide. *Eur. J. Immunol.* **42,** 27–34 (2012).

259. Schneider, C. A., Rasband, W. S. & Eliceiri, K. W. NIH Image to ImageJ: 25 years of image analysis. *Nat Meth* **9,** 671–675 (2012).
260. Eliceiri, K. W. *et al.* Biological imaging software tools. *Nat Meth* **9,** 697–710 (2012).
261. Massi, D. *et al.* A reappraisal of the histopathologic criteria for the diagnosis of cutaneous allogeneic acute graft-vs-host disease. *American journal of clinical pathology* **112,** 791–800 (1999).
262. Fischer, A. *et al.* Histopathologic Features of Cutaneous Acute Graft-Versus-Host Disease in T-Cell-Depleted Peripheral Blood Stem Cell Transplant Recipients. *The American Journal of dermatopathology* **37,** 523–529 (2015).
263. Kanitakis, J. The challenge of dermatopathological diagnosis of composite tissue allograft rejection: a review. *Journal of cutaneous pathology* **35,** 738–744 (2008).
264. Schmittgen, T. D. & Livak, K. J. Analyzing real-time PCR data by the comparative C(T) method. *Nat Protoc* **3,** 1101–1108 (2008).
265. Law, C. W. *et al.* RNA-seq analysis is easy as 1-2-3 with limma, Glimma and edgeR. *F1000Res* **5,** 1408 (2016).
266. Cooke, K. R. *et al.* An experimental model of idiopathic pneumonia syndrome after bone marrow transplantation: I. The roles of minor H antigens and endotoxin. *Blood* **88,** 3230–3239 (1996).
267. Hill, G. R. *et al.* Total body irradiation and acute graft-versus-host disease: the role of gastrointestinal damage and inflammatory cytokines. *Blood* **90,** 3204–3213 (1997).
268. Barrett, D. M. *et al.* Relation of clinical culture method to T-cell memory status and efficacy in xenograft models of adoptive immunotherapy. *Cytotherapy* **16,** 619–630 (2014).
269. Finck, R. *et al.* Normalization of mass cytometry data with bead standards. *Cytometry* **83A,** 483–494 (2013).
270. Shekhar, K., Brodin, P. & Davis, M. M. Automatic classification of cellular expression by nonlinear stochastic embedding (ACCENSE). in (2014). doi:10.1073/pnas.1321405111/-/DCSupplemental
271. Meyer, D., VR, C. A., Bitarello, B. D., DY, C. B. & Nunes, K. A genomic perspective on HLA evolution. *Immunogenetics* **70,** 5–27 (2018).
272. Kabat, E. A., National Institutes of, Health. Columbia, University. *Sequences of proteins of immunological interest*. (U.S. Dept. of Health and Human Services, Public Health Service, National Institutes of Health, 1991).
273. Chothia, C. & Lesk, A. M. Canonical structures for the hypervariable regions of immunoglobulins. *Journal of Molecular Biology* **196,** 901–917 (1987).
274. El-Awar, N., Lee, J. H., Tarsitani, C. & Terasaki, P. I. HLA class I epitopes: recognition of binding sites by mAbs or eluted alloantibody confirmed with single recombinant antigens. *Human Immunology* **68,** 170–180 (2007).
275. Hilton, H. G. & Parham, P. Direct binding to antigen-coated beads refines the specificity and cross-reactivity of four monoclonal antibodies that recognize polymorphic epitopes of HLA class I molecules. *Tissue Antigens* **81,** 212–220 (2013).
276. Lamarche, C. & Levings, M. K. Guiding regulatory T cells to the allograft. *Current Opinion in Organ Transplantation* **23,** 106–113 (2018).

277. Lam, A. J., Hoeppli, R. E. & Levings, M. K. Harnessing Advances in T Regulatory Cell Biology for Cellular Therapy in Transplantation. *Transplantation* **101,** 2277–2287 (2017).
278. Cao, J. *et al.* Potent anti-leukemia activities of humanized CD19-targeted Chimeric antigen receptor T (CAR-T) cells in patients with relapsed/refractory acute lymphoblastic leukemia. *Am J Hematol* **93,** 851–858 (2018).
279. Lamers, C. H. *et al.* Treatment of metastatic renal cell carcinoma with autologous T-lymphocytes genetically retargeted against carbonic anhydrase IX: first clinical experience. *J. Clin. Oncol.* **24,** e20–2 (2006).
280. Safdari, Y., Farajnia, S., Asgharzadeh, M. & Khalili, M. Antibody humanization methods - a review and update. *Biotechnology and Genetic Engineering Reviews* **29,** 175–186 (2013).
281. Johnson, L. A. *et al.* Rational development and characterization of humanized anti-EGFR variant III chimeric antigen receptor T cells for glioblastoma. *Science Translational Medicine* **7,** 275ra22 (2015).
282. Sun, M. *et al.* Construction and evaluation of a novel humanized HER2-specific chimeric receptor. *Breast Cancer Res* **16,** R61 (2014).
283. Qian, L. *et al.* The novel anti-CD19 chimeric antigen receptors with humanized scFv (single-chain variable fragment) trigger leukemia cell killing. *Cellular Immunology* **304-305,** 49–54 (2016).
284. Teplyakov, A. *et al.* Structural insights into humanization of anti-tissue factor antibody 10H10. *MAbs* **10,** 269–277 (2018).
285. Schwaigerlehner, L., Pechlaner, M., Mayrhofer, P., Oostenbrink, C. & Kunert, R. Lessons learned from merging wet lab experiments with molecular simulation to improve mAb humanization. *Protein Eng Des Sel* (2018). doi:10.1093/protein/gzy009
286. Choi, Y., Hua, C., Sentman, C. L., Ackerman, M. E. & Bailey-Kellogg, C. Antibody humanization by structure-based computational protein design. *MAbs* **7,** 1045–1057 (2015).
287. Zeevi, A., Marrari, M., Feingold, B., Webber, S. & Duquesnoy, R. J. Human leukocyte antigen epitope analysis to assess complement- and non-complement-binding donor-specific antibody repertoire in a pediatric heart transplant recipient. *Human Immunology* **73,** 48–51 (2012).
288. Ramos, C. A. & Dotti, G. Chimeric antigen receptor (CAR)-engineered lymphocytes for cancer therapy. *Expert Opinion on Biological Therapy* **11,** 855–873 (2011).
289. Davenport, A. J. *et al.* Chimeric antigen receptor T cells form nonclassical and potent immune synapses driving rapid cytotoxicity. *Proc. Natl. Acad. Sci. U.S.A.* **115,** E2068–E2076 (2018).
290. Jensen, M. C. *et al.* Antitransgene rejection responses contribute to attenuated persistence of adoptively transferred CD20/CD19-specific chimeric antigen receptor redirected T cells in humans. *Biol. Blood Marrow Transplant.* **16,** 1245–1256 (2010).
291. Elinav, E., Adam, N., Waks, T. & Eshhar, Z. Amelioration of colitis by genetically engineered murine regulatory T cells redirected by antigen-specific chimeric receptor. *Gastroenterology* **136,** 1721–1731 (2009).
292. Pierini, A. *et al.* T cells expressing chimeric antigen receptor promote immune tolerance. *JCI Insight* **2,** 1–17 (2017).

293. Nervi, B. *et al.* Factors affecting human T cell engraftment, trafficking, and associated xenogeneic graft-vs-host disease in NOD/SCID beta2mnull mice. *Exp Hematol* **35,** 1823–1838 (2007).
294. Zhang, N. *et al.* Regulatory T cells sequentially migrate from inflamed tissues to draining lymph nodes to suppress the alloimmune response. *Immunity* **30,** 458–469 (2009).
295. Arroyo Hornero, R. *et al.* CD45RA Distinguishes CD4+CD25+CD127-/low TSDR Demethylated Regulatory T Cell Subpopulations With Differential Stability and Susceptibility to Tacrolimus-Mediated Inhibition of Suppression. *Transplantation* **101,** 302–309 (2017).
296. Boardman, D. A. & Levings, M. K. Cancer immunotherapies repurposed for use in autoimmunity. *Nat Biomed Eng* **3,** 259–263 (2019).
297. Pierini, A. *et al.* T cells expressing chimeric antigen receptor promote immune tolerance. *JCI Insight* **2,** 763 (2017).
298. Kim, Y. C. *et al.* Engineered antigen-specific human regulatory T cells: immunosuppression of FVIII-specific T- and B-cell responses. *Blood* **125,** 1107–1115 (2015).
299. Kumar, P., Bhattacharya, P. & Prabhakar, B. S. A comprehensive review on the role of co-signaling receptors and Treg homeostasis in autoimmunity and tumor immunity. *Journal of Autoimmunity* **95,** 77–99 (2018).
300. Long, A. H. *et al.* 4-1BB costimulation ameliorates T cell exhaustion induced by tonic signaling of chimeric antigen receptors. *Nature Medicine* **21,** 581–590 (2015).
301. Song, D. G. *et al.* In Vivo Persistence, Tumor Localization, and Antitumor Activity of CAR-Engineered T Cells Is Enhanced by Costimulatory Signaling through CD137 (4-1BB). *Cancer Research* **71,** 4617–4627 (2011).
302. van der Stegen, S. J. C., Hamieh, M. & Sadelain, M. The pharmacology of second-generation chimeric antigen receptors. *Nat Rev Drug Discov* **14,** 499–509 (2015).
303. Salmikangas, P., Kinsella, N. & Chamberlain, P. Chimeric Antigen Receptor T-Cells (CAR T-Cells) for Cancer Immunotherapy - Moving Target for Industry? *Pharm Res* **35,** 152 (2018).
304. Guedan, S. *et al.* ICOS-based chimeric antigen receptors program bipolar TH17/TH1 cells. *Blood* **124,** 1070–1080 (2014).
305. Guedan, S. *et al.* Enhancing CAR T cell persistence through ICOS and 4-1BB costimulation. *JCI Insight* **3,** 6106–18 (2018).
306. Fedorov, V. D., Themeli, M. & Sadelain, M. PD-1- and CTLA-4-based inhibitory chimeric antigen receptors (iCARs) divert off-target immunotherapy responses. *Science Translational Medicine* **5,** 215ra172 (2013).
307. Nowak, A. *et al.* CD137+CD154- Expression As a Regulatory T Cell (Treg)-Specific Activation Signature for Identification and Sorting of Stable Human Tregs from In Vitro Expansion Cultures. *Front Immunol* **9,** 199 (2018).
308. Golovina, T. N. *et al.* CD28 Costimulation Is Essential for Human T Regulatory Expansion and Function. *J. Immunol.* **181,** 2855–2868 (2008).
309. Tai, X., Cowan, M., Feigenbaum, L. & Singer, A. CD28 costimulation of developing thymocytes induces Foxp3 expression and regulatory T cell differentiation independently of interleukin 2. *Nat Immunol* **6,** 152–162 (2005).

310. Zhang, R. *et al.* An obligate cell-intrinsic function for CD28 in Tregs. *J. Clin. Invest.* **123,** 580–593 (2013).
311. Okkenhaug, K. *et al.* A point mutation in CD28 distinguishes proliferative signals from survival signals. *Nat Immunol* **2,** 325–332 (2001).
312. Walker, L. S. K. & Sansom, D. M. The emerging role of CTLA4 as a cell-extrinsic regulator of T cell responses. *Nat. Rev. Immun.* **11,** 852–863 (2011).
313. Nakaseko, C. *et al.* Cytotoxic T Lymphocyte Antigen 4 (Ctla-4) Engagement Delivers an Inhibitory Signal through the Membrane-Proximal Region in the Absence of the Tyrosine Motif in the Cytoplasmic Tail. *Journal of Experimental Medicine* **190,** 765–774 (1999).
314. Chopra, M. *et al.* Exogenous TNFR2 activation protects from acute GvHD via host T reg cell expansion. *J. Exp. Med.* **213,** 1881–1900 (2016).
315. Pierini, A. *et al.* TNF-alpha priming enhances CD4+FoxP3+ regulatory T-cell suppressive function in murine GVHD prevention and treatment. *Blood* **128,** 866–871 (2016).
316. Bridgeman, J. S., Hawkins, R. E., Hombach, A. A., Abken, H. & Gilham, D. E. Building better chimeric antigen receptors for adoptive T cell therapy. *Curr Gene Ther* **10,** 77–90 (2010).
317. Dotti, G., Gottschalk, S., Savoldo, B. & Brenner, M. K. Design and development of therapies using chimeric antigen receptor-expressing T cells. *Immunol. Rev.* **257,** 107–126 (2014).
318. Hamieh, M. *et al.* CAR T cell trogocytosis and cooperative killing regulate tumour antigen escape. *Nature* **568,** 112–116 (2019).
319. June, C. H. & Sadelain, M. Chimeric Antigen Receptor Therapy. *N Engl J Med* **379,** 64–73 (2018).
320. Lim, W. A. & June, C. H. The Principles of Engineering Immune Cells to Treat Cancer. *Cell* **168,** 724–740 (2017).
321. Kim, H.-J. *et al.* Stable inhibitory activity of regulatory T cells requires the transcription factor Helios. *Science* **350,** 334–339 (2015).
322. Nakagawa, H. *et al.* Instability of Helios-deficient Tregs is associated with conversion to a T-effector phenotype and enhanced antitumor immunity. *Proc Natl Acad Sci USA* **113,** 6248–6253 (2016).
323. Skadow, M., Penna, V. R., Galant-Swafford, J., Shevach, E. M. & Thornton, A. M. Helios Deficiency Predisposes the Differentiation of CD4(+)Foxp3(-) T Cells into Peripherally Derived Regulatory T Cells. *The Journal of Immunology* **203,** 370–378 (2019).
324. Thornton, A. M. *et al.* Helios(+) and Helios(-) Treg subpopulations are phenotypically and functionally distinct and express dissimilar TCR repertoires. *Eur. J. Immunol.* **49,** 398–412 (2019).
325. Polansky, J. K. *et al.* DNA methylation controls Foxp3 gene expression. *Eur. J. Immunol.* **38,** 1654–1663 (2008).
326. Hou, T. Z., Qureshi, O. S. & Sansom, D. M. Measuring CTLA-4-Dependent Suppressive Function in Regulatory T Cells. *Methods Mol. Biol.* **1899,** 87–101 (2019).

327. Wang, A. Y. *et al.* Adenoviral-transduced dendritic cells are susceptible to suppression by T regulatory cells and promote interleukin 17 production. *Cancer Immunol. Immunother.* **60,** 381–388 (2010).
328. Bin Dhuban, K. *et al.* Coexpression of TIGIT and FCRL3 identifies Helios+ human memory regulatory T cells. *The Journal of Immunology* **194,** 3687–3696 (2015).
329. Josefowicz, S. Z., Lu, L.-F. & Rudensky, A. Y. Regulatory T cells: mechanisms of differentiation and function. *Annu. Rev. Immunol.* **30,** 531–564 (2012).
330. Cheng, J., Montecalvo, A. & Kane, L. P. Regulation of NF-κB induction by TCR/CD28. *Immunol Res* **50,** 113–117 (2011).
331. Takeda, K. *et al.* CD28 stimulation triggers NF- B activation through the CARMA1-PKC -Grb2/Gads axis. *Int. Immunol.* **20,** 1507–1515 (2008).
332. Grinberg-Bleyer, Y. *et al.* NF-κB c-Rel Is Crucial for the Regulatory T Cell Immune Checkpoint in Cancer. *Cell* **170,** 1096–1108.e13 (2017).
333. Long, M., Park, S.-G., Strickland, I., Hayden, M. S. & Ghosh, S. Nuclear Factor-κB Modulates Regulatory T Cell Development by Directly Regulating Expression of Foxp3 Transcription Factor. *Immunity* **31,** 921–931 (2009).
334. Messina, N. *et al.* The NF-κB transcription factor RelA is required for the tolerogenic function of Foxp3+ regulatory T cells. *Journal of Autoimmunity* **70,** 52–62 (2016).
335. Oh, H. *et al.* An NF-κB Transcription-Factor-Dependent Lineage-Specific Transcriptional Program Promotes Regulatory T Cell Identity and Function. *Immunity* **47,** 450–465.e5 (2017).
336. Du, T., Nagai, Y., Xiao, Y., Greene, M. I. & Zhang, H. Lysosome-dependent p300/FOXP3 degradation and limits Treg cell functions and enhances targeted therapy against cancers. *Exp. Mol. Pathol.* **95,** 38–45 (2013).
337. Ghosh, S. *et al.* Regulatory T Cell Modulation by CBP/EP300 Bromodomain Inhibition. *J. Biol. Chem.* **291,** 13014–13027 (2016).
338. Nagai, Y., Lam, L., Greene, M. I. & Zhang, H. FOXP3 and Its Cofactors as Targets of Immunotherapies. *Engineering* **5,** 115–121 (2019).
339. Akhmetzyanova, I. *et al.* CD137 Agonist Therapy Can Reprogram Regulatory T Cells into Cytotoxic CD4+ T Cells with Antitumor Activity. *The Journal of Immunology* **196,** 484–492 (2016).
340. Yang, S., Wang, J., Brand, D. D. & Zheng, S. G. Role of TNF–TNF Receptor 2 Signal in Regulatory T Cells and Its Therapeutic Implications. *Front Immunol* **9,** 372 (2018).
341. Golovina, T. N. *et al.* CD28 Costimulation Is Essential for Human T Regulatory Expansion and Function. *J. Immunol.* **181,** 2855–2868 (2008).
342. Kastenhuber, E. R. & Lowe, S. W. Putting p53 in Context. *Cell* **170,** 1062–1078 (2017).
343. Lienart, S. *et al.* Structural basis of latent TGF-beta1 presentation and activation by GARP on human regulatory T cells. *Science* **362,** 952–956 (2018).
344. Zaitsu, M., Issa, F., Hester, J., Vanhove, B. & Wood, K. J. Selective blockade of CD28 on human T cells facilitates regulation of alloimmune responses. *JCI Insight* **2,** (2017).
345. Seddiki, N. *et al.* Expression of interleukin (IL)-2 and IL-7 receptors discriminates between human regulatory and activated T cells. *Journal of Experimental Medicine* **203,** 1693–1700 (2006).

346. Kordasti, S. *et al.* Deep phenotyping of Tregs identifies an immune signature for idiopathic aplastic anemia and predicts response to treatment. *Blood* **128,** 1193–1205 (2016).
347. Bengsch, B. *et al.* Deep immune profiling by mass cytometry links human T and NK cell differentiation and cytotoxic molecule expression patterns. *J Immunol Methods* (2017). doi:10.1016/j.jim.2017.03.009
348. Lowther, D. E. *et al.* PD-1 marks dysfunctional regulatory T cells in malignant gliomas. *JCI Insight* **1,** (2016).
349. Chew, V. *et al.* Delineation of an immunosuppressive gradient in hepatocellular carcinoma using high-dimensional proteomic and transcriptomic analyses. *Proc. Natl. Acad. Sci. U.S.A.* **114,** E5900–E5909 (2017).
350. Law, J. P. *et al.* The importance of Foxp3 antibody and fixation/permeabilization buffer combinations in identifying CD4+CD25+Foxp3+ regulatory T cells. *Cytometry A* **75,** 1040–1050 (2009).
351. Liu, W. *et al.* CD127 expression inversely correlates with FoxP3 and suppressive function of human CD4+ T reg cells. *Journal of Experimental Medicine* **203,** 1701–1711 (2006).
352. Baecher-Allan, C., Brown, J. A., Freeman, G. J. & Hafler, D. A. CD4+CD25high regulatory cells in human peripheral blood. *J. Immunol.* **167,** 1245–1253 (2001).
353. Elghetany, M. T. & Davis, B. H. Impact of preanalytical variables on granulocytic surface antigen expression: a review. *Cytometry B Clin Cytom* **65,** 1–5 (2005).
354. Turac, G. *et al.* Combined flow cytometric analysis of surface and intracellular antigens reveals surface molecule markers of human neuropoiesis. *PLoS ONE* **8,** e68519 (2013).
355. Bendall, S. C. *et al.* Single-cell mass cytometry of differential immune and drug responses across a human hematopoietic continuum. *Science* **332,** 687–696 (2011).
356. Tricot, S. *et al.* Evaluating the efficiency of isotope transmission for improved panel design and a comparison of the detection sensitivities of mass cytometer instruments. *Cytometry A* **87,** 357–368 (2015).
357. Seddiki, N. *et al.* Human antigen-specific $CD4^+$ $CD25^+$ $CD134^+$ $CD39^+$ T cells are enriched for regulatory T cells and comprise a substantial proportion of recall responses. *Eur. J. Immunol.* **44,** 1644–1661 (2014).
358. Shekhar, K., Brodin, P., Davis, M. M. & Chakraborty, A. K. Automatic Classification of Cellular Expression by Nonlinear Stochastic Embedding (ACCENSE). *Proc. Natl. Acad. Sci. U.S.A.* **111,** 202–207 (2014).
359. Thome, J. J. & Farber, D. L. Emerging concepts in tissue-resident T cells: lessons from humans. *Trends Immunol.* **36,** 428–435 (2015).
360. Bjornson, Z. B., Nolan, G. P. & Fantl, W. J. Single-cell mass cytometry for analysis of immune system functional states. *Curr. Opin. Immunol.* **25,** 484–494 (2013).
361. Pham, M. N., Herrath, Von, M. G. & Vela, J. L. Antigen-Specific Regulatory T Cells and Low Dose of IL-2 in Treatment of Type 1 Diabetes. *Front Immunol* **6,** 1007–9 (2016).
362. Trzonkowski, P. *et al.* Hurdles in therapy with regulatory T cells. *Science Translational Medicine* **7,** 304ps18–304ps18 (2015).

363. Hombach, A. A., Kofler, D., Rappl, G. & Abken, H. Redirecting human CD4+CD25+ regulatory T cells from the peripheral blood with pre-defined target specificity. *Gene Ther* **16,** 1088–1096 (2009).
364. Vahl, J. C. *et al.* Continuous T cell receptor signals maintain a functional regulatory T cell pool. *Immunity* **41,** 722–736 (2014).
365. Dawson, N. A. J. & Levings, M. K. Antigen-specific regulatory T cells: are police CARs the answer? *Transl Res* 1–6 (2017). doi:10.1016/j.trsl.2017.06.009
366. Brentjens, R. J. *et al.* Safety and persistence of adoptively transferred autologous CD19-targeted T cells in patients with relapsed or chemotherapy refractory B-cell leukemias. *Blood* **118,** 4817–4828 (2011).
367. Eshhar, Z., Waks, T., Gross, G. & Schindler, D. G. Specific activation and targeting of cytotoxic lymphocytes through chimeric single chains consisting of antibody-binding domains and the gamma or zeta subunits of the immunoglobulin and T-cell receptors. *Proc. Natl. Acad. Sci. U.S.A.* **90,** 720–724 (1993).

Appendices

Appendix A Gating strategies for in vivo signaling domain CAR Treg studies (Chapter 4)

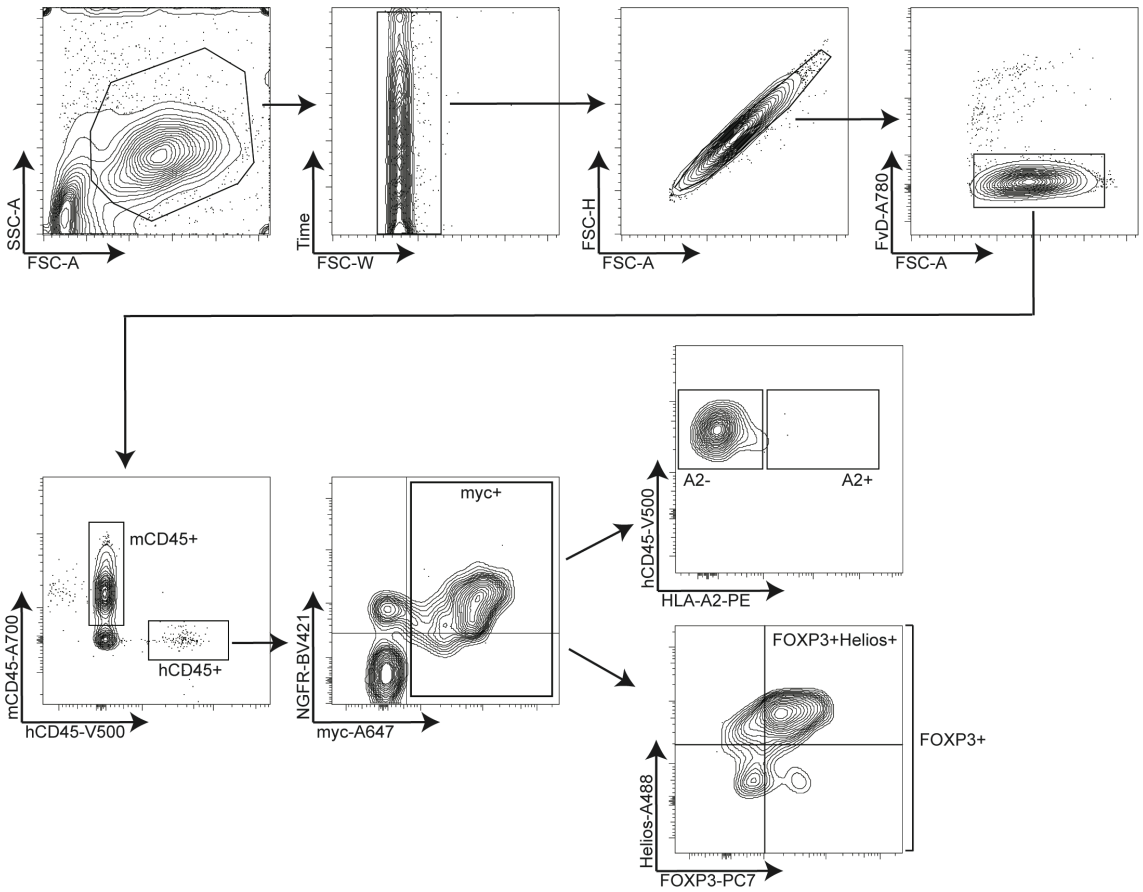

Figure A.1 Gating strategy for flow cytometry analysis of xenoGVHD experiments (Chapter 4).
Gates are as marked. CD28wt-CAR Tregs from a high ratio mouse at day 7 is shown as an example.

Appendix B Supplemental tables supporting RNA sequencing pathway analyses

Table B.1 Gene set enrichment analysis of transcription factor targets and hallmark pathways supporting Figure 4.13B

Group: PD-1, TNFR2, CTLA-4mut, CTLA-4wt, CD3zeta			Group: CD28wt		
Enriched transcription factor targets	**NES**	**Adj. p val.**	**Enriched transcription factor targets**	**NES**	**Adj. p val.**
CREBBP	-1.92	0.0333	MYB	2.00	0.0192
EP300	-1.92	0.0333	ORC2	1.99	0.0213
			RB1	1.94	0.0329
			E2F4	1.90	0.0192
			MCM2	1.87	0.0402
			MCM3	1.87	0.0402
			MCM4	1.87	0.0402
			MCM5	1.87	0.0402
			MCM6	1.87	0.0402
			MCM7	1.87	0.0402
			RELA	1.62	0.0402
			NFKB1	1.45	0.0449
Enriched hallmark pathways	**NES**	**Adj. p val.**	**Enriched hallmark pathways**	**NES**	**Adj. p val.**
HALLMARK_INTERFERON_ALPHA_RESPONSE	-2.01	0.001	HALLMARK_MYC_TARGETS_V1	3.43	0.001
HALLMARK_INTERFERON_GAMMA_RESPONSE	-1.73	0.001	HALLMARK_MYC_TARGETS_V2	3.08	0.001
HALLMARK_HEME_METABOLISM	-1.60	0.004	HALLMARK_E2F_TARGETS	2.97	0.001
			HALLMARK_MTORC1_SIGNALING	2.62	0.001
			HALLMARK_UNFOLDED_PROTEIN_RESPONSE	2.58	0.001
			HALLMARK_G2M_CHECKPOINT	2.50	0.001
			HALLMARK_OXIDATIVE_PHOSPHORYLATION	2.07	0.001
			HALLMARK_GLYCOLYSIS	2.05	0.001
			HALLMARK_DNA_REPAIR	2.04	0.001
			HALLMARK_UV_RESPONSE_UP	1.86	0.001
			HALLMARK_ADIPOGENESIS	1.83	0.001
			HALLMARK_FATTY_ACID_METABOLISM	1.48	0.022

Table B.2 Gene set enrichment analysis of transcription factor targets and hallmark pathways supporting Figure 4.13C

Group: 4-1BB, TNFR2			Group: CD28wt		
Enriched transcription factor targets	**NES**	**Adj. p val.**	**Enriched transcription factor targets**	**NES**	**Adj. p val.**
IKBKG	-1.93	0.0194	ORC2	1.98	0.0190
CREBBP	-1.90	0.0190	MCM2	1.83	0.0473
EP300	-1.90	0.0190	MCM3	1.83	0.0473
			MCM4	1.83	0.0473
			MCM5	1.83	0.0473
			MCM6	1.83	0.0473
			MCM7	1.83	0.0473
			E2F4	1.71	0.0190
			MYB	1.63	0.0194
Enriched hallmark pathways	**NES**	**Adj. p val.**	**Enriched hallmark pathways**	**NES**	**Adj. p val.**
HALLMARK_MYC_TARGETS_V2	-2.76	0.003	HALLMARK_INTERFERON_ALPHA_RESPONSE	2.20	0.003
HALLMARK_MYC_TARGETS_V1	-2.74	0.003	HALLMARK_INTERFERON_GAMMA_RESPONSE	2.08	0.003
HALLMARK_E2F_TARGETS	-2.60	0.003	HALLMARK_TNFA_SIGNALING_VIA_NFKB	1.52	0.007
HALLMARK_G2M_CHECKPOINT	-2.21	0.003	HALLMARK_HEME_METABOLISM	1.41	0.037
HALLMARK_MTORC1_SIGNALING	-2.08	0.003			
HALLMARK_UNFOLDED_PROTEIN_RESPONSE	-2.08	0.003			
HALLMARK_UV_RESPONSE_UP	-1.59	0.006			
HALLMARK_GLYCOLYSIS	-1.48	0.013			
HALLMARK_IL2_STAT5_SIGNALING	-1.44	0.013			

Table B.3 Gene set enrichment analysis of transcription factor targets and hallmark pathways supporting Figure 4.13D

Group: PD-1			Group: CD3zeta		
Enriched transcription factor targets	**NES**	**Adj. p val.**	**Enriched transcription factor targets**	**NES**	**Adj. p val.**
STAT6	-1.96	0.0325	MYB	2.06	0.0276
STAT2	-1.88	0.0420	E2F4	1.46	0.0430
STAT3	-1.69	0.0420			
Enriched hallmark pathways	**NES**	**Adj. p val.**	**Enriched hallmark pathways**	**NES**	**Adj. p val.**
HALLMARK_P53_PATHWAY	-1.42	0.0140	HALLMARK_MYC_TARGETS_V1	2.70	0.0007
			HALLMARK_MYC_TARGETS_V2	2.50	0.0007
			HALLMARK_MTORC1_SIGNALING	2.32	0.0007
			HALLMARK_E2F_TARGETS	2.11	0.0007
			HALLMARK_UNFOLDED_PROTEIN_RESPONSE	2.09	0.0007
			HALLMARK_CHOLESTEROL_HOMEOSTASIS	2.03	0.0007
			HALLMARK_TNFA_SIGNALING_VIA_NFKB	1.90	0.0007
			HALLMARK_ESTROGEN_RESPONSE_LATE	1.83	0.0007
			HALLMARK_G2M_CHECKPOINT	1.81	0.0007
			HALLMARK_OXIDATIVE_PHOSPHORYLATION	1.79	0.0007
			HALLMARK_GLYCOLYSIS	1.76	0.0007
			HALLMARK_FATTY_ACID_METABOLISM	1.71	0.0007
			HALLMARK_IL2_STAT5_SIGNALING	1.60	0.0019
			HALLMARK_ANDROGEN_RESPONSE	1.56	0.0125
			HALLMARK_UV_RESPONSE_UP	1.43	0.0181
			HALLMARK_HYPOXIA	1.43	0.0181
			HALLMARK_ADIPOGENESIS	1.41	0.0170
			HALLMARK_XENOBIOTIC_METABOLISM	1.41	0.0249
			HALLMARK_INFLAMMATORY_RESPONSE	1.38	0.0340
			HALLMARK_DNA_REPAIR	1.38	0.0340

Table B.4 Gene set enrichment analysis of transcription factor targets and hallmark pathways supporting Figure 4.14A

Group: CD28mut			Group: CD28wt		
Enriched transcription factor targets	**NES**	**Adj. p val.**	**Enriched transcription factor targets**	**NES**	**Adj. p val.**
STAT1	-1.91	0.0336	E2F4	1.70	0.0269
Enriched hallmark pathways	**NES**	**Adj. p val.**	**Enriched hallmark pathways**	**NES**	**Adj. p val.**
HALLMARK_WNT_BETA_CATENIN_SIGNALING	-1.75	0.0124	HALLMARK_E2F_TARGETS	2.52	0.0013
HALLMARK_INTERFERON_GAMMA_RESPONSE	-1.67	0.0014	HALLMARK_MYC_TARGETS_V1	2.45	0.0013
HALLMARK_ALLOGRAFT_REJECTION	-1.56	0.0064	HALLMARK_G2M_CHECKPOINT	2.35	0.0013
HALLMARK_INTERFERON_ALPHA_RESPONSE	-1.51	0.0208	HALLMARK_MTORC1_SIGNALING	2.28	0.0013
			HALLMARK_MYC_TARGETS_V2	2.02	0.0013
			HALLMARK_PROTEIN_SECRETION	1.96	0.0013
			HALLMARK_MITOTIC_SPINDLE	1.78	0.0013
			HALLMARK_UNFOLDED_PROTEIN_RESPONSE	1.72	0.0030
			HALLMARK_FATTY_ACID_METABOLISM	1.68	0.0032
			HALLMARK_XENOBIOTIC_METABOLISM	1.67	0.0032
			HALLMARK_SPERMATOGENESIS	1.56	0.0209
			HALLMARK_ANDROGEN_RESPONSE	1.54	0.0209
			HALLMARK_PEROXISOME	1.54	0.0209
			HALLMARK_OXIDATIVE_PHOSPHORYLATION	1.50	0.0093
			HALLMARK_COMPLEMENT	1.50	0.0148
			HALLMARK_ADIPOGENESIS	1.50	0.0129
			HALLMARK_GLYCOLYSIS	1.43	0.0239

Table B.5 Gene set enrichment analysis of transcription factor targets and hallmark pathways supporting Figure 4.14B

Group: Tconv CD28wt			Group: Treg CD28wt		
Enriched transcription factor targets	**NES**	**Adj. p val.**	**Enriched transcription factor targets**	**NES**	**Adj. p val.**
REL	-2.34	0.0082	SPI1	2.03	0.0082
MYB	-2.07	0.0082	DAXX	1.93	0.0230
RBL1	-2.04	0.0230	GLI2	1.85	0.0331
RBL2	-2.04	0.0230			
MCM2	-1.93	0.0230			
MCM3	-1.93	0.0230			
MCM4	-1.93	0.0230			
MCM5	-1.93	0.0230			
MCM6	-1.93	0.0230			
MCM7	-1.93	0.0230			
E2F4	-1.90	0.0082			
RB1	-1.83	0.0294			
ORC2	-1.82	0.0331			
FOS	-1.71	0.0309			
Enriched hallmark pathways	**NES**	**Adj. p val.**	**Enriched hallmark pathways**	**NES**	**Adj. p val.**
HALLMARK_MYC_TARGETS_V1	-3.71	0.0011	HALLMARK_INTERFERON_ALPHA_RESPONSE	2.06	0.0011
HALLMARK_MYC_TARGETS_V2	-3.38	0.0011	HALLMARK_CHOLESTEROL_HOMEOSTASIS	1.88	0.0013
HALLMARK_E2F_TARGETS	-2.88	0.0011	HALLMARK_HYPOXIA	1.87	0.0013
HALLMARK_UNFOLDED_PROTEIN_RESPONSE	-2.41	0.0011	HALLMARK_HEME_METABOLISM	1.80	0.0013
HALLMARK_DNA_REPAIR	-2.18	0.0011	HALLMARK_APOPTOSIS	1.80	0.0011
HALLMARK_G2M_CHECKPOINT	-2.16	0.0011	HALLMARK_INTERFERON_GAMMA_RESPONSE	1.80	0.0013
HALLMARK_OXIDATIVE_PHOSPHORYLATION	-1.95	0.0011	HALLMARK_UV_RESPONSE_DN	1.75	0.0013
HALLMARK_MTORC1_SIGNALING	-1.78	0.0011	HALLMARK_COMPLEMENT	1.75	0.0016
HALLMARK_UV_RESPONSE_UP	-1.50	0.0079	HALLMARK_IL6_JAK_STAT3_SIGNALING	1.70	0.0063
			HALLMARK_TNFA_SIGNALING_VIA_NFKB	1.69	0.0013
			HALLMARK_P53_PATHWAY	1.65	0.0013
			HALLMARK_MITOTIC_SPINDLE	1.57	0.0016
			HALLMARK_IL2_STAT5_SIGNALING	1.57	0.0016
			HALLMARK_MYOGENESIS	1.55	0.0074

Enriched hallmark pathways	NES	Adj. p val.	Enriched hallmark pathways	NES	Adj. p val.
			HALLMARK_APICAL_JUNCTION	1.53	0.0063
			HALLMARK_EPITHELIAL_MESENCHYMAL_TRANSITION	1.49	0.0114
			HALLMARK_BILE_ACID_METABOLISM	1.49	0.0244
			HALLMARK_TGF_BETA_SIGNALING	1.49	0.0385
			HALLMARK_ALLOGRAFT_REJECTION	1.48	0.0087
			HALLMARK_PROTEIN_SECRETION	1.47	0.0241
			HALLMARK_KRAS_SIGNALING_DN	1.43	0.0337
			HALLMARK_KRAS_SIGNALING_UP	1.40	0.0275

Table B.6 Gene set enrichment analysis of transcription factor targets and hallmark pathways supporting Figure 4.15A

Group: Treg TCR (CD3+CD28)			Group: Treg CAR CD28wt		
Enriched transcription factor targets	**NES**	**Adj. p val.**	**Enriched transcription factor targets**	**NES**	**Adj. p val.**
			HIF1A	1.88	0.0216
			CREB1	1.81	0.0216
Enriched hallmark pathways	**NES**	**Adj. p val.**	**Enriched hallmark pathways**	**NES**	**Adj. p val.**
HALLMARK_MYC_TARGETS_V2	-2.41	0.0019	HALLMARK_CHOLESTEROL_HOMEOSTASIS	1.84	0.0024
HALLMARK_MYC_TARGETS_V1	-2.32	0.0019	HALLMARK_MITOTIC_SPINDLE	1.79	0.0019
HALLMARK_DNA_REPAIR	-1.44	0.0167	HALLMARK_HYPOXIA	1.77	0.0019
			HALLMARK_INTERFERON_GAMMA_RESPONSE	1.74	0.0019
			HALLMARK_IL2_STAT5_SIGNALING	1.74	0.0019
			HALLMARK_TNFA_SIGNALING_VIA_NFKB	1.72	0.0019
			HALLMARK_SPERMATOGENESIS	1.67	0.0043
			HALLMARK_HEME_METABOLISM	1.65	0.0019
			HALLMARK_INFLAMMATORY_RESPONSE	1.64	0.0024
			HALLMARK_INTERFERON_ALPHA_RESPONSE	1.62	0.0055
			HALLMARK_REACTIVE_OXIGEN_SPECIES_PATHWAY	1.60	0.0197
			HALLMARK_MTORC1_SIGNALING	1.60	0.0024
			HALLMARK_KRAS_SIGNALING_UP	1.60	0.0024
			HALLMARK_P53_PATHWAY	1.56	0.0024
			HALLMARK_APOPTOSIS	1.54	0.0044
			HALLMARK_PROTEIN_SECRETION	1.50	0.0182
			HALLMARK_ANDROGEN_RESPONSE	1.50	0.0182
			HALLMARK_G2M_CHECKPOINT	1.44	0.0043
			HALLMARK_FATTY_ACID_METABOLISM	1.42	0.0192
			HALLMARK_ALLOGRAFT_REJECTION	1.39	0.0182
			HALLMARK_COMPLEMENT	1.38	0.0245
			HALLMARK_XENOBIOTIC_METABOLISM	1.38	0.0254

Table B.7 Gene set enrichment analysis of transcription factor targets and hallmark pathways supporting Figure 4.15B

Group: Tconv TCR (CD3+CD28)			Group: Tconv CAR CD28wt		
Enriched transcription factor targets	**NES**	**Adj. p val.**	**Enriched transcription factor targets**	**NES**	**Adj. p val.**
MYB	-1.69	0.0124	REL	1.97	0.0175
E2F4	-1.59	0.0175	NFKB1	1.86	0.0124
			RELA	1.84	0.0124
			FOS	1.75	0.0234
Enriched hallmark pathways	**NES**	**Adj. p val.**	**Enriched hallmark pathways**	**NES**	**Adj. p val.**
HALLMARK_G2M_CHECKPOINT	-2.57	0.0010	HALLMARK_TNFA_SIGNALING_VIA_NFKB	2.04	0.0010
HALLMARK_MYC_TARGETS_V1	-2.42	0.0010	HALLMARK_INTERFERON_ALPHA_RESPONSE	2.03	0.0010
HALLMARK_E2F_TARGETS	-2.17	0.0010	HALLMARK_INFLAMMATORY_RESPONSE	1.90	0.0010
HALLMARK_MYC_TARGETS_V2	-1.96	0.0010	HALLMARK_P53_PATHWAY	1.84	0.0010
HALLMARK_MITOTIC_SPINDLE	-1.83	0.0010	HALLMARK_IL2_STAT5_SIGNALING	1.80	0.0010
HALLMARK_UV_RESPONSE_DN	-1.72	0.0010	HALLMARK_INTERFERON_GAMMA_RESPONSE	1.77	0.0010
HALLMARK_UNFOLDED_PROTEIN_RESPONSE	-1.36	0.0487	HALLMARK_XENOBIOTIC_METABOLISM	1.62	0.0026
HALLMARK_MTORC1_SIGNALING	-1.32	0.0429	HALLMARK_REACTIVE_OXIGEN_SPECIES_PATHWAY	1.50	0.0451
			HALLMARK_APOPTOSIS	1.50	0.0104
			HALLMARK_IL6_JAK_STAT3_SIGNALING	1.46	0.0475
			HALLMARK_UV_RESPONSE_UP	1.46	0.0194
			HALLMARK_EPITHELIAL_MESENCHYMAL_TRANSITION	1.44	0.0248
			HALLMARK_COMPLEMENT	1.41	0.0248
			HALLMARK_KRAS_SIGNALING_UP	1.40	0.0328
			HALLMARK_APICAL_JUNCTION	1.37	0.0429

Appendix C Gating strategies for mass cytometry studies

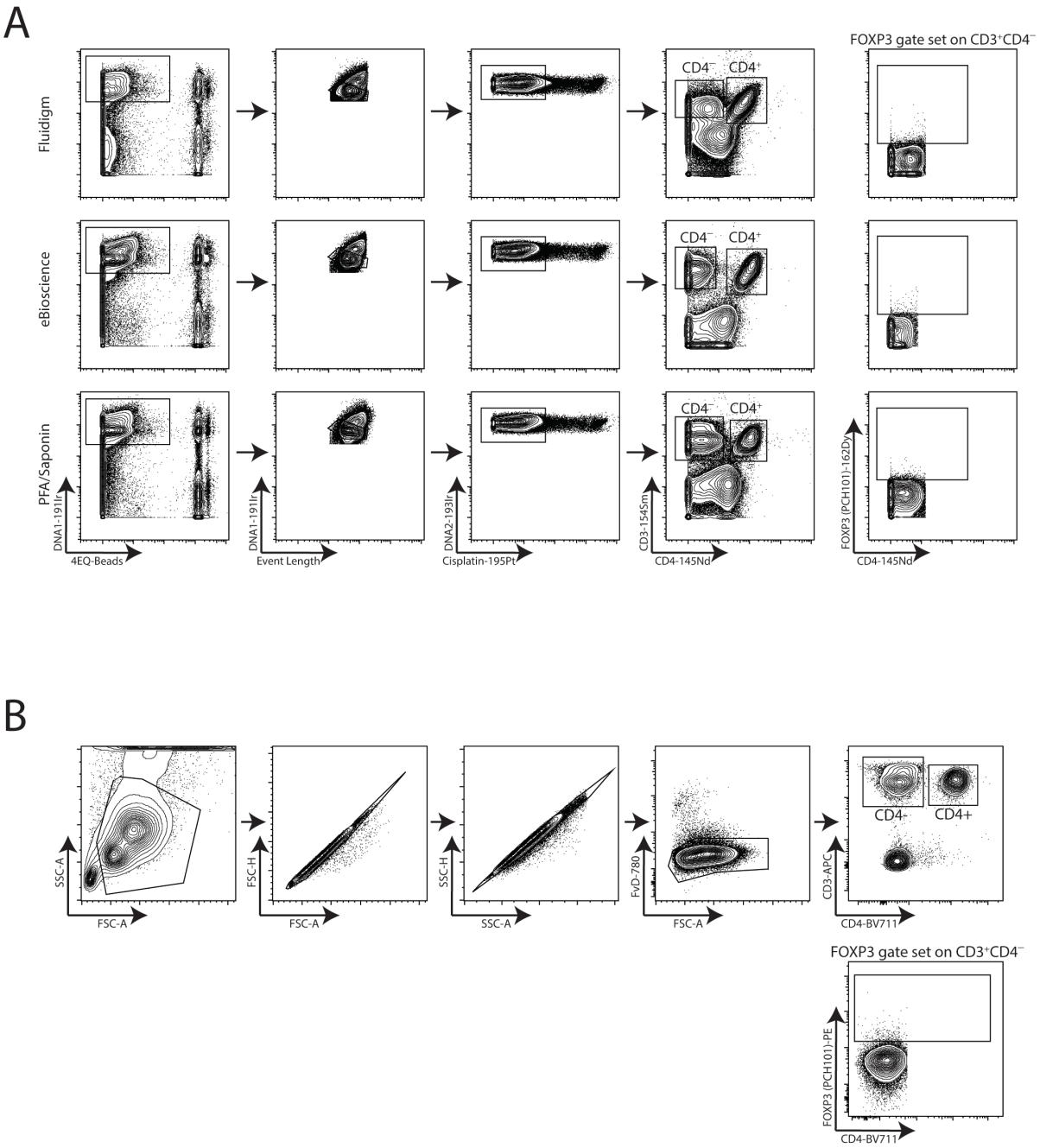

Figure C.1 Example gating strategies for mass cytometry studies (Chapter 5).
(A) Gating strategies for mass cytometry optimization of FOXP3 staining methods. PBMCs were prepared using various fixation/permeabilization methods as in Figure 5.1 and analyzed by mass cytometry. Viable (cisplatin$^-$) bead$^-$DNA1$^+$DNA2$^+$CD3$^+$CD4$^-$ single cells were used to set the FOXP3$^+$ gates which were then applied to CD4$^+$ cells to analyze the proportion of FOXP3$^{+/-}$ cells. **(B)** Example flow cytometry gating strategy for comparison to mass cytometry. Ex vivo or cryopreserved PBMC were stained using eBioscience FOXP3 staining buffers as described in Figure 5.1. Shown is an example gating strategy for gating viable (fixable viability dye–) CD3$^+$CD4$^-$ single cells to set a FOXP3$^+$ gate, which was then applied to the corresponding CD4$^+$ cells to analyze the proportion of FOXP3$^+$ cells.